TEMPERATURE INDUCED PRESSURE DIFFERENTIALS IN HIGH-RISE BUILDINGS

by

Kyu-Hyun Lee

A thesis submitted to the School of Graduate Studies
in partial fullfillment of the requirements of
the degree of

Doctor of Philosophy
in the
Department of Mechanical Engineering
University of Ottawa
Ottawa, Canada
1986

ISBN 0-315-36503-X

UNIVERSITÉ D'OTTAWA
UNIVERSITY OF OTTAWA

ABSTRACT

An analytical and experimental study of the characteristics of the distributions of the pressure differentials induced by temperature difference across the building envelope (which is termed in general as " thermal effect ") is presented in this thesis. The thermal effect in the buildings is investigated analytically and experimentally in two major categories: thermal effect without considering the effect of floor separations and thermal effect considering the effect of internal flow resistance imposed by floor separations.

Emphasis was placed on the effect of the floor separations within the building on the profiles and patterns of the pressure differentials across the building envelope induced by thermal effect, the effect of non-uniform temperature distribution of air, and the effect of mechanical ventilation.

To verify the analytical study, two different types of simulated high-rise model buildings were used, which were made of copper tubes having 50.8 mm I. D., 2.5 mm in thickness, and 18.3 m in length. One of the model buildings was designed to have only the exterior wall openings distributed along its elevation without floor separations, while the other was designed to have five floor levels divided by the specially made cassette plate assemblies that

enable floor openings between floor separations to be simulated.

The results of the present analysis, based on the energy equations applied to the two different types of high-rise model buildings, have been shown to agree fairly well with those obtained from the present experimental programs. The study showed that the thermal effect equations can correctly estimate the pressure differentials across the exterior enclosures of buildings induced by the temperature differences if the value of the neutral pressure level is known so that the thermal effect in the high-rise buildings could be characterized with neutral pressure level(NPL).

The study also confirmed that the distribution of the pressure difference due to the thermal effect is strongly affected by the relative magnitude of resistance to flow the in exterior envelope to the resistance to flow across floor separations, and that their relationships can be characterized with a non-dimensional parameter A_p^*.

However, the present analysis applied to the actual buildings showed that the effect of floor separations on the pressure differentials across the wall is not significant in the actual buildings due to sufficient interconnections between floor separations. As a result, the thermal effect in the actual buildings appeared to be governed mainly by the distributed patterns of the openings on the exterior wall of the building with elevation.

It also has been shown in the study that the the pressure differential induced from the operation of mechanical ventilation appeared to be almost linearly additive to the pressure differential due to the thermal effect if the air is introduced or taken out of the building space uniformly by the mechanical ventilation. The result has been shown that depending on its applied pattern, the mechanical ventilation appeared to result in shifting up or down of NPL and the profile of pressure differentials across the exterior wall due to the thermal effect.

ACKNOWLEDGEMENTS

The author wishes to express his deep sense of gratitude and appreciation to Dr. Yung Lee who initiated and supervised this work. His valuable suggestions, guidances and encouragement throughout this work have made it possible to achieve the desired objectives and results.

The author also wishes to extend his deep gratitude to Dr. H. Tanaka, Department of Civil Engineering, who frequently provided guidance and encouragement throughout the duration of this study.

Sincere thanks are also due to both the technical and administrative staff members of the Department of Mechanical Engineering, who extended their helps and cooperation in various ways.

Very special thanks are due to the author's wife, Myung-Ae, who offered great help and encouragement during time of difficulty, and the typing of this thesis.

TABLE OF CONTENTS

LIST OF FIGURES

LIST OF TABLES

NOMENCLATURE

A	Area, m^2.
A_p^*	Ratio of floor opening area to exterior wall opening per floor, A_p/A_w.
$A_{p\,crt}^*$	Critical value of A_p^* which shows a negligible pressure difference across floor partition
b	Temperature slope of air or wall with elevations
C	Friction factor, defined in Eq.3.3.6.
D	Diameter, m.
f	friction factor
g	Acceleration of gravity, m/s^2.
H	Height of building or height, m.
K'	Constant, defined in Eq.1.1
K_c	Minor loss factor due to sudden contraction
K_{ext}	Minor loss factor due to sudden expansion
K_{fl}	Form loss factor
K_{re}	Minor loss factor due to re-entrant
L	Length of openings, m.
NPL	Neutral Pressure Level, m.
P	Pressure, Pa.
R	Gas constant, J/kg.K.
Re_d	Reynold number, $\rho vD/\mu$.
T	Temperature or absolute temperature, $^{\circ}C$ or K.
y	Crack perimeter or width, m.
v	Velocity, m/s.

z	Elevation or height, m.
z_n	Neutral Pressure Level, m.

SUBSCRIPTS

1	Opening at bottom level, Fig.3.3.1.
2	Opening at top level, Fig.3.3.1.
a	Flow section a of opening, Fig.3.3.1.
b	Flow section b of opening, Fig.3.3.1.
crt	Critical value
e	Equivalent
i	Inside; opening below NPL
in	Inward; inside
j	Opening above NPL
o	Outside
out	Outward; outside
p	Floor~~-partition~~
v	Mechanical ventilation
vs	Mechanical ventilation plus thermal effect

GREEK SYMBOLS

ρ	Density of air, kg/m^3.
μ	Viscosity of air, $N.s/m^2$.
Δ	Difference

CHAPTER I

INTRODUCTION

Studies on the energy consumption for the buildings show that over one half of the energy consumed in the commercial and residential buildings is for space heating and cooling [1]. This space air conditioning load is caused by losses or gains due to heat transmission, by air infiltration, and controlled ventilation by operation of mechanical ventilation system.

In contrast with the relatively easy process of predicting the heat transmission loads in heating, ventilation, and air conditioning (HVAC) of the building, the infiltration is the most complicated problem which results in an uncontrolled air flow into buildings. Recently, as buildings are constructed so as to be further insulated thermally, air infiltration becomes a more important component in the design and operation of building space air conditioning systems.

When the building, especially in the heating season, is subject to the environment associated with the temperature difference between inside and outside, and the wind, it unavoidably experiences air leakage or infiltration through the cracks or crevices existing on the exterior enclosure at various levels. The operation of the mechanical ventilation

system for air conditioning may also contribute to the air leakage.

The air leakage or the air infiltration into the building is known to be the direct result of the pressure differences due to the driving forces mentioned above. The air infiltration resulting from the forces has been shown to have a significant influence on the various aspects of the building performances in a number of ways [2, 3].

The air infiltration due to the thermal force, induced from the difference in the density of the air inside and outside, appears to be substantial in high-rise or multi-story buildings during the heating season, especially where a considerable difference of temperature is observed [2, 4, 5, 6, 7].

Even for one- or two-storey houses, the thermal effect in the heating season is known to be a major source resulting in air infiltration [8].

Since the thermal effect, or force, is shown to be the major source causing the air infiltration in high-rise buildings, it is very important to have correct information about the characteristics and behaviours of the thermal effect in the buildings for an accurate estimation of HVAC load.

In the winter season in the building, if not affected by the other forces like wind or mechanical ventilation, the dense air outside tends to displace the lighter air inside by forcing its way in at the bottom of the building, and pushes the warmer air out at the top. The air infiltration, therefore, is induced, and this affects the heating or cooling loads in the air-conditioning system, as well as the cost of the building operation.

The air flow induced by the thermal effect can also cause functional problems in building operations, and discomfort or hazardous environment for the building occupants [2, 3]. These problems may include the following:

1) Uncomfortable air currents and annoying wind noise may occur in the vicinity of doors, elevator shafts, stairwells, and fire tower doors.

2) Due to the infiltration or the exfiltration induced, the thermal load may differ significantly from design values in some local areas, such as a reduced temperature of the main entrance floor, thus requiring excessive quantities of heat to provide a more comfortable space conditioning.

3) In the case of fire in high-rise buildings, the smoke dispersion through stairways, service and elevator shafts could be a potential hazard.

4) Moisture condensation and freezing problems as the air exfiltrates from upper floors.

5) An excessive pressure difference across a particular enclosure may cause difficulty in its operation(e.g., the door openings such as the main entrance door, the roof-top doors, and the elevator doors).

The problems mentioned above can be reduced by a number of modifications and designs in the building construction, but this process requires a firm understanding of the characteristics of the thermal effect. For example, if an excessive force is needed to open a single door, the use of a revolving door or two-door vestibules in the critical areas, such as the main entrance, can be a way to reduce the functional problems. Interrupting doors in stairways may also provide a means of controlling air currents and pressure differences between floors.

Another alternative is to pressurize or depressurize the particular areas by excessive air supply or exhaust through the air handling systems, but this involves an addition of heating or cooling load in the building operations.

It requires a thorough understanding of the thermal effect imposed on the building under consideration in order to determine the methods or modifications needed for reducing the air infiltration and functional problems.

The thermal effect in the building is the same as the stack effect in the chimney. The natural draft force produced in the chimney depends on the temperature differences between the flue gas and the outside air, as well as the height of the chimney.

When the air temperature inside a building is higher than that of the outside, the thermal effect certainly produces a negative inside pressure, and an inward air flow at the low level openings and a positive inside pressure and an outward air flow at the high level openings.

During the cooling season, the flow directions and the pressure pattern within the building are reversed when the inside temperature is lower than that of the outside. However, their effects are generally much less significant than the previous case because of the relatively small magnitudes of temperature difference.

The nature of the thermal effect of the building in the heating season can be explained with aid of the graphical presentation in Fig.1.1 qualitatively.

Since the pressure difference is zero at mid-height, the distribution of the pressure differences across the exterior wall would be shown as in Fig.1.1.

The pressure difference caused by the thermal effect increases with the temperature difference between inside and outside, and with the height of the building. Hence, it

would be appropriate to consider the thermal force to be one of the major causes of air infiltration in high-rise or multi-story buildings, during the heating season.

It is usually known that the pressure difference due to the thermal can be calculated from the following equation:

$$(\Delta P) = K' \left(\frac{1}{T_o} - \frac{1}{T_i} \right)(z_n - z) \qquad (1.1)$$

where

(ΔP) = pressure difference across exterior wall induced by thermal effect$(P_o - P_i)$, Pa.

T_i = inside air temperature, K.

T_o = outside air temperature, K.

K' = 3.44×10^3 Pa.K/m.

z_n = neutral pressure level, m.

z = height of opening from reference, m.

Assuming that the neutral pressure level exists at the mid-height of the building, and neglecting the effect of resistance to flow within the building, the estimated thermal effect per story would be 0.1 Pa/°C.story (one story being assumed to be 3.6 m) from Eq.1.1.

In reality, the construction of the high-rise or multi-story buildings are not as simple as the case illustrated in

Fig.1.1. The buildings are not completely open inside, nor are the interior separations between stories completely airtight. There are passages for air to flow directly through the floors, and there are stairwells, elevators and other various service shafts that allow the air to permeate through the floors.

Furthermore, the leakage openings existing in the exterior walls of a building are not always distributed simply from bottom to top. If the openings at the bottom or top are sufficiently larger than others, the resulting pressure distributions would be different than that of the previous one. In addition, the temperature profile of air within the building also may be varied along the height due to the induced flow by thermal effect.

Intuitively, the distributions and profiles of the pressure difference due to the thermal effect may depend upon the resistance to flow or the air permeability of the building components, such as the exterior walls and the interior separations within the building, as well as the temperature environments imposed.

In buildings with no internal floor separations or a relatively small internal resistance to flow, the pressure differences induced by the thermal effect act on the induced flow paths existing at the exterior enclosures of the building.

In building constructions with floor separations, the resistance to flow within the building is supposed to be increased due to serial resistance caused by the floor separations. Hence, the resulting pressure differentials across the building enclosure may be reduced. Therefore, in this particular case, the thermal effect or force may depend upon the relative magnitudes of the resistance to air flow at the exterior enclosure to that of the interior separation within the building.

In addition, the profiles of the pressure differentials induced by thermal effect also may depend upon the distributed patterns of air temperatures in the building environments.

Little information is provided, at the present, about the characteristics and behaviour of the thermal effect in the high-rise or multi-story buildings. The information about the prediction of the thermal effect in the building assessed thus far is mostly provided by the ASHRAE HANDBOOK [9], but its availability is very limited. Even the only method presented by ASHRAE is found to be incorrect [10]. Particularly, the information about the effect of internal separations and temperature distributions of air along elevation on the distributions and patterns of pressure differentials, and the relationship of the resistance to flow at exterior openings to the resistance to flow at the

interior separations within the building is entirely unknown.

In this study, the major problems aforementioned will be analyzed through analytical modelling and experimentally investigated using simulated model building, specially designed for these purposes.

The thermal effect equations and the computational models for various types of the building constructions and environments will be developed first. Then, the computed profiles and patterns of the pressure differentials will be compared with the experimental results from the simulated building model.

As a last step, the characteristics and behaviour of the thermal effect in the building, including the neutral pressure level will be studied in detail, with variations of important pertinent parameters using the analytical model tested in the second step.

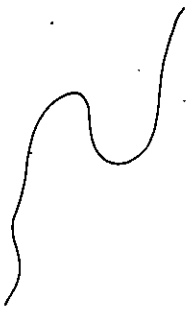

CHAPTER II

LITERATURE REVIEW

With the advent of a priority status for energy conservation, the importance of air leakage, or infiltration rate of buildings has become of great concern recently.

In this chapter, the characteristics of the air infiltration and the study results thus far, including the comparisons of measuring techniques, will be reviewed briefly.

In the first part, the physiological aspects of air infiltration and the major measurement techniques will be discussed. In the second part, the methods used to estimate air infiltration are reviewed and compared. In the third part, the field measurement results on the thermal effect in actual buildings will be reviewed.

2.1 AIR INFILTRATION AND ITS MEASUREMENTS

The air infiltration is defined to be the uncontrolled flow of air into the opening in the building envelope driven by the pressure difference across the exterior wall due to the ambient effect.

Infiltration is balanced by an equal amount of exfiltration since there can be no net storage of air in the building, except for transient conditions.

As stated earlier, understanding infiltration is critical to any building energy conservation program, since it is a primary source of energy loss in the buildings.

Furthermore, it has been shown that the air flow induced by the pressure forces, such as the thermal effect or the wind, could also cause functional problems in the building operations, and discomfort or a hazardous environment for the building occupants [2, 3].

However, at the present time, we are far more capable of predicting and calculating the heat transmission losses through the enclosure than the losses due to the air infiltration [11]. Several explanations with respect to this disparity need to be mentioned.

The heat transmission losses through the building envelope can be easily predicted because the heat transfer is shown to be linearly proportional to the temperature difference, and does not depend strongly on any other driving forces.

The air infiltration, on the other hand, depends on the pressure difference between the interior and the exterior of the building but is not linearly proportional to it. Furthermore, the driving forces or the pressure differences resulting in the air infiltration are caused by the uncontrolled ambient physical effects, such as the local direction and speed of wind, and temperature differences between inside and outside of the building [12].

The heat transmission losses can be characterized by means of one parameter, the thermal resistance. But the air infiltration, until now, has had no equivalent quantity. It is, therefore, obvious that it is more difficult to predict and to model the air infiltration than the heat transmission.

Due to these reasons outlined above, for a careful analysis of the energy requirements and better environmental conditions for the buildings, the air infiltration is required to be measured directly. However, this process is not always practicable or easy to manage.

There are two major methods of measuring the air leakage rate or air tightness of a building at the present time; the tracer gas dilution method and the fan pressurization technique.

2.1.1 Tracer Gas Measurement

The tracer gas measurement technique is a well known standard method for the direct measurement of air infiltration under the variables of ambient wind and temperature conditions. This method is based on the basic principle that an inert or inactive gas can be easily detected in dilute quantities.

If the tracer gas does not react and is not absorbed on the materials of the building and furnishings installed, its flow rate through the building envelope would provide an

accurate analog the air infiltrated into the building. ASTM Standard E741-83 specifies a standard tracer dilution method for air infiltration measurement [11].

A great advantage of measuring the infiltration with the tracer gas method is that it provides a means to measure the air infiltration rate under more or less natural conditions. However, it is expensive and time consuming to obtain a complete characterization of air infiltration using this method. It is also considered to be difficult to use on a large scale structures, such as the high-rise buildings for a routine test [13].

The tracer gas measurement of the air infiltration rate is based upon the principle that the tracer gas diffuses uniformly throughout the ventilated space in the building, and the decrease in concentration as a function of time elapsed is monitorted.

The rate of change in the amount of the tracer gas in a ventilated space may be represented as the following relationship [13]:

$$V \frac{dc}{dt} = c_o \dot{v} + G - c \dot{v} \qquad (2.1.1)$$

where

V = volume of ventilated space.

c = concentration of tracer gas in ventilated space at the time of t.

c_o = concentration of tracer in the outside air

$\dot{v}$ = rate at which air leaves the ventilated space in volume per unit time.

G = net rate of generation of tracer in the ventilated space.

If the concentration of the tracer gas in the inflow air is negligibly small (that is, $c_o = 0$) and if no tracer gas is generated or absorbed within the space, Eq.2.1.1, reduces to

$$\frac{dc}{dt} = - \frac{\dot{v}}{V} c \qquad (2.1.2)$$

which may be solved to give

$$\text{Ln} \frac{c}{c_{init}} = - \frac{\dot{v}}{V} t = - I t \qquad (2.1.3)$$

where

c_{init} = initial concentration of tracer at t = 0.

I = air change rate per unit time ($\dot{v}/V$).

If the right hand side of Eq.2.1.3 is plotted against elapsed time in hours, the slope of the line becomes - I and it represents the infiltration rate.

The plot of concentration vs. time on a semi-log graph gives a straight line if the tracer concentration is uniform in volume and the infiltration rate is constant. Several

periodic injections would give a group of straight lines. The slope of each straight section is the air infiltration rate for that time interval.

Some characteristics of ideal tracer gas have been listed by Lagus et al. [9, 13].

Helium and hydrogen are among the first gases used as the tracer gases. Helium can be determined in concentrations of the order of 0.5 percent using thermal conductivity measurements.

Hydrogen, although less compatible than helium, can be measured in lower concentrations. Kathometers for this purpose have been used [9, 13].

The thermal conductivity of the air containing tracer gases, such as helium and hydrogen, is determined relative to the initial thermal conductivity. Helium has great stability and is known to be non-toxic. The low molecular weight of helium gas makes the measurement of thermal conductivity easy to perform.

Carbon dioxide (CO_2) has also been used as a tracer gas. Nondispersive infrared gas analyzers have been developed now, which can analyze the carbon dioxide gas in concentrations as low as a few parts per million. Carbon dioxide is easy to monitor, but it has some disadvantages. For instance, there are background concentrations of CO_2 in the order of 400 to 600 ppm in the building air, and the occupants generate significant quantities of it.

Sulfur hexafluoride (SF_6) has become popular as a tracer gas [13]. It can be conveniently detected and measured in concentrations of a few parts per billion with electron capture detector.

Sulfur hexafluoride is known to be non-flammable and comparatively non-toxic. The high sensitivity with which the tracer gas may be measured is not without certain problems. For example, the leakage from regulators and other sources that might go unnoticed with other gases can lead to significant contamination and measuring error when SF_6 is used as a tracer gas.

On the other hand, the high sensitivity makes it eminently feasible to perform tracer measurements in large buildings [13].

Mixing problems have been shown to present a major source of error in the measurement of air infiltration by the tracer gas dilution method [9].

Use of Eq.2.1.3 implies that the tracer gas must be uniformly mixed throughout the test space, so that the concentration of tracer gas which is measured accurately represents the concentration in the space. In multi-room structures this may not always be feasible and special procedures are required.

Apart from the problems of a non-uniform mixing rate, which would invalidate the assumptions leading to Eq.2.1.3, there are other non-instrumental difficulties that can arise.

The loss of tracer gas by means of other than leakage can be a good example. For instance, the condensation of gas may occur or the chemical reaction may change tracer concentration in a manner which causes confusion in the results obtained [9].

Another non-instrumental difficulties can be the recirculation of air and tracer gas via adjoining rooms and external air intakes. It is often possible for the air containing tracer to be removed from the region of interest and returned at a lower concentration at some later time. This recirculation would result in an air infiltration rate that is lower than the actual one in the structure.

2.1.2 Fan Pressurization

The tracer gas procedures provide a measure of air leakage rates under more or less natural conditions, since they are conducted under the natural ambient variables.

These procedures are time consuming, expensive and not easy to handle in practice, based on the fundamental assumption, that air and tracer gas are uniformly mixed throughout the measurement intervals. It is, therefore, obvious that the tracer gas method is subject to certain degrees of uncertainties due to its own inherent characteristics outlined previously.

Where the air tightness, or leakage characteristics of the building are of major concern, apart from weather conditions, the fan pressurization or depressurization

methods have been applied widely [8, 14, 15]. Since the fan, or blower is employed for the infiltration measurement in this method, this particular procedure can characterize the air leakage rate in the building, independent of weather parameters, such as wind and temperature.

Equipment required for the measurements include a blower, a flow meter, a pressure gage, and possibly a smoke source, or an infrared scanning device to locate leaks [9, 11, 15].

A fan, or blower is sealed into the building envelope such as a window or doorway, and allowed to move air into or out of the building at a measured rate. The pressure difference between inside and outside is measured as a function of flow rate of air.

A scaled down version of this approach is also applied for measuring air leakages of building components, such as windows, doors, and wall sections [14]. One of the applications of the method in particular, is to identify the air leakage paths in the building enclosures. By alternatively sealing different parts of the house, or building with plastic sheets, Tamura [15] was able to determine the fraction of the total air leakage through different components of the building envelope such as the roof, window, and doors.

The principle of the method is based on the flow through a orifice area, which may be expressed by

$$Q = C\,(\Delta P)^n \qquad (2.1.4)$$

where

Q = flow rate in volume per unit time

C = flow coefficient

P = pressure difference measured between inside and outside.

n = flow exponent.

Eq.2.1.4 would have a form of a straight line in a log-log plot where n is the slope of the line. Dividing both sides of the equation by the volume of the ventilated space, V, converts the air flow rates into the air changes per unit time.

One of the advantages of the fan pressurization method is that it is comparatively easy to perform the measurement, except for large buildings, and would be useful to predict the overall characteristics of air leakage or tightness of the building components.

Using the pressurization method, one is confronted with the problem of comparing leakiness from house to house or from building to building. Kronvall [11] attempted to make such comparisons for a number of Swedish houses using the parameter Q/A (flow rate/ surface area), and then derived

a relationship between pressurization tests and the natural infiltration. The results showed that this process appears to be limited and not successful.

Fan-induced air exchange rates are usually shown to present much larger values than the normal or natural air leakage rate, obtained from the tracer gas method [11].

Some study results showed that there may be a small difference between pressurization and depressurization, due to elements in the building enclosures, which can act somewhat as flap valves, causing errors arising from the blower rating calibration [11].

2.2. METHODS OF CALCULATION FOR AIR-INFILTRATION

Most of the models or methods for estimating the infiltration developed thus far are shown to be air leakage models in general [9]. In the methods presented, it has been shown that assumptions should be made as to which components of the building are subjected to infiltration and which are subjected to exfiltration, in order to convert the leakage calculations to the air infiltration estimates.

ASHRAE and others have presented several methods or models for estimating and calculating the air infiltration into the building [9, 11, 12]. Here the representative methods are outlined and discussed.

2.2.1. Air Change Method

The ASHRAE [9] recommends an air change method for the calculation of air infiltration rates for a building. This method is known to be a rule of thumb approximating the amount of air infiltration with the past experience in practice.

This method suggests dividing the total leakage rate obtained from the procedures by two to achieve the estimated infiltration rate into the building.

This method also cautions that the air change method mentioned above has a size effect, in which the extra large rooms with relatively small window areas (e.g., extra high ceilings) could be expected to have a lower volumetric exchange rate than small rooms with large window areas.

The results of the estimated infiltration rate in the houses obtained from the air change method have been compared with those from the tracer gas measurements [13]. In the study it has been reported, that in a particular case the differences between both results could be more than 50 %.

Consequently, it can be seen that the air change method can provide only a gross estimate in the prediction of infiltration at best, for the residential housings, because it is mainly based on the approximations gathered from the past experiences for residential housings, as represented above.

2.2.2 Empirical Estimation Methods

Another method is the empirical method, based on past experiments and observations in the field study of infiltration in actual residential buildings [9, 11, 16]. It is possible to consider this method as a compromise method between the air change method, and the crack method which will be discussed later in the study.

As mentioned earlier, the air infiltration into the building is not only a function of the tightness of the building envelopes, but is also influenced by the wind velocity and the temperature difference between the inside and outside. The main concept of this method, is to correlate air infiltration with the major influential factors affecting on it from an empirical view point, and derive an empirical correlation equation.

A number of empirical equations for correlating the air infiltration with the parameters mentioned above have been developed.

Dick and Thomas [11] have carried out a study of two groups of houses. One was in a comparatively exposed location so that the wind had a dominant effect on the infiltration. The other group of houses was located in more protected areas, so that under some conditions the effect of the wind was predominant, and under other conditions the effect of the thermal forces was dominated the air infiltration rate.

Their results have shown that the relative effect of the wind pressure to the thermal force appeared to be $V^2/\Delta T$, where V was wind speed in miles per hour and T was the inside-outside temperature differences in F. From the results obtained they developed an experimental graph, which is shown in Fig.2.2.1, where I/V and $I/\Delta T^{0.5}$ are plotted against $\log V^2/\Delta T$, where I is the infiltration rate.

The figure shows that when $\log V^2/\Delta T > 0.3$, $I/\Delta T^{0.5}$ increases as $V^2/\Delta T$ increases, since the thermal effect induced by temperature difference no longer dominates the mechanism, and the effect of the wind force becomes the governing factor.

When $\log V^2/\Delta T < 0.3$, I/V increases as $V^2/\Delta T$ decreases, the effect of the thermal effect is predominant. Thus, in this particular study, they proposed that the air infiltration rate may be represented in terms of the parameters of T and V.

Bahnfleth et al. [17] have conducted measurements of air infiltration by using the tracer gas method in residential houses, and their results indicated that under constant wind speed, the infiltration rate was shown basically to have a linear functional relationship with the temperature differences between the inside and outside, while under constant temperature differences, it was shown to be linearly proportional to the wind speed.

ASHRAE [9], and Coblentz and Achenbach [11] presented relationships of the parameters found in the study by Bahnfleth et al.[17] mentioned above in the form of the following empirical correlation equation.

$$I = A + BW + CT \qquad (2.2.1)$$

where

W = wind speed.

T = inside-outside temperature difference.

A, B, C = empirical constants derived from measurements at the site.

In the study, it has been shown that the constants, A, B, and C, in the equation vary significantly from site to site. It was proposed that one should account for the location of the house when using this empirical equation as a predictive model of infiltration rate for a house.

Some typical values of the constants suggested for different classes of residential houses are presented in the form of tables in the ASHRAE HANDBOOK [9].

Sepsy et al. [11] reported the results of measurements on several houses, logging nearly 2000 hours of data. In their study a number of correlation formulae were developed and tested, considering such factors as wind velocity, wind direction, temperature difference, crack lengths, and other parameters. From the results obtained, they proposed the following empirical formula:

$$I = B\ G\ \sqrt{4\Delta P_{th} + 2\Delta P_w} \qquad (2.2.2)$$

where

B = a statistical regression coefficient.

G = total crack length over infiltration exposures.

ΔP_{th} = pressure difference due to temperature difference.

ΔP_w = pressure difference due to wind effect

The equation presented above was developed as a compromised estimating method between the optimum predictive values, considering various pertinent parameters that have an influence on the infiltration, with the simplicity of the empirical correlation model suggested by Coblentz et al. [9, 11] including the crack lengths, etc.

By including the crack length, G , in the above relationship, they found that the same relationship could be applied with a reasonable accuracy for all of the houses studied.

It has been shown that the empirical methods discussed above will provide a useful means for gross approximations of air infiltration. However, there are important areas where one should be careful before applying the method in the calculation of infiltration.

For example, the wind direction and the sheltering effect provided by the surrounding environment, such as other buildings and trees, were not considered sufficiently in its formulation to warrant accurate estimation.

Furthermore, the empirical methods reported hitherto are made from experimental observations conducted for small residential houses or buildings with low structures [9]. Therefore, it is obvious that these methods have limitations in their application for estimating infiltration.

2.2.3 Crack Method

The next method is the crack method, which is known to be the most common and representative one. It is usually regarded as more accurate and reliable than others as long as the pressure differentials and leakage characteristics of the building are evaluated properly.

The method is based on the fundamental concept that a building may be considered as having a certain porosity or permeability of air with overall leakiness through enclosures, such as windows, window frames, doors, door frames, etc.

It is well understood that air infiltration is the natural uncontrolled flow of air through cracks, holes, etc., across the building envelopes by the driving forces. As a result, the infiltration may be correlated with the pressure difference induced by the ambient driving forces which is acting on the flow paths involved.

The crack method calculates the air flow produced by the pressure differences acting on each air leakage path. This method is also applied as the basic principle for the air leakage test of building enclosures or building components mentioned above, using the pressurization technique with a blower or fan [9, 11].

From the concept aforementioned, it might be assumed that the air flow through cracks is proportional to the applied or acting pressure difference across the flow passage raised to some power. Hence, the basic equation which serves to characterize the conditions above may be presented as follows:

$$Q = C\,(\Delta P_t)^n \qquad (2.2.4)$$

where

Q = volume flow rate of air

C = flow coefficient, volumetric flow rate per unit length of crack, or unit area, at a unit pressure difference

ΔP_t = total pressure difference across the building envelope

n = flow exponent, depending on the character of the flow ($0.5 < n < 1.0$)

Since the method conveys the fundamental assumption that the air leakages into the buildings through cracks and crevices can be expressed as a function of the pressure differences, it requires the determination of the quantity of driving forces that cause the air leakages correctly.

The total pressure difference resulting in the infiltration in the building, shown in Eq.2.2.3, can be considered to be the pressure differences caused by the wind, the thermal effect, and the mechanical ventilation. With the assumption that these forces could be linearly additive, it may be written as:

$$\Delta P_t = (\Delta P)_w + (\Delta P)_{th} + (\Delta P)_{vent} \qquad (2.2.4)$$

where

ΔP_w = pressure difference induced by wind.

ΔP_{th} = pressure difference induced by thermal effect.

ΔP_{vent} = pressure difference induced by mechanical ventilation.

If the correct information on each major component of the pressure differences constituting the total pressure

force inducing the infiltration, as shown in Eq.2.2.4, is available, the air infiltration can be easily predicted accurately, provided that the value of C and n are known.

However, at the present time, it has been shown that a reliable procedure for estimating these components of the total pressure difference as well as the interaction between the components constituting the driving force resulting the air leakages have not yet been developed [9, 11].

The pressure difference due to the wind is the difference between the outside and inside pressure caused by the wind on the building. The pressure difference due to the wind has been shown to depend on the elevation because the wind varies with elevation, the characteristics of the enclosure, and the wind direction.

It is well known that the air flow due to the wind around and over a building creates localized regions in which the static pressure is above or below that of the undisturbed airstream.

The wind pressure is positive on the windward side, resulting in an inflow of air into the building. Conversely, it is negative on the leeward side, resulting in an outflow of air from the building. Pressure on the other sides is negative or positive, depending on the wind angle and shape of the building under consideration.

The characteristics of the wind pressure in the building aforementioned are confirmed through the wind tunnel testing of a building model by Lee et al. [18]. In

that study, they also reported that the linear summation of pressure differentials due to the wind action and mechanical ventilation cannot be taken as the equivalent of the pressure differential due to the combined action of the two.

ASHRAE [9] has shown that the pressure difference across the windward wall due to the wind action alone can be given as:

$$P_w - P_i = \frac{P_w - P_L}{1 + (A_w/A_L)^{1/n}} \qquad (2.2.5)$$

where

P = wind pressure.

A = leakage area.

n = flow exponent

and subscripts are

w = windward.

i = inside.

L = leeward.

As shown in Eq.2.2.5, the pressure difference due to the wind action is affected by the ratio of A_w/A_L which represents the wind direction and leakage area.

ASHRAE refers to a number of papers on the wind effect [9]. In the referenced results, it has shown that square type building with a quartering wind angle, which is 45 degrees to the wall, experience an infiltration leakage into the building on two sides and out of the building on the

other two sides.

It shows also that for the case of a wind which is normal to one wall, infiltration occurs through one-quarter of the sides. Thus, the result shows that the effective wind pressure is influenced strongly by the wind direction.

In estimating the wind pressure, one has to account for the effect of the terrain on the wind velocity, which is due to large-scale roughness near the structure and provides a shielding effect in the building [9]. For a tall building, the variations of wind velocity with elevation should also be considered.

Hill and Kusuda [19] measured the infiltration in a sealed room with a window crack of given dimensions. With a simultaneous monitoring of the pressure difference across the crack they found that the flow due to the wind appeared to be a pulsed dynamic phenomenon, and that the air change rates measured by the tracer gas method were less than those predicted from the average pressure differences across the cracks, particularly at wind velocities greater than 8 Km/h.

The results showed that under the wind effect, the air infiltration is primarily the result of a pulsation process at the cracks, and that the air flow occurs into and out of the room simultaneously.

The ASHRAE [9] also referred to a number of papers about the thermal effect. In order to determine the pressure difference across the exterior wall due to thermal effect,

Eq.1.1 was proposed. For the determination of the neutral pressure level(NPL), ASHRAE recommended the following equation;

$$z_n = \frac{H}{1 + (\frac{A_1}{A_2})^2 (\frac{T_i}{T_o})} \qquad (2.2.6)$$

where

A_1 = area of lower opening.

A_2 = area of top opening.

H = height of building.

The method to estimate the NPL shown in Eq.2.2.6, which is derived by neglecting flow resistances at the openings, is applicable only for a simple case having exterior wall openings at the top and bottom levels only with no internal floor partitions between floors, and uniform temperature distributions along elevation. It has been shown by an analytical and experimental investigation using a model building [10] that Eq.2.2.6 is not correct for the simple opening cases described before.

Available information on the NPL for different types of building construction is very limited. Since the real building is not as simple as in the case of Eq.2.2.6, it is evident that the method could not be used in the actual situations.

The distributions and patterns of pressure differentials induced by thermal effect in the building are affected by the internal partitions, stairwells, elevator shafts, utility ducts, vents, and mechanical supply, and the exhaust system.

As stated earlier in this study, the estimation of infiltration using the crack method depends on the information about the pressure force. However, the accuracy of the crack method for calculating the air infiltration, as presented before, is restricted by the difficulty of a correct estimation of pressure differences induced by the major components, such as temperature and wind, even though it is known to be an accurate method for the prediction of infiltration, provided that the values of C and n are correctly known or available.

The study results reported hitherto [11] have shown that due to incorrect estimation of the pressure difference caused by the driving forces, the crack method presented the results either too low or too high from the actual one [11].

Hunt et al. [11] demonstrated that by overestimating the pressure difference, which is about 25 Pa, an air exchange rate calculated from the crack method can be more than three times the one measured for an apartment building with the tracer gas method.

Bahnfleth et al. [17], on the other hand, reported a reasonable agreement between the infiltration rates by the

crack method, and those obtained by the helium tracer gas measurements. Doeffinger [11] reported that for a measured pressure difference of 7 Pa, the infiltration values were approximately 10 % of the tracer-measured values.

Janssen et al. [16] showed that the crack method tends to overestimate the infiltration in small houses and underestimate infiltration in large residential houses.

2.3 FIELD MEASUREMENTS OF THERMAL EFFECT IN BUILDINGS

The major purpose of the field investigation was to evaluate the overall characteristics of air infiltration and the patterns of the pressure differences caused only by the thermal effect, or in combination with the effects of the wind, and the mechanical ventilation.

Tamura and Wilson [5] have investigated the distribution of the pressure differences in a nine storey office building under the influence of the thermal effect only as well as under the combined actions of the mechanical ventilation and the thermal effect. The height of the building above the ground was about 34 m to the main roof level, and 41 m to the top of the penthouse. The internal dimensions of a typical floor were 23 m x 81 m and 3.6 m between the floors.

The pressures were measured at varoius time in the evening when the building was not occupied during periods of low wind speed to provide wide range of outside temperature.

Prior to the tests, all windows, entrance doors and connecting doors between inside partitions were closed. The pressure differences across the exterior wall were then measured by using a portable pressure gage at four floor levels. Pressure measurements were also conducted under conditions of turning off the mechanical ventilation and closing dampers in the ducts joining the interior zone air-conditioning units to the fresh air shaft. The profile of the pressure differences along the elevations which was obtained from this test is shown in Fig. 2.3.1(a). Other measurements were taken when the fresh air shaft intake, the return air shaft exhaust dampers, and the connection between the stairwell and penthouse were also sealed.

This additional sealing, as shown in Fig. 2.3.1(b), presented a noticeable effect on the pressure profile, indicating that a significant air flow occur through the closed dampers prior to sealing. Due to the additional sealing, the location of the NPL was shown to be moved from 72 % of the height of the building to 62 %.

The results, obtained from measurements taken over a wide range of the outside air temperatures, showed that the NPL was not affected by the temperature differences between the inside and outside under the provided conditions of crack openings, but the slope of the pressure difference line was shown to be increased in proportion to the temperature difference between the inside and outside of the building.

The pressure measurements across the stairwells and elevator doors were conducted with mechanical ventilation both on and off. Concerning the direction of the air flow in the building, the results ~~showed~~ that without operation of the mechanical ventilation, the air flow is upward across each floor, except from the first floor to the basement, and air flows into the lower half of the vertical shafts from the first floor and out of the upper half into the floor area.

With the mechanical ventilation system on, the effect of pressurization on the pressure distribution line was observed. The effect of the operation of the mechanical ventilation resulted in lowering the NPL, causing a decrease in pressure difference across the entrance, and an increase across the top level.

Tamura and Wilson [6] also have conducted other subsequent measurements on three multi-story commercial buildings. Buildings A and B, consisted of 44 and 34 stories respectively and were commercial office buildings in Montreal. Building C, 17 stories, was a government office building in Ottawa.

All the buildings were rectangular in shape, with stairwells, elevators and various service shafts located in the core of the buildings. Pressure measurements to investigate the thermal effect were carried out over a range of outside air temperatures when the buildings were not occupied.

To minimize the effect of the wind action on the data reduction, the measurements were taken when the wind speed was under 16 Km/h. With the mechanical ventilation system on and off, the pressure measurements were carried out for the three buildings.

The results obtained in these tests indicated a general similarity with the previous results for the nine story building. In the results, it has been shown that the slope of the pressure distribution line representing the pressure differences across the exterior wall along height had the same trends that presented in Eq.1.1.

The location of the neutral pressure levels in the three buildings are shown to be approximately 40, 35, and 52% of the building height for Building A, B, and C, respectively. The measurements made over a various range of outside air temperatures indicated that the neutral pressure levels in the buildings appear not to be affected by the temperature differences as were found in the previous measurements.

The pressure differences across the exterior wall are shown to be approximately linearly proportional to the corresponding absolute temperature differences.

The measured results indicated that in all the buildings investigated, the pressure differences between floors in the building were shown to be relatively small, except between the ground and the first floor due to sufficient openings provided by exhaust ducts, elevator and

service shaft cracks, etc.

Large pressure differences between floors were observed in all buildings wherever there were air tight separations between floors. Especially large pressure differences were shown to exist between the ground floor and the following upper floors, presenting a considerable effect of the internal floor separations on the pressure profile.

With the operation of the mechanical ventilation system, the pressurization effect was observed in Building B and C, which caused a corresponding shift of the pressure differential curve across the exterior wall to the left in general, lowering the neutral pressure level. On the other hand, the effect of the operation of the mechanical ventilation in Building A was shown not apparent.

The results also showed, that the pressure difference across the various internal separations were increased by the operation of the mechanical ventilation system, and in some cases there was a non-uniform pressurization between floors with the ventilation system in operating conditions.

Lee et al. [4] have conducted a measurement of pressure distributions on a twenty-story compartmentalized building which was a student residence at the University of Ottawa, for 5 months of the winter season. The building was approximately 56 m high, 22 m x 27 m in floor section and 3.6 m high between floors.

The pressure differences across exterior walls were measured at four different floor levels. The results showed

that the pressure difference across the doors in the same floor within the building were negligibly small.

For the reduction of the thermal effect, the measurements for the pressure differences were carried out when the wind speed was less than 1.0 m/s.

The neutral pressure level in the building was found to be located at 70 % of the height of the building when it was not occupied. However, it was raised to 90 % of the height of the building during the occupied period, when the mechanical ventilation system and elevators were operating.

The results obtained showed that the thermal effect was one of the major driving forces for the pressures differences causing the infiltration all through the winter season.

The resulting pressure difference due to thermal effect only was shown to be comparable to the pressure of the wind induced with a positive pressure of local mean speed of 12 m/s. The effect of the mechanical ventilation system on the pressure profiles in the building was found to be less than a quarter of that caused by the thermal effect.

The results above indicates that for cold weather or heating season the thermal effect comprises the major portion of the driving forces causing the infiltration in the high-rise buildings.

2.4 NUMERICAL ESTIMATIONS OF THERMAL EFFECT

Barret and Locklin [3] have carried out a computational analysis of the thermal effect in the high-rise building using a hypothetical 75 storey office building model with curtain wall construction.

In the analysis, the example building was divided into a total of 37 unique spaces comprising 7 occupied zones, 13 elevator shafts, 1 stairway, 3 equipment floors, and 13 elevator machine rooms.

By assuming the flow characteristics of all paths and a linear pressure profile with elevation given by Eq.1.1 for the building, the thermal effect air flow quantities and the pressure differentials were evaluated for all building components.

The calculation of the air flow quantities for the flow paths involved were determined from the conventional crack flow equation using iterative procedures until the results were met the balanced condition of mass conservation in total.

Through the analysis it has been shown that a computational analysis of this type is useful to identify the nature and location of problems created by the thermal effect in a particular building. Tamura and Wilson [20] have carried out a computational analysis of the distribution of the pressure differences due to the thermal effect using a mathematical model with equivalent orifice openings in the major building enclosures including the

floor separations.

In the analysis, the mass flow through the orifice openings was based on the crack flow equation, Eq.2.2.3, assuming flow exponent of 1/2 to 1.0. Initially a model was made of a three story building, which was expanded up to ten stories later.

Using the model, a computer program was formulated to solve all the unknown pressures inside the building using the crack flow equation of Eq.2.2.3 and flow balance through the orifice openings of the external walls, the floors and the vertical shafts.

In the results, it has been shown that with a high resistance to upward flow within the building, the pressure differences across the exterior walls was reduced, and those across the interior floor partitions were increased. The results also indicated, that with a significant resistance to upward air flow, it is possible to minimize the effect of the thermal pressure differences.

The study also presented, that providing an excess air supply or exhaust at the corresponding floor could be another alternative to reduce the pressure difference causing infiltration due to thermal effect.

Tamura and Shaw [21] presented an air infiltration model of the thermal effect which was derived from the crack flow equation of Eq.2.2.3 and the thermal effect equation of Eq.1.1.

In the development of the model a correction factor was introduced to Eq.1.1, in order to consider the effect of the resistance to flow within the building on the distributions of pressure difference across the exterior wall, due to the interior floor partitions and the vertical distribution pattern of exterior openings in the wall.

Assuming a constant cross sectional area, and a uniform distribution of leakage opening with height, the following model was presented:

$$Q_s = C_w S \left(0.034 \gamma p \frac{T}{T_i T_o} \right) \frac{(\beta H)^{n_w + 1}}{n_w + 1} \qquad (2.4.1)$$

Q_s = total rate of infiltration due to thermal effect, cfm/s.

C_w = flow coefficient, cfm/sq.ft.in of water.

γ = correction factor.

p = barometric pressure, lb/sq.in.

h = vertical distance from NPL, ft.

T = temperature difference, $T_i - T_o$, F

β = ratio of building height to NPL.

H = height of building, ft.

n_w = flow exponent for exterior wall.

S = perimeter of the building, ft.

For the calculations of the air infiltration, they suggested the use of the values of n_w and C_w, determined by the field measurement, using fan pressurization in actual

building with an arbitrary assumption of the correction factor, γ.

The values of the flow exponent and the flow coefficient, n_w and C_w, were presented in three major groups according to the air tightness of the building envelope from their air leakage tests in buildings using the fan pressurization tests [15, 23, 25]. However, the values of the correction factor, γ, and the NPL were assumed arbitrarily in the calculations of air infiltration in the method.

Since the NPL and the value of the correction factor are not only unknown, but also not easy to determine for various actual situations, it is very doubtful that the proposed method can be a correct and a predictive one.

2.5 CONCLUDING REMARKS

From the overview the study results reported thus far, it is clear that the air leakage or the infiltration in the buildings appeared to be very difficult to quantify because it is not only a function of building tightness and configuration but also of the ambient variables, and the mechanical ventilation.

Several standard formulas have been developed to estimate the air infiltration rates [9], but they still are rough approximations at best, since the information on the mechanisms inducing the air leakages is not well understood due to its inherent complexity resulting from the

unpredictable parameters, such as ambient variables.

Existing test results also showed that the validity of the models for an estimation of the air infiltration described in Section 2.2, mainly depends upon the correctness of the information provided about the pressure difference acting on the flow paths, as well as the characteristics of the openings in the buildings.

The leakage characteristics of the building enclosures can be found through the fan pressurization method indirectly [9, 23, 25, 26]. However, the pressure differentials resulting in the infiltration still is shown to be very difficult to determine correctly.

Hence, for the correct estimation of the air infiltration, a method which is reliable and correct, should be developed to quantify the pressure differentials governing the infiltration into the building.

As presented previously, information on the infiltration measurements of actual buildings is still very limited and rare, especially in the high-rise or multi-story buildings.

As indicated earlier in this study, most of the predictive or calculating models for infiltration have been made on single family homes or low level residential units.

Through a number of field measurements in multi-story buildings, it has been observed that the pressure differences due to thermal effect, can be one of the major forces which induce air infiltration in the high-rise or

multi-story building during the heating season.

Therefore, it is very important to have a complete understanding about the characteristics of the thermal effect in the building correctly in order to estimate air infiltration in high-rise buildings. However, the information obtained on the thermal effect in the high-rise building has been very limited [9]. Furthermore, the existing method that serves for this purpose is shown to apply only to simple, and limited cases, and is not reliable due to its incomplete performance [10].

Direct measurements of the air infiltration due to the thermal effect in actual high-rise buildings can be conducted, but this is not always feasible and easy to process, nor is it economical to manage in practice.

Moreover, from the logical point of view, it is not practical to isolate the other effects, such as wind, and mechanical ventilation, from direct measurement results, conducted for the purpose of studying the thermal effect in the actual buildings.

There may also be other errors expected from the air flow paths, like supply and exhaust ducts, used for the air conditioning of the building space, and the operations of elevators, etc., which contribute to sufficient interconnections of air flow between floors affecting the measured results.

To obtain accurate and practical information about the characteristics and behaviors of the thermal effect in real buildings, it is very important to carry out both analytical and experimental investigations by using specially designed experimental models, which can isolate the thermal effect from the other factors described above.

CHAPTER III

ANALYSIS

3.1 THERMAL EFFECT IN BUILDINGS

As stated earlier, the thermal effect in buildings has a close physical similarity with the stack effect in the natural draft chimney. The natural draft force produced in the chimney is well known to be dependent upon the temperature differences between the flue gas and the air outside, as well as on the height of the chimney.

In the heating season, a similar action takes place in the building, even though the temperature difference of the air between inside and outside is much less than that of the chimney.

The thermal effect occurring in the building can be illustrated by the aid of the graphical representations for different types of buildings, as shown in Figs.3.1.1 to 3.1.6.

In Fig.3.1.1, a heated building which has no internal floor separations and uniform temperature distributions with height, is presented. The building in the figure is shown to have a single opening at the bottom level only. The distributions of the pressure both inside and outside with height are shown in the figure.

In this particular case, the maximum value of the pressure difference due to the thermal effect occurs at the top level, as shown in the figure, and the profile of

pressure differentials with height is expected to be governed by the bottom opening.

Since steady and uniform distributions of temperatures are assumed for both sides of the building, in the absence of wind and mechanical ventilation, the pressure of the inside and outside of air should be equal at the level of the bottom opening.

As can be seen in the figure, the pressures both inside and outside of the building are shown to decrease with elevation because of the reduction of air column weight acting above.

The figure also indicates that since the air outside is more dense than that inside, the variation of the pressure with the height outside is more rapid than that of the inside. Therefore, the pressure within the building is higher than that at the outside at all levels above the opening.

The example shown in Fig.3.1.1 can also have a similarity with an extreme case of a building with sufficiently larger single opening at the bottom than others.

Fig.3.1.2 illustrates another example, showing the reverse case of Fig.3.1.1. In this building, the single opening is placed at the top level of the building.

As a result, the pressure of both inside and outside of the building would be equal at the top level, and the pressure of the air inside is expected to be less than that

at the outside at all lower level. Hence, the maximum pressure difference due to the thermal effect would act at the bottom level as shown in the figure.

In actual buildings the openings through which air may infiltrate or exfiltrate are distributed in the exterior wall of the building at various vertical elevations.

Fig.3.1.3 illustrates an example of an idealized heated building with no internal floor separations, having openings of equal size and shape in the exterior wall at the top and bottom level only. Since the air within the building is lighter than that at the outside due to heating, it tends to rise upward and escape through the top opening, whereas the colder air outside flows into the bottom opening to displace it.

In addition, since the openings at the top and bottom are of equal size and shape, the resistance to flow imposed by the openings is expected to be the same at both openings. Consequently, the distributions of the pressure differences due to the thermal effect at both openings would be of equal in magnitude.

As shown in the figure, the lines representing the pressures are shown to cross at the mid-height of the building at the point where there is no pressure difference across the exterior wall.

This level, where the inside and outside pressures of the building is identical, is called "the neutral pressure level (NPL)". Therefore, in the example shown in Fig.3.1.1,

the neutral pressure level is placed at the bottom opening level. Conversely, as in the case shown in Fig.3.1.2, the neutral pressure level exists at the top opening level.

In the figures, it may be noted that the pressure difference across the exterior wall is shown to increase in proportion to the distance from the neutral pressure level. From a theoretical point of view, as shown in Eq.1.1, the difference in the slopes of the lines representing inside and outside pressure is expected to increase as the temperature difference between inside and outside increases. Therefore, the pressure differences across the exterior wall would increase correspondingly.

If the opening at the bottom level, as shown in the figure, is larger than than that at the top, imposing less resistance to flow, the pressure difference across the opening at the bottom would be less than that across the opening at the top. The opposite case would occur if the opening at the top level is larger than that of the bottom. This alteration of the resistance to flow in the openings result in a shift of the inside pressure line and the location of the neutral pressure level in the building.

Suppose a building with a very large single opening at the top or bottom with respect to the other openings at different level. In this case, the resulting profile of the pressure difference across the exterior wall would be the same as shown in Fig.3.1.1 or Fig.3.1.2, correspondingly.

The characteristics of the thermal effect for the simple case presented in Fig.3.1.3 have been investigated both experimentally and analytically [10]. The study has shown that the behavior of the thermal effect in this type of building depends upon significantly the characteristics of the exterior openings.

Fig.3.1.4 illustrates another variation of the case which was shown in Fig.3.1.3. In this case exterior openings of equal size and shape are distributed with elevation in the exterior wall.

In this case, the line representing the pressure of the air inside within the building may be somewhat different from the case which is shown in Fig.3.1.3, depending on the distributed patterns of the exterior wall openings. If the resistance to flow imposed by each opening is exactly same, the neutral pressure level is expected to be located at the mid-height of the building.

If the distributed pattern of the exterior wall openings along the height is non-uniform, on the other hand, the lines representing the air pressure inside and outside would cross somewhere between the bottom and top opening level.

In this case, as has been shown in figure, the air outside would infiltrate through the openings below the NPL and the air inside would exfiltrate through the openings above the NPL.

Fig.3.1.5 represents a hypothetical building with completely air-tight floor separations at each floor level, and openings of equal size and shape in the exterior wall of each story, at the top and bottom. Thus, it can be assumed that there can be no upward flow of air between floor separations.

Since there is no air flow through the floor separations in this case, each floor level may act independently, and the thermal effect in each story is expected to be unaffected by that of another level. It can also be seen that there would be an inflow at the bottom opening and an outflow at the top opening of each floor, since each floor has its own particular NPL.

In theory, the sum of the pressure differences across the floor levels, plus the pressure difference across the exterior walls at the top and bottom of the building should be equivalent to the total thermal effect for the total building height which has been presented in Fig.3.1.1 or Fig.3.1.2.

In practice, the high-rise or multi-story buildings are not completely open inside, as has been shown in Fig.3.1.4, nor are the floor separations between floors completely air tight, as illustrated in Fig.3.1.5. It is well known that there are various passages for the air to flow through the floor separations in the actual buildings. The interconnections providing the air flow paths between floors usually consist of the stairwells, elevator and various

service shafts that extend through the floors.

A typical example of the case described above is illustrated in Fig.3.1.6, which represents a heated building with uniform distribution of the openings in the exterior wall and floor separations.

The general pattern of the air flow induced by thermal effect is expected to be the same as that presented in Fig.3.1.4. The air infiltrates into the building at the bottom, flows upwards through the openings in the floor separations, and exfiltrates through the exterior wall openings in the upper level.

Since steady and uniform distribution of the temperature with height in both inside and outside are assumed, the slope of the line representing the inside pressure would be the same as shown in Fig.3.1.4 or Fig.3.1.3. However, there may be a discontinuity of the inside pressure line at each floor due to the resistance to flow within the building, contributed by the floor separations as illustrated in the figure.

In the analysis of the thermal effect in the building, it is necessary to consider the effect of the resulting flow due to the pressure difference on the building environment.

The flow occurring within the building may cause a variation in the heating load from floor to floor, and therefore would have some implications for the distributions of the air temperature inside with elevations.

With regard to the distribution of the pressure differentials due to the thermal effect in the buildings, as demonstrated before, there could be two extrema: the open type buildings which have negligibly small resistance to flow within the building as shown in Fig.3.1.4, and the story type buildings which have air tightness between floors as illustrated in Fig.3.1.6.

This implies that one can represent the building relative to the value of the resistance to flow or to the permeability of the building components separating floors.

The permeabilty to air can be described as the property of a building component to let air pass when it is subject to pressure difference, which is another representation of the resistance to flow, exerted by a building component.

In a building with an open type construction, which is the case shown in Fig.3.1.4, the influence of thermal effect on air infiltration would be substantial. On the other hand, in the story type building, which is the case shown in Fig.3.1.6, there are small buoyancy effects only within every floor due to discontinued floor permeability, and consequently the air infiltration due to thermal effect is small. Thus, it is advantageous to have air-tight floor partitions to minimize air infiltration.

3.2 THERMAL EFFECT EQUATIONS

3.2.1 General Description

We may choose a differential element of mass of air, dm, with sides dx, dy, and dz as shown in Fig.3.2.1. The element of air in the column shown in the figure can be considered as stationary relative to the stationary coordinate system presented in Fig.3.2.1. From simple force equilibrium in the differential element, we understand that the only two components of forces may be applied on it. These forces are: body force and surface force. The only body force that must be considered in this problem is due to gravity.

For the differential air element, the body force, dF_B, is

$$dF_B = g\ dm = g \rho\ dV \qquad (3.2.1)$$

where g is local gravity, is the density of air, and dV is the volume of the element. In the coordinate system shown, dV = dx dy dz, so

$$dF_B = \rho\ g\ dx\ dy\ dz \qquad (3.2.2)$$

Since the air in the column is assumed to be static, no shear stresses can be present. Thus the only surface force is the pressure force.

Let the pressure at the center, O, of the element be P. To determine the pressure force at the faces of the element in the direction considered, we may use a Taylor series expansion of the pressure about O. By using this representation, the pressure at bottom face of the element is

$$P_{bottom} = P - \frac{dp}{dz}\frac{dz}{2} \tag{3.2.3}$$

The pressure on the upper face of the element is

$$P_{up} = P + \frac{dp}{dz}\frac{dz}{2} \tag{3.2.4}$$

Combining all such forces gives the net surface force acting on the element. Thus,

$$dF_s = \left(P - \frac{dp}{dz}\frac{dz}{2} \right) dx\, dy - \left(P + \frac{dp}{dz}\frac{dz}{2} \right) dx\, dy \tag{3.2.5}$$

Collecting and canceling the terms, we obtain

$$dF_s = \left(- \frac{dp}{dz} \right) dx\, dy\, dz \tag{3.2.6}$$

Since no other kinds of force may be present in the present model, it is allowed to combine surface and body forces that we have developed to obtain the total force acting on the air element. Therefore, we have

$$dF = dF_s + dF_B$$

$$= \left(- \frac{dp}{dz} + \rho g \right) dx\, dy\, dz \qquad (3.2.7)$$

or on a unit volume basis

$$\frac{dF}{dx\, dy\, dz} = - \frac{dp}{dz} + \rho g \qquad (3.2.8)$$

Since we are dealing with the static element of air, it becomes

$$\frac{dF}{dV} = a \rho = 0 \qquad (3.2.9)$$

where a is acceleration of the element.

Substituting for dF/dV from Eq.3.2.8, we obtain

$$- \frac{dP}{dz} + \rho g = 0 \qquad (3.2.10)$$

This equation is the basic pressure-height relation of static fluid. This equation also indicates that it has been formulated on the assumption that the pressure is independent of the coordinates, x and y, and it only is

dependent upon z. To determine the pressure distribution in the static air field, Eq.3.2.10 may be integrated with the appropriate boundary conditions applied.

3.2.2 Thermal Effect Equation with Uniform Temperature Distributions in Vertical Elevations

In order to determine the pressure from Eq.3.2.10, as stated earlier, the variation of the density of fluid, ρ and the gravity force, g, must be known as function of elevation.

It has been shown that the pressure variation in the static air column can be described by the basic pressure-height relation of the static fluid;

$$\frac{dP}{dz} = -\rho g \qquad (3.2.11)$$

The air can be taken as an ideal gas and have the ideal gas equation of state is;

$$P = \rho R T \qquad (3.2.12)$$

where R is the gas constant and T the absolute temperature.

In a particular situation, in which the variation of the air temperature with elevation of the building is minimal, it may be assumed that the distribution of the air temperature is uniform with height.

Hence, with this idealization that the temperature distribution of the inside and outside of the building is constant, and uniform with height, we have that $T_o(z) = T_i(z) = \text{constant}$.

Using these assumptions, Eq.3.2.12 becomes

$$\frac{dP}{dz} = -\rho g = \text{constant} \qquad (3.2.13)$$

With the simplification through the substitution of Eq.3.2.12 into Eq.3.2.13 and with its rearrangement, the following is obtained:

$$\frac{dP}{P} = -\frac{g}{RT}\,dz \qquad (3.2.14)$$

To determine the distributions of the pressure, Eq.3.2.14 should be integrated by applying the appropriate boundary conditions.

If the pressure at the reference level, z_o, is designated as P_r, then the pressure, P, at the elevation z is found by the integration of Eq.3.2.14 as:

$$\text{Ln}\left(\frac{P}{P_r}\right) = -\left(\frac{g}{R\,T}\right)(z - z_r) \qquad (3.2.15)$$

Therefore, the pressure variations with the elevation of the air within the building would be

$$P_i = (P_r)_i \exp\left[-\frac{g}{RT_i}(z-z_r)\right] \qquad (3.2.16)$$

where the subscript i is the air inside.

Since the thermal effect is defined as the pressure differentials across the exterior wall of building, the pressure difference between inside and outside at the difference of the elevation from the reference level, $(z-z_r)$, would be

$$\Delta P(z-z_r) = P_o(z-z_r) - P_i(z-z_r) \qquad (3.2.17)$$

By substitution of Eq.3.2.16 into Eq.3.2.17, we have the following;

$$\Delta P(z-z_r) = (P_r)_o \exp\left[-\frac{g}{RT_o}(z-z_r)\right] - (P_r)_i \exp\left[-\frac{g}{RT_i}(z-z_r)\right] \qquad (3.2.18)$$

In order to determine the pressure differential from Eq.3.2.18, we may assume that there exists a particular

elevation where the pressure difference between inside and outside of the building becomes zero owing to the different pressure gradient of the air at both sides. This level was defined as the neutral pressure level.

With the application of the assumption, and taking the neutral pressure level as the reference level, we obtain

$$(\Delta P_{th}) = (P_o)_n \left\{ \exp\left[-\frac{g}{RT_o}(z_n - z)\right] - \exp\left[-\frac{g}{RT_i}(z_n - z)\right] \right\} \quad (3.2.19)$$

where subscripts, th and n, refer to the pressure difference induced by thermal effect, and the neutral pressure level, respectively.

For the determination of the pressure difference due to the thermal effect in a more simplified manner, we may use a series method for the exponential terms in Eq.3.2.19. Neglecting the higher order terms, we have

$$(\Delta P) = K' \left(\frac{1}{T_o} - \frac{1}{T_i} \right)(z_n - z) \quad (3.2.20)$$

where $K' = P_o g/R$

The equation presented above, Eq.3.2.20, is the basic thermal effect equation which relates the pressure difference across the exterior wall to the temperature difference between the air inside and outside, and the building height. This is also applicable for the case having uniform temperature distributions along elevationboth inside and outside.

3.2.3 Thermal Effect Equation with Non-Uniform Temperature Distributions with Building Elevations

As presented previously, information on the temperature distribution is required to determine the pressure difference across the exterior wall. As a result, a temperature profile within building with height must be assumed to determine the distribution of the pressure differences considering a non-uniform temperature distribution of the air inside.

In order to obtain the pressure difference under these temperature conditions within the building, it will be assumed that the temperature distribution of the air within the building depends upon elevation only, and is a linear distribution with height as follows:

$$T_i(z) = T_i(z_r) \pm b_i z$$

where b_i is temperature gradient of the inside ($^{\circ}C/m$).

Substituting the one above into Eq.3.2.14, the pressure distribution within the building can be expressed as

$$\frac{dP}{P} = -\frac{g}{R}\frac{dz}{[T_i(z_r) \pm b_i z]} \qquad (3.2.21)$$

If the pressure at the reference level, z_r, is denoted as P_r, then the inside pressure, P_i, at elevation z is found by integration of Eq.3.2.21:

$$\text{Ln}\left[\frac{P(z-z_r)}{P(z_r)}\right]_{in} = \mp \frac{g}{b_i R}\,\text{Ln}\left[\frac{T_i(z_r) \pm b_i(z-z_r)}{T_i(z_r)}\right] \qquad (3.2.22)$$

where the subscript, in, refers to the inside of the building.

Hence, the pressure difference between inside and outside the building at a certain level can be written as follows:

$$\Delta P(z-z_r) = P_o(z_r)\exp\left[-\frac{g}{RT_o}(z-z_r)\right] - P_i(z_r)\left[\frac{T_i(z_r) \pm b_i(z-z_r)}{T_i(z_r)}\right]^{\mp \frac{g}{b_i R}} \qquad (3.2.23)$$

With the assumption that the pressure difference between inside and outside at the neutral pressure level is nil and taking the level as the reference elevation, the following equation is obtained:

$$(\Delta P)_{th} = P_o(z_n)\exp\left[-\frac{gz}{RT_o}\right]\left\{1 - \exp\left[-\frac{gz_n}{RT_o}\right]\left[\frac{T_i(z_o)\pm b_i z}{T_i(z_o)\pm b_i z_n}\right]^{\mp \frac{g}{b_i R}}\right\} \qquad (3.2.24)$$

where z_o denotes the bottom opening level.

The equation, Eq.3.2.24, is the thermal effect equation, which determines the pressure differentials across the exterior wall at the given level due to the thermal

effect, under a non-uniform distribution of the air temperature inside alone.

To apply this equation for the case with a negative slope of the air temperature inside, the sign of the temperature slope, b, correspondingly will be altered.

As shown in the derivations, it is subjected to the restrictions that the temperature distribution of the air inside depends on the vertical direction only and has a linear form of distribution with elevations. From Eq.3.2.24 we can see that for the calculation of the pressure differential in this case, it is required to have the information on the neutral pressure level and the gradient of the air temperature inside.

Thus far, as has been demonstrated in the derivation of Eq.3.2.24, we have only taken into account the effect of the non-uniform distributions of the air temperature inside on the pressure difference due to thermal effect in the building.

However, in practical situations, it can be expected that both the air temperature inside and outside may vary with the elevations. To determine the pressure differentials due to the thermal effect considering these temperature variation both inside and outside, the same assumptions are applied in the derivation of Eq.3.2.24 will be applied for the outside air and inside air. Hence, the temperature of the air outside is;

$$T_o = T_o(z_r) \pm b_o z \qquad (3.2.25)$$

where the subscript o denotes the outside.

Substituting Eq.3.2.25 into Eq.3.2.14, and taking the same procedures used in the derivation of Eq.3.2.24, the following is obtained:

$$\Delta P(z) = P_o(z_n) \left[\frac{T_o(z_o) \pm b_o z}{T_o(z_o)} \right]^{\mp \frac{g}{b_o R}} - \left[\frac{T_o(z_o) \pm b_o z_n}{T_o(z_o)} \right]^{\mp \frac{g}{b_o R}} \left[\frac{T_i(z_o) \pm b_i z}{T_i(z_o) \pm b_i z_n} \right]^{\mp \frac{g}{b_i R}} \qquad (3.2.26)$$

This is the basic equation for the thermal effect to determine the pressure differential due to thermal effect considering a linear temperature distributions of the air inside and outside with the elevations in the building. As shown in the equation, the temperature gradient of the air inside and outside and the neutral pressure level should be given in order to evaluate the pressure differentials with the elevations of the building. Also the equation is subjected to the restrictions were applied in its derivations.

3.3 ANALYTICAL MODEL FOR THERMAL EFFECT ANALYSIS

3.3.1 Model without considering Effect of Internal Floor Partitions

It is expected that the profile and distribution of the pressure differentials induced by the thermal effect in high-rise building may depend upon factors related to the constructions, the design, and the environment of the building involved, such as the distributed pattern of the exterior wall opening holes, the types of floor separations, and the temperatures.

In the building with a relatively loose air tightness between floor separations, the flow resistance within the building will be shown to be negligible, causing no pressure difference across the floor partitions provided.

As a result, it is possible to consider that the pattern and the distribution of the pressure differentials produced by the thermal effect will be governed mainly by the conditions and designs of the exterior openings existing in the wall.

On the other hand, in the building with air tight floor separations, the distributions of the pressure differentials induced by thermal effect may be the result of the interaction between the exterior wall openings, and the floor openings provided.

For the solution of the problems outlined above, the case of a particular type of building with negligible resistance to flow inside, having sufficient

interconnections of air flow between floors, will be regarded in the analysis first.

The schematic diagram of the analytical model for this type of building is presented in Fig.3.3.1, in which only the exterior wall openings are distributed along the elevations of the building. In the model, the opening holes associated with cracks or crevices in the exterior enclosures contributed by the doors and the windows, are represented by the equivalent orifice opening area of the exterior wall (A_w).

For the analysis of the thermal effect in this type of building, the following major assumptions would be introduced:

(1) The air temperature inside the building is higher than that of the air outside with elevations.

(2) The conditions of the flow field at the opening hole involved are steady, laminar and hydrodynamically smooth.

(3) There is no wind or mechanical ventilation acting on the building.

From these assumptions, the pressure difference across the exterior enclosures of the building will be solely due to the temperature differences between inside and outside. Hence, it is expected that the resulting pressure differences induce an air flow field at the openings, existing on the exterior enclosures as represented in Fig.3.3.1.

The pressure differentials induced by thermal effect resulting in these air flows in the building may be represented by the steady flow energy equation for the flow at the corresponding opening hole involved, which is an expression of the conservation of energy.

Applying the assumptions made above and the energy balance relation, the pressure difference across an opening hole in the enclosure can be represented as follows:

$$(\Delta P)_k = (\Delta P_{loss})_k \qquad (3.3.1)$$

where subscript k refers to the position of the opening considered, ΔP_{loss} denote all the pressure losses occurred in the flow path, respectively.

The term associated with the pressure loss, shown in the left side of Eq.3.3.1, at the flow through the opening hole consists of the pressure loss contributed by the friction loss due to the inner surface of the opening, the form losses at the entrance and exit, due to abrupt alterations of the flow area at the opening considered. Hence, we have

$$(\Delta P)_k = (\Delta P_{fl} + \Delta P_{fr})_k \qquad (3.3.2)$$

where subscripts, fl and fr refer to form losses and friction losses, respectively.

Also applying the respective definitions described above, the pressure losses can be represented as

$$(\Delta P_{fl})_k = [(K_c + K_{ext}) \frac{1}{2} \rho v^2]_k \qquad (3.3.3)$$

and

$$(\Delta P_{fr})_k = f \frac{L}{D} \frac{1}{2} \rho v^2 \qquad (3.3.4)$$

With the application of the assumption that the induced air flow at the opening holes is steady and smooth in transition, the friction coefficient, f, shown in Eq.3.3.4 may be represented as

$$f = \frac{\overline{C}}{Re_d} \qquad (3.3.5)$$

where

$$\overline{C} = \frac{\int_0^L C_x \, dx}{\int_0^L dx} \qquad (3.3.6)$$

and

$$C_\infty = 64 \qquad (3.3.7)$$

With the substitution of Eqs.3.3.3 to Eq.3.3.5 into the basic equation, Eq.3.3.2, and by rearranging, the pressure difference across the opening hole due to the induced flow is given as

$$(\Delta P)_k = \frac{1}{2} \rho V^2 [\ \Sigma K_{fl} + f \frac{L}{D}\ ]_k \qquad (3.3.8)$$

where ΣK_{fl} is the summation of the form loss factors at the opening involved such as K_{ext}, K_c, and K_{re}.

If the configuration of the crack or crevices of the opening is assumed to be a thin rectangular type, in which spacing y is very small as shown in Fig.3.3.2, then the flow can be treated as that between parallel plates and the equivalent diameter of the crack hole, De, would be $D_e = 2y$, where y is the spacing between plates.

Hence, the friction factor in Eq.3.3.4, assuming fully developed laminar, for this particular case will be:

$$f = 4 \left(\frac{16}{\phi\ Re_{De}} \right) \qquad (3.3.9)$$

where

$$D_e = \frac{2(y_1 y_2)}{(y_1 + y_2)} \qquad (3.3.10)$$

and ϕ may be given by Fig.3.3.3 [27].

From the physical considerations of the flow induced by the thermal effect, the flow of air below the neutral pressure level is inward. Thus, taking the pressure differentials resulting in an inward flow into the building as the negative pressure difference, the energy equation, Eq.3.3.8, can be represented as

$$(\Delta P)_k = \pm \frac{1}{2} [\rho V^2 (\Sigma K_{fl}) + \bar{C} V \frac{\mu L}{D^2}]_k \qquad (3.3.11)$$

Hence, applying Eq.3.3.11 for the present model represented in Fig.3.3.1, the pressure differentials across the opening holes are given as follows:

For openings placed below the NPL

$$(\Delta P)_m = \frac{1}{2} [\rho_a V_a^2 (K_c + K_{ext}) + \rho_b V_b^2 (K_{re}) + \bar{C}_a V_a (\frac{\mu L}{D^2})_a + \bar{C}_b V_b (\frac{\mu L}{D^2})_b] \qquad (3.3.12)$$

And for openings placed above the NPL

$$(\Delta P)_n = - \frac{1}{2} [\rho_a V_a^2 (K_c + K_{ext}) + \rho_b V_b^2 (K_e) + \bar{C}_a V_a (\frac{\mu L}{D^2})_a + \bar{C}_b V_b (\frac{\mu L}{D^2})_b] \qquad (3.3.13)$$

where subscripts, m and n denote the position of openings placed below and above the NPL, respectively.

For the solution of the problems in the present model, in addition to the energy equation presented, we can formulate a relation of the mass conservation in the induced flow field in the model.

From the physical considerations in the model, the amount of the inflow of air into the system due to thermal effect, should be equal to that of the outflow from the system. Thus, the mass balance in the building can be written as:

$$\sum_{i=1}^{M}(\rho V A)_{in} = \sum_{j=1}^{N}(\rho V A)_{out} \qquad (3.3.14)$$

where M and N are the summation of the opening number existing below and above the NPL, respectively.

In order to formulate the analytical model to obtain a numerical solution for the present model, the corresponding number of energy equations of Eq.3.3.8 can be set for the exterior openings in the building shown in the figure. In addition, the continuity equation, Eq.3.3.14, can be made for the system, corresponding to the number of the exterior openings provided.

For the purpose of formulating the analytical model in the building, it is required to rearrange the pressure terms shown in the left hand side of Eq.3.3.8 appropriately through manipulations, using the energy balance relations between the openings to be interrelated.

Since the pressure terms representing the inside and outside pressure at the given elevations of the openings can be interrelated between the opening positions by the energy conservation corresponding to the difference of elevations, the computational model to calculate the pressure differentials due to thermal effect finally, is reduced to the set of non-linear equations, having the corresponding number of unknowns of the openings involved in the induced flow by thermal effect in the building.

3.3.2 Model considering Effect of Floor Partitions

As we know, in practice multi-story or high-rise buildings are neither open in the inside nor airtight between floor separations.

For the purpose of obtaining more realistic solutions of the thermal effect in buildings, the presence of the floor separations within the building as well as their interactions with the openings existing in the exterior enclosures should be taken into account.

As a result, it will be expected that the patterns of distribution of the pressure differentials induced by the thermal effect in this situation will show differences to the profile of the pressure differentials compared to that for the case discussed in Section 3.3.2.

Intuitively, for a building having considerable air-tightness between floors, there can be minimal air flow between floor partitions, so that each floor may act independently and the thermal effect induced may not be influenced by others.

On the other hand, for buildings with plenty of interconnections between floor separations, the resultant thermal effect may be influenced by other floors owing to the upward movement of the air inside resulting from reduced resistance to flow within the building.

For the correct estimation of the pressure differentials of this case, a complete understandings about the characteristics and behavior of the thermal effect in this type of building, is strongly required.

The schematic diagram of the analytical model of the building with internal floor separations is illustrated in Fig.3.3.4. In the figure, it shows that for this type of model the openings in the floor separations as well as the openings in the exterior wall are distributed with elevations.

In the analytical model, the opening holes associated with cracks or crevices in the floor separation, which are formed by the elevator doors, stairwells, and various service shafts, are lumped together and represented by an equivalent orifice opening hole in the floor separation (A_p). Conversely, the cracks or crevices formed by the window and doors, existing at the exterior wall per unit

floor level, are represented by the equivalent exterior orifice opening of the wall (A_w).

In the model, the exterior wall openings at each floor are made to be placed at the top and bottom of each floor, and the opening in the floor separation is made at the the floor partition of each floor, as presented in the figure.

In order to formulate the analytical model, the major assumptions to be applied in this type of building would be the same as that of the case which has been discussed in Section 3.2.

Additional assumptions to be made for this case are, that the air flow within building is upward and steady, and that the resistance to flow imposed by the floor separation is not negligible.

With the application of the assumptions described above, the pressure differentials across the openings can be presented from the energy balance relations as follows:

For the openings placed at the exterior wall

$$(\Delta P)_k = (\Delta P_{fl} + \Delta P_{fr})_k \qquad (3.3.15)$$

where the subscript, k, denotes the position of exterior openings at the wall.

For the openings existing at the floor separations

$$(\Delta P)_p = (\Delta P_{fl} + \Delta P_{fr}) \qquad (3.3.16)$$

where subscript, p, refers to the position of the floor separation.

With the application of the basic assumptions made above, the energy equations representing the pressure differences across the opening holes for the present model, can be presented as follows, taking the pressure difference inducing inward flow into building as the negative quantity:

For the exterior openings

$$(\Delta P)_k = \pm \frac{1}{2} [\rho V^2 (\Sigma K_{fl}) + \bar{C} V (\frac{\mu L}{D^2})]_k \qquad (3.3.17)$$

For the openings existing at the floor partitions

$$(\Delta P)_p = \frac{1}{2} [\rho V^2 (\Sigma K_{fl}) + \bar{C} V (\frac{\mu L}{D^2})]_p \qquad (3.3.18)$$

where subscript, p, denotes the position of the floor partition in the building.

In addition to the formulation of the energy equations showing the pressure differences across the openings involved, the mass balance relationship in the flow system in the building induced by thermal effect can be made.

Since the total inflow into the building should be balanced with the total outflow from it, the mass conservation in the model as a whole, can be represented as follows:

$$\sum_{i=1}^{M} (\rho V A)_{in} = \sum_{j=1}^{N} (\rho V A)_{out} \qquad (3.3.19)$$

where M and N are the total numbers of the exterior openings undergoing an inward and outward flow in the building respectively.

As presented earlier, the number of the energy equations showing the pressure difference across the openings and the mass conservation equations to be formulated depend upon the corresponding number of the openings in the building involved in the air flow caused by thermal force, including the openings in the floor partitions, for the solution of the problem.

For the purpose of processing the analytical model formulated from mass and energy balance in the building for the computational work in order to determine the pressure difference across the openings, it is required to rearrange the pressure terms shown in the left hand side of each energy equation to be interrelated with the one in the other equations.

Since the terms representing the inside and outside pressure at the given elevations can be interrelated with another from the relation of energy balance between the

openings, the analytical model is finally transformed into a set of non-linear equations, having the same number of unknown of flow velocities.

In this computational model, consequently, the number of equations of energy and mass balance is increased more than that of the previous case with no floor partitions. Hence, the process of the computational works to be done can be more complicated and difficult than that of the previous model.

3.4 NEUTRAL PRESSURE LEVEL

As shown in the derivations of the thermal effect equations in Section 3.2, the distribution of pressure differentials across the exterior wall due to the thermal effect are shown to be increased with distances from the neutral pressure level.

As discussed in the derivations of the thermal effect equations, the neutral pressure level is very important information in the calculation of the pressure differentials induced by the thermal effect in the buildings. It is shown that if the neutral pressure level is given, the pressure difference can be determined from the thermal effect equation for various cases.

The method of finding the neutral pressure level can be obtained from the analytical model developed in Section 3.3. By interrelating the steady flow energy equations with the thermal effect equation at the corresponding opening, the

neutral pressure-level can be calculated.

First, the case with a uniform temperature distribution with elevation will be considered. From the logical point of view, if the thermal effect equation, Eq.3.2.20, has a validity for these cases, the pressure difference across the opening to be considered should be identical with that of the pressure differential obtained from the analytical model described in Section 3.3.

Applying this physical condition to an opening existing on the exterior wall, we may proceed as follows:

For any opening below the NPL, the pressure difference across the opening can be given from the energy equation:

$$(\Delta P)_i = (P_{out} - P_{in})_i$$

$$= -\frac{1}{2} [\rho V^2 (\Sigma K_{fl}) + \bar{C} V (\frac{\mu L}{D^2})]_i \qquad (3.4.1)$$

where the subscript i denotes the position of the opening below NPL in the exterior wall.

For any opening above the NPL, the energy equation is as follows:

$$(\Delta \bar{P})_j = (P_{out} - P_{in})_j$$

$$= \frac{1}{2} [\rho V^2 (\Sigma K_{fl}) + \bar{C} V (\frac{\mu L}{D^2})]_j \qquad (3.4.2)$$

where subscript, j, refers to the opening position above the NPL, in the exterior wall.

If we let

$$X = \frac{1}{2}\left[\rho V^2\left(\Sigma K_{fl}\right) + \bar{C}\, V\left(\frac{\mu L}{D^2}\right)\right] \tag{3.4.3}$$

Then,

$$(\Delta P)_i = X_i$$

$$(\Delta P)_j = -X_j \tag{3.4.4}$$

From the thermal effect equation, Eq.3.2.20, the pressure differentials across the openings induced by thermal effect are given as follows:

$$(\Delta P)_i = \frac{(P_o)_n\, g}{R}\left(\frac{1}{T_o} - \frac{1}{T_i}\right)(z_n - z_i) \tag{3.4.5}$$

$$(\Delta P)_j = \frac{(P_o)_n\, g}{R}\left(\frac{1}{T_o} - \frac{1}{T_o}\right)(z_n - z_j) \tag{3.4.6}$$

where z_i and z_j refer to the opening level existing below and above the NPL, respectively.

If we let

$$A' = \frac{(P_o)_n g}{R}\left(\frac{1}{T_o} - \frac{1}{T_i}\right) \tag{3.4.7}$$

Then,

$$(\Delta P)_i = A'(z_n - z_i) \qquad (3.4.8)$$
$$(\Delta P)_j = A'(z_n - z_j)$$

Equating Eq.3.4.4 with Eq.3.4.8, and simplifying by collecting terms, the following is obtained:

$$z_n = \frac{z_j + (X_j/X_i)\, z_i}{1 + (X_j/X_i)} \qquad (3.4.9)$$

The equation above, that is, Eq.3.4.9, is the generalized solution for determining the neutral pressure level of the case with a uniform temperature distribution of the air inside and outside with elevations. As has been shown in the derivations, it is subject to the restriction that the pressure differentials due to the thermal effect can be predicted by the thermal effect equation, Eq.3.2.20.

From Eq.3.4.9, the value of the neutral pressure level can be obtained. As can be seen in the equation, the NPL is shown to have a close relationship with the resistance to flow at the openings, which is represented in terms of X_i and X_j. Hence, it is obvious that the neutral pressure level depends upon the characteristics of the opening in the building enclosures, as expected.

If we consider a simple case with the exterior openings at top and bottom level only, then, it becomes that in Eq.3.4.9 $z_i=0$ and $z_j=H$. Denoting 1 and 2 as the opening

positions at the top and bottom levels of the building, respectively, we have

$$z_n = \frac{H}{1 + (X_2/X_1)} \tag{3.4.10}$$

where

$$X_1 = \frac{1}{2}\left[\rho V^2(\Sigma K_{f1}) + \bar{C}\, V(\frac{\mu L}{D^2})\right]_1$$

$$X_2 = \frac{1}{2}\left[\rho V^2 (\Sigma K_{f1}) + \bar{C}\, V(\frac{\mu L}{D^2})\right]_2$$

For an ideal case, particularly, in which the flow resistance to flow in the openings is neglected, Eq.3.4.10 simply becomes as:

$$z_n = \frac{H}{1 + (\frac{A_1}{A_2})^2(\frac{T_i}{T_o})} \tag{3.4.11}$$

The equation above, Eq.3.4.11, as shown in the derivations, is applicable only in the particular case with openings at the top and bottom level only, in the building having a uniform temperature distributions and a negligible resistance to the flow in the openings involved. Thus, it is to be applied only where these restrictions can be satisfied for the physical situations.

In addition, it is interesting to note that Eq.3.4.11 is identical with the expression on the NPL which is recommended by ASHRAE [9] for the present case. Hence, it

can be deduced that the method provided by ASHRAE [9] is only applicable for the simple and idealized cases, in which the resistance to flow imposed by openings is neglected.

As described in the derivations of the thermal equations, Eq.3.2.24 and Eq.3.2.26, one can consider the cases with a non-uniform distribution of the temperatures with elevations in the buildings.

In these particular cases, the solution for the neutral pressure level also can be found by applying the same procedures taken in the development of Eq.3.4.9.

As an example of the process, consider the case with a non-uniform temperature distribution of the air inside only, in which the variation of temperature with respect to elevation is $T_i(z)=T_i(z_o)\pm b_i z$.

Interrelating the energy equation, Eq.3.4.4, into the thermal effect equation for this case, Eq.3.2.24, at the corresponding openings, the following is obtained:

For any opening below the NPL

$$X_i=P_o(z_n)\exp[\mp\frac{gz_i}{RT_o}]\left\{1-\exp[\mp\frac{gz_n}{RT_o}][\frac{T_i(z_o)\pm b_i z_i}{T_i(z_o)\pm b_i z_n}]^{\mp\frac{g}{b_i R}}\right\} \qquad (3.4.12)$$

For any opening above the NPL

$$X_j=-P_o(z_o)\exp[\mp\frac{gz_i}{RT_o}]\left\{1-\exp[\mp\frac{gz_n}{RT_o}][\frac{T_i(z_o)\pm b_i z_i}{T_i(z_o)\pm b_i z_n}]^{\mp\frac{g}{b_i R}}\right\} \qquad (3.4.13)$$

Collecting and simplifying the terms, the following is obtained:

$$\frac{X_j}{X_i}\exp\left[\mp\frac{g}{RT_o}(z_j-z_i)\right]+\frac{\left\{1-\exp\left[\mp\frac{gz_n}{RT_o}\right]\left[\frac{T_i(z_o)\pm b_i z_j}{T_i(z_o)\pm b_i z_n}\right]^{\mp\frac{g}{b_i R}}\right\}}{\left\{1-\exp\left[\mp\frac{gz_n}{RT_o}\right]\left[\frac{T_i(z_o)\pm b_i z_i}{T_i(z_o)\pm b_i z_n}\right]^{\mp\frac{g}{b_i R}}\right\}} \qquad (3.4.14)$$

This is the NPL equation for the case with a non-uniform temperature distribution of the air inside only with height. This equation is subject to restrictions, that Eq.3.2.24 can be valid, and that the air inside only has a linear variation of temperature with height.

As illustrated in Eq.3.4.14, the final expression for the neutral pressure level is shown as not being as simple as that of the case with a uniform distribution of the temperature. To determine the NPL, as shown in Eq.3.4.14, an iterative method is required, assuming an appropriate initial value corresponding to the given physical conditions as expected from the solution.

In this case, it can be seen that the neutral pressure level depends upon the characteristics of the openings as well as the temperature distribution of the air inside.

Additionally, another different case can be considered with a non-uniform temperature distributions of the air inside and outside with elevations. Applying the identical procedures used in the derivations in Eq.3.4.14, the following is obtained:

For the openings below the NPL

$$X_i = P_o(z_n) \left[\frac{T_o(z_o) \pm b_o z_i}{T_o(z_o)}\right]^{\mp \frac{g}{b_o R}} - \left[\frac{T_o(z_o) \pm b_o z_n}{T_o(z_o)}\right]^{\mp \frac{g}{b_o R}} \left[\frac{T_o(z_o) \pm b_i z_i}{T_i(z_o) \pm b_i z_n}\right]^{\mp \frac{g}{b_i R}} \tag{3.4.15}$$

For the openings above the NPL

$$X_i = -P_o(z_n) \left\{\left[\frac{T_o(z_o) \pm b_o z_i}{T_o(z_o)}\right]^{\mp \frac{g}{b_o R}} - \left[\frac{T_o(z_o) \pm b_o z_n}{T_o(z_o)}\right]^{\mp \frac{g}{b_o R}} \left[\frac{T_o(z_o) \pm b_i z_i}{T_i(z_o) \pm b_i z_n}\right]^{\mp \frac{g}{b_i R}}\right\} \tag{3.4.16}$$

Simplifying and putting the terms as follow:

$$A = \left[\frac{T_o(z_o) \pm b_o z_i}{T_o(z_o)}\right]^{\mp \frac{g}{b_o R}} - \left[\frac{T_o(z_o) \pm b_o z_n}{T_o(z_o)}\right]^{\mp \frac{g}{b_o R}} \left[\frac{T_o(z_o) \pm b_i z_i}{T_i(z_o) \pm b_i z_n}\right]^{\mp \frac{g}{b_i R}}$$

$$B = \left[\frac{T_o(z_o) \pm b_o z_i}{T_o(z_o)}\right]^{\mp \frac{g}{b_o R}} - \left[\frac{T_o(z_o) \pm b_o z_n}{T_o(z_o)}\right]^{\mp \frac{g}{b_o R}} \left[\frac{T_o(z_o) \pm b_i z_i}{T_i(z_o) \pm b_i z_n}\right]^{\mp \frac{g}{b_i R}}$$

Then, finally, we obtain

$$\frac{X_i}{X_i} - \frac{B}{A} = 0 \tag{3.4.17}$$

Owing to the variation of both the air temperature outside and inside, the expression of the NPL solution for this case is shown to be somewhat lengthy and complicated. In this case, to determine the NPL an iterative method is required assuming an appropriate initial value, which corresponds to the physical conditions in the building.

3.5 METHOD OF SOLUTION

In the development of the analytical models, as stated earlier, it has been shown that the energy equations formulated, corresponding to the number of openings involved in the building, should be rearranged to obtain a feasible solution by interrelating between the openings at different levels with applications of energy balance in order to determine the pressure differentials analytically.

In addition, it has been shown that in the process of such manipulations, the terms representing the velocity in the energy equation, as shown in the right hand side of Eq.3.4.2 also can be interrelated using mass conservation between the openings at different levels.

Through these processes, the computational model results in a set of equations represented in terms of the velocity. The total number of equations, as well as the number of unknowns in the computational model, are identical to the numbers of the openings involved in the flow field induced by the thermal effect in the building. In the computational model, the set of equations which is processed

with the procedures above takes the following mathematical functional form:

$$
\begin{aligned}
&f_1(v_1^2, v_2^2, \ldots v_n^2, v_1, v_2, \ldots v_n) = 0 \\
&f_2(v_1^2, v_2^2, \ldots v_n^2, v_1, v_2, \ldots v_n) = 0 \\
&\cdot \\
&\cdot \\
&f_n(v_1^2, v_2^2, \ldots v_n^2, v_1, v_2, \ldots v_n) = 0
\end{aligned}
\qquad (3.5.1)
$$

or simply

$$
\begin{aligned}
&f_1(V) = 0 \\
&f_2(V) = 0 \qquad \text{where } V = \begin{bmatrix} v_1 \\ v_2 \\ \cdot \\ \cdot \\ v_n \end{bmatrix} \\
&\cdot \\
&\cdot \\
&f_n(V) = 0
\end{aligned}
\qquad (3.5.2)
$$

In Eqs.3.5.1 and 3.5.2, v and subscript n is the velocity, and the number of the openings to be considered in the problem, respectively.

In general, a system of n equations in n unknowns, x_1, x_2, $\cdots$, x_n, is called nonlinear if one or more of the equations is nonlinear because it cannot be written as [28]:

$$ax + by + cz + \cdots\cdots = \text{constant}$$

where x, y, z are unknowns and a, b, c are arbitrary constants.

Since the equations formulated in the computational model to calculate the pressure differentials, as shown in Eq.3.5.1, include non-linear terms, a special method to solve the problem presented is required.

In the present study, two types of computational models are formulated for two different kinds of building construction. One of these models is for the building without floor partitions, and the other for the building with floor partitions.

In the model for the building with no floor partitions, it is designed to execute the calculation of pressure differentials with variations in the number of the exterior wall openings along the height of the building as well as various pertinent parameters, such as the characteristics of the openings, temperature distributions, etc.

On the other hand, in the computational model for the building with floor partitions, the calculation of the pressure differentials is designed to be carried out with variations in the number of floors as well as various pertinent parameters, including the opening characteristics, physical dimensions of the building, and temperature distributions, etc.

Both of types of computational models are also designed to calculate the neutral pressure level using the method

presented in Section 3.3, after having completed the computations of the pressure differentials for each opening.

The method used in the solution of the set of non-linear equations in the computational model is based on Newton's method which is known to have an advantage of converging quadratically if the initial guesses are near the roots [28]. In the method, the values for the unknowns are determined by calculating the given function with a small perturbation for each of the variables in turn, to improve the accuracy of the estimation.

In both of the computational models, the computations are made to be initiated with the initially assumed values of the velocity of air in the openings involved for the case under consideration. When the convergence is obtained, the next procedure to satisfy mass conservation in the system to be analyzed is taken.

In the program of the computational models, several decision making steps are provided to check convergence, and error finding routines are used. For the case resulting in discrepancy between energy and mass balance, the program is also made to reiterate the velocity terms until the mass balance is met in the building as a whole.

All the computation carried out to obtain the numerical solutions of the computational models are performed by using the main frame computing facilities (Amdahl A) at the University of Ottawa.

The values for the coefficient, $\bar{C}_x$, as has been presented in Eq.3.3.6, are estimated from reference [29]. The examples of the calculated values for $\bar{C}_x$ using Eq.3.3.6 are presented in Table 3.5.1.

The values for the viscosity of air used in the computations are calculated from the empirical correlation suggested by Sutherland as follows [27]:

$$\mu = \mu_o \left(\frac{T}{T_o} \right) \left(\frac{T_o + S}{T + S} \right) \qquad (3.5.3)$$

where

μ = viscosity of air, $N.s/m^2$.

T_o = Reference Temperature(273.0 K)

μ_o = Reference μ ($1.72 \times 10^{-5} N.s/m^2$)

S = empirical constant(110.0).

In the computations for the cases with an uniform temperature distribution with elevation, the air temperatures in the openings in the flow are taken the same as the wall temperature at the corresponding level, measured in the experiment.

For the cases with a non-uniform temperature distribution, the air temperature in the openings is made the same as the corresponding wall temperature profile along the elevation, measured in the experiment.

The effect of a small amount of perturbation in the air temperature in the openings involved in the flow appeared marginal on the calculated results, such as the pressure differentials, and NPL, for both computational models.

The values of form loss factor which is used for the computation of the present models are; K_c=0.5, K_{ext}=1.0 and K_{re}=1.0 respectively.

CHAPTER IV

EXPERIMENTAL STUDIES

In the previous discussion, a theoretical analysis of the characteristics of the thermal effect was examined for the various different cases that most likely could be encountered in buildings in practice.

In addition, the basic equations to determine the pressure differentials induced by thermal effect also were developed for these cases.

Since the main objectives of the present study are to obtain an accurate means to predict the pressure differentials due to the thermal effect and to provide better insight into the characteristics and behaviour of the thermal effect, it is required to conduct sufficiently informative investigations through experimental studies.

To study in detail the characteristics and behaviour of the thermal effect for various different situations which may be expected in the actual building, the problems to be investigated in the study are classified into two major fundamental categories:

(1) thermal effect neglecting the effect of floor separations within building and

(2) thermal effect considering the presence of floor separations within building.

For the purpose of studying the problems outlined above, two types of specially designed model buildings are made, of which one is non-partitioned and the other floor partitioned.

Using these experimental model buildings, the characteristics and behaviors of the thermal effect in the buildings are investigated experimentally for various ranges of temperatures, for different distributions of exterior and interior partition openings, for ventilated conditions and for different number of floors. The details of the experimental apparatus, instruments, and experimental procedures will be discussed in the following sections.

4.1 EXPERIMENTAL APPARATUS

4.1.1 Model Building with No Internal Floor Partitions

A schematic configuration of the experimental apparatus used for simulation of thermal effect in buildings with no internal floor separations is shown in Fig.4.1.1.

The model building is basically made of a main test section, pressure and temperature measuring devices, power supply and control system with measuring loops, a ventilation system consisting of a blower and piping system with flow control and measurements, and a data acquisition system.

The essential configurations and dimensions of the major components constituting the system are illustrated in Figs.4.1.1 to 4.1.6. The details of the systems are presented in the followings.

A. Test Section:

A plan view of the test section set-up used for the cases with no internal floor partitions is shown in Fig.4.1.1.

The basic concept of the test section design for this particular cases is to simulate a high-rise building with negligible effect of floor separations on the air flow within building due to sufficient interconnections between floors.

In this type of building construction, as discussed previously, the flow resistance within the building imposed by internal floor separations may be considered insignificant due to existence of various interconnections between floors such as stairwells, elevator and service shafts, and exhaust ducts, etc.

In this building environment, it can be anticipated that the distribution of the pressure differentials with elevation induced by the thermal effect is mainly governed by the condition provided by the exterior openings existing on the external wall of building.

In order to meet the requirements prescribed above, a special test section shown in Fig.4.1.1 is fabricated. For this purpose the test section has distribution of the exterior wall openings with height only, having no provisions of internal floor partitions within it.

The test section is made of a copper tube with 50.8 mm I.D. and 18.3 m in length. Both ends of the test section are connected to a piping system which leads to the ventilation system with flow control loop by using 25.0 mm copper reducers.

The outer surface of copper tube for the test section is drilled at the designated positions to install the exterior opening tubes, pressure and thermocouple taps which will be explained later.

The details of the major components for the test section assembly and the place where the set-up of the testing apparatus is situated will be discussed in the following pages.

B. Exterior Openings:

In order to simulate the equivalent crack openings in the exterior wall of the building, six openings are provided on the test section in four different elevations as shown in Fig.4.1.2.

In this test section, two openings of identical size and shape are installed at top and bottom levels respectively.

All openings are made of copper tubing as is the test section tube. The configuration and dimensions of the exterior wall openings installed are illustrated in Fig.4.1.2.

As shown in the figure, the construction of each opening hole is made of two sections, a and b, which have different flow areas to exemplify the effect of flow resistance at the openings.

Section a is made of 2.5 mm drilled hole in the test section tube. Section b is made of copper tubing of 5.0 mm I.D. and 55 mm long. The tubings are soldered on the drilled hole which is made in the test section.

Subsequent to these solderings, each opening is trimmed to remove remaining debris or chips.

C. Heating Sections:

One of the most important experimental requirements to achieve the simulation of thermal effect in the building is to produce the designated temperature distributions along the testing section.

To accomplish the temperature distributions in the model building, as required by the objectives of this study, the heating system of the test section is designed in a particular manner.

The heating system in the test section is made of multi-zone systems which divides the test section into twenty independent heating sections.

Each heating section in the test section is 0.91 m in length. The power supply and control for each heating section is designed to be manipulated independently by its own variable transformer.

As a preparatory step to fabricate the heating sections on the test section body, the outer surface of the copper tube in the test section is entirely covered with layers of thermal resistant electric insulating paint.

After finishing the above electric insulation carefully, the coated surface of the test section is again wrapped with three layers of 50.0 mm wide fiberglass tapes to secure electric insulation between the heating wire and the test section body.

As the next step, seventeen gage nichrome wires (20 % Cr, 80 % Ni, resistivity 1.3352 Ω/m) as a heating element, are then wound around the electrically insulated test section surface described above. The winding is in 40.0 mm pitches over every 0.91 m length of the test section.

As a result, twenty independent heating sections in total are made. Then, each heating section is connected to its own electric power supply circuit loops consisting of a variable transformer and a power supply with measuring loops.

D. Thermocouples:

For the measurement of temperatures in the present experimental studies, K-type (Chromel-Alumel) thermocouples are used.

A schematic diagram of the thermocouples installed on the test section is illustrated in Fig.4.1.4.

In order to measure the temperature distribution of the test section wall with respect to height, as shown in the figure, one thermocouple is spotwelded at the center of each heating section before the electric insulation procedures mentioned above are done.

In addition, another six thermocouples are spotwelded at various levels of the test section as shown in Fig.4.1.4 to supplement temperature measurement at the corresponding positions with the same procedures described above.

The thermocouples used for temperature measurements of the inside and outside air of the test section will be represented in detail later in the following subsection which deals with the instrumentations.

E. Ventilation System:

To investigate the effect of the mechanical ventilation on the profile and pattern of the pressure differentials induced by the thermal effect, a ventilation system is installed for the test section as shown in Fig.4.1.5.

The system is designed to carry out the function of pressurization and depressurization on the test section spaces, with excess supply or exhaust of air at the top or bottom elevations of test section as shown in the figure. The system consists of a blower with capacity of 1.4 m^3/min, flow control system and flow measuring devices.

The supply and exhaust line of air into the test section is made of 25.0 mm I.D copper tube and is then connected to the test section by copper pipe reducers at the top and bottom of the test section as shown in Fig.4.1.5. The flow loop of the air is designed to pass through a control system consisting of three sets of rotameters (Brooks type: R-8M-25-4F, range: 0.1 to 71.0 L/hr) and directional control valves.

The flow control system in the test section is designed to perform the flow rate adjustment and to choose flow directions according to the experimental requirements for the purpose of pressurization or depressurization at the top or bottom position of the test section.

4.1.2 Model Building with Internal Floor Partitions

A schematic view of the experimental apparatus used for investigations of the thermal effect in the buildings with internal floor partitions is presented in Fig.4.1.7.

The model building is basically similar to the test system described in the subsection 4.1.1. It consists of a main test section, pressure and temperature measuring

devices, power supply control and measuring loop, and a data acquisition system.

In the system, as shown in Fig.4.1.7, the main test section has floor partitions and no ventilation system. The essential configuration and dimensions of the major components of the model building are illustrated in Figs.4.1.7 to 4.1.11.

A. Test Section:

A schematic view of the test section set-up for the experimental study to examine the characteristics and behavior of thermal effect in the cases with internal floor separations is shown in Fig.4.1.7.

The fundamental purpose of this test section design is to simulate a multi-story or high-rise building with significant internal flow resistances.

In practical situations, in actual building construction, we know that no buildings are open in the inside or air tight between floors. Hence, for more practical interpretations on thermal effect in the buildings, the effect of internal separations should be included in the problems to be investigated.

To accomplish the requirements explained above, the test section shown in Fig.4.1.8 was designed. To simulate the floor partitions in the real buildings the test section is designed to have five floor separations along the height

which have a floor opening hole as well as the exterior wall openings at each floor.

The test section is made of copper tube with 50.8 mm I.D. and 18.3 m long in total height. It is internally separated into five stories along the height by four cassette plates inserted between flanges mounted every 3.6 m length of the test section tube.

The height of each floor in the test section is designed to be 3.6 m long the same as the usual floor level height of actual buildings. The cassette plates separating each floor are made of aluminium plate of 3.0 mm thick.

The flanges for mounting the cassette plates are designed to allow removal and re-insertion of the cassette plates at the gap of the corresponding flanges. They are also designed to maintain air tightness between floors except for the floor partition opening hole at the center of each cassette plate.

As shown in Fig.4.1.9, each set of cassette plates is designed to have a circular opening hole which is made to be placed at the center of the cross section of the test section after being inserted into the flange to simulate the equivalent floor partition openings in the floor separations in the buildings.

The flanges for jointing the test section tubes and mounting of cassette plates are made of copper plates 20.0 mm thick.

The details of the flange design and construction are shown in Fig.4.1.9.

The flanges, machined according to the design specifications as shown in Fig.4.1.9, are soldered with test section copper tube at both ends and assembled by joint bolts with insertion of an asbestos gasket 2.0 mm thick between the upper and lower flanges.

Subsequent to assembling the flanges, the test section tube is then drilled at the designated positions according to design details to install the pressure and temperature measuring taps, and exterior wall openings.

B. Exterior and Floor Partition Openings:

To simulate the exterior wall crack openings existing in the building wall, four openings are provided at each floor section of the test section, of which two openings are installed at the top and the other two at the bottom of each floor section as shown in Fig.4.1.8.

All exterior wall openings are made of copper tubing 5.0 mm I.D. and 75 mm long. The openings are soldered at the drilled positions of the test section and then trimmed to remove remaining debris or chips.

The floor partition openings between floors are simulated by the opening hole in the cassette plates described before. To investigate the effect of the variations of the area of floor opening between floors on

the pressure profile, fifteen sets of cassettes plates, which have different opening diameters ranging from 1.0 to 20.0 mm, are fabricated for each flange.

All the cassette plates in the identical set for a flange are designed and machined to have the same tolerance for fitting into the corresponding flange gaps except for the diameter of the opening hole that is made to be placed at the center of the cross section of the test section.

C. Heating System:

For the purpose of achieving any required wall temperature distribution of the test section along elevations, each floor of the test section is constructed with four heating sections, which becomes then twenty sections in total for the whole test section.

In the construction of the heating section for this test section, the identical method and design of fabrication described in subsection 4.1.1 are applied. Each heating section is 0.91 m in length and its own power supply is controlled by its individual control circuit loop consisting of a variable transformer and measuring circuit.

D. Thermocouples:

In order to measure the temperature distribution of the test section K-type thermocouples are used in the experiments as before.

To measure the wall temperatures in the test section with height, one K-type thermocouple is spotwelded on the outer exposed surface of the test section at the center of each heating section before constructing the heating sections aforementioned.

All other thermocouples installed to measure the temperatures of inside and outside air will be described later in detail in the following subsection on instrumentation.

4.1.3 Installation of Test Sections

For the completion of installing both the test sections, several preparatory steps described below are taken.

After finishing the fabrication of the heating sections, the entire test section is again carefully wrapped with two layers of 40 mm wide fiberglass tape to protect and to insulate heating wire as shown in Fig.4.1.12.

Following the above step, the performance of the electric insulation between the test section tube and heating wires at each heating sections are tested with an electric resistance meter (mega ohm tester).

In this testing process, if any faults or defects are found, the procedures are done again from the beginning. When these testing procedures are carried out successfully, the test section is then covered entirely with 40 mm thick glassfiber

thermal insulation, by providing careful attention to the taps of pressure and temperature measurements, exterior openings, and the wiring of thermocouples and heating sections in order to reduce the heat loss through the test section wall.

As noted previously, the primary objective of the present study is to carry out an investigation on the characteristics and behaviors of the thermal effect in building. Hence, it is very important to perform these experimental studies under favorable situations which can eliminate wind effect and external adverse interferences induced by gusty air streams and disturbances due to surrounding environment, or the other factors.

To avoid as much as possible the adverse effect of the surrounding environment and due to the unusual height of the test sections, both test sections are situated in the stairwell of the D section of Colonel By Hall of the University of Ottawa.

An example of the plan view of the installed test section is illustrated in Fig.4.1.6. As can be seen in the figure all the wiring from the test sections is extended through the walls into the adjacent laboratory room(D006 of Colonel By Hall) where the data acquisition system and power controls are situated.

4.2 INSTRUMENTATION

4.2.1 Temperature Measurements

A. Experiments with No Floor Partitions:

In the experimental apparatus with no floor partitions thirty eight K-type thermocouples in total are used for temperature measurement of the test section wall, and of the inside and outside air at different elevations of the test section.

As mentioned in the fabrication of the test section, twenty thermocouples are spotwelded on the surface of the test section at the center position of each heating section to measure the wall temperature of the test section with height.

In addition, another eight thermocouples are spotwelded at various levels of the test section as presented in Fig.4.1.4 to supplement the temperature measurements at those positions.

To measure the temperature distribution of the air within the test section with height, five K-type thermocouples, which are sheathed with stainless steel tube with 152 mm length and 0.82 mm O.D., are inserted into the temperature measuring taps provided in the test section at five different elevations. These taps are made of seventeen gage stainless tubing and silver-soldered at the predetermined positions during fabrication of the test section. Example of the thermocouple tapping is illustrated in Fig.4.1.4.

Five additional thermocouples are mounted on the outside surface of the completed test section at the same elevations of the thermocouple taps that are measuring the temperature of the air inside, to measure the temperature distributions of the surrounding outside air along the height.

The positions of the thermocouples installed in the test section are illustrated in Fig.4.1.4, in which thermocouples are represented as positions #1 to #38. The positions #1 to #20 represent the thermocouples for wall temperature measurements, the positions #21 to #25 are the thermocouples for inside air temperature, and the positions #26 to #30 are the thermocouples for outside air temperature measurements, respectively.

Another eight thermocouples, represented as #31 to #38, are the thermocouples supplementing at the positions.

B. Experiments in Test Section with Floor Partition:

In the test section with five floor partitions, forty one K-type thermocouples in total are used for the measurements of temperatures.

As described in the fabrication of the test section, twenty thermocouples are spotwelded on the surface of the test section at the center of each heating sections to measure the wall temperature of the test section with height.

Another six thermocouples are spotwelded to supplement the twenty thermocouples mentioned above at top and bottom level of each floor of the test section.

To measure the inside air temperature distributions with height ten stainless sheathed K-type thermocouples, 152 mm long and 0.82 mm O.D., are inserted into the temperature measuring taps of the test section and its end tips are placed at the center of the cross section of the test section.

Another five thermocouples are installed on the outside wall of the completed test section at the mid-height of each floor to measure the temperature distributions of the outside air with elevations.

The positions of the thermocouples installed in the test section with floor partitions are illustrated in Fig.4.1.11.

C. Measurements:

All the thermocouples from both the test sections are connected to the terminal board of the control panel which is situated in the adjacent laboratory room (D006 of Colonel By Hall) with extensions and linked to a switching board made of three sets of two way rotary switches.

The control panel for the thermocouples is designed to measure temperature at a specific point by turning the rotary switch in sequence through a specially designed circuit loop.

The positive side of each thermocouple is connected so as to pass through the ice-junction point via the rotary switch.

An example of the detailed circuit diagram of the thermocouple connection is shown in Fig.4.2.1. By turning the rotary switches to a selected position in sequence the EMF in D.C. from each thermocouple is processed by the data acquisition system through the predetermined channel of the scanner which will be described later.

4.2.2. Pressure Measurements

The measurement of the pressure differentials across the wall of the test section in both experiments are carried out with MKS Baratron type 220B pressure transducers with maximum pressure head of one torr (133.3 Pa) and 0.15 % error at full scale.

In the experiments using the test section with no floor partitions, seven sets of the pressure transducers are employed. For the experiments using the test section with floor partitions, ten sets of the pressure transducers are used.

The positions of the pressure taps and transducers installed in both test sections can be found in Figs.4.1.3. and 4.1.10, respectively.

All static pressure taps in both test sections are made of seventeen gage stainless steel tubing 76 mm long. Before

installing the heating section on the test sections these taps are silver-soldered at the designated drilled hole and then trimmed. A typical installed configuration of the static pressure taps in both test sections can be found in Fig.4.2.2.

In the present study, the measurements of the pressure differentials across the exterior wall of the test sections at the specific level have been referenced to the outside pressure of the test sections at the corresponding level of the static pressure tap installed.

To measure the pressure differentials between the inside and the outside of the test section at the elevations of the static pressure taps, one of the two pressure ports, the positive side, of each pressure transducer is connected to the static pressure tap installed in the test section at the corresponding elevations with flexible tygon plastic tubing.

The other pressure port of each transducer is connected to a 90° bend of seventeen gage stainless steel tubing which is mounted on the insulated outer wall of the test section at the same level of the static pressure tap with the same kind of plastic tubing. Fig.4.2.2. illustrates an example of the completed connection of pressure taps at the test section.

Since the positive side of all the pressure transducers is connected to the static tap of the test section in the installations, the pressure differential causing the air

infiltration is designated as the negative quantity in the study.

The D.C. signal from the pressure transducers installed in the test sections is linked to the channels of a HP scanner in the data acquisition system with shielded electric cable of three wires from the test section to the laboratory room(D006 of Colonel By Hall) where the data acquisition system is situated.

Since the pressure measurements in the present experiments are at the order of Pascal, which is extremely small, simultaneous measurements of the pressure differentials at all elevations is very important to obtain the accuracy and reliability of experimental data acquired. For the accomplishment of this purpose, the pressure data readings are taken simultaneously through the channels of the scanner corresponding to the number of static pressure taps installed in the test sections.

In the cases of experiments with no floor partitions, the measurements of pressure differentials generated in the form of D.C. signals are taken through seven channels of the scanner, channels #2 to #8, of the data acquisition system. For the case of experiments using the test section with floor partitions, the D.C. signals from the transducers are taken through ten channels of the scanner, channels #2 to #11, of the data acquisition system.

4.2.3. Power Supply, Control and Measurement

Following the completion of the fabrication and the performance testing of the heating sections in both test sections, both end terminal wires of each heating section are connected to its own power cable (600 V, 15 A, three wires). The power cables are then extended from the test section through the walls to the control panel situated in Room D006 of Colonel By Hall as shown in Fig.4.1.6.

To assure the proper performance of the wirings and electric insulation of each heating section in the test sections, another performance test is taken with an electric resistance tester (mega-ohm tester) carefully.

In the experiments of both test sections, twenty sets of variable transformers with 1 Kw capacity, 110 V and 10 A are used to supply and control the power required for heating of the test section to produce the thermal effect.

As mentioned before, each heating section is designed to have its own circuit loop supplying and measuring the power to it. The power supply to the heating section is measured by both a digital voltmeter and ammeter using a control panel consisting of five power bars, groups of sockets, and two rotary switches. A plan view of the set-up of power supply and control panel is shown in Fig.4.2.3.

4.3 CALIBRATION OF INSTRUMENTS

4.3.1 Thermocouples

Every thermocouple bead to be installed in both test sections was made by a thermocouple welder, taking careful standard procedures. The thermocouples, K-type(chromel-alumel), used in the present study are calibrated indirectly using a thermocouple which is made from the same spool of wire.

The thermocouples made for the testing purpose are calibrated against a Fisher NR 15-155 standard precision thermometer having a temperature controlled oil bath in the range from 20 °C to 100 °C. An example of the thermocouple calibration is presented in Fig.4.3.1.

As can be seen in the figure, in all range of calibrations, which is within the experimental operations, the thermocouples made from the same spool of wire are shown to indicate fairly close agreement with the temperature readings from the precision thermometer.

4.3.2 Pressure Transducers

In addition to the temperature measurement, the correct measurement of the pressure differentials is another very important requirement that should be fulfilled. Due to the great importance of the correct measurement of the pressure differentials induced by the thermal effect,

several demanding testing procedures are taken before any pressure measurements are executed in all the experiments.

As the initial step of installing the pressure transducers in the test section, all the pressure transducers to be used are calibrated against the original calibration record of each unit supplied by the manufacturer in order to check whether or not it performs properly in the calibrated ranges according to the specifications.

For this calibration procedure, first, the pressure transducer is zero-adjusted according to the manufacturer's instruction manual until it meets the tolerance of 0.001 V of D.C. output(0.013 Pa) by connecting the positive side of each transducer to its own negative side port with the same size plastic tubing as the pressure port diameter.

After the above zero-adjustment procedures are done properly, each pressure transducer is then calibrated to obtain a correlation of the pressure measurement in units of D.C. output voltage against the static water pressure head in units of Pa by using a specially made device shown in Fig.4.3.2. The device is made of a precision type height gage with level adjustment knob and two glass tubes connected to the pressure port with plastic tubing.

The D.C. output of the pressure transducers is obtained by changing the increment of head height of the positive side port alone by turning the knob of height gage.

All D.C. output readings are taken by a digital voltmeter with an auto calibration function, which constitutes the data acquisition system for the present study.

The results are compared with the original calibration record of its own unit supplied by the manufacturer. An example of this result is presented in Fig.4.3.3. The result shows that the agreement between the testing results and the calibrated records supplied by the manufacturer appears to be fairly good, especially in the measuring ranges of the present experiments.

The pressure transducers that were taken through the above calibration procedures satisfactorily were installed in the test section at the designated positions. Before taking any measurements, the pressure transducers are zero adjusted again at the installed position if required.

4.4 DATA ACQUISITION

4.4.1 Data Acquisition System

The data acquisition system used in all aspects of the present experimental studies is a system consisting of a Hewlett Packard (HP) desk top computer and four other HP peripheral instruments.

Fig.4.4.1 illustrates a schematic diagram of the data acquisition system used in the present study.

The details of the data acquisition system will be presented in Appendix A-1.

4.4.2. Data Acquisition Procedures

The data acquisition for the present experimental works is designed to have the following systematic procedures to acquire and process the experimental data:

(Step #1) In this first step of the data acquisition process, all the variables and arrays for data reading and processing are initialized and all the instruments are addressed.

(Step #2) This stage includes the branching routines for all errors expected to be encountered in the instrument malfunctions, storage medium overflow. etc., as the debugging process.

(Step #3) In this step, the computer requires a file name for the data storage of the current experiment to be fed into the computer.

(Step #4) In this step of the data acquisition process, the preliminary test of the temperature distributions with elevations for those test sections having predetermined openings or partitions are executed.

Temperatures of the inside air, the wall, and the outside air of the test section along the height of the building are scanned for all the positions where thermocouples are placed as shown in Fig.4.4.1 through the HP Scanner by turning the 2 channel rotary switch knob in sequence. This preliminary measurement of temperatures is repeated until the inside air and the wall temperatures of the test section are stabilized and meet to the required conditions of the present experiment along all the elevations of the test section.

(Step #5) This is the step executing the temperature measurement for the present experiment. Subsequent to obtaining the required temperature distributions in the test section, the temperatures at all the positions where thermocouples are installed are measured through the HP scanner by turning the 2 channel rotary switches in sequence manually.

(Step #6) This is the step of the data acquisition loop designed to execute the pressure measurement. In this step, the computer starts to measure the pressure differentials across the exterior wall of the test section at the designated elevation under predetermined temperature difference and opening conditions.

The pressure measurements are taken in sequence for all the pressure taps installed in the test section shown in Fig.4.1.3 and Fig.4.1.10. Each measurement at a position is taken as the arithmetic average of 50 individual readings for a time period of 20 seconds. All of these measurements of the pressure differentials are automatically performed by the system using channels #2 to #11 of the HP Scanner.

(Step #7) In this step, the voltage and current supplied to each heating sections of the test section are read with an ammeter and a handheld type digital voltmeter by manually turning the rotary switches placed on the power control panel in sequence from heating sections #1 to #20 shown as in Fig.4.1.4 or Fig.4.1.11. The data acquired from this step are fed into the computer manually.

(Step #8) After all the data are acquired, they are processed and stored in the cassette tape cartridge. In addition, a hard copy printout of the processed data is also produced from the printer/plotter.

(Step #9) As the final step of the data acquisition, the system either starts a new set of experiment or stops and ends at the request of the operator. The flow chart of the data acquisition procedures outlined above can be found in Fig.4.4.2.

4.5 EXPERIMENTAL PROCEDURES

4.5.1 Preliminary Testing of System

Before performing any data acquisition procedures described in the previous sections in the experiments for both the case with no floor partitions and the case with floor partitions, several preliminary procedures are taken to assure the performance of the experimental apparatus and to provide favorable conditions required to create the thermal effect in the test sections.

A. Inspection of Electric Wirings and Insulations

Since a significant number of electric and thermocouple wirings are involved in both test sections, as described earlier in the experimental apparatus, it is necessary to inspect thoroughly the performances of all wiring and the electric insulation of the thermocouples and of the heating sections to ensure the proper implementation of the testing systems.

Following the test of the electric insulation of each heating section installed in the test section with electric resistance meter, the power for each heating section is switched on at the predetermined voltage scale of the variable transformer for three hours. Then, they are checked again to test if there are any malfunctions in their performance such as the failure of electric insulation or local overheating, etc.

Finishing the previous testing of the performance of heating sections, the connected wirings and performance of the electric insulation of the thermocouples, including the measuring loops, are inspected with an electric resistance meter and a digital voltmeter.

In this testing procedures, the electric insulation between thermocouples spotwelded in the test sections and the A.C power supply for pressure transducers and the heating sections is especially emphasized to prevent the D.C signals generated by thermocouples from interference by any A.C signals which could come from improper electric insulation.

B. Testing of Test Sections

Subsequent to conducting the inspections in the step A described above, the experimental systems are switched on and set to idle for more than 12 hours at the designated experimental condition to obtain a stabilized temperature distributions of the inside air in the test section in both types of experiment.

In the aforementioned testing operation of the experimental apparatus, the power supply to the test sections is adjusted to have the temperature difference about 60 °C between the inside and the outside of the test section along the height through continuous monitoring of power supply and temperatures distributions in the test sections.

After obtaining the uniform and steady temperature difference between the inside and outside of the test sections along the elevations, the performance of both test sections and each pressure transducer installed in the test section is inspected using the well known intrinsic attributes of the thermal effect in the building under uniform temperature differences with height, which is represented in Section 3.1 of Chapter.

In the testing procedures for the test section with no floor partitions, the exterior openings provided in the wall shown in Fig.4.1.2 are closed except the one positioned at the bottom level.

For the above opening arrangement and temperatures, as presented earlier, the pressure difference at the bottom opening should be nil and the maximum pressure difference induced by thermal effect would occur at the top level of the test section logically as shown in Fig.3.1.1.

Due to the given temperature distributions the profile of the pressure differentials due to thermal effect should be linear with elevation, and the magnitude of the maximum pressure difference which occurs at top opening level can be calculated from Eq.3.2.15 of the thermal effect equation. This characteristic of the thermal effect has been shown in the previous study[10].

Consequently, this characteristic of the thermal effect could be employed as the testing criteria of the performance of the test section to check whether it has any leakage of

heated air except for the opening at the bottom or top level. Also it could provide an excellent criteria for indirect performance testing of the differential type pressure transducers to be used in the present experiments.

Applying the steps mentioned above, the test sections as well as all the pressure transducers are tested before taking them into experimental operations.

The functional test of pressure transducers is carried out by measuring the pressure differentials at different elevations through interchanging the connecting tygon plastic tubing with the others at different levels in sequence at the installed position. Then, the measured results are compared to the calculated differentials from Eq.3.2.15 for each given condition.

The identical procedures are also applied in the performance test of the test section with floor partitions. In this case the test section is tested for two different modes.

First, the test section is tested in the same manner as the one without floor partitions by removing all four cassette plates from the flanges and closing its gaps with sealing tape as well as enclosing the exterior openings except a single opening at the top level. Under this particular condition of the exterior wall opening arrangements, ten pressure transducers installed on the test section with floor separations are also checked applying the same procedures taken previously.

Secondly, subsequent to conducting the above test successfully, the functional test of each floor in the test section is carried out after inserting a cassette plate with no opening hole into the corresponding flanges which provides a complete air tightness between the floors. A typical example of this particular testing result for the test section as well as the pressure transducers, by the procedures described above, are presented in Figs.4.5.1 to 4.5.2.

4.5.2 Simulation of Thermal Effect

A. Experiments using Test Section with No Partitions

The simulation of the thermal effect in the test section is carried out through careful and cautious adjustment of the power supply to each heating section with continuous measurement of the current and voltages supplied and the temperature distributions of the wall and inside air with elevation.

This procedure is continued until the desired temperature distribution of wall and inside air with height are achieved with maximum allowable deviations of $\pm 3\,^{\circ}C$ at each level or point from the designated temperature for the experiment.

The temperature difference between the inside and the outside of the test section to simulate the thermal effect in the test section is referenced to the average air temperature of the outside along the height, where the test

section is situated. The range of the temperature difference across the test section wall applied for these experiments were between 25 and 60°C (25, 30, 40, 50 and 60).

The simulation of the distributed patterns of the exterior wall openings of the building were carried out by opening or closing the exterior wall openings provided in the test section wall in sequence under the imposed temperature difference for the experiment.

The pressure differentials across the exterior wall with elevations are measured for different arrangements of the exterior wall openings while maintaining the temperature differences required for the ongoing experiment through continuous monitoring of power supply and temperatures in the test section.

Subsequent to the completion of the measurements of the pressure profiles due to thermal effect alone for the various distributed pattern of exterior wall openings and different temperature difference, another series of pressure measurements are also carried out with operation of the ventilation system of the experimental apparatus described in Section 4.1.

The measurements of the pressure differentials for investigating the effect of the mechanical ventilation on the thermal effect are carried out for the given opening mode under thermal effect alone as well as under the operation of ventilation system with variations of air flow rate.

The air flow is either exhausted out of or supplied into the test section while keeping the designated temperature differences for the ongoing experiment through continuous monitoring of power supply and temperature.

The pressure measurements also are conducted with variations of the position of supplying or exhausting air into or out of the test section by alternating the flow directions as well as flow rate in the flow control loops. In both tests the flow rates are varied from 0.47 L/hr to 3.0 L/hr.

B. Experiments using Test Section with Floor Partitions

The temperature difference between inside and outside of the test section to simulate thermal effect in the test section, as in the case with no partitions, is referenced to the average temperature of the outside air where the test section is situated. The range of the temperature difference across the test section wall applied for these experiments was between 25 and 60 °C (25, 30, 40, 50 and 60), which is the same as the previous cases.

The procedures taken to obtain the required temperature distribution in the test section in this experimentation are the same with those taken in the case with no partitions.

The simulation of exterior wall openings are conducted by opening or closing of the exterior wall openings in sequence.

The number of floor levels are simulated by altering or removing the number of the cassette plates installed in the flanges. Whenever an alteration of floor number in the test section is required, the identical testing procedures described in the subsection 4.5.1 are conducted again to test the test section prior to execution of experiments.

The variation of the opening hole in the floor separations are carried out by interchanging the cassette plates installed with another one in the same set having different opening holes at the corresponding levels.

C. Experiments having A Non-Uniform Temperature Distributions with Elevation

The distribution of a non-uniform temperature of the air inside along the height of the test section are simulated through adjustments of the power supply to each heating sections in both the test sections, which results in a temperature profile of the test section wall with elevation corresponding to the patterns of the power supplied.

In both experiments, using the test section without floor partitions and the test section with floor partitions, two different profiles of the temperature differences along the test section height are employed; $\Delta T(z)=30.0 + 3.3z$ and $\Delta T(z)=90.0-3.3z$.

In addition, the temperature difference across the exterior wall for these cases, the same as before, is referenced to the air temperature of the outside where the test sections are situated.

For the measurement of the pressure differentials with elevation for the above non-uniform temperature distribution of inside air with variations of exterior openings, floor openings, and number of floors, the identical procedures aforementioned in the experiments of A and B are taken in both experiments of the case without partitions and the case with floor partitions.

CHAPTER V

RESULTS AND DISCUSSIONS

5.1 VALIDITY OF THERMAL EFFECT EQUATIONS

In the present study, the validity of the thermal effect equations, Eqs. 3.2.20 and 3.2.24, are examined through comparisons with the corresponding experimental results.

As the first attempt, Eq.3.2.20, which is for the case with uniform temperature distributions of both inside and outside air with elevation, is tested.

As shown in Eq.3.2.20, the pressure differentials across the wall for this particular case at given temperatures and building height are presented to depend upon the value of the coefficient K' which represents the slope of the pressure difference profile due to the thermal effect.

In order to verify Eq.3.2.20 as the one to determine the pressure differentials, the coefficient K' obtained from theory is compared to the experimental results.

The values of K' from the experimental results are obtained for different arrangements of exterior wall openings, internal floor openings distributions, and floor partitions under various temperature differences.

Fig.5.1.1 shows the results for the case with no internal floor partitions, and Fig.5.1.2 is for the case with floor partitions. In the figures, the value of K' is plotted against the difference of the reciprocal of the absolute temperature between the inside and outside of building.

The tests shown in Fig.5.1.1 were carried out with variation of distributed patterns of exterior wall openings along the elevations under different temperature differences between inside and outside of the test section. The test results presented in Fig.5.1.2 were carried out with variations of exterior wall openings, floor partition openings, and number of floors under different temperature differences between inside and outside.

The theoretical value of the coefficient K' can be obtained as follows, assuming that the atmospheric pressure is 1 atm at ground level:

$$K' = \frac{P_o g}{R} \qquad (5.1.1)$$

$$= 3.47 \times 10^{3} \text{ K/m}$$

where

g = acceleration due to gravity (9.81 m/sec^2)

P_o = standard atmospheric pressure (101.3 KPa).

R = gas constant of air (286.8 J/Kg.deg C).

In all the test results, as represented in the figures, the values of the coefficient K' obtained from the experiments of both partitioned and non-partitioned cases are fairly constant and close to the calculated value from the theory given by Eq.5.1.1.

For the case with no internal floor partitions it is shown to be approximately equal 3.53×10^3 Pa.K/m. In the results from the case with internal floor partitions, it is shown to be about 3.50×10^3 Pa.K/m. The slight difference between both experimental results is believed to be mainly due to the different atmospheric pressure at the time of experiments.

The test results, as demonstrated above, show that the agreement between the theoretical and the experimental value of the coefficient K'is excellent in both cases.

From these results, it can be stated that the value of K' is not affected by the distributed patterns of exterior wall openings, the presence of floor partitions within the building, and the temperature difference between inside and outside.

It is also interesting to note that the behavior of the air movement in high-rise buildings is well predicted by the ideal gas equation of state, and that the assumptions applied in the derivation of Eq.3.2.20 are well justified.

The results presented in Fig.5.1.1 also agree well with the finding in the measurement in an actual building reported by Lee et al.[4] with respect to Eq.3.2.20, which

showed that the value of K' is consistent, and neither affected by the temperature differences across the exterior wall nor by the wall opening distributions.

From these results, consequently, we may conclude that for the case with uniform temperature distributions with height of building the thermal effect equation, Eq.3.2.22, can be used with great confidence to determine the pressure differentials across the exterior wall induced by thermal effect if the neutral pressure level (NPL) is known.

In the present study, the validity of the thermal effect equation for the case with non-uniform distributions of air temperature with elevation is also attempted.

In theory, as presented in Section 3.2 of Chapter III, the pressure differentials due to thermal effect having a non-uniformity of temperature along the elevation is believed to be determined from Eq.3.2.24 or Eq.3.2.26 depending on the temperature environment of the air.

In the developments of Eqs.3.2.24 and 3.2.26, both the profiles of the inside and outside temperatures of air are assumed to be linear along the elevation.

In the present study, the validity of the thermal effect equation, Eq.3.2.24, which is for the particular case with non-uniform temperature distributions of the air inside only, is examined by using the experimental results.

For the purpose of testing the validity of the thermal effect equation for this particular case, the computed pressure differentials across the exterior wall, which is

from Eq.3.2.24 using the value of the neutral pressure level obtained from experiment, are compared with the pressure differentials across the exterior wall measured from the experiments.

Fig.5.1.3 presents an example of the test results compared with the computed pressure differentials from Eq.3.2.24 for the case with non-uniform temperature distributions of the air inside only along the height, in which the temperature difference between inside and outside air with elevations is given as $\Delta T(z) = 30.0 + 3.3z$ (°C/m) and $T_o(z) = 283.0$ K.

Fig.5.1.4 illustrates another test result for the case with the reversed temperature profile of Fig.5.1.3, in which the temperature difference between the inside and outside air with elevations is $\Delta T(z)=90.0 - 3.3z$ (°C/m) and $T_o(z)=283.0$ K.

Fig.5.1.5 presents the test result obtained from the experiments using the test section with four floor levels having sufficiently large floor partition opening in each floor separations.

Fig.5.1.6 illustrates an other example of the test results obtained from the test section with two floors having sufficiently large opening in the floor partition. In both figures, Figs.5.1.5 and 5.1.6, the temperature difference between inside and outside with elevations is $\Delta T(z)=30.0 + 3.3z$ (°C/m) under constant outside air temperature which is

$T_o(z)$=283.0 K.

As shown in all the test results, it can be seen that the agreements between experiment and theory are fairly good in all the cases investigated. Consequently, it leads us to conclude that Eq.3.2.29 can be applied to determine the pressure differentials across the exterior wall due to thermal effect having this particular type of temperature profile.

5.2 THERMAL EFFECT IN BUILDING WITH NO FLOOR PARTITIONS AND UNIFORM TEMPERATURE DISTRIBUTIONS.

5.2.1 Effect of Exterior Wall Opening Distributions

In buildings with construction of negligibly small resistance to flow within the inside, as stated earlier, it could be expected that the total pressure forces induced by the thermal effect may be mainly distributed along exterior wall openings.

As a result, the profile of the pressure differentials across the exterior wall due to thermal effect is believed to be affected by the distribution of the exterior wall openings in the building along the height.

In the present study, the relationship of the profile of pressure differentials across the exterior wall with the distribution of the exterior wall openings along the elevation is examined for the building of the type described above in both experiment and analysis.

In the experimental study, the distribution of the pressure differentials across the exterior wall with elevations are measured for a wide range of temperature differences with variation of distributions of the exterior wall openings using the test section with no internal floor partitions, which is presented in Fig.4.1.2 of Chapter IV.

Figs. 5.2.1 to 5.2.3 represent the examples of the results showing the pressure profiles obtained from these experiments using the test section with no floor partitions.

In the experiments, the variation of the exterior openings distribution along the height are achieved by opening or closing the opening holes installed in the test section in the vertical direction according to the predetermined sequence and procedures.

Fig.5.2.1 represents the profiles of the pressure differentials across the exterior wall which are measured from the experiments having a temperature difference of 60 °C between inside and outside of the test section with variations of distributed patterns of exterior wall openings in the test section.

Figs. 5.2.2 and 5.2.3 illustrate another examples of the profiles pressure differentials obtained with the temperature differences of 40°C and 25°C, respectively.

As can be found in the figures, these results indicate distinctively that under the imposed temperature difference between inside and outside, the profiles of the pressure differentials across the exterior wall due to thermal effect

appear to be affected significantly by the distribution of the exterior wall openings along the elevation.

In the results, in addition, one can observe that the location of the neutral pressure level in this type of building clearly depends on how the exterior wall openings are distributed along the elevation, whereas the slope or gradient of the pressure profile is constant for a given temperature difference.

To examine the accuracy of the present analytical model for this type of building, the profiles of the pressure differentials across the exterior wall with elevations are also calculated from the model shown in Section 3.3.1 of Chapter III by applying the identical experimental conditions.

The examples of the computed results from the numerical model are presented in Figs. 5.2.4 to 5.2.6, in which the results are compared to the corresponding experimental.

Fig.5.2.4 illustrates the comparison of the pressure differential profiles obtained from the present model with the experiment for the case with four vertical distribution of exterior wall openings.

Figs. 5.2.5 and 5.2.6 represent other examples of the comparison of the computed pressure profile from the analytical model with the experiments for different distribution of exterior wall opening in the test section.

No comparisons, except for the cases with openings at top and bottom, of the present results with ASHRAE recommendation are possible since ASHRAE has provided only the information only for the case with openings at the top and bottom.As can be seen from the figures, the analytical and experimental results show an excellent agreement in all the cases studied.

Consequently, it can be said that the accuracy of the numerical solution from the present model is satisfactory and reasonable. In the analytical results, it is also revealed that the pressure profiles and the location of the neutral pressure level are strongly influenced by the patterns of the distributions of the exterior wall openings.

From the present results, we may conclude that for the building of construction having small resistance to air flow inside, the profiles of the pressure differentials across the exterior wall due to thermal effect and the location of the neutral pressure level mainly depend upon the distributed patterns of the exterior wall openings in the vertical direction as well as the resistance to the induced flow imposed by the exterior wall openings.

It also can be seen that in this particular type of building, the prediction of the pressure profile due to the thermal effect requires advanced knowledge of the distributed patterns of the exterior wall openings as well as the characteristics of the openings.

5.2.2 Effect of Temperature Difference across Exterior Wall

As discussed in Section 5.1, the thermal effect equation, Eq.3.2.20, has shown that the pressure differentials across the exterior wall due to thermal effect are proportional to the difference of the reciprocal of absolute temperature difference between inside and outside of the building.

To investigate the effect of temperature difference on the patterns and profiles of the pressure differentials across the exterior wall, the measurements of the pressure differentials along the height of the test section are conducted with variations of temperature differences for the given distributed pattern of the exterior wall openings in the test section.

In the experiments for this purpose, the temperature differences across the wall of the test section are varied from 25 C to 60°C (25, 30, 40, 50, 60).

Figs. 5.2.7 to 5.2.10 represents the examples of the results obtained from these experiment and analysis.

In the figures, the pressure differentials across the exterior wall with elevations are plotted against temperature differences across the exterior wall under given distributed exterior wall opening pattern.

Fig.5.2.7 illustrates the result for the case with uniform distributions of exterior wall openings in the test section vertically. Figs. 5.2.8 to 5.2.10 present other examples of the pressure profiles obtained from the cases

with different temperature differences as well as different exterior wall opening arrangements.

For the purpose of testing the accuracy of the present model for this case, the profiles of the pressure differentials across the exterior wall are also calculated from the analytical model by applying the identical set of data imposed in the experiments. The calculated results are represented in the corresponding figures as shown in Figs. 5.2.7 through 5.2.10.

From the examination of Figs. 5.2.7 to 5.2.10, it can be seen that the agreements between the computed results from the present model and the experimental results are fairly close in all the cases investigated. Furthermore, it confirms again that the accuracy of the present analytical model for all the cases is reasonable and satisfactory, including the basic assumptions employed.

In the results presented in the figures, one can observe an important characteristic of the thermal effect in the building which should be noted. The characteristic is that the neutral pressure level (NPL) in this particular type of building construction is shown to be hardly affected by the temperature difference across the exterior wall but influenced mainly by the distributed patterns of the exterior wall openings along the elevation.

Fig.5.2.10 illustrates a typical test result of the particular case having a single exterior wall opening at the top level only, which is a good illustration of the accuracy

of the experimental procedures taken.

In all experiments executed, this important characteristic of the pressure profile due to thermal effect is employed as the accuracy testing criteria for the experimental procedures, the performance of test sections, and the pressure transducers installed in the test section. This requirements were also fulfilled in all the experimental cases investigated in the present study.

5.2.3 Neutral Pressure Level (NPL)

Since the pressure differences across the exterior wall can be computed from Eq.3.2.20 as long as the correct value of the neutral pressure level is known, the neutral pressure level can be the most useful parameter in characterizing the thermal effect in the buildings. Therefore, it is desirable to find a reliable method to predict the neutral pressure level for the different building construction and environment.

In the results demonstrated in Sections 5.2.1 and 5.2.2, it has been found that for the building having uniform temperature distributions along the height and negligibly small resistance to flow inside, the neutral pressure level is significantly influenced by the distributed patterns of exterior wall openings but almost independent of the temperature difference between the inside and the outside of the building.

As stated earlier, Eq.3.4.9 is proposed to determine the neutral pressure level for this particular type of building analytically. To evaluate the accuracy and dependability of the method presented in the present model, which is shown as Eq.3.4.9, a series of tests are carried out for various cases.

Typical results of the tests executed for the purpose are presented in Fig.5.2.11 to Fig.5.2.13, in which $[NPL-NPL_{(exp)}]/NPL_{(exp)} \times 100$ is plotted against temperature difference for different pattern of exterior wall openings since the neutral pressure level already appears to be invariant.

Fig.5.2.11 shows the comparison of the neutral pressure level for the case with uniform exterior wall openings along the elevation. Figs. 5.2.12 and 5.2.13 represent other examples of the comparisons for different exterior wall openings.

As can be seen in the figures, it has been shown that the agreement between the present model shown as Eq.3.4.9 and the experimental results are excellent in all cases illustrated, in which the maximum deviation between both results is less than 5.0 %. Consequently, it has been demonstrated again that the present analytical model developed in Section 3.4 of Chapter III is dependable and satisfactory.

5.2.4 Characteristics and Behavior of Thermal Effect in Buildings with Uniform Temperature Distributions and No Internal Floor Partitions

It has been shown in the previous discussion that the pressure differentials due to the thermal effect can be determined directly from the thermal effect equations by knowing the value of NPL for given state of building construction and environment.

Hence, it is obvious that the thermal effect in building can be represented by the characterization of NPL in actual states for practical purposes.

In the previous discussion, it has been shown that our analytical model, Eq.3.4.9, appears to be in excellent agreement with experimental results and to be a reasonable method to predict NPL. Hence, we can apply the present model confidently to study the characteristics and behavior of the thermal effect in the building.

In the present study, a series of analyses are carried out to investigate the attributes and behaviour of the thermal effect with variations of pertinent parameters by using the model of Eq.3.4.9 for the building having negligibly small resistance to flow within the inside.

Fig.5.2.14 illustrates the relationship of the NPL with the temperature differences across the exterior wall for various distributed patterns of exterior wall openings.

In the figure, it confirms again that the NPL appears to be almost independent of the temperature differences but appears only to depend upon the distributed patterns of the exterior wall openings with elevations. In the figure, the results of the experiments are also presented with the analytical results.

This observation on the characteristics of NPL presented in Fig.5.2.14 is consistent with the field test result reported by Tamura [5] and a previous study by the present author [10].

Consequently, it can be deduced that to predict the thermal effect for the building having insignificant internal flow resistance under given temperature difference, the correct information on the distributed patterns as well as the characteristics of the exterior wall openings is required.

Another attempt to investigate the relationship of the physical dimensions of the building with thermal effect is conducted with the present model. Fig.5.2.15 illustrates the effect of the building height or the vertical dimensions of the building on the NPL obtained from the present analysis.

In the figure, the ratio of the NPL to building height, NPL/H, is plotted against the ratio of building height to the reference height of the test section used in experiments (18.3 m), H^*.

The tests are done for various distribution of exterior wall openings. In the results, the NPL appears to be hardly affected by the physical dimension of the building in the vertical direction for all the cases studied as presented in the figure.

Fig.5.2.16 illustrates an example of the analytical result where only the opening hole at the bottom or top level of building is varied whereas the other exterior openings are kept constant at the initial condition.

In the figure, the ratio of the NPL to building height, NPL/H, is plotted against the ratio of the opening hole area, at the bottom or the top level, to the original total exterior wall opening area in the exterior wall, A_{wb}^*, or A_{wt}^*, respectively.

The result shows that the relative magnitude of a single opening at the bottom, or the top level to the total opening area appears to have strong effect on the location of the NPL depending on its magnitude comparable to others. As A_{wb}^*, or A_{wt}^* increases, NPL/H shifts down or up rapidly as shown in the figure.

It indicates that when A_{wb}^* or A_{wt}^* is 60 or over the NPL reaches at the bottom or top exterior wall opening level. From this result, it can be deduced that, if the exterior wall opening existing at the bottom or the top level for this particular type of building is significantly larger than others, the pressure differential profile across the exterior wall due to thermal effect could be identical

to that of the case with a single exterior wall opening at bottom or top level only.

5.2.4 Effect of Ventilation on Thermal Effect

The air infiltration or leakage into the building, as mentioned earlier, is the direct result of the pressure differentials across the exterior envelope caused by thermal effect, wind and the mechanical ventilation within building.

In the results obtained from field measurements of the pressure differentials in the actual buildings, the thermal effect is found to be a major factor in air infiltration in the heating season [1, 2, 4, 5, 6].

In high-rise or multi-story buildings, in general, the operation of the mechanical ventilation is shown to have a pressurization or depressurization effect on the existing pressure distributions within building. Depending on its applied pattern, it may result in shifting down or up the neutral pressure level, and decrease or increase in the pressure difference across the exterior wall at the corresponding levels [5, 6].

It is also generally assumed that the pressure force induced by mechanical ventilation is linearly additive to the pressure difference due to the thermal effect for estimation of the total pressure force resulting in infiltration in the building.

This effect of mechanical ventilation on the profiles of pressure differentials induced by the thermal effect is observed in field measurements of pressures in actual buildings by Tamura et al. [5, 6].

In the present study, a series of experiments were conducted to investigate the effect of mechanical ventilation on the profiles of the pressure differentials across the exterior wall induced by the thermal effect in a building with no internal floor partitions.

The experiments for this purpose were performed by using the testing apparatus presented in Fig.4.1.1. The experiments evaluating the effect of ventilation were conducted after achieving a predetermined temperature difference across the test section wall uniformly with height to produce the pressure profiles due to the thermal effect.

Subsequent to achieving the designated temperature differences with height, the pressure differentials across the exterior wall of the test section with elevations induced by thermal effect are measured for given distributed wall opening patterns without operation of the ventilation system.

Following the procedure stated above, new pressure measurements are then conducted with operation of the mechanical ventilation system supplying or exhausting air into or out of the test section space. In the experiments, the effect of the mechanical ventilation on the pressure

profile due to thermal effect only is carried out by supplying air into, or by exhausting air from, the test section space inside with operations of the mechanical ventilation system shown in Fig.4.1.5. The flow rate of air supplied or exhausted into or out of the test section space by the ventilation system are varied from 0.47 to 2.82 L/hr, which is the proper rate for the test.

In the process of all the experimental measurements of investigating the mechanical ventilation, there are no apparent observation of adverse experimental conditions, such as disturbances, or disruptions of pressure differential profiles, and temperature distributions along the elevations of the test section due to the operations of the mechanical ventilation system.

This is believed to result from the fact that the rate of air flow supplied into or exhausted out of the test section space is negligibly small compared to the volume of the test section, so that it takes more than three hours to accomplish one air change with the usual experimental conditions imposed.

Figs.5.2.17 to 5.2.18 illustrate the typical examples of results obtained from the experiments investigating the effect of the mechanical ventilation on the pressure profile due to the thermal effect only.

Fig.5.2.17 presents the experimental results obtained for the case with openings at the top and the bottom level only under temperature difference of 60°C.

Fig.5.2.18 illustrates other examples of the experimental results having four exterior wall openings along height.

In all the results presented in the figures, as expected, the operation of the mechanical ventilation system has resulted in a pressurization or depressurization effect on the pressure differential profiles across the exterior wall due to thermal effect only, depending upon the imposed ventilation mode of excess supply or exhaust of air.

By supplying excess air into the inside space of the test section, it has been shown that the effect of pressurization of inside space appears at all elevations uniformly, and results in the corresponding decrease and increase of pressure differentials across the exterior wall with elevations. In the figures, it can be seen that shifting down of the neutral pressure level and the pressure profile depend on the amount of the air supplied into the test section.

Conversely, it shows that when the air within the test section is discharged out by the blower in excess of supply, the effect of uniform depressurization with elevations is observed, which shows exactly the opposite result of the case above.

From the results shown in Fig.5.2.17, it is important to note that the magnitude of shifting the pressure profile and the NPL due to supply or exhaust of air appears to be not linearly proportional to the air flow rate supplied or

exhausted.

This can be explained from the functional relationship of the flow rate with the pressure difference acting on the flow paths, which depends on the characteristics of the flow as well as the opening.

The comparison of Fig.5.2.17 and Fig.5.2.18 can be a good illustration of this particular case. As can be seen in the figures, the case with openings at the top and the bottom only has resulted in a larger pressurization or depressurization for the same air flow rate than the case having four exterior wall openings along height. This is believed to result from the different opening characteristic of the building.

This result can be explained obviously from the fact that, as the enclosure of the building has more opening wall holes, therefore, it would have a reduced effect on the resulting pressure profile due to the mechanical ventilation since it has more leakage areas.

Fig.5.2.19 shows an example of the experimental results representing the effect of mechanical ventilation on the thermal effect in the case with four exterior wall openings with elevations.

In the figure, the profiles of the pressure differentials obtained from different temperature difference as well as different patterns of mechanical ventilation are compared.

The mechanical ventilation, as shown in the figure, resulted in pressurization or depressurization on the pressure profile for all different temperature difference. The resulting pattern of the pressure profile, which is pressurized or depressurized, is shown only to depend on the ventilation mode applied for the test section space. The same trends are observed in all other experiments for the cases having different exterior wall opening patterns.

In this particular result, it should be noted that the gradient of the pressure differential profile with elevation is consistent for a given temperature difference in spite of the fact that there is the effect of mechanical ventilation causing pressurization or depressurization on the building space.

In the study, the effect of applying position of mechanical ventilation on the pressure profile due to thermal effect only is also investigated.

The study for this purpose is carried out by supplying air into, or by exhausting air from the test section either at the top or at the bottom of the test section as shown in Fig.4.1.5.

Since the thermal effect results in an upward flow in the building inside, it is possible to assume that the profile of pressure differentials along elevations resulting from thermal effect plus mechanical ventilation may be affected by the position at which the mechanical ventilation is applied.

The air supplying into the heated building space at the top by mechanical ventilation is in opposite flow direction to the air flow due to thermal effect within building, in which the supplied air flow by the ventilation would be in a " counter flow " with that of the thermal effect.

On the other hand, the air exhausting from the heated building space at top by the mechanical ventilation is in the same direction with the air flow within the building resulted from thermal effect, in which the exhausting air flow by the ventilation would be be in a " parallel flow " with that of the thermal effect.

Hence, it can be expected that the resultant profile of the pressure differentials across the exterior wall from both mechanical ventilation and thermal effect may be affected by the pattern of the air flow applied into the building space by mechanical ventilation.

In Figs. 5.2.17 and 5.2.18, the profiles of the pressure differentials which result from mechanical ventilation of different applied position are shown, in which the mechanical ventilation is applied either at the top or at the bottom of the test section.

Fig.5.2.20 shows the effect of position of application of mechanical ventilation on the pressure differentials along the height due to thermal effect only for the case having four exterior wall openings with height and temperature difference of 60 °C.

In the figure, the pressure difference between the absolute pressure differential of the ventilation plus thermal effect, $| P_{vs} |$, and the absolute pressure differential with the thermal effect only, $| P_s |$, at the corresponding elevation, is plotted against height of the test section for different air flow rate of the ventilaion.

From the result shown in Fig.5.2.19, it can be seen that there appears to be some effect of the position of application of the ventilation on the resultant pressure profile, especially in the counter flow mode, ranging from -0.6 to 0.8 Pa.

However, due to small magnitudes of the resulting difference above, the overall effect of the position of application of mechanical ventilation appears to be the corresponding elevation, is plotted against height of the test section for different air flow rate of the ventilation.

From the results presented in Figs. 5.2.17 to 5.2.19, it has been shown that, for the range of the parameters studied, the pressure differentials induced by the mechanical ventilation appears to be almost linearly additive to the pressure differentials due to thermal effect only if the pressure imposed by the mechanical ventilation is applied uniformly on the building space.

The results described above can be interpreted from straightforward logic, in that the resulting internal pressure of any confined space due to the external source, such as mechanical ventilation, depends upon the

characteristic of the openings existing in the enclosures as well as the distribution of the pressure across the exterior enclosure.

Since there are no disturbances of the exterior pressure due to external sources, such as due to wind, and the mechanical ventilation is applied uniformly into the test section space in the present experiment, the pressure difference across the exterior wall in the building should be the direct result of the thermal effect plus the mechanical ventilation applied, depending on the characteristic of the exterior wall openings.

Consequently, it can be concluded that the variation of the profile of the pressure differentials across the exterior wall due to both thermal effect and the mechanical ventilation is related directly to the opening characteristics as well as the applied pattern of mechanical ventilation.

5.3 Thermal Effect in Building with Internal Floor Partitions and Uniform Temperature Distributions

5.3.1 Effect of Internal Floor Partitions

In the previous discussion, we only considered the effect of the resistance to flow due to the exterior wall openings on pressure differences across the exterior wall. This was based on the basic assumption that the internal resistance to air movement within inside is negligibly small

due to the presence of sufficient interconnections between floor separations.

However, the real multi-story or high-rise buildings are neither completely open nor air tight between floor partitions. Hence, it is obvious that for more realistic and accurate prediction of the characteristic and behavior of the thermal effect, the effect of the flow resistance or the permeability of air flow within the building on the resulting profiles of pressure differentials across the exterior wall should be interpreted correctly.

For the solution for this type of problem, therefore, it is desirable to find a parameter which can represent a relative permeability of air flow or relative resistance to air flow between the building components existing in the exterior envelopes and the floor separations.

In the present study, in both experiment and analysis, the relative magnitude of the resistance to air flow in the floor partitions to that of the exterior walls are characterized with the ratio of the opening hole area existing in the floor separation (A_p) to the opening hole area existing in the exterior wall for each floor (A_w), A_p^*. Thus, the resistance to flow imposed by the floor separations is represented by the multitudes of A_w in the results obtained.

To investigate the effect of the internal floor partitions on the pressure differential due to the thermal

effect, the measurements of the pressure differentials across the exterior wall with elevations are carried out over various temperature differences and different arrangements of the opening holes in the exterior wall and floor partitions by using the partitioned test section described in Fig.4.1.10 of Chapter IV.

Fig.5.3.1 illustrates an example of the profile of pressure differentials across the exterior wall obtained from the experiment of the case with two floors.

In this experiment, the height of each floor level is made to be 7.2 m by removing the partitions installed at H_1 and H_3 position and using the cassette plate with no hole at H_4 in Fig.4.1.10 to magnify the pressure drop across the floor separation at H_2 position.

As shown in Fig.5.3.1, the pressure difference across the floor partition, appears to decrease gradually as the floor opening is increased more than the exterior wall openings at each floor. In the experiments, the value of A_p^* is varied from 0.1 to 1.5 by interchanging the cassette plate at H_2 position of the figure with the one having different opening diameter.

For a very small value of A_p^*, as expected, the pressure difference across floor partition increases significantly due to the increased resistance to air flow in the floor partition. Correspondingly, the thermal effect in each floor appeared to be less affected by other floors.

The analytical result obtained from the present model for this case shows that the agreement with experimental results is shown to be excellent at all values of A_p^*.

Fig.5.3.2 shows another example of the experimental and analytical results obtained for the case with four floors. In this study, the height of each floor level is made to be 3.6 m, and the floor partition at H_4 in Fig.4.1.10 is closed by installing the cassette plate with no opening hole.

In the figure, the pressure differential profiles across the exterior wall with elevations are represented in terms of the ratio of A_p/A_w as in Fig.5.3.1 for given temperature and exterior wall opening pattern.

Fig.5.3.3 presents another example of the study result which was conducted for a case with a different variation in the distribution of the floor openings with height from the case shown in Fig.5.3.2. In this experiment, the floor opening at the position H_1 is varied only while the others are kept constant as $A_p^* = 10.0$ for the same conditions of temperature and exterior opening pattern shown in Fig.5.3.2. In the figure, the analytical result for this case is also presented together.

From the examination of Figs. 5.3.1 to Fig.5.3.3, we can observe distinctively the effect of the relative magnitude of flow resistance of floor opening to exterior wall openings on the profile of pressure differential across the exterior wall along elevations, and that the effect can

be predicted analytically.

As the ratio of the floor opening area to the exterior wall opening area increase, in both experimental and analytical results, the pressure difference across floor separations decreased correspondingly, and at a sufficiently large value of A_p^*, the profile of pressure differentials with height finally appears to form of a straight line along height regardless of the presence of the floor separations.

Since the pressure differential across enclosures of the building should be related closely with the characteristics of the openings existing on it, the variation of the pressure differential profiles, which are illustrated in Figs.5.3.1 to 5.3.3 corresponding to the value of A_p^*, are obvious and coincide with that anticipated in advance in the analysis of Chapter III.

With reduced resistance to flow between floor separations, the thermal effect in each floor is shown to be influenced mutually due to increased upward air movement from lower floor to floor above, and finally the pressure profile develops the same pattern of the non-partitioned building presented in Section 5.2.

As shown in the figures, it can be seen that for the case with sufficiently large value of A_p^*, the profiles of the pressure differentials across the exterior wall are shown to be governed solely by the distributed pattern of

the exterior wall openings with height.

Conversely, it shows that if the resistance to flow imposed by the floor separations is substantial compared to that of the exterior wall openings, the resulting profile of pressure differential across the exterior wall would be " the story type " as shown in Fig.3.1.5, in which the thermal effect in each floor appears to be independent from others due to significant resistance between floors.

In this particular case, the thermal effect in each floor acts independently, and hence each floor has its own particular NPL corresponding to the distributed pattern of exterior wall openings at the floor level, and results in a smaller pressure differentials across the exterior wall.

For the prediction of the thermal effect, consequently, in the types of building constructions with floor partitions, it is very important to have correct knowledge of the relative magnitude of resistance to flow of floor separations to the exterior openings at each floor as well as the distributed patterns of the exterior walls along the elevation.

In the results shown in Fig 5.3.3, another interesting example of the thermal effect in a building having different arrangement of floor partition openings with elevation can be found.

In this particular example, as shown in the figures, the floor opening at position of H_1 is varied only from A_p^* = 0.25 to 10.0 while the others are kept at A_p^* =10.0.

As the floor opening area at the floor separation at H_1 position decreases, the pressure drop across the floor increases correspondingly. Hence, it results in a reduced pressure differential across the exterior wall at the floor level.

With this particular type of floor opening arrangement in the floor separations, the bottom floor appears to be split from the upper levels due to the increased resistance to air flow at the H_1 position.

The result, presented in Fig.5.3.3, shows that with increased air tightness of a specific floor separation, the interaction of the thermal effect at the corresponding floor from others can be reduced.

In the results presented in Figs.5.3.1 to 5.3.3, it is worthwhile to note that the profile of the pressure differential is consistent for the given temperature difference in all cases despite the presence of the floor partitions with height. This characteristic of the thermal effect is mentioned in the discussion of the validity test of the thermal effect equations in Section 5.1.

In addition, the results presented in the figures also confirm that the accuracy of the numerical method of the present model for this type of thermal effect analysis is quite feasible and reasonable in all the cases studied.

5.3.2 Effect of Temperature Difference

From the previous discussions, one can realize that, for the building with no floor partitions, the pressure differentials across the exterior wall due to thermal effect, are shown to be proportional to the difference of the reciprocal of absolute inside and outside temperature for the given value of the neutral pressure level.

Furthermore, it has been shown that, for this particular type of building, the neutral pressure level appeared to be invariant with the temperature difference, while it is strongly affected by the distributed patterns of the exterior wall openings.

However, information about the effect of temperature difference on the thermal effect in buildings with floor partitions is little available.

In the present study, the investigation of the effect of temperature difference across the exterior wall on the pressure profiles in the building with floor partitions is conducted in both experiment and analysis.

A series of experiments for this purpose are carried out for various ranges of temperature differences with different arrangements of exterior and interior floor openings, as well as the number of floors by using the test section described in Fig.4.1.10.

Figs.5.3.4 to 5.3.7 represent typical examples of these experimental results. In the figures, the analytical results obtained from the present model are also presented together and compared.

In the results, it can be found that, for the cases with floor partitions, the pressure differentials across the exterior wall due to thermal effect are also proportional to the reciprocal of absolute temperature differences between the inside and the outside for given opening arrangements.

In addition, it represents that the neutral pressure level for the provided opening conditions appears to be not affected by the temperature differences. This observation exactly coincide with the characteristics of the thermal effect in the building with no internal floor partitions presented in Section 5.2.

Consequently, it can be concluded from these results that, for the floor partitioned type of building, the profiles of pressure differentials across the exterior wall, are mainly governed by the characteristics of the openings involved in the induced flow by thermal effect, and the effect of the temperature difference on the thermal effect in this particular building has a similarity with that of the building without floor partitions.

5.3.3 Existence of Critical Ratio of Floor Opening Area to Exterior Wall Opening Area

As demonstrated earlier, the prediction of the profiles of the pressure differentials across exterior wall with elevations becomes more difficult when internal floor separations exert resistance to flow within the building.

Also it has been shown that, in the partitioned building, the pressure difference across the exterior wall has a functional relationship between the resistance to flow through exterior wall relative to that through the floor separations.

In the results shown in the previous section, the ratio, A_p^*, is presented to be an important parameter showing a significant effect on the resulting pressure differential profiles due to the thermal effect in the building with floor partitions.

As the value of A_p^* becomes sufficiently large, the profile of the pressure differential with elevation appears to have close similarity with that of the building with no partitions as if there were no floor separations with height.

Conversely, as the ratio of A_p^* decreases considerably, each floor, in effect, is shown to be an independent single story building at the situated levels, and the profile of the pressure differentials in the whole building appears to have a series of sharp turns between each floor separation.

Hence, it results in a considerably reduced pressure differences across the exterior wall at top and bottom level.

In the results, it has been shown that there exist a particular value of the ratio of A_p^*, which presents negligibly small pressure difference between the floor separations with elevations, and finally represents a straight pressure differential line from the top to the bottom elevations of the building for the given number of floor separations as well as distributed patterns of the exterior wall openings at each floor.

In dealing with the thermal effect in the building with floor partitions, the particular ratio of A_p^*, showing negligibly small pressure drop between the floors with elevations, could be a very convenient indicator in the analysis of the problems involved.

For this purpose, the parameter, P^*, is introduced in the study. The parameter, P^*, represents the ratio of pressure difference across a certain floor partition (ΔP_p) to the total pressure differential induced by the thermal effect at the corresponding floor (ΔP_s) for given floor height and temperature difference.

In doing so, a non-dimensional parameter, $A_{p\,crt}^{**}$, will be considered in the present study. The parameter is defined as the particular value of the ratio of A_p to A_w resulting in a value of P^* is less than 0.01 between floors with elevations of the building, is to be considered.

Hence, from the respective definitions above, it can be seen that, as the ratio of A_p^* approaches to $A_{p\,crt}^*$ for the corresponding floor numbers and distributed pattern of exterior wall opening at each floor, P^* becomes nearly zero and the profile of the pressure differentials across the exterior wall would be in the shape of straight line from top to the bottom of the building.

In this particular case, the profile of the pressure differentials across the exterior wall with elevations becomes identical to that of " the open shaft type building " as shown in Fig.3.1.4, in which the resulting pressure differential profile is mainly governed by the distributed patterns of exterior wall openings due to negligible resistance to flow within the building.

Conversely, when A_p^* becomes smaller than $A_{p\,crt}^*$, the pressure difference between the floors increases, and the resulting pressure profile with the building height has sharp turns at each floor separation as shown in Fig.5.3.2.

If the value of A_p^* is substantially smaller than $A_{p\,crt}^*$, the profiles of the pressure differentials across the exterior wall would be the same as that of " the story type building " as shown in Fig.3.1.5.

In the results presented in Figs.5.3.1 to 5.3.2, it has been shown that the value of $A_{p\,crt}^*$ has a functional relationship with the number of floors as well as the distributed patterns of the exterior wall openings at each

floor. Figs.5.3.1 to 5.3.3 show that, for the building with two and four levels, the values are shown to be 1.5 and 7.0, respectively.

The existence of the critical value of A_p^* in the pressure differential profile across the exterior wall in the building has very important significance in the understanding of the characteristics and behavior of the thermal effect in the high-rise buildings.

With the assumption that all the openings in each floor partitions as well as in the exterior wall elevations are identical in size and shape in the building, a correlation of the critical value of A_p^* to the number of floors for different distributed pattern of exterior wall openings in each floor is computed from the analytical model which is presented in Section 3.3.

The computational model for this analysis is made to handle the number of floors from 2 floors up to 30. In this analysis, the dimensions of exterior wall and floor openings and floor height of each floor are assumed to be the same as those of the test section shown in Fig.4.1.8.

Fig.5.3.8 illustrates the relationship of the critical value of A_p^* to the number of floors obtained from the present model. In the figure, the $A_{p\,crt}^*$ is plotted against the number of floors for different modes of exterior wall opening distributions at each floors.

As shown in the figure, the critical value of A_p^* increases gradually as the number of floors increases as expected.

The results also show that, depending on the distributed pattern of exterior wall openings at each floor, the critical value of A_p^* can vary for the given number of floor levels.

However, the critical value of A_p^* becomes almost asymptotic, reaching a certain limiting value for the given distributed pattern of exterior wall opening at each floor despite the number of floors increases.

From the thermal effect equation, Eq.3.2.20, it can be seen that, for the imposed temperature difference, the pressure difference across the exterior wall due to the thermal effect increases with height of building correspondingly. Hence, as the number of floors in the building become progressively higher, the pressure force induced by the thermal effect enlarges proportionally.

Also the serial resistance to air flow within the building, which is imposed by the floor separations, increases in proportion to the number of floors in the building. However, the resistance to flow within the building contributed by the series of floor partitions may not to be enlarged rapidly compared to the pressure force caused by the thermal effect for the imposed temperature difference and provided building height.

The limiting value of the critical value of A_p^* for the cases shown in Fig.5.3.8, is between 8 and 18, depending on the distributed pattern of the exterior wall openings at each floor. Based on this result, it can be said that, if the distribution and configuration of the openings in the exterior wall and floor separations at each floor with height in the buildings is identical to the cases shown in Fig.5.3.8, the critical value of A_p^* will not exceed more than 18 for any number of floors.

In the analysis made thus far for the characteristics of $A_{p\,crt}^*$, the openings existing in the exterior wall and floor partitions are assumed to be an orifice type opening as shown in Fig.4.1.8.

In addition, the floor openings in the floor separations within building are made to be a single orifice hole placed at the center of each floor cross section with elevations as illustrated in Fig.4.1.9.

In actual building constructions, it is well known that the crack openings in the floor separations are not placed in a single place, especially such as the elevator door cracks and service shaft cracks. In addition, these crack shapes, including exterior wall cracks, are usually shown to be in thin rectangular shapes in practice as shown in Fig.3.3.2.

Consequently, it is necessary to take account of the relationship of the shape as well as the number of the openings in the building components with the characteristics

of the critical value of A_p^*. These problems will be discussed in Section 5.6 later.

5.3.4 Characteristics of Thermal Effect in Partitioned Buildings.

Since it is known that the pressure differentials can be determined from the information on the neutral pressure level, as stated earlier, it is important to have complete understanding about the characteristics of the neutral pressure level for the accurate prediction of thermal effect in the building.

The characteristics and behavior of the neutral pressure level in the partitioned building are also investigated in the present study in both experiment and analysis.

Fig.5.3.9 illustrates an example of the result showing the effect of number of floors on the neutral pressure for the case in which A_p^* is greater than $A_{p\,crt}^*$.

In the figure, the ratio of NPL to building height, NPL/H, is plotted against number of floors. For this analysis, the height of each floor is made to be 3.6 m and the distributed exterior wall openings at each floor are made equal in size and shape as shown in Fig.4.1.8.

As shown in the figure, the neutral pressure level appears to be not affected by the number of floor separations for the cases if A_p^* is greater than $A_{p\,crt}^*$.

But the neutral pressure level for this particular case is shown to be influenced by the distributed modes of exterior wall openings at each floor.

Fig.5.3.10 illustrates another result presenting the effect of temperature difference across the wall on the neutral pressure level for the case with four floor levels, in which the ratio of NPL to building height, NPL/H, is plotted against temperature differences ranging from 10 to 60°C.

In the analysis, the distributed type of exterior wall openings at each floor is varied as shown in the figure. As can be seen in the figure, NPL is shown to be not affected by the temperature difference across the wall in all the cases studied.

This characteristic of the thermal effect is exactly identical with that of the case with no internal floor partition. Consequently, it can be concluded that, for the partitioned building, the neutral pressure level is also hardly affected by the temperature difference, and is mainly governed by the distributed patterns of the exterior wall openings as well as the floor openings.

Fig.5.3.11 represents an example of the analytical result showing the effect of enlargement of a single exterior wall opening placed at the bottom or top level shown in the figure while keeping the others unchanged.

In the figure, the ratio of NPL to building height is plotted against the ratio of the single opening hole area to

the original total exterior wall opening area formed by all exterior wall openings (A_{wtot}).

This example can be an interesting case for the thermal effect in actual buildings in which large top or bottom openings are exist in the building.

In the figure, the case I is the case of enlarging the bottom hole only, and the case II is the case of enlarging the top hole only, respectively. As can be seen in the figure, when the single hole at bottom or top level increases the neutral pressure level shift down or up rapidly.

For the extreme case, in which A_{wb}^{*} or A_{wt}^{*} is 60 or greater, the NPL is shown to be located at the elevation of the bottom or the top opening of the building as if the building had only one single opening at the corresponding elevation. The analysis is based on the assumption that the analytical model based on Eq.3.3.8 can be applicable.

5.4 EFFECT OF NON-UNIFORM TEMPERATURE DISTRIBUTIONS ON THERMAL EFFECT

In actual buildings, the patterns of the pressure differentials across the exterior wall with elevation and the induced air flow caused by the thermal effect are shown to be complex combinations of the components including the effect of the distributed pattern of the exterior wall openings, the resistance to flow of series of internal floor partitions, and the excess supply or exhaust air brought by the mechanical ventilation system.

These patterns of the air flow induced by the thermal effect are evident from the profiles and magnitudes of the pressure differentials across the exterior wall in the buildings which are presented in the previous discussions.

Considering the flow pattern of air within the building described above, it is probable to expect that the induced upward air flow or air current through various floor separations caused by thermal effect may result in an non-uniform distributions of the temperature with elevation within the building environment.

As a result, it can be estimated that this non-uniform distribution of inside air with elevations would have a certain effect on the patterns and profiles of the pressure differentials across the exterior wall due to thermal effect.

Thus far, with respect to the temperature distributions of inside and outside air, we have only applied the assumption that the temperature distributions of both outside and inside air are uniform along the height of the building. Hence, it is required to investigate the effect of this non-uniformity of temperature distributions on the thermal effect in the buildings.

In the present study, the investigation of the effect of non-uniform distribution of the inside air temperature on the pressure differential profiles resulting from the thermal effect are carried out by both experiment and analysis for the partitioned and non-partitioned building cases.

In the experiments, in both non-partitioned and partitioned test section model buildings, the temperature differences across the wall are made to have a linear distribution along the height, which is $\Delta T(z) = 30.0 + 3.3z$ ($^{\circ}C$) or $\Delta T(z)=90.0-3.3z$ ($^{\circ}C$) for the given outside air temperature conditions where the test section is situated.

5.4.1 Effect of Non-Uniform Temperature Distributions of Inside Air on Thermal Effect in Non-Partitioned Building

Fig.5.4.1 illustrates an example of the experimental results showing the pressure differential profiles across the exterior wall of the test section with elevations for different exterior wall opening arrangements under a non-uniform temperature distributions of inside air.

In these experiments, the temperature difference with height is made to increase with elevations, in which $\Delta T(z)=30.0+3.3z$ ($^{\circ}C$) for given outside air temperature as shown in the figure.

Fig.5.4.2 presents other examples of the experimental results showing the effect of non-uniform temperature distributions of inside wall in the non-partitioned building for various distributed patterns of exterior wall openings. In this specific case, the inside wall temperatures are made to decrease with elevations as shown in the figure, in which temperature difference is $\Delta T(z)=90.0-3.3z$ ($^{\circ}C$).

In Figs. 5.4.3 and 5.4.4, it can be found that the profile of the pressure differentials across the exterior wall with elevations is shown to be in the form of curves due to the non-uniformity of temperature difference with elevations.

However, it should be noted that the location of the neutral pressure level appears to depend upon the distributed pattern of the exterior wall openings while the curvature of the pressure profiles is consistent for the provide temperature profile in all the cases studied.

With application of the present analytical model, the effect of the temperature gradient of the inside wall on the profile of pressure differentials with elevations due to thermal effect are examined. Fig.5.4.5 illustrates an example of the result for the case with uniform distribution of exterior wall openings with elevation. In the analysis,

the temperature gradient of the inside wall is varied from 0.1 to 3.4^{o}C/m.

As can be seen in the figure the pressure differentials across the exterior wall increase as the temperature slope of inside air increases as expected, but the location of the neutral pressure level for a given pattern of exterior wall openings appears to be nearly independent of the temperature slope of the inside air.

It is interesting to note in this result that as temperature gradient b reduces, the profile of the pressure differentials across the exterior wall approaches to the linear shape. This is identical to that is observed in the results of the uniform temperature distributions with elevations, and is expected from the analytical solution.

Fig.5.4.6 illustrates another example of the analytical result representing the effect of the temperature slope of the inside air on the neutral pressure level for various exterior wall opening distributions.

In the analysis, the temperature difference between the inside and the outside with elevations, is assumed to be $\Delta T(z) = 30.0 + bz$. The slope of the inside temperature is varied from 0.0 to 4.0^{o}C/m while the outside temperature is kept constant. In the figure, the ratio of NPL to building height, NPL/H, for different patterns of exterior wall openings is plotted against the temperature slope of inside air.

The neutral pressure level appears to increase slightly initially as the temperature slope of the inside air increases for all different patterns of exterior wall openings, but it becomes almost asymptotic and constant beyond the temperature slope of $0.8^{\circ}C/m$ in all the cases studied as shown in the figure. For $b > 0.8^{\circ}C/m$, the neutral pressure level appears to be independent of the temperature difference across the exterior wall along the height, which is identical to the characteristics of the neutral pressure level observed in the cases having uniform temperature distributions with elevations.

Compared to the NPL of the case with uniform temperature distributions, the value of the NPL obtained from the non-uniform temperature distribution of the building inside has shown approximately 4.2 % higher value when b is over $0.8^{\circ}C/m$ in all the cases examined.

From observation of the result presented in Fig.5.4.6, we can conclude that the effect of the inside air temperature slope on the pressure differentials induced by the thermal effect appears to be marginal in the buildings with no partitions if the temperature slope of the inside air is less than $0.8^{\circ}C/m$ with elevations.

Fig.5.4.7 illustrates the analytical result showing the effect of the building height on the NPL with variations of exterior wall opening distributions. In the analysis, the temperature difference between the building inside and

outside is assumed to be $\Delta T(z) = 30.0 + 3.3\ z\ (^{o}C)$ with elevations.

In the figure, the ratio of NPL to building height, NPL/H, is plotted against the ratio of building height to the reference height of the test section which is 18.3 m.

This result exactly coincides with the characteristic of NPL observed in the previously discussed cases with uniform temperature distributions along the height.

5.4.2 Effect of Non-Uniform Temperature Distributions of Inside Wall on Thermal Effect in Building with Partitions

The effect of non-uniform temperature distributions of inside wall on the profile of pressure differential due to thermal effect in the buildings with floor partitions is investigated by both experiment and analysis.

For the experimental investigations, the test section with floor partitions which is presented in Fig.4.1.8 of Chapter IV is used. For the analytical studies, the model developed in Section 3.3 of Chapter III is applied.

Fig.5.4.8 illustrates an example of the pressure differential profiles across the exterior wall with elevation for the case of four floor levels with non-uniform temperature distributions of inside air.

In the experiment, the temperature profile of the inside air with height is made to be the same as the one shown in Fig.5.4.1, and the floor openings at each floor are varied by interchanging cassette plates with different

opening diameter.

As presented in the figure, it shows that as the ratio of floor opening area to the exterior wall opening area in each floor, A_p^*, increases, the pressure difference across floor separations reduces, and at sufficiently large value of A_p^*, the pressure curve becomes almost continuous from the top to the bottom of the test section.

It is also interesting to note from this result that the pressure differential curves of different A_p^* develop symmetrically at the mid-height of the test section as A_p^* increases while the curvature of the pressure differential line is consistent.

In this particular case, when A_p^* is 8.0, the pressure difference across floor separations appears to be negligible, and the profile of the pressure differentials with height becomes almost a continuous curve. To test the accuracy of the present model for this particular case, the corresponding analytical results are also presented in the figure together. The agreement between experiment and analysis is shown to be fairly close in all the cases as illustrated.

With applications of the present analytical model, the effect of non-uniformity of inside wall temperature distributions on the thermal effect in the floor partitioned buildings is examined further.

Fig.5.4.9 presents an example of the results showing the critical value of A_p^* for the case with non-uniform

distributions of inside air temperature with height for various of number of floors. In the analysis, the configurations of floor and exterior wall openings at each floor are assumed to be identical, and the profile of the temperature difference with elevations is made to be $\Delta T(z) = 30.0 + 3.3z$ (^{o}C). Also the height of each floor is assumed to be 3.6 m.

As illustrated in the figure, the critical value of A_p^* increases as the number of floor separations increases due to the effect of serial resistance to air flow within the building by the floor partitions. This is identical to what we observed in the results for the building with floor partitions having a uniform temperature difference along the height.

The resultant value of the critical value of A_p^* obtained from this case appears to be nearly the same as that of the partitioned building with uniform temperature distributions. From these results, it can be deduced that the effect of the non-uniform distributions of inside wall is shown to be insignificant on the critical value of A_p^*.

Figs.5.4.10 to 5.4.11 present the results showing the effect of the temperature slope of the inside wall on the pressure differential profile due to thermal effect for the different exterior opening distributions in the building with four floors.

In the analysis, the ratio of floor opening to the exterior wall opening at each floor (A_p^*) is made to be

greater than $A_{p\,crt}^{*}$ in all the cases, and the slope of inside wall temperature along elevations is varied from 0.1 to 3.4°C/m.

It can be seen in the figures that the pressure differentials increases as the temperature difference across exterior wall increases, and that the profile of pressure differentials with height becomes almost linear when the temperature slope of the inside wall reduces increasingly. These results coincide with the those found in the results of the thermal effect without partitions under non-uniform temperature distributions.

Applying the same conditions employed for the case in Fig.5.4.11, the study to examine the characteristics of the thermal effect in partitioned building under non-uniform distributions of inside air is extended further.

The results representing the effect of the temperature slope of the inside wall on the neutral pressure level for various distributed exterior openings are illustrated in Fig.5.4.12. In the figure, the ratio of NPL to building height, NPL/H, is plotted against the temperature slope of the inside wall with height.

In the figure, we can observe that the different distributed mode of exterior wall opening at each floor is shown to have its own distinctive location of the neutral pressure level for given floor opening condition.

It also shows that, as the temperature slope of the inside wall with elevation increases, the ratio of NPL to

building height, NPL/H, increase initially but becomes almost constant beyond b = 0.8 °C/m in all cases studied.

The effect of temperature slope of the inside wall on the NPL, which is shown above, is identical with that observed in the non-partitioned case discussed in the previous section. The values of NPL over b = 0.8 °C/m obtained from this case are shown to be approximately 4.2 % higher than that of the case having floor partitions with uniform temperature distribution.

Hence, if we consider this substantial magnitude of the limiting value of the temperature slope of the inside wall, resulting in 4.2 % of the relative difference with the NPL from uniform temperature distributions, it can be said that, in practice, the effect of non-uniform temperature distributions of inside wall on the neutral pressure level is marginal.

Fig.5.4.13 illustrates an example of the analytical result showing the effect of physical dimensions of the building on NPL can be found, in which NPL/H is plotted against the ratio of building height to the reference heightof the test section used, 18.3 m.

In the results presented in the figures, we can confirm again that the effect of physical dimensions, vertical, of

the building on the thermal effect is also shown to be negligibly small in the partitioned building under non-uniform temperature distributions of the inside wall with elevations alone.

Consequently, we can reconfirm from the analysis that the pressure differential profiles induced by the thermal effect in the building with floor separations is mainly governed by the distributed mode of the exterior wall openings as well as the openings in the floor separations including the number of floors even if it is under the effect of the non-uniform temperature distributions of inside wall with elevations.

5.4.3 Effect of Both Non-Uniform Temperature Distributions of Inside Wall and Outside Air with Elevations on Thermal Effect

In the present study, thus far, only the effect of the non-uniform distributions of the inside wall temperature with elevations of building on the pressure differential profiles due to the thermal effect is taken into consideration.

However, in real situations, it is possible that both the inside wall and outside air temperature may vary with elevations. As a result, it is worthwhile to examine the

effect of the non-uniform distributions of both the inside wall and outside air temperatures on the thermal effect in the buildings.

With applications of the present analytical model developed in Section 3.3 of Chapter III, the investigations for this purpose are carried out. Since the pressure differentials across the exterior wall at given elevations can be found from the thermal effect equations if the NPL is known, the analysis for this study is mainly done on the characteristics of the neutral pressure level under the effect of both non-uniform distributions of the inside wall and outside air temperatures.

Fig.5.4.14 illustrates a typical example of the analytical results obtained for the purpose mentioned previously for the case with floor partitions, in which A_p^* is greater than Ap^*_{crt}. In the figure, the ratio of NPL to building height, NPL/H, is plotted against the height of the building for given distributed pattern of exterior wall and floor opening at each floor. The profile of temperature distribution of both sides with height is assumed to be linear in the analysis and its respective profiles of temperature are indicated in the figure.

The analytical results obtained from four different profiles of temperature difference distributions along the building elevation are presented in the figure. Type I is the case with non-uniform temperature distributions of the inside wall only, type II is the case with uniform

temperature distribution of both the inside wall and outside air, type III is the case having linear increase of both the inside wall and outside air temperature with height, and type IV is the case in which outside air temperature is decreasing with height whereas the inside wall temperature is increasing with elevation, respectively.

In the results, as represented in the figure, we can observe that the case of type I, having non-uniform distributions of the inside wall alone, is shown to have higher value of NPL/H than others. Conversely, the case of type IV has appeared to give lower NPL/H than others.

As shown in the figure, the maximum difference between the highest and the lowest value of the NPL/H is shown to be less than 5.0 % in these particular results. The same trends are also observed in other cases with different distributed exterior wall opening patterns, and also in the case with no floor partitions.

Based on these results, we can obtain several interesting conclusions. First, the effect of non-uniform distributions of inside or outside air temperature with height is shown to be marginal on the value of NPL within practical ranges of temperature differences between the inside wall and outside air in the building.

Secondly, considering the substantial magnitudes of the assumed temperature slope of the outside air compared to the standard atmospheric air [30], which is less than $-0.01\ ^{\circ}C/m$, the actual temperature distribution of outside air may be

considered to be uniform in the problem analysis of the thermal effect in the high-rise buildings.

Finally, considering the magnitudes of the relative errors, as shown in the figure, between maximum and minimum values of the NPL under the effect of non-uniform distributions of the inside and outside air temperature, the effect of the non-uniform temperature distributions of the inside wall on the profiles of pressure differential due to thermal effect in the actual building environment also can be considered to be insignificant.

5.5 CALCULATION OF AIR-INFILTRATION OF THERMAL EFFECT

5.5.1 General Descriptions of Air Infiltration due to Thermal Effect

As stated earlier, the patterns of the pressure differentials across the exterior wall induced by the thermal effect in the actual buildings are shown to be dependent on the complicated interactions of the distributed patterns of exterior wall openings and floor openings in the internal floor separations as well as the temperature environment.

The patterns of the air flow induced by the thermal effect in the building enclosures are obviously evident from the profiles and magnitudes of the pressure differentials across the various building components represented in the previous discussions.

The amount of air infiltrated or exfiltrated through an opening hole existing in the building enclosures may be calculated on the basis of the total pressure difference across a crack opening hole which occurs from the air flow induced by the thermal effect.

As presented earlier, it has been shown that the method of calculating the air leakage or infiltration through building enclosure by using the pressure differences acting on the leakage path or component is known as the crack flow method which is expressed by:

$$Q = C\ (\Delta P)^n \qquad (5.5.1)$$

For the application of this method to determine the amount of flow through the opening, one can see that the correct information on the pressure differentials across the opening, the flow coefficient, C, and the flow exponent of the building enclosures is required.

However, it should be noted that the equation of the type shown in Eq.5.5.1 lacks generality because it is not dimensionally homogeneous. That is, it is in conflict with a fundamental law of fluid mechanics; Reynolds law of similitude. Therefore, the derived crack flow equation in the investigation for a specific case can only be valid for identical cases, and hence it has limitations in its

applications.

The total pressure drop across an opening hole occurring in the air flow due to the thermal effect in the building enclosure can be presented by the energy equations as illustrated in the analytical models discussed in Section 3.3 of Chapter III.

The total pressure difference across an opening hole in the induced air flow in the building enclosure is estimated to consist of four major components: form losses due to sudden contractions of flow area at the openings; the form losses due to sudden expansions of flow area at the openings; the friction loss due to inner surface of the openings

Hence, it can be written as

$$\Delta P_{total} = \Delta P_{fr} + \Delta P_{ent} + \Delta P_{ext} \qquad (5.5.2)$$

where

ΔP_{total} = total pressure difference across the opening.

ΔP_{fr} = friction loss due to inner surface

ΔP_{ent} = form losses due to sudden contractions at the opening.

ΔP_{ext} = form losses due to sudden expansions at the openings.

Applying the above respective descriptions for the total pressure differences across the opening, we have

$$\Delta P_{total} = \frac{1}{2}\rho v^2 [K_{ent} + K_{ext} + f\frac{L}{D}] \qquad (5.5.3)$$

As a result, from the above functional relationship of the pressure difference with the flow in Eq.5.5.3, one can see that the velocity of air flow through the opening hole can be expressed in terms of the total pressure drop as

$$v_h = \sqrt{[\frac{2}{\rho}\frac{1}{(K_{ent}+K_{ext}+f\frac{L}{D})}\Delta P_{total}]} \qquad (5.5.4)$$

Consequently, it can be found that the velocity of air flow through the opening hole can be calculated if the total pressure differentials across the opening hole as well as the characteristics of the opening hole are both known.

As demonstrated in the previous discussions, it has been shown that the analytical models, developed in Section 3.3 of Chapter III, are shown to be reliable and accurate to calculate the pressure differentials across the openings due to thermal effect for various temperature distributions, for different types of distributed patterns of exterior wall openings as well as for different building floor constructions.

Furthermore, the thermal effect equations, presented in Chapter III, are also proved through experimental tests to be a method to determine the pressure differentials across the exterior wall induced by thermal effect if the value of NPL is known accurately.

Also it has been shown that the characteristics of the the thermal effect in the building could be characterized by the NPL, which has been extensively investigated for various types of building environment and constructions in the present study.

Consequently, it can be seen that the velocity of the air flow through the opening hole induced by the thermal effect can be determined since the pressure differentials due to thermal effect acting on the flow path can be found from the present analytical model for given characteristics of the opening.

Hence, with knowledge of the air flow velocity, the amount of air infiltration through an opening hole can be calculated by continuity relation at the corresponding opening as

$$Q_h = V_h A_h \tag{5.5.5}$$

where

Q_h = amount of air flow through the opening (m^3/sec).

V_h = velocity of air flow through the opening (m/sec).

A_h = area of the opening hole (m^2).

If a building is considered as having a certain porosity with overall leakiness, then the total flow balance for the building can be expressed as

$$\int_{in} QdA = \int_{out} QdA \tag{5.5.6}$$

where

$\int_{in} QdA$ = sum of air flow into the building

$\int_{out} Q_{out}$ = sum of air flow out of the building

Since the openings placed below NPL induce infiltration and the openings placed above NPL experience exfiltration, the total air flow balance can be also represented as

$$\sum_{i=1}^{N} (C \Delta P^n)_i = \sum_{j=1}^{M} (C \Delta P^n)_j \tag{5.5.7}$$

where

i = openings below NPL

j= openings above NPL

N= total number of openings below NPL

M= total number of openings above NPL

5.5.2 Correlation of Air Infiltration Calculation due to Thermal Effect

As mentioned earlier, it has been shown that, the pressure differentials across the opening hole due to thermal effect can be determined from the present model,

developed previously, for different types of building construction and temperature profiles. In addition, the pressure differentials across the opening holes in the test sections are also measured experimentally for various cases.

Consequently, using the pressure differentials obtained from the above procedures, it is possible to determine the amount of air flow through the opening holes from the numerical method presented in Section 5.5.1.

Since the amount of air flow and the pressure differentials across the opening hole are available, we can proceed to correlate the crack flow equation, Eq.5.5.1, with the pressure differences and air flow rate through the opening hole.

By re-writing the crack flow equation, Eq.5.5.1, in the logarithmic representation, we have

$$\mathrm{Ln}(Q_h) = \mathrm{Ln}(\ C\ ) + n\ \mathrm{Ln}(\Delta P) \qquad (5.5.8)$$

Since the amount of air infiltration through the opening hole, Q_h, and the pressure differentials across the hole are known, the plot of a logarithmic linear graphic representation for different flow rate and pressure differentials is possible. Therefore, it is straightforward to find the value of the flow coefficient, C, and the flow exponent, n.

A computer program has been formulated to calculate the numerical values of the flow coefficient and the flow exponent for different types of building construction, which is the partitioned cases and the non-partitioned cases, with variations of the characteristics of the opening holes.

In the computations, the pressure differentials across the opening hole due to thermal effect are varied from 5.0 to 30 Pa, which are the pressure differences measured at the temperature differences between 25 and 60°C by using the test sections in the present study.

In the analysis, the characteristics of the opening hole are represented as the ratio of the opening hole length to opening hole diameter, L/D, which is varied from 0.5 to 300.0 in the computations.

Fig.5.5.1 illustrates an example of the correlated result for the cases with no internal floor partitions. In the figure, two different types of exterior wall opening patterns are compared.

For the case with openings at top and bottom level only, the correlated equation is shown to be;

$$Q_h = 3.02\times10^{-6}(\Delta P)^{0.81} \qquad (5.5.9)$$

For the case with four openings in vertical

$$Q_h = 3.43\times10^{-6}(\Delta P)^{0.53} \qquad (5.5.10)$$

In the figure, the case having four exterior wall openings with elevation is shown to have a larger value of flow coefficient and a smaller value of flow exponent than that of the case having openings at the top and the bottom only, due to the increased number of opening holes per unit wall area.

Fig.5.5.2 presents another example of the correlated result of the pressure differentials across the opening hole with the flow rate for the cases with internal floor partitions.

In this analysis, the value of A_p^* is taken to be greater than $A_{p\,crt}^*$ for given conditions, having the same distributed pattern of exterior wall openings at each floor. In the figure, the results of the two cases, of two floors and of four floors, are compared.

The correlated equations of both cases are shown to be almost identical even though there is a difference in the number of floor partitions since the value of A_p^* for the partitioned case is greater than $A_{p\,crt}^*$.

Fig.5.5.3 illustrates a result representing the effect of floor separations on the correlated equation of the pressure difference with the flow rate. In this figure, the case without floor partitions is compared to the case with two floor partitions having identical exterior opening mode.

The correlated equation for the case with no floor partitions appears to have a significantly larger value of C than that of the case without partition, whereas the flow patterns in both cases are quite similar.

The result shown in the figure indicates that the flow coefficient is related to the pressure differences as well as the characteristics of the openings representing the resistance to flow in the building enclosure.

As stated earlier, the correlated equations presented in Figs.5.5.1 to 5.5.3 are valid only for buildings with identical characteristics of the openings as the model buildings of the present study.

The study to examine the relationship of the opening hole characteristics with the flow coefficient, C, and the flow exponent, n, have been carried out for both partitioned and non-partitioned cases with variations of the ratio of hole length to hole diameter. In the analysis, for the partitioned cases, the A_p^* is made to be greater than $A_{p\,crt}^*$ for the corresponding floor number and exterior opening distributions.

Fig.5.5.4 shows an example of the results showing the relationship of the flow exponent, n, with the ratio of the opening hole length to opening hole diameter, L/D, for the case with no floor partitions. Fig.5.5.5 illustrates another example of the results obtained for the case with floor partitions.

The flow exponent, n, increases as the ratio of L/D increases. Also the value of the flow exponent is shown to vary from 0.5 to 1.0 as expected from the theoretical point of view, relating the flow rate to the pressure drop in the flow path. This also agrees with the range of the flow exponent, n, in ASHRAE HANDBOOK [10].

It is interesting to note in Fig.5.5.4 that, for the case with four exterior wall openings along the elevation, the flow exponent, n, increases much slower than for the case with openings at top and bottom only as the ratio of L/D increases.

This illustrates a good example showing the relationship of the flow exponent to the resistance to flow. Since the case with four exterior openings has less flow resistance than the latter, the effect of increased ratio of L/D appears to be less sensitive initially.

Fig.5.5.5 represents another result showing the effect of opening characteristics on the flow exponent for partitioned cases.

In the figure, both cases of two floor partitions and four floor partitions are compared.

It can be found in the figure that, for the partitioned cases, the effect of increasing the ratio of L/D on the flow exponent appears to be slight difference in both cases, even though there exists a difference of floor numbers. However, the value of the flow exponent, n, is between 0.5 and 1.0 as shown in Fig.5.5.5.

The relationship of the flow coefficient, C, with the opening hole characteristic is also investigated for both partitioned and non-partitioned cases. In the analysis, the same conditions employed in the study of the flow exponent are applied.

Fig.5.5.6 presents an example of the result showing the relationship of the flow coefficient, C, with the ratio of L/D for the cases with no floor partitions.

The minimum value of the flow coefficient, C, is supposed to be zero, which can be the case with no opening hole in the enclosures for sufficiently large value of L/D. In this result, the maximum value of the flow for the case is shown to be 19.53 x 10^{-6} $m^3/s.Pa^n$ for very small value of L/D.

In the comparisons of both cases in the figure, it can seen that the effect of the ratio of L/D on the flow coefficient appears to be affected by the characteristic of the openings existing in the wall, which implies the relationship of the flow coefficient with the flow resistance.

In the figure, it also shows that, for the case with four exterior wall openings, the flow coefficient appears to be reduced less slowly initially than in the case with top and bottom openings only.

Fig.5.5.7 illustrates another example of the result showing the relationship of the flow coefficient with the ratio of L/D for the case with partitions. In this result,

it can be found that the maximum value of the flow coefficient, C, is approximately 9.5×10^{-6} $m^3/s.Pa^n$, and is shown to be significantly lower than that of the case with no floor partitions due to the effect of the floor partitions.

It also show that the effect of the opening characteristics on the flow coefficient, C, is almost identical in both case due to the existence of floor partitions.

From the overview of the present study results, it can be seen that the calculation of air infiltration due to thermal effect is possible from the crack flow equation, Eq.5.5.1, by applying the pressure differences obtained from the present study.

Moreover, the present result has shown that the analysis of the relationship of the flow coefficient, C, and flow exponent, n, with the various types of opening characteristics provides an insight on the characteristic of air infiltration due to thermal effect in the building. However, the equations, 5.5.9 and 5.5.10, are only valid for a specific case having the identical opening characteristics presented in the present study.

5.6 APPLICATION OF PRESENT STUDY

5.6.1 A Parametric Study applied to a Large Model Building

As presented previously, the analysis of the thermal effect in the building, thus far, is made only for the cases of the simple models, and these results have been evaluated through the experimental observations of the idealized model buildings.

Since the analytical models developed in the present study have been shown to be reliable and accurate, it is possible to extend its application for the analysis of the thermal effect in actual buildings.

In the construction of actual buildings, it is well known that the crack openings in the floor separations are not situated in a single place like the model building used in the present study. Furthermore, the configuration of the crack openings, including the exterior wall openings, are usually shown to be in thin rectangular shapes in effect, as presented in Fig.3.3.2.

Consequently, it is necessary to conduct the present analysis of the thermal effect in the building by taking account of the opening condition pointed out above as well as by applying the data of actual building dimensions.

As the first part of these analyses, the concept of the equivalent opening diameter, which is shown in Eq.3.3.10, is applied for the exterior wall and floor partition openings

in the computation of the pressure profile using the present analytical model. In the analysis, the floor height and area are made to be 3.6 m and 50 m x 50 m, respectively, to simulate actual buildings.

Fig.5.6.1 presents the analytical result showing the effect of the crack opening shape on the value of $A_{p\,crt}^{*}$. In the figure, the value of $A_{p\,crt}^{*}$ is plotted against the number of floors for two different types of distributed pattern of exterior wall openings at each floor.

In the results, it can be seen that the effect of the configuration of crack openings on the value of $A_{p\,crt}^{*}$ appears not to be significant in all the cases studied, and the overall trends in the analysis are almost identical to the result presented previously in Section 5.3.

In actual buildings, the crack openings in the floor separations, such as the elevator and stairway door cracks, the cracks in the various service shafts, etc., are neither situated in one place nor existed as one single opening in any floor partition. As a result, these opening conditions described above should be included in the analysis.

Fig.5.6.2 shows an example of the analytical result presenting the effect of dividing the single floor opening into multi-holes on the value of $A_{p\,crt}^{*}$ for the cases of having two floors and four floors.

In the analysis, the number of floor openings per floor partition, which is assumed to be the same in the shape and the dimensions at each floor, is varied from 1 to 25 for the

different number of floors. In this analysis, the total opening area occupied by the holes in each floor separation is kept constant and the same as the $A_p{}^*_{crt}$ for the case having one single floor opening.

As shown in the figure, the value of $A_p{}^*_{crt}$ increases gradually as the number of floor opening in a floor separation increases. This is believed to result from the increased resistance to flow in the floor partition by dividing the $A_p{}^*_{crt}$ of the single hole case into multi-openings.

Fig.5.6.3 presents other examples of the analytical result showing the effect of dividing the floor opening in each floor separation into multi-holes on the value of $A_p{}^*_{crt}$ for a building, in which the fractions of floor opening at each floor partition, $A_n{}^*$, is varied from 1 to 10 for different number of floor levels as shown in the figure.

In the analysis, the floor height, the floor dimensions, and the floor opening length of the building are made to be 3.6 m, 25 m x 40 m, and 200 mm, respectively. Also the equivalent diameter and the crack length of the exterior wall openings are assumed to be 2.0 mm and 75.0 mm. The dimensions and configuration of the openings, and the floor plan of the building are made to be similar to Building C which is shown in Table 5.6.1.

As shown in the figure, it can be seen that by dividing one single floor opening into multi-openings at each floor, the value of $A_p{}^*_{crt}$ is increased. The results indicate that

the value of $A_p^*{}_{crt}$ is increased much more than that of the case with one floor opening, shown in Fig.5.3.15, due to the extended length of floor crack opening as well as the effect of dividing the floor opening at each floor into multi-openings. The figure also shows that the value of $A_p^*{}_{crt}$ increases asymptotically as the number of floors increases for different value of A_n^*. For the case of twenty floors, the value of $A_p^*{}_{crt}$ is shown to be from 32 to 43 depending on the A_n^*.

5.6.2 Application of Present Analysis to Actual Buildings

The profile of the pressure differentials due to thermal effect is obtained from the present analytical model for several real buildings listed in Table.5.6.1. In the analysis, the data shown in Table.5.6.1 are applied. The results of these analyses are presented in Figs.5.6.4 to 5.6.6.

Fig.5.6.4 shows the result for Building A of Table.5.6.1, which is a compartmentalized residence building for students in the University of Ottawa. In the figure, the present result is compared with the experimental test result by Lee et al [4].

In Fig.5.6.5, the present analytical result for Building E which is a nine story government office building in Ottawa, listed in Table.5.6.1, is presented with the field test result by Tamura and Wilson [5]. Fig.5.6.6 shows

the present analysis for Building C which is a seventeen story government office building, listed in Table.5.6.6.

As can be seen in the figures, the profile of the pressure differentials from the present analysis appears to be linear along the elevations for all the buildings analyzed. In addition, as has been shown in Figs.5.6.4 to 5.6.5, the pressure profile of the present result appears to be quite close to that of the measured result for the actual buildings.

These results can be explained from the fact that in actual buildings, as can be seen in Table.5.6.1, there exist a large number of various cracks which interconnect the air flow within the building between floors.

As shown previously, the profile and distribution of the pressure differentials along height in the building having floor partitions are shown to be closely related with the relative magnitude of resistance to flow in the exterior wall opening to the resistance to flow in the floor separations.

The results shown in Fig.5.6.3 indicates that the maximum value of $A_p^*{}_{crt}$ is not greater than 45 for the cases investigated. As shown in Table.5.6.1, it can be seen that even if one single door crack of the elevator alone is considered in the actual buildings, the value of A_p^* is significantly greater that the value of $A_p^*{}_{crt}$ presented above.

From the overview of the results shown above, one can conclude that the effect of the floor separations on the pressure profile due to the thermal effect is negligibly small because of sufficient interconnections between floors which are formed by various cracks in the floor partition, such as the elevator doors and shafts, the stairways and stair shafts, the exhaust air ducts, and the various service shafts.

Moreover, it has been shown that the analytical model presented in the present study can accurately predict the thermal effect in actual buildings.

CHAPTER VI

CONCLUDING REMARKS

In the present study, the characteristics and behaviors of the thermal effect in high-rise buildings are investigated both analytically and experimentally. From the present study results, the following major conclusions can be drawn:

(1) Validity of Thermal Effect Equations

The thermal effect equations for different temperature distributions of air along the building elevation are derived from the assumption that the air in the building environment can be considered in a static state, and the assumption that the air can be modelled from the equation of state of ideal gas.

Through experimental tests using model buildings, the thermal effect equations have been shown to be valid for determining the pressure differentials across the exterior wall with elevations due to thermal effect if the neutral pressure level is known correctly.

(2) Significance of Neutral Pressure Level in prediction of the Thermal Effect

Since the thermal effect equations are shown to be reliable to estimate the pressure differentials across the exterior wall of the building induced by thermal effect as long as the neutral pressure level is provided accurately, it has been shown that the thermal effect in the buildings can be characterized with the neutral pressure level for various different types of building constructions and temperature differences.

(3) Effect of Temperature Differences Across Exterior Wall on Thermal Effect

The pressure differentials across the exterior wall due to the thermal effect are shown to be proportional to the reciprocals of the absolute temperature differences between inside and outside of the building.

However, the temperature difference between inside and outside appears to have little influence on the neutral pressure level in all the cases investigated.

(4) Effect of A Non-Uniform Distribution of Inside Wall Temperature with Elevation

In the present study results, it has been found that the distribution and profile of the pressure differentials

across the exterior wall with elevation depend on the distributed pattern of the air temperature inside and outside with elevation.

However, the present result has shown that the effect of a non-uniform distribution of the temperature of the building inside on the neutral pressure level appears to be not significant within the practical range of temperature in actual building environments.

(5) Profiles of Pressure Differentials Across the Exterior Wall Induced by Thermal Effect

The present study result has been shown that the thermal effect in the high-rise buildings can be categorized into the two distinctive types depending on the relative magnitudes of resistance to flow in the exterior enclosures to the resistance to flow within the building: the case of " open shaft type " in which the pressure profile has no sharp turns along the elevation due to the negligible effect of floor separation, and the case of the " story type " in which the thermal effect in each floor appears to act independently, resulting in the pressure profile having a sharp turn along the elevation due to the effect of floor separations.

In the case of the " open shaft type ", the profile of pressure differentials across the exterior wall has been shown to be mainly affected by the distributed pattern of

the exterior wall openings with elevations.

In the second case of the " story type ", the profile of the pressure differentials has been shown to be dependent on the relative magnitude of the resistance to flow in the exterior wall openings to that in the openings of the interior floor separations.

In the extreme case, which has significant resistance to flow in the floor separations compared to that in the exterior enclosures, the profile of the pressure differentials along height are shown to be a discontinued type between floor levels, and it has resulted in the reduction of pressure differences across the exterior wall correspondingly.

The study result has shown that, for this particular type of building construction, the thermal effect can be characterized with a non-dimensional parameter, A_p^*, which represents the relative resistance to flow in the exterior openings to the resistance to flow imposed by the openings in the floor separations which are consisted of the cracks of the various shafts, service ducts, and etc., within the building.

The result has also presented that, in this type of building, there exists the critical value of A_p^* representing the particular value of A_p^*, resulting in a negligible pressure drop between floor separations for given distributed patterns of exterior wall openings per floor as well as the floor numbers.

The study result has been shown that the value of $A_{p\,crt}^{*}$ appears to be dependent on the number of floor and the distributed pattern of exterior wall openings at each floor.

(6) Effect of Mechanical Ventilation on Thermal Effect

The effect of mechanical ventilation on the thermal effect has been investigated in the present study experimentally.

The investigated result has been shown that the mechanical ventilation results in the effect of pressurization or depressurization on the profile of pressure differentials across the exterior wall due to the thermal effect depending on the applied pattern of the ventilation. The result has also shown that, if the mechanical ventilation is applied uniformly into the building space, the pressure profile appears to be shifted uniformly along elevation depending on the applied pattern of the ventilation.

In the present study results, it has been shown that the position of applying mechanical ventilation into the building space, which supplies or exhausts the air into or out of the building space, appears to result in a negligible effect on the profile and distribution of the pressure differentials along elevation due to thermal effect plus mechanical ventilation.

(7) Effect of Physical Dimensions of Building on Thermal Effect

In the study results, it has been shown that the effect of the physical dimensions of building, lateral or vertical, appears to be not significant on the profile and distributions of the pressure differentials induced by the thermal effect.

(8) Estimation of Air Intiltration due to Thermal Effect

The present study result has been shown that the air infiltration due to the thermal effect can be estimated with the crack method. The results obtained from the crack method have shown that the flow coefficient, C, and the flow exponent, n, appear to have a functional relationship with the distributed patterns of the exterior wall openings as well as the opening characteristics in the floor separations.

It has also been shown that if the characteristics of the openings in the building are identical to that of the present model, the air infiltration due to thermal effect can be calculated from the present method presented here by knowing the pressure differentials.

(9) Significance of Present Study Results in Engineering Practice

The following important conclusions may be drawn from the present study results in the view points of engineering applications:

a) The pressure differentials due to the thermal effect can be computed by applying the energy equations to the flow paths in the building enclosures, and that the present analytical models developed from the energy equations is accurate and reliable.

b) The pressure differentials due to thermal effect in the building can be estimated accurately from the thermal effect equation if the correct information on the neutral pressure level is available.

c) The effect of resistance to air flow in actual buildings, which is imposed by the floor separations, is shown to be negligibly small on the profiles of the pressure differentials across the exterior wall induced by the thermal effect due to sufficient interconnections between floors provided by various shafts and cracks.

In the results, it has been shown that even one single elevator door crack in the existing buildings can provide sufficient opening area to result in negligible pressure difference between floors.

d) The pressure differences of the mechanical ventilation and the thermal effect in the building appear to be linearly additive if the mechanical ventilation is introduced uniformly along the elevation on the entire building space.

e) Since the effect of floor separations on the pressure differentials due to thermal effect is shown to be insignificant, the profile of pressure differentials with elevations due to thermal effect in the actual buildings could be considered as the one which is observed in " the open shaft type building ".

Therefore, the distribution of the pressure differentials across the exterior envelope due to the thermal effect are estimated to be mainly dependent on the distributed pattern of the exterior wall openings with elevations in the building.

f) For the building having airtightness between floor separations, the pressure differentials due to thermal effect across the exterior wall becomes small.

However, for the building having sufficient interconnections between floor separations, the pressure differentials across the exterior wall due to thermal effect is larger than that of the case above. In this particular type of building, the pressure difference induced by the thermal effect can be one of the major force resulting in air infiltration.

REFERENCES

1. P. W. O'Callaghan, Building from Energy Conservation, Pergamon Press, Oxford, ch.1, 1978.

2. George L. Smith," Air Leakage due to Stack Effect in Multi-Story Buildings ", ASHRAE Journal, p.73, July, 1958.

3. R. E. Barret and D. W. Locklin," Computer Analysis of Stack Effect in High-Rise Buildings ", ASHRAE Transactions,Vo1.74, part.II, p.155, 1968.

4. Y. Lee, H. Tanaka and C. Y. Shaw," Distribution of Wind and Temperature Induced Pressure Differences across the Walls of Twenty Story Compartmentrized Building ", Journal of Wind Engineering and Industrial Aerodynamics, Vo1.10, p.287, 1982.

5. G. T. Tamura and A. G. Wilson," Pressure Differences for a Nine Story Building as Result of Chimney Effects and Ventilation System Operation ", ASHRAE Transactions, Vo1.72, pt.I, p.180, 1966.

6. G. T. Tamura and A. G. Wilson," Pressure Differences Caused by Chimney Effect in Three High Buildings", ASHRAE Transactions, Vo1.73, pt.II, 1982.

7. T. C. Min," Winter Infiltration through Swinging Door Entrance in Muti-Story Building ", ASHVE Transactions, Vo1.64, p.421, 1958.

8. C. Y. Shaw," Air Tightness and Air Infiltration of School Buildings", ASHRAE Transactions, Vo1.85, p.85, 1979.

9. ASHRAE," 1981 HANDBOOK of FUNDMENTALS ", Chap.22, ASHRAE, 1981.

10. K. H. Lee," Thermal Effect of High-Rise Buildings ", Thesis of Master of Applied Science, Dept. of Mech. Eng., Univ. of Ottawa, 1983.

11. C. M. Hunt," Air Infiltration: A Review of Some Existing Measurement Techniques and Data ", ASTM STP 719, p.3, ASTM, 1980.

12. Max H. Sherman and D. T. Grimsurd," Infiltration Pressurization Correlation: Simplified Physical Modelling ", ASHRAE Transactions, Vol.86, pt. II, 1980.

13. P. L. Lagus, " Air-leakage Measurement by Tracer Dilution Method - A Review ", Building Air Exchange Rate and Infiltration Measurements, ASTM STP 719, p.36-49, ASTM, 1980.

14. J. R. Sasaki and A. G. Wilson," Air Leakage Values for Residential Windows ", ASHRAE Transactions, Vol.71, pt. II, 1965.

15. G. T. Tamura and C. Y. Shaw," Studies on Exterior Wall Air Tightness and Air Infiltration of Tall Buildings ", ASHRAE Transactions, Vol.82, pt. I, 1976.

16. J. E. Jansen, T. J. Hill and A. N. Pearman," Calculating Infiltration : An Examination of Handbook Models ", ASHRAE Transactions, pt.II, 1980

17. D. R. Bahnfleth, T. D. Moseley and W. S. Harris," Comparison of Variables Affecting Infiltration ", ASHAE Transactions, Vol.63, p.453, 1957

18. Y. Lee, T. H. Liang, and H. Tanaka, " Non-linearity of Pressure Differentials Induced by Wind and Mechanical Ventilation ", Journal of Wind Engineering and Industrial Aerodynamics, p.47-58, 15(1983).

19. J. E. Hill and T. Kusuda," Dynamic Charateristics of Air Infiltration ", ASHRAE Transactions, Vol.81, pt.I, p.168, 1975.

20. G. T. Tamura and A. G. Wilson," Building Pressures Caused by Chimney Action and Mechanical Ventilation ", ASHRAE Transactions, Vol.73, pt.II, 1967.

21. C. Y. Shaw and G. T. Tamura," The Calculation of Air Infiltration Rates by Wind and Stack Action for Tall Buildings ", ASHRAE Transactions, Vol.83, pt.2, p.145, 1977.

22. G. T. Tamura and A. G. Wilson," Building Pressures Caused by Chimney Action and Mechanical Ventilation ", ASHRAE Transactions, Vol.73, pt.II, 1967.

23. C. Y. Shaw, D. M. Sander and G. T. Tamura," Air Leakage Measurements of the Exterior Walls of Tall Buildings ", ASHRAE Transactions, Vol.79, pt.11, p.40, 1973.

24. A. K. Blomsterberg and D. T. Harrje," Approaches to Evaluation of Air Infiltration Energy Losses in

Buildings ", ASHRAE Transactions, Vol.85, pt.I, p. 797, 1979.

25. C. Y. Shaw," A Correlation between Air Infiltration and Air Tightness for Houses in A Developed Residential Area ", ASHRAE Transactions, Vol.87, pt.II, p.333, 1981.

26. G. T. Tamura," Studies on Exterior Wall Air Tightness and Air Infiltration of Tall Buildings ", ASHRAE Transactions, Vol.82, pt. I, 1976.

27. Warren M. Rohsenow and H. Y. Choi," Heat, Mass and Momentum Trasfer ", ch.4, Prentice-Hall, Inc., 1961.

28. Curtis F. Gerald, " Applied Numerical Analysis ", 3rd.ed. Ch.2, Addison-Wesley Publishing Company, 1984.

29. Kailash C. Goel," Effect of Free Stream Turbulent on Fluid Flow and Heat Transfer ", Thesis of Master of Applied Science, Dept. of Mech. Eng., University of Ottawa, 1972.

30. The U. S. Standard Atmosphere, U. S. Government Printing Office, 1962, p.10-14, Washington D.C., U. S. A.

31. W. M. Kays, " Loss Coefficients for Abrupt Changes in Flow Cross Section with Low Reynolds Number Flow in Single and Multiple Tube System ", ASME Transactions, Vol.72, p.1067-1074, 1950.

32. D. W. Etheridge, " Crack Flow Equations and Scale Effect ", Building and Environment, Vol.12, p.181-189, Pergamon Press, 1977.

33. P. Lagus, A. K. Persily, " A Review of Tracer Gas Techniques for Measuring Airflows in Buildings ", ASHRAE Transactions, Vol.91, pt.2, 1985.

34. Joel E. Peterson, " Estimating Air Infiltration into House ", ASHRAE Journal, January, p.60-62, 1979.

35. ASTM, " Standard Practice for Measuring Air Leakage Rate by the Tracer Dilution Method ", ASTM E741-83, ASTM.

36. C. Y. Shaw," The Calculation of House Infiltration Rates ", ASHRAE Transactions, Vol.85, pt.I, p.58, 1979.

37. H. Tanaka, K. H. Lee. and Y. Lee," The Influence of Non-Uniform Temperature Distribution on Stack Effect ", Proceedings of 10th CANCAM, University of Western Ontario, June 2-7, 1985.

38. H. D. Ross," Significance of Air Infiltration on

Building Energy Conservation Design, Standards, and Codes ", ASTM STP 719, Building Air change Rate and Infiltration Measurements, p.153, 1980.

39. P. E. Condon, D. T. Grimsurd, M. H. Sherman, and R. C. Kammerud," An Automated Controlled-flow Air Infiltration Measurement System ", Building Air Change Rate and Infiltration Measurements, ASTM STP 719, p.60, 1980.

40. V. W. Goldschmidt, R. G. Leonard, J. E. Ball and D. R. Wilhelm," Wintertime Infiltration Rates in Mobile Homes ", Building Air Change Rate and Infiltration Measurements, ASTM STP 719, p.107, 1980.

41. W. G. Brown, A. G. Wilson and K. R. Solvason," Heat and Moisture Flow through Openings by Convection ", ASHRAE Journal, September, p.49, 1963.

42. R. C. Jordan, G. A. Erickson and R. R. Leonard, " Infiltration Measurements in Two Research Houses ", ASHRAE Transactions, Vol.69, p.344, 1963.

43. Frank W. Sinden," Wind, Teprerature and Natural Ventilation - Theoretical Considerations ", Energy and Buildings, p.275-280, 1(1977/78).

44. ASTM," Standard Practice for Measuring Air Leakage by Fan-Pressurization Method ", ASTM E779-81, ASTM.

45. ASTM," Standard Practice for Field Measurement of Air Leakage through Installed Exterior Windows and Doors ', ASTM E783-81, ASTM.

46. H. Feustel, CH. Zuercher, R. Diamond, B. Dickinson, D. Grimsud and R. Lipschutz, " Temperature and Wind Induced Air Flow Patterns in a Staircase - Computer Modelling and Experimental Verification ", Energy and Buildings, p.105-122, 8(1985).

47. Frank W. Sinden," Multi-Chamber Theory of Air Infiltration ", Building and Environment, Vol.13, p.21, Pergamon Press, 1978, U. K.

48. G. T. Tamura," Measurement of Air Leakage Characteristics of House Enclosures ", ASHRAE Transactions, Vol.81, Pt.I, p.202, 1975.

49. R. K. Beach," Relative Tightness of New Housing in the Ottawa Area ", Division of Building Research Report 149, NRC, Canada, 1979.

50. C. W. Coblentz and P. R. Achenbach," Field Measurements of Air Infiltration in Ten Electrically Heated Houses ", ASHRAE Transactions, Vol.60,p.358,

1963.

51. F. S. Wang, Sr., and C. F. Sepsy," Field Studies of Air Tightness of Residential Buildings ", ASTM STP 719, ASTM, p.24, 1980.

52. S. Uvslokk," Field Verification of Air Infiltration Model Used in the Computer Program ENCORE ", ASHRAE Transactions, Vol.89, pt.2B, p.149, 1983.

53. G. T. Tamura and C. Y. Shaw," Air Leakage Data for the Design of Elevator and Stair Shaft Pressurization Systems ", ASHRAE Transactions, Vol.82, pt.2, p.179, 1976.

54. J. P. Cockroft and P. Robertson," Ventilation of an Enclosure through a Single Openings ", Building and Environment, Vol.11, p.29, Pergamon Press, 1976.

55. G. T. Tamura," Computer Analysis of Smoke Movement in Tall Building ", ASHRAE Transactions, Vol.75, pt.II, p.81, 1969.

56. A. G. Wilson," Influence of the House on Chimney Effect ", ASHRAE Journal, Vol.2, No.12, December, 1960.

57. C. P. Crall," Development of Air Infiltration Model for the Energy Performance Design System ", ASHRAE Transactions, Vol.89, pt.2B, p.201, 1983.

58. M. P. Modera, M. H. Sherman and P. A. Levin," A Detailed Examination of the LBL Infiltration Model Using the Mobile Infiltration Test Unit ", ASHRAE Transactions, Vol.89, pt.2B, p.157, 1983.

59. D. M. Sander and G. T. Tamura," A FORTRAN IV Program to Simulate Air Movement in Multi-Storey Buildings ", Division of Building Research Computer Program No.35, NRC, Canada, 1973.

60. R. R. Laschober and J. H. Hearly," Statistical Analysis of Air Leakagee in Split-Level Residence ", ASHRAE Transactions, Vol.70, p.364, 1964.

61. D. W. Etheridge and J. A. Nolan," Ventilation Measurement at Model Scale in a Turbulent Flow ", Building and Environment, Vol.14, p.53, Pergamon Press, U.K., 1979.

62. M. W. Liddament," The Air Infiltration Center's Program of Model Validation ", ASHRAE Trransactions, Vol.89, pt. 2B, p.129, 1983.

63. B. H. Jennings and J. A. Armstrong," Ventilation Theory and Practice ", ASHRAE Transactions, Vol.77,

pt.I, p.50, 1971.

64. D. T. Grimsurd, M. H. Sherman, R. C. Diamond, P. E. Condon, and A. H. Rosenfeld," Infiltration-Pressurization Correlations: Detailed Measurements on a California House ", ASHRAE Transactions, Vol.85, pt.I, p.851, 1979.

65. A. K. Persily and G. T. Lintris," A Comparison of Measured and Predicted Infiltration Rates ", ASHRAE Transactions, Vol.89, pt.2B, p.183, 1983.

66. A. Marin," Influence of Stack Effect on the Heat Loss in Tall Buildings ", ASHRAE Transactions, Vol.40, p.377, 1934.

67. D. W. Etheridge and D. K. Alexander," The British Gas Multicell Model for Calculating Ventilation ", ASHRAE Transactions, Vol.80, pt.II, p.808, 1980.

68. John R. Taylor," The study of Uncertainties in Physical Measurements", University Science Books, Mill Valley, California, 1981.

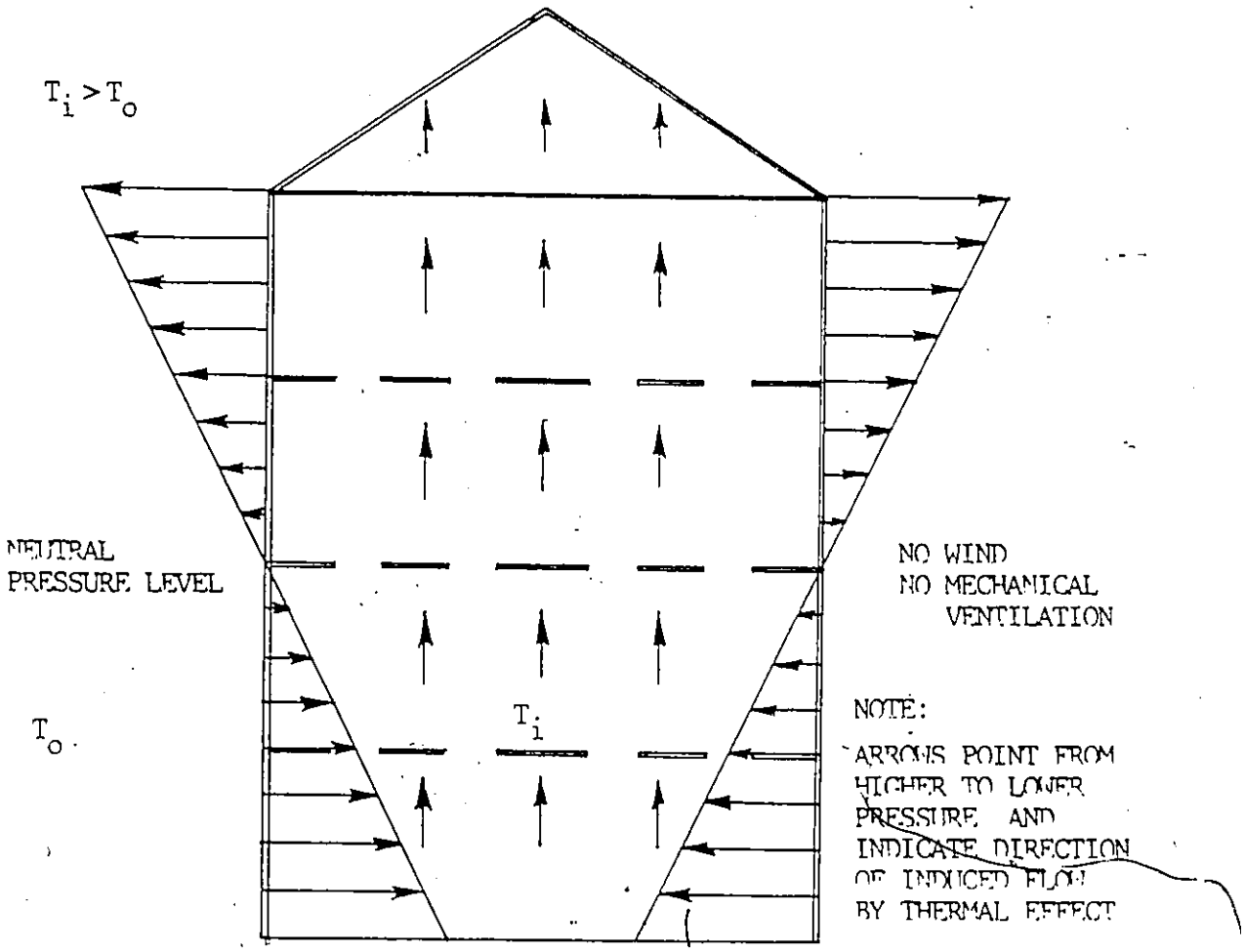

Fig.1.1 Pressure Difference Across Wall caused by Thermal Effect for a Typical Building Structure

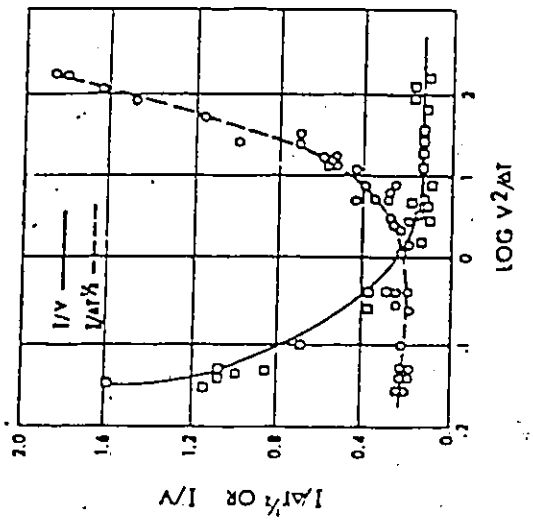

Fig.2.2.1 Empirical Relation of Air Infiltration [11]

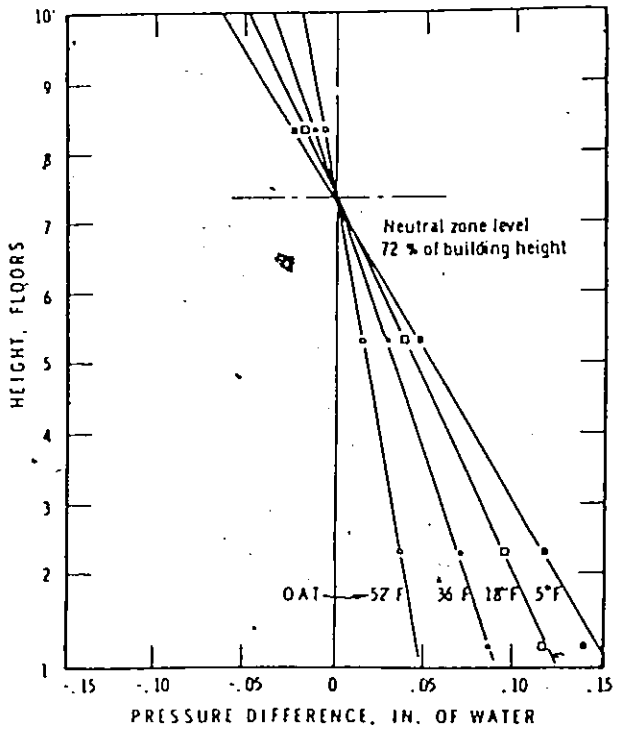

(a) Exterior Wall Pressure Difference induced by thermal effect

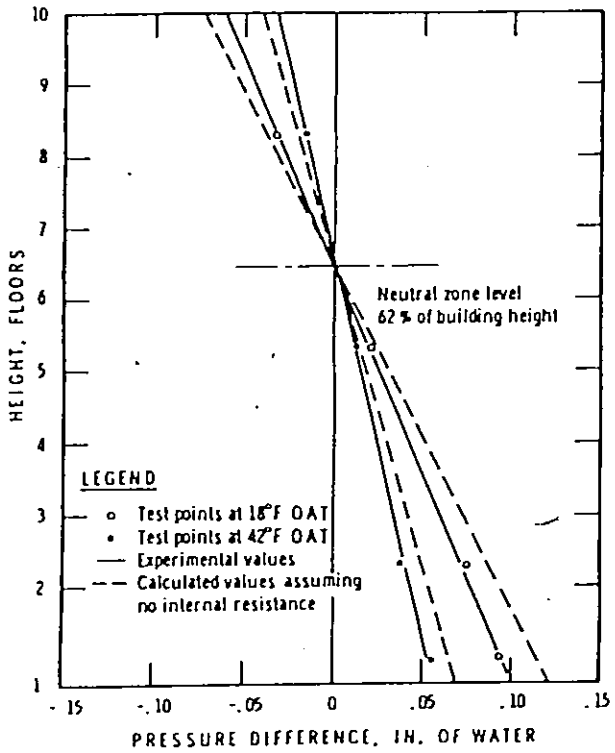

(b) Exterior Wall Pressure difference caused by stack effect with vertical air shaft sealed.

Fig.2.3.1 The Result of A Field Measurement of A Nine Story Building by Tamura and Wilson[5]

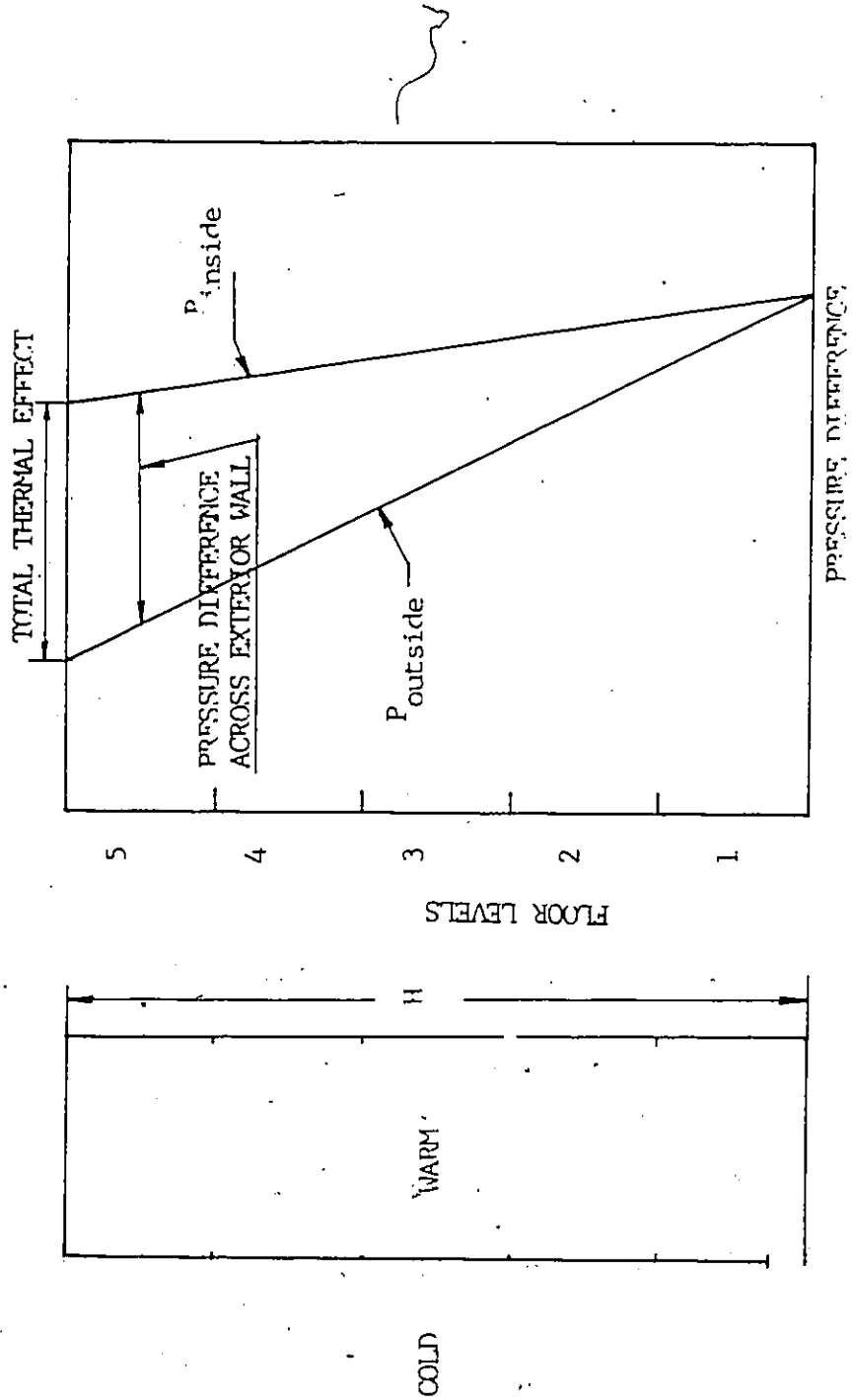

Fig.3.1.1 Idealized Building with Bottom Opening Only

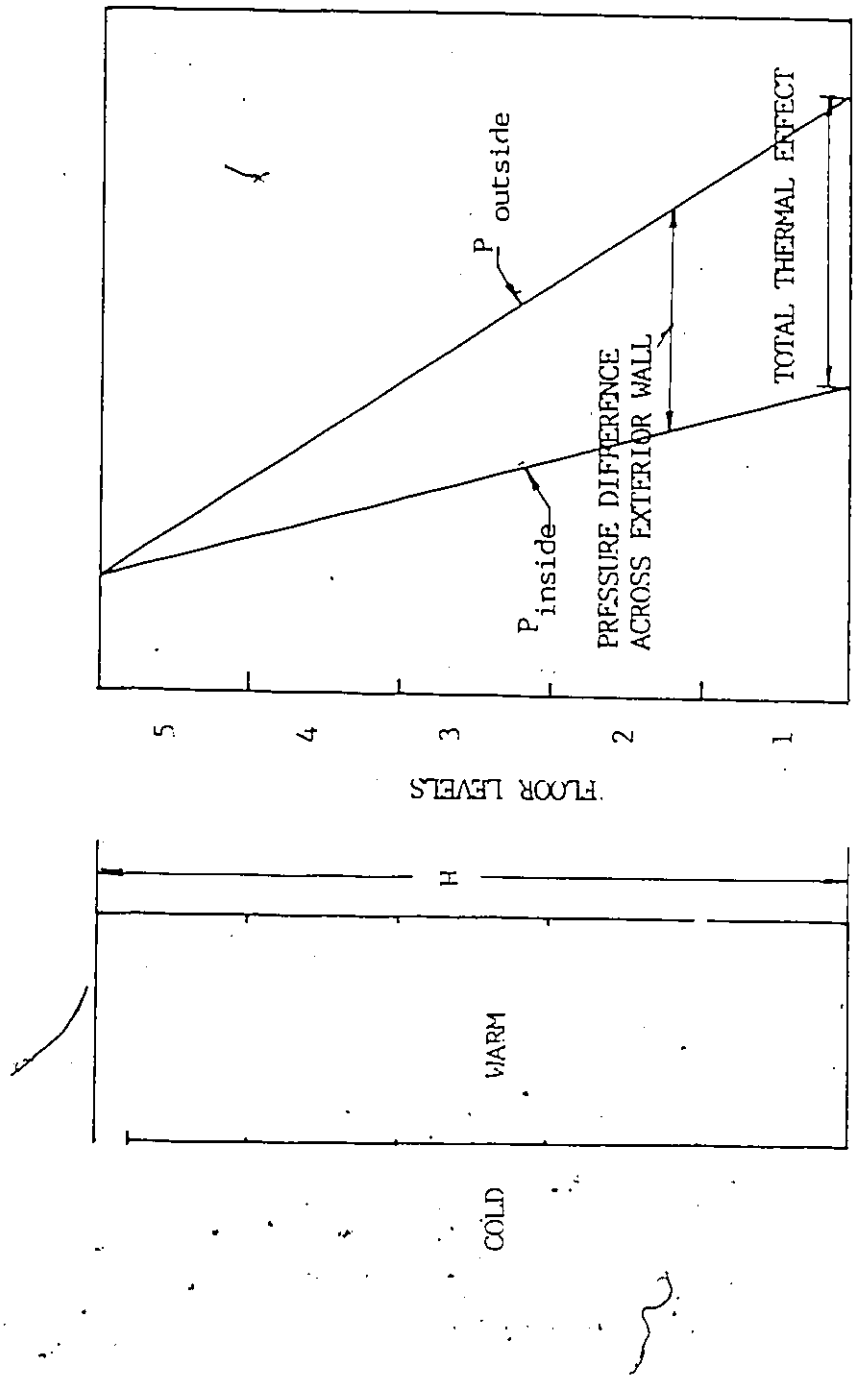

Fig.3.1.2 Idealized Building with Top Opening Only

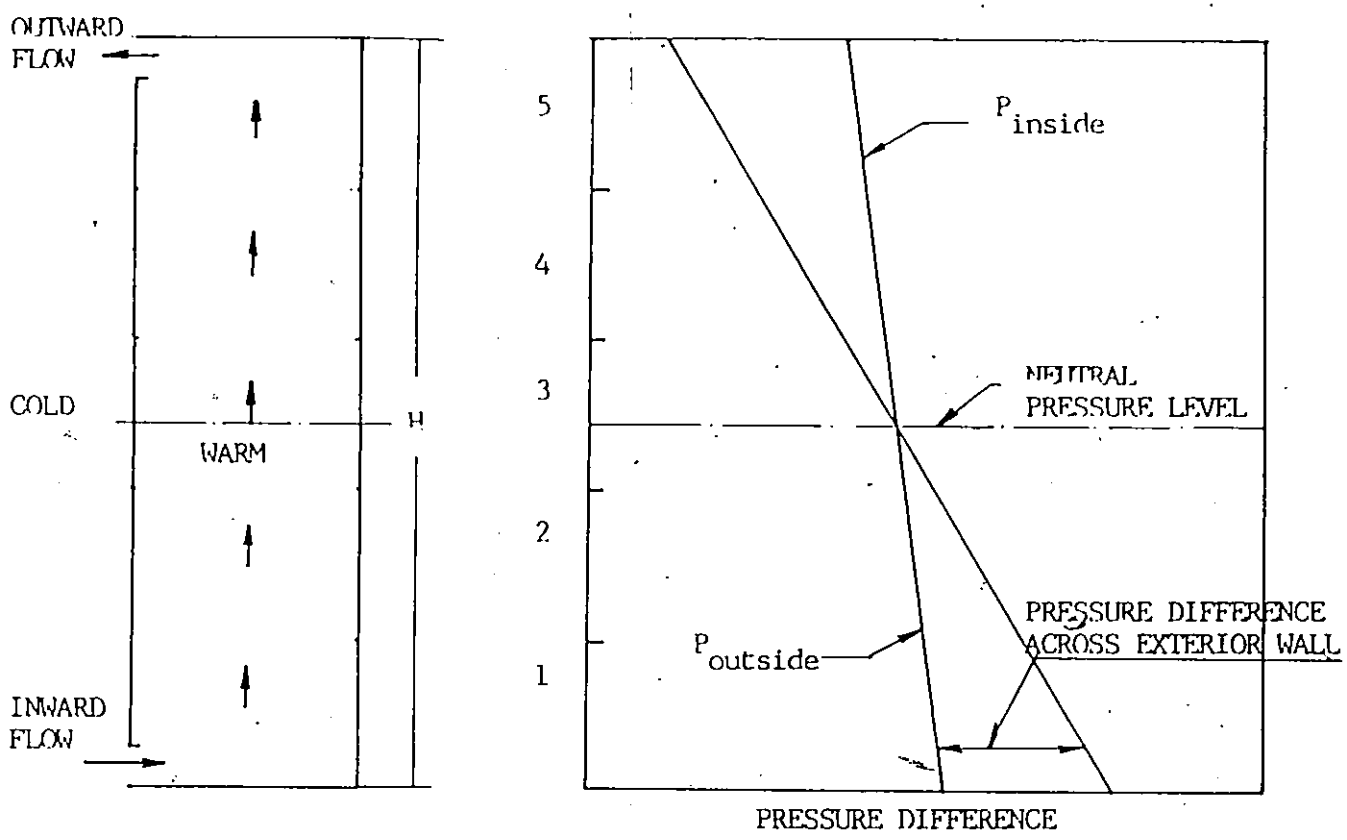

Fig.3.1.3 Idealized Building with Top and Bottom Opening Only

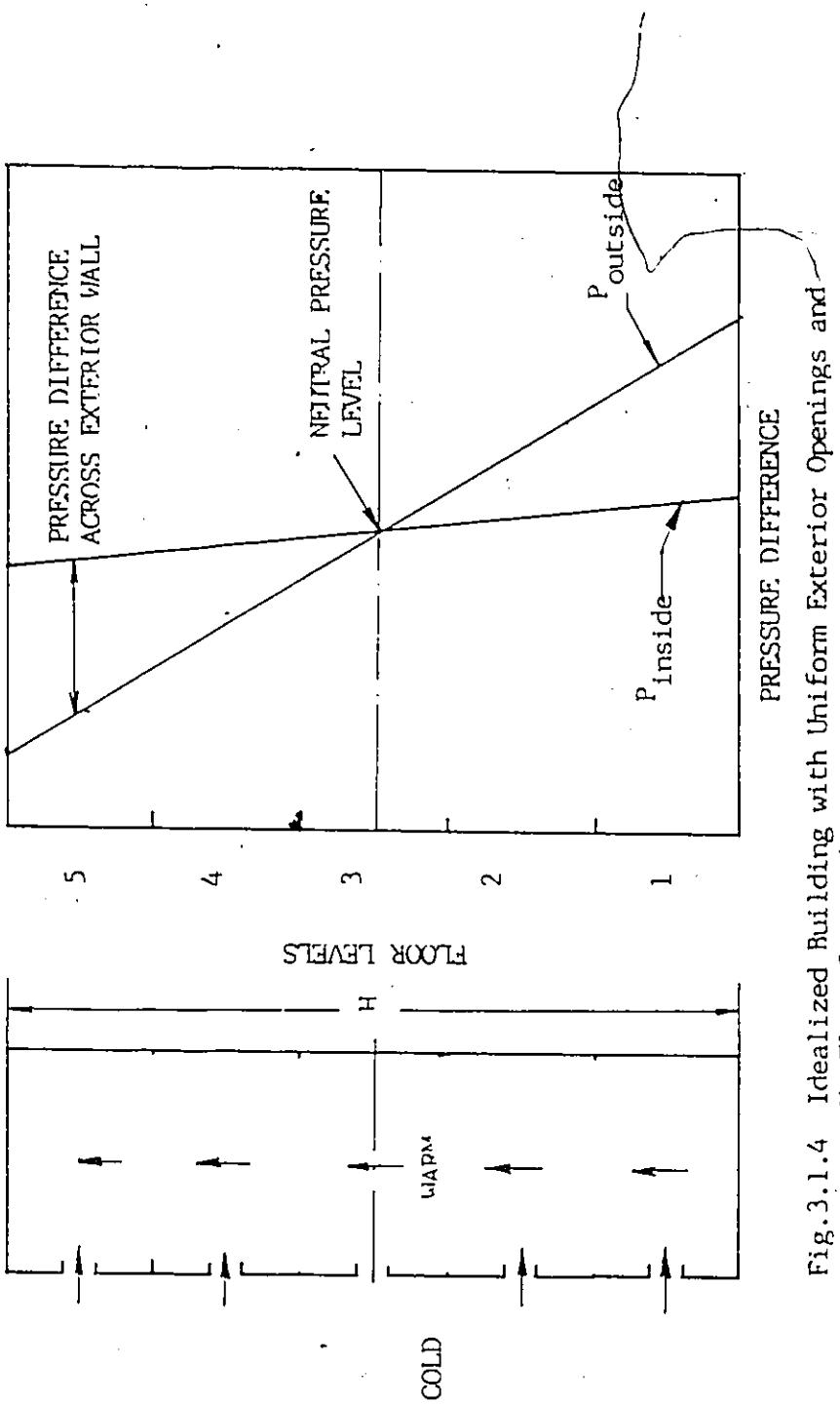

Fig.3.1.4 Idealized Building with Uniform Exterior Openings and No Floor Separations

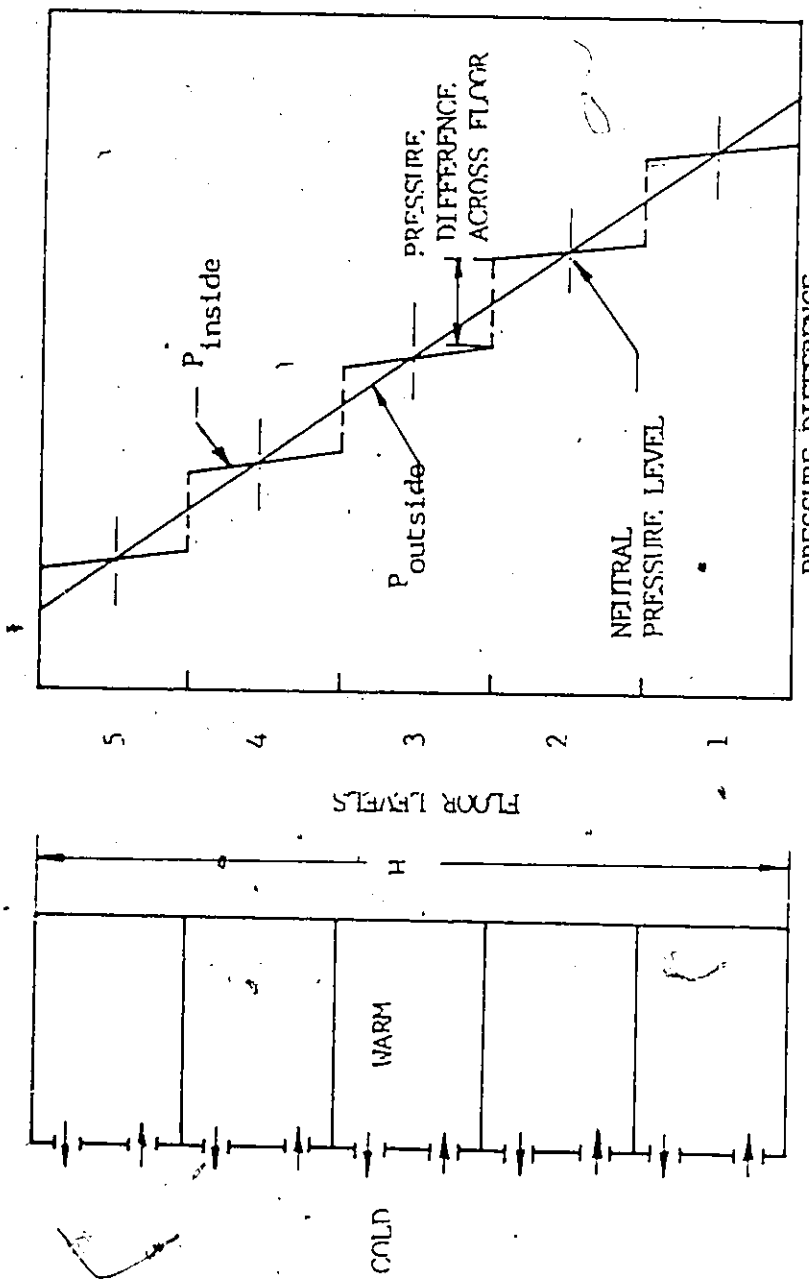

Fig.3.1.5 Idealized Building with Complete Floor Separations

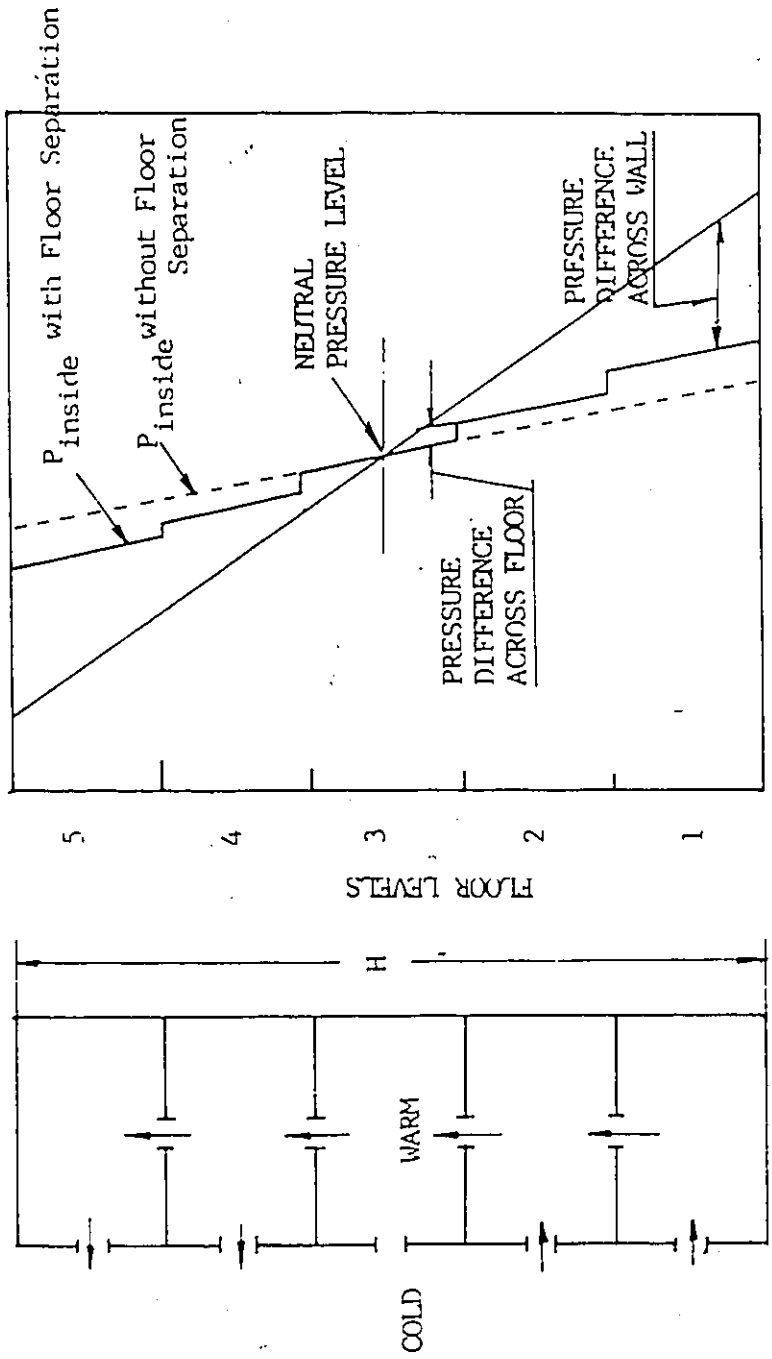

Fig.3.1.6 Idealized Building with Exterior Wall and Floor Openings

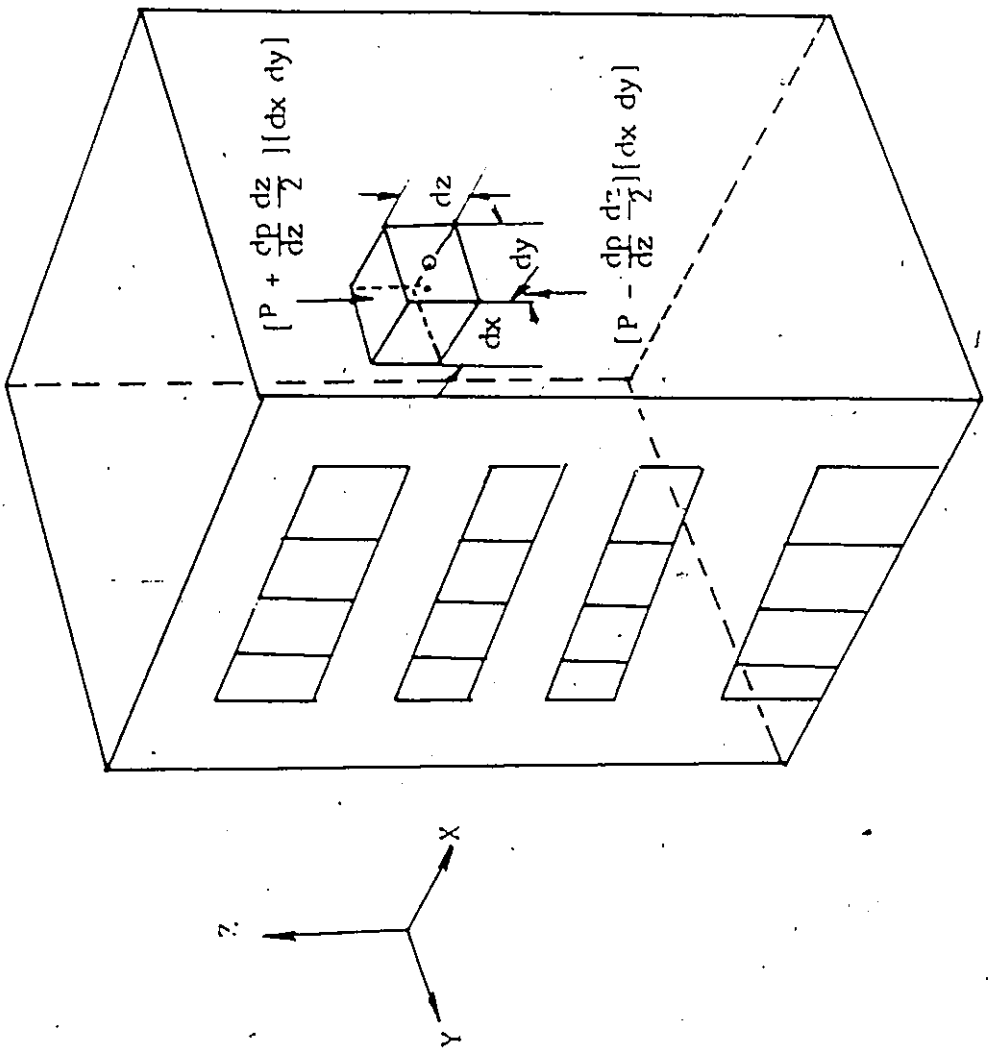

Fig.3.2.1 Differential Element of Air in Building

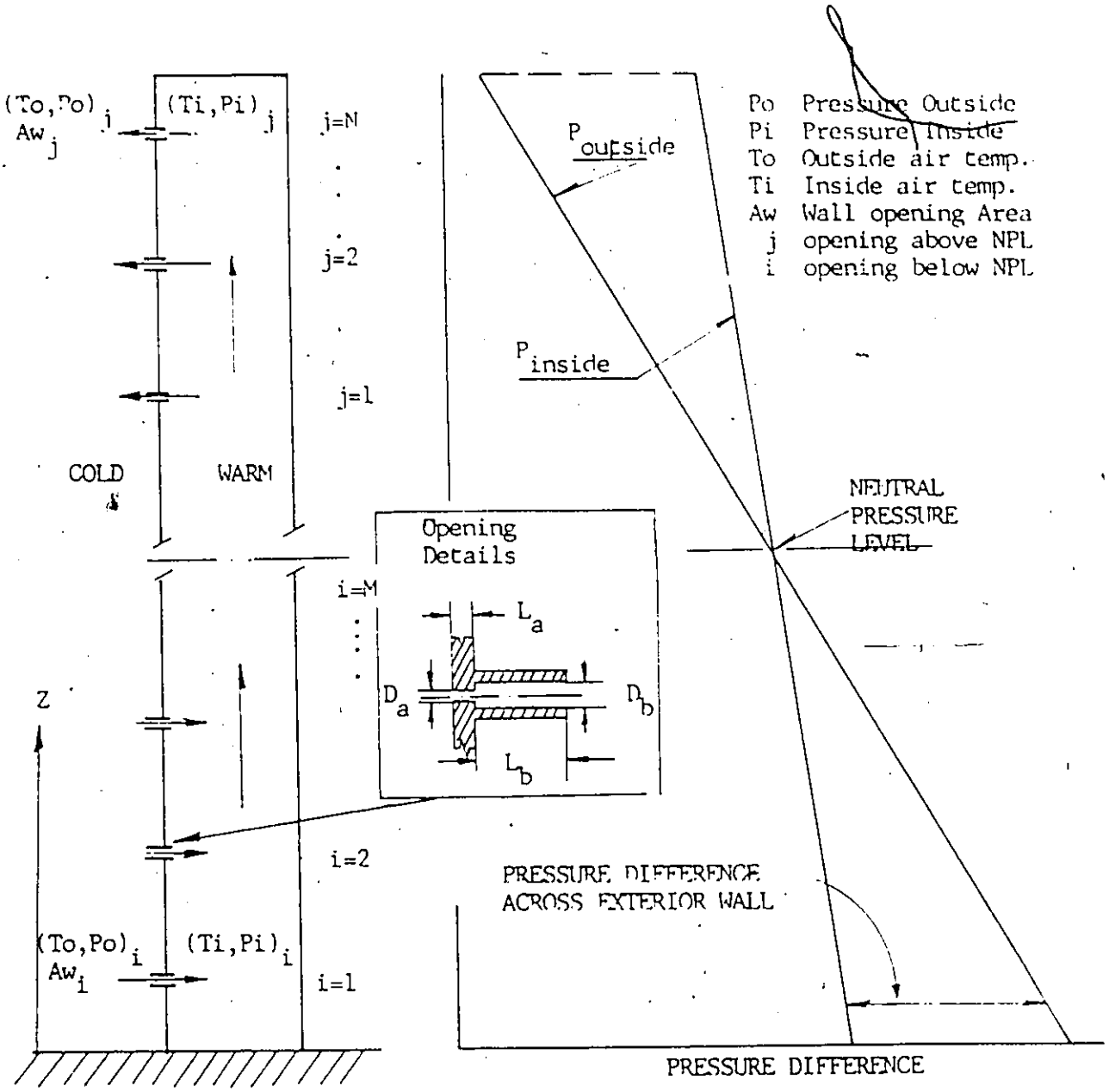

Fig.3.3.1 Idealized Model Building with Exterior Wall Openings and negligible resistance to flow inside

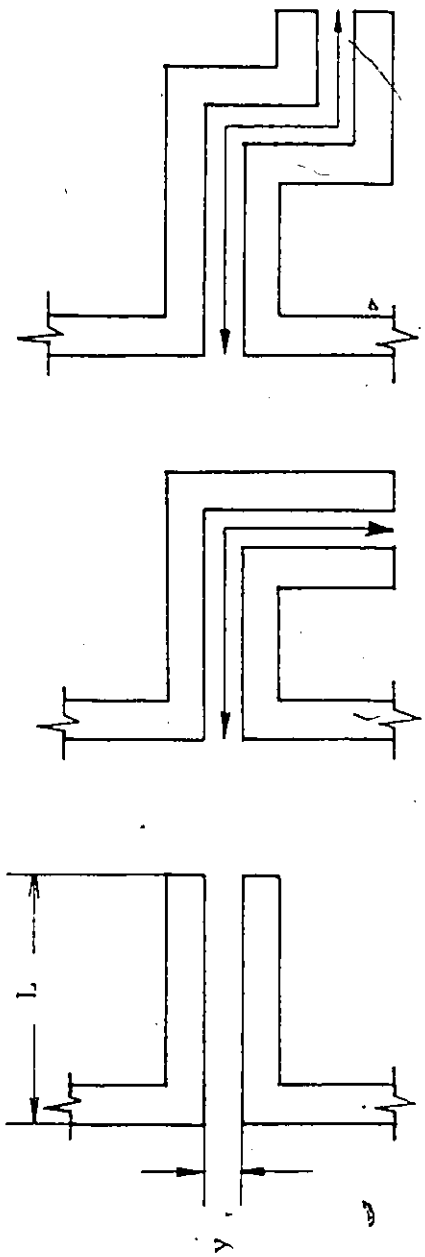

Fig.3.3.2 Typical Configurations of Cracks encountered in Buildings

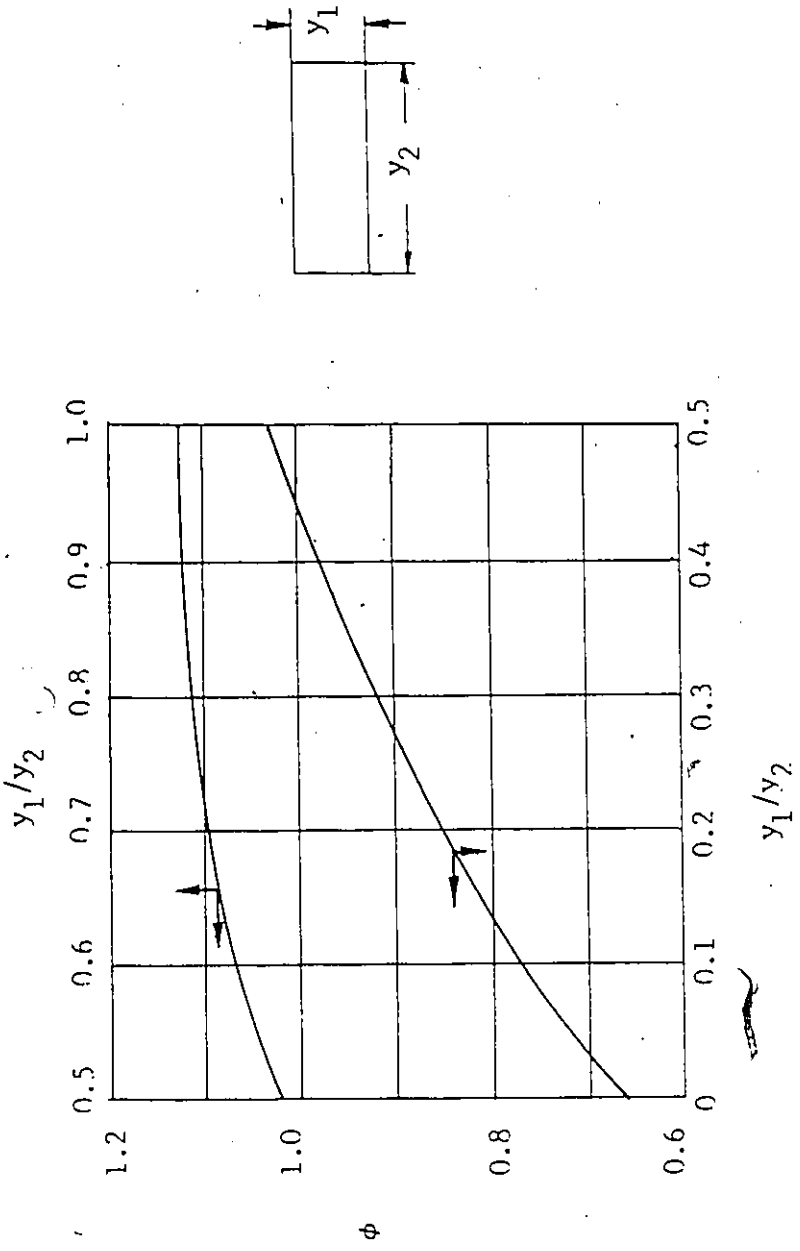

Fig.3.3.3 Values of ϕ for rectangular ducts[27].

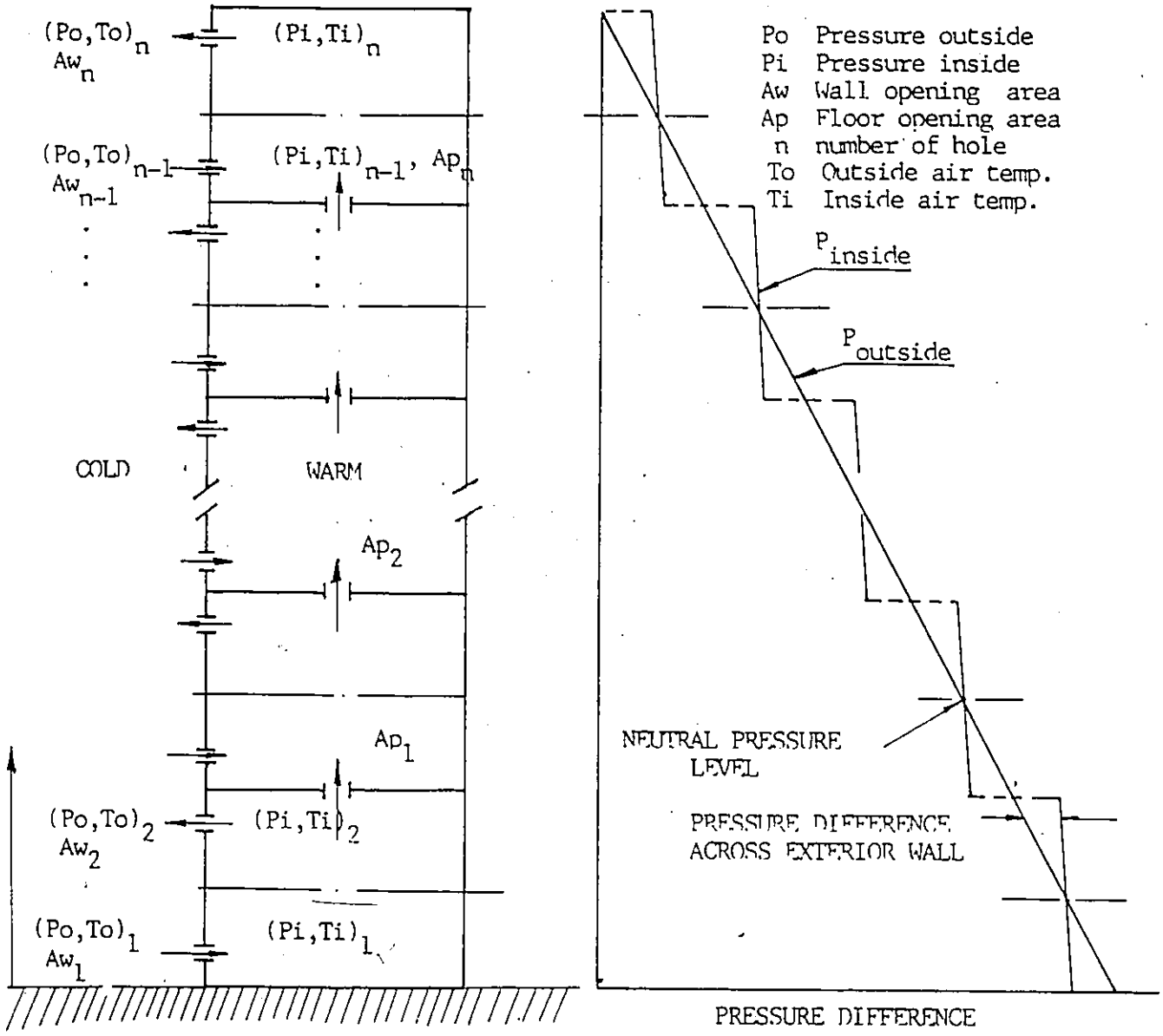

Fig.3.3.4 Idealized Model Building with Exterior Wall Openings and Floor Openings

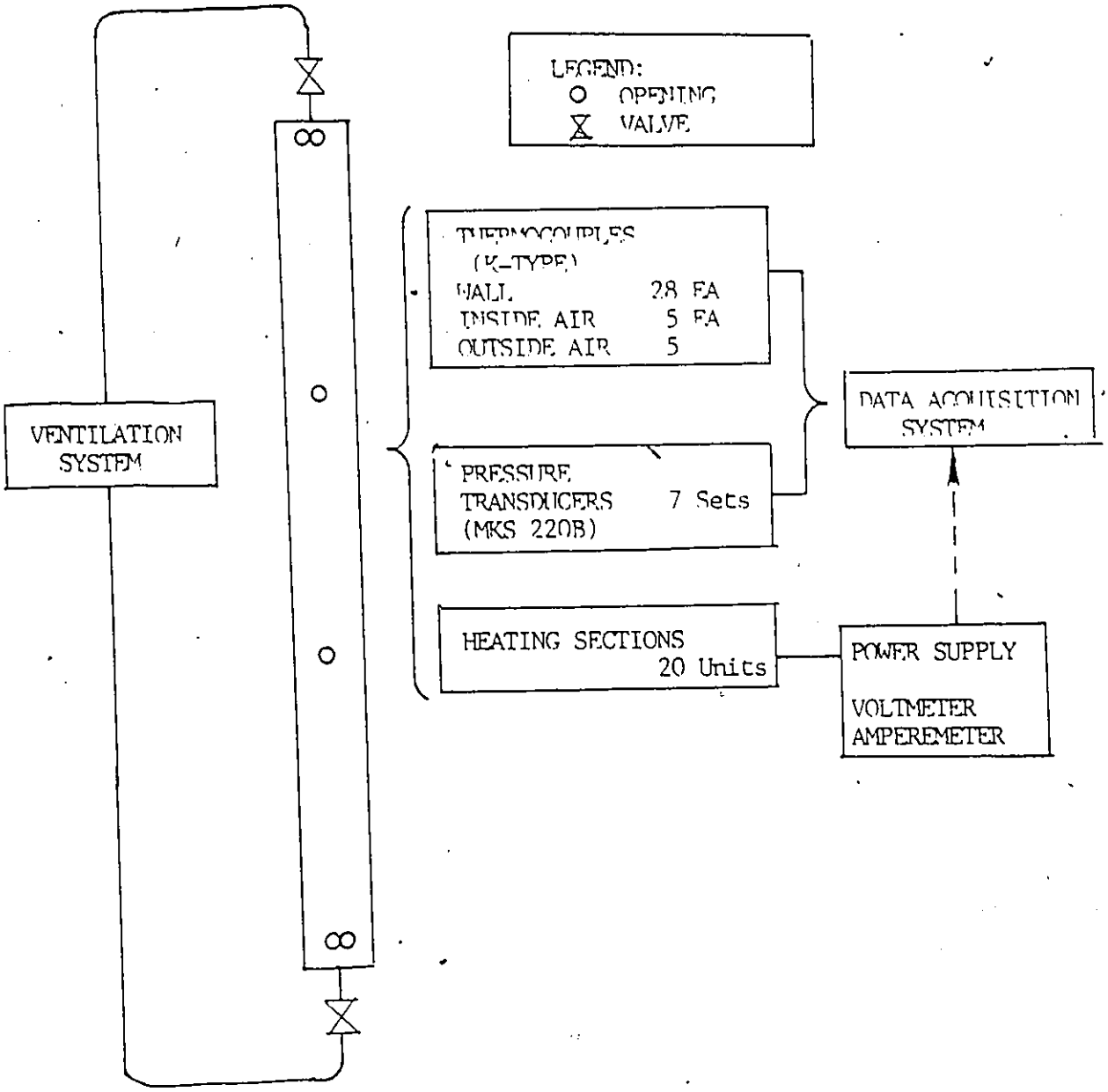

Fig. 4.1.1. Schematic Diagram of Testing Apparatus without Partitions

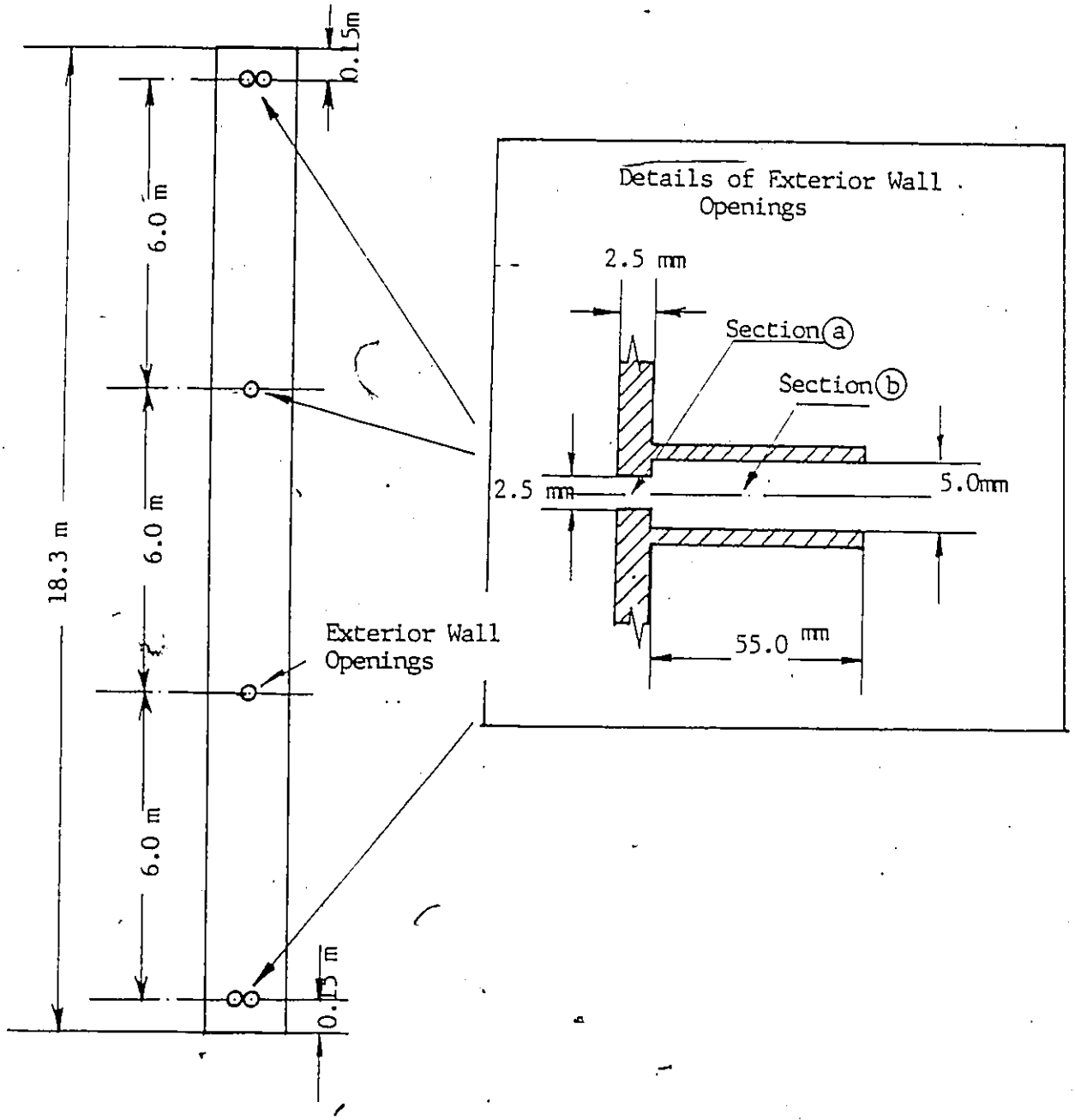

Fig.4.1.2 Configuration of Test Section with No Partitions

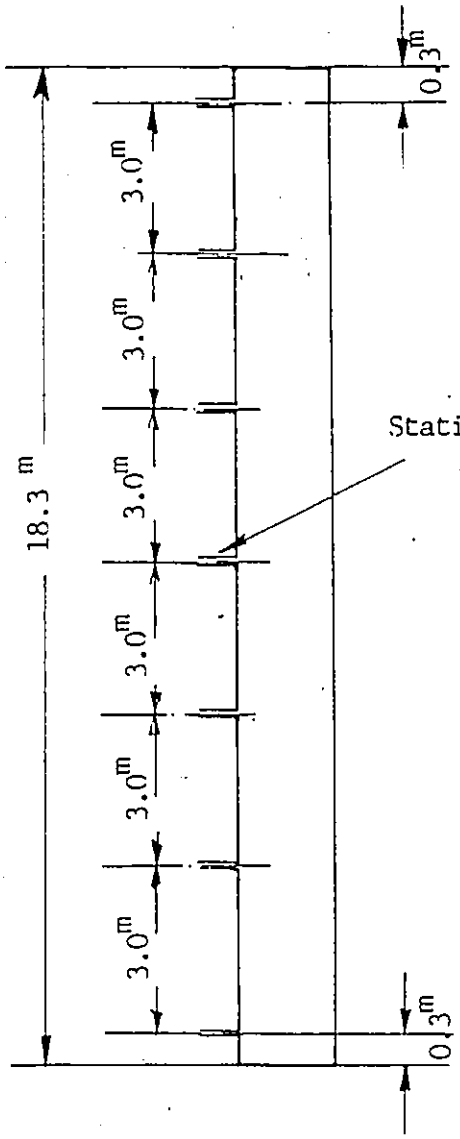

All Static Pressure Taps are 76 mm long, 17 Gage Stainless Steel Tube

Static Pressure Tap

Fig.4.1.3 Installation of Static Pressure Taps in Test Section with No Partitions

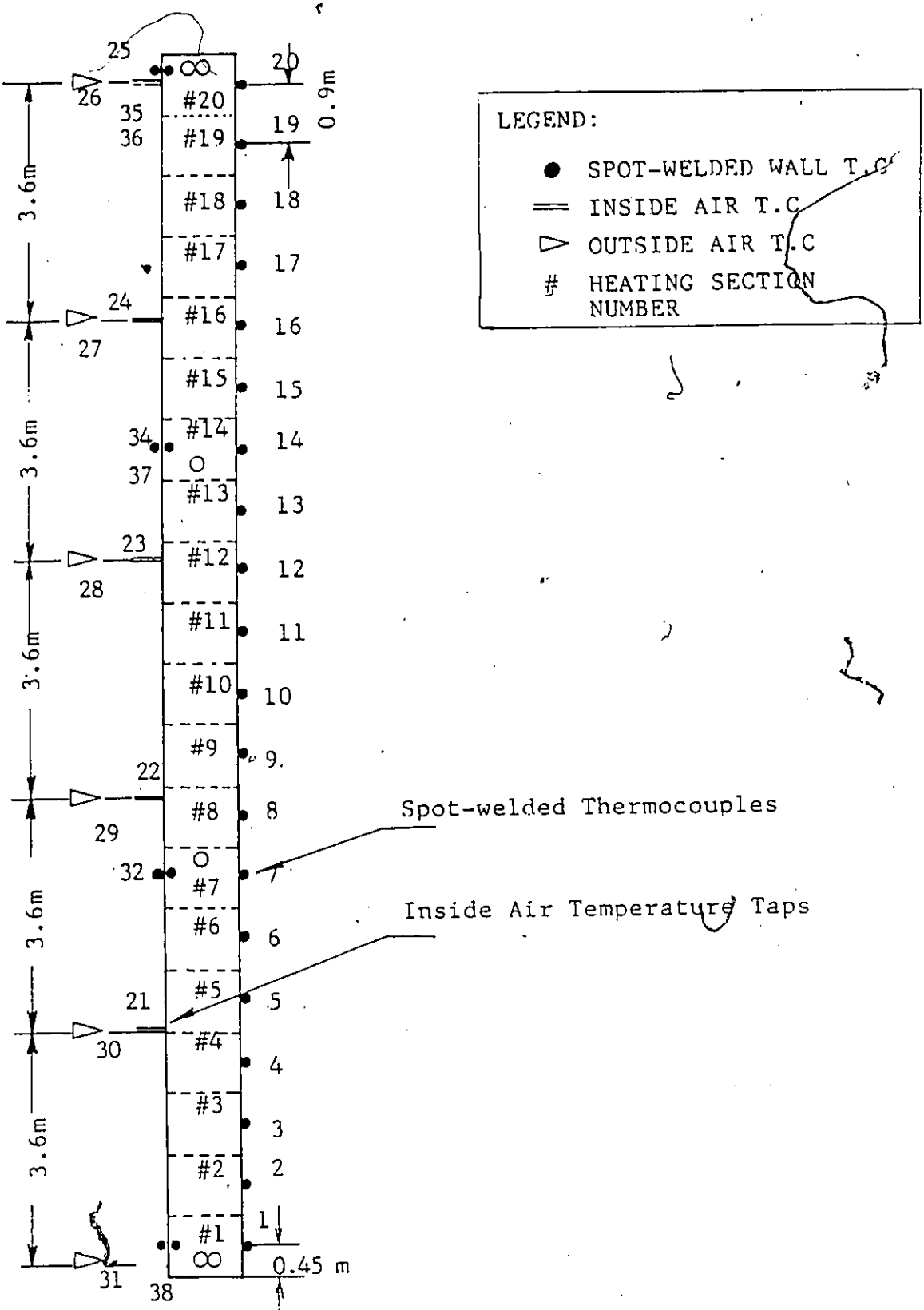

Fig.4.1.4 Schematic View of Installed Thermocouples in Test Section without Partitions

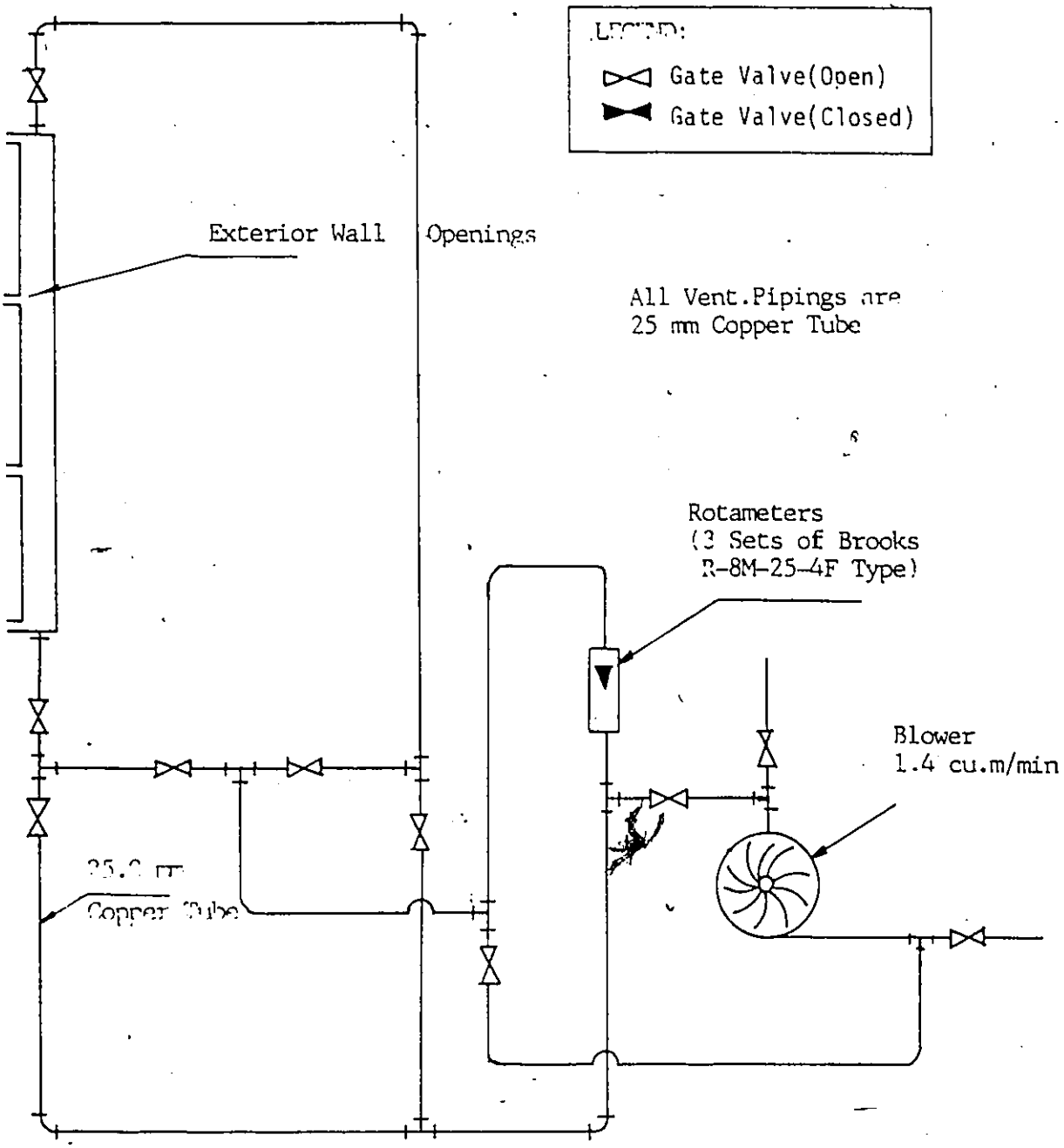

Fig.4.1.5 Mechanical Ventilation System for Test Section with No Floor Partitions

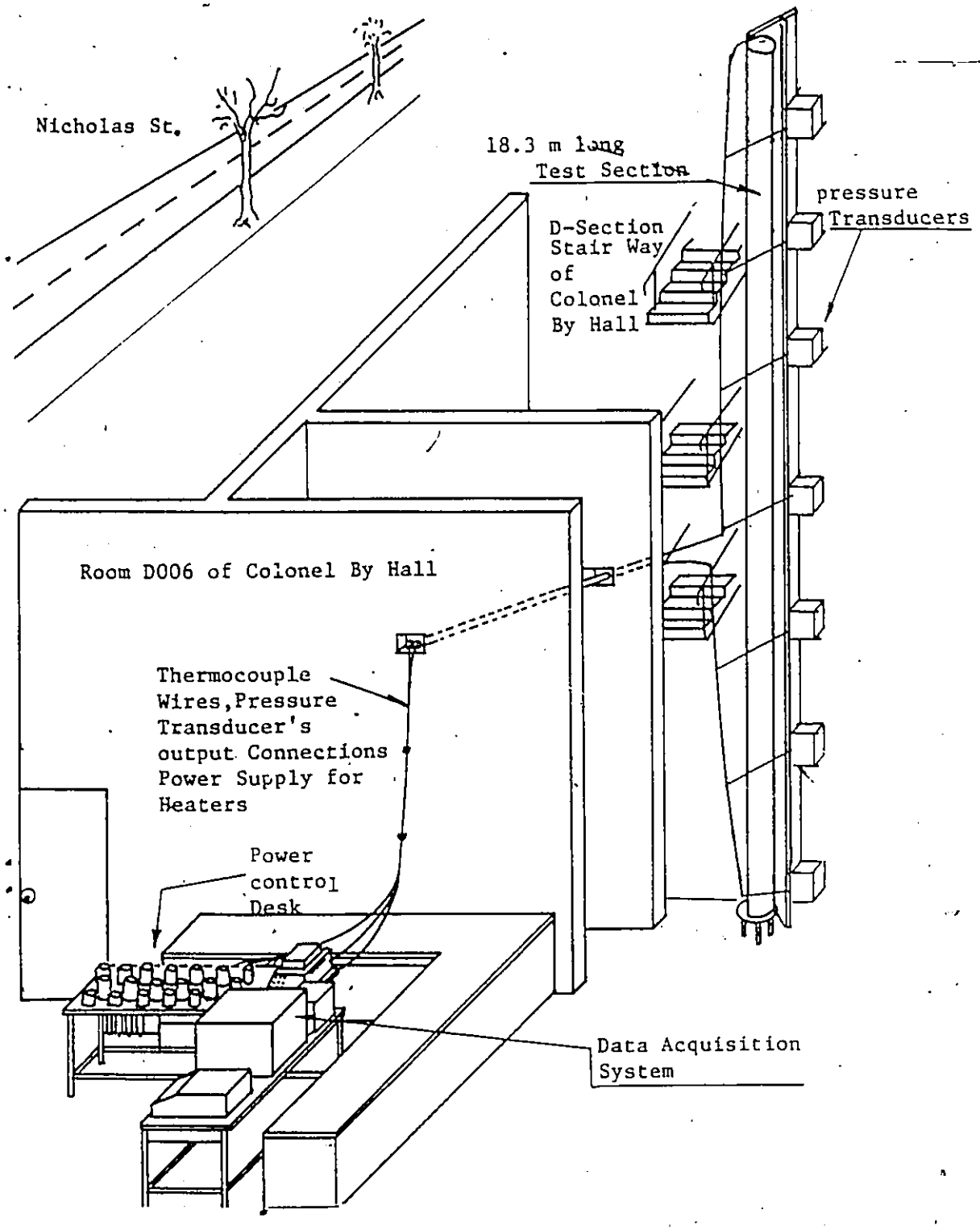

Fig.4.1.6 Situated View of Testing Apparatus

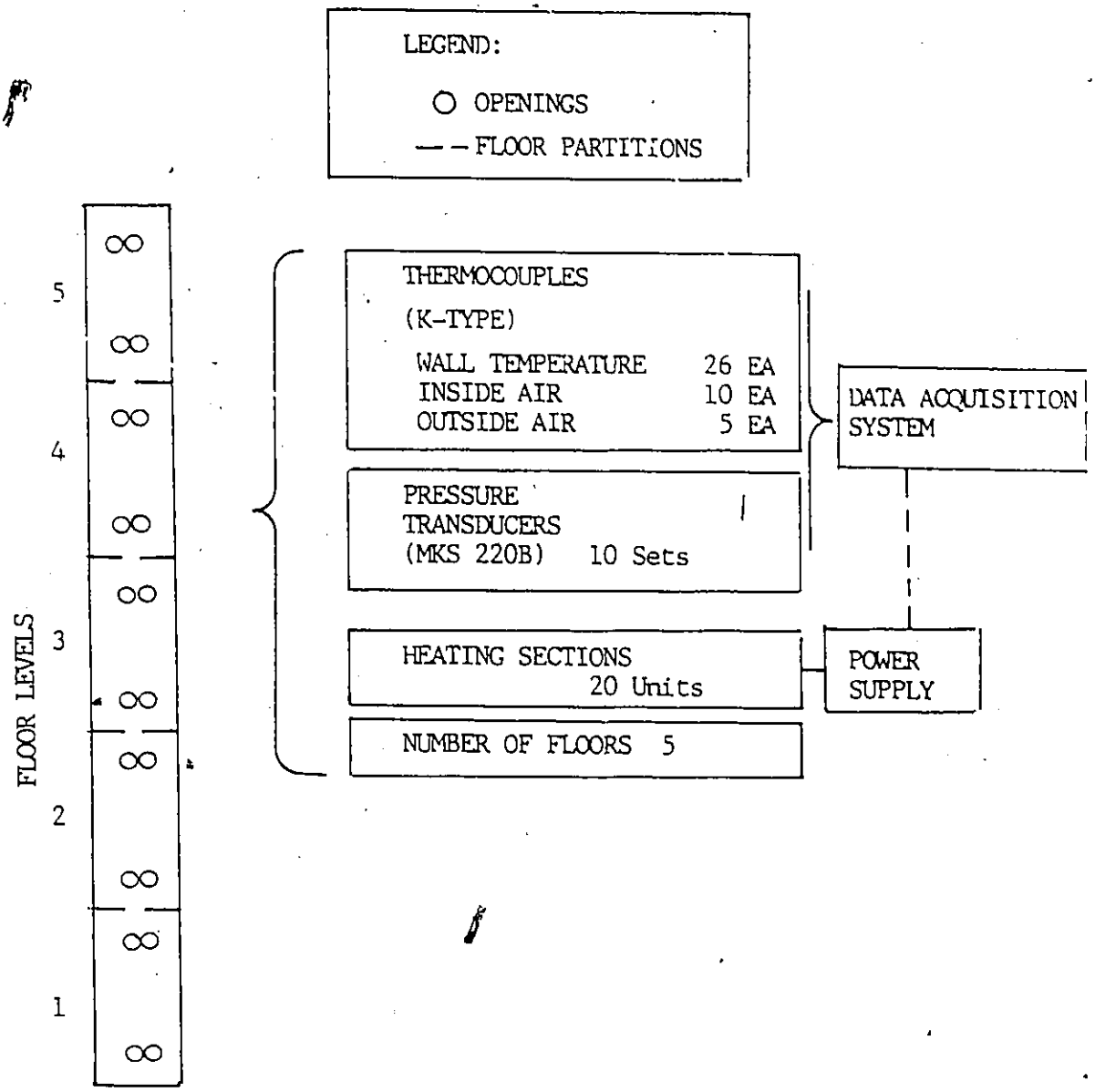

Fig.4.1.7 Schematic Diagram of Testing Apparatus with Floor Separations

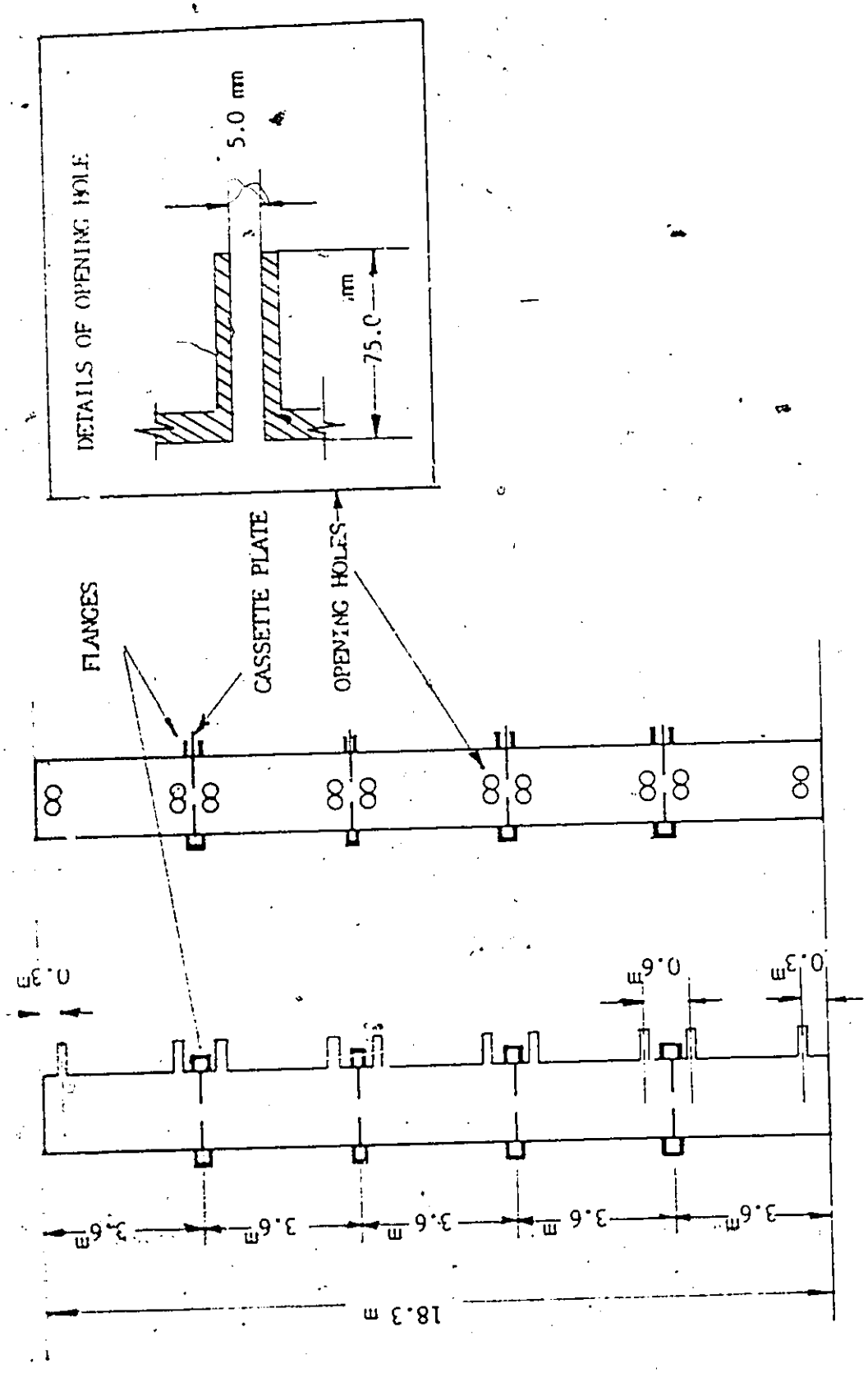

Fig.4.1.8 Design Configuration of Test Section with Floor Partitions

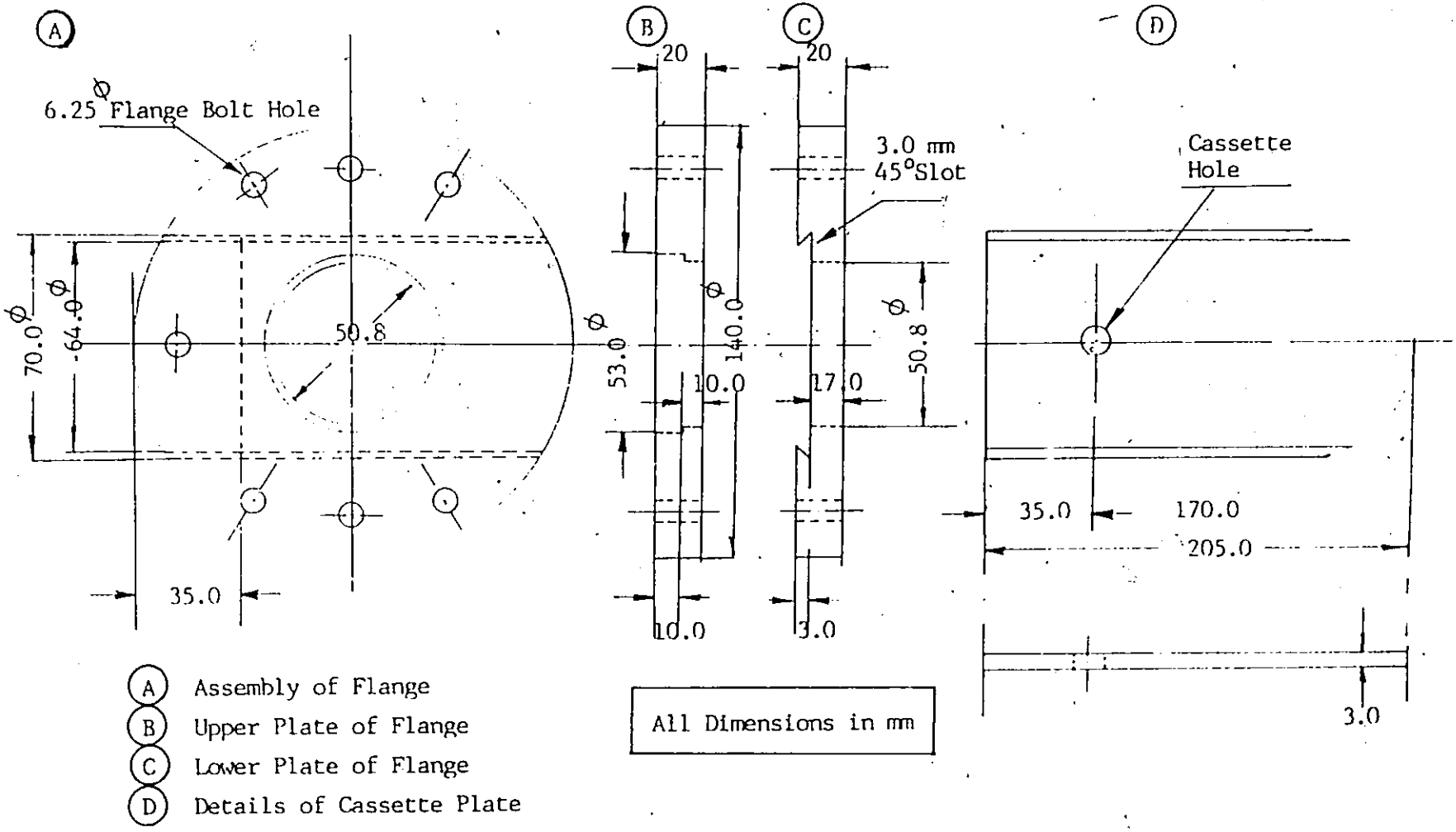

Fig.4.1.9 Design of Flanges and Cassette Plates for Floor Partitions in Test Section

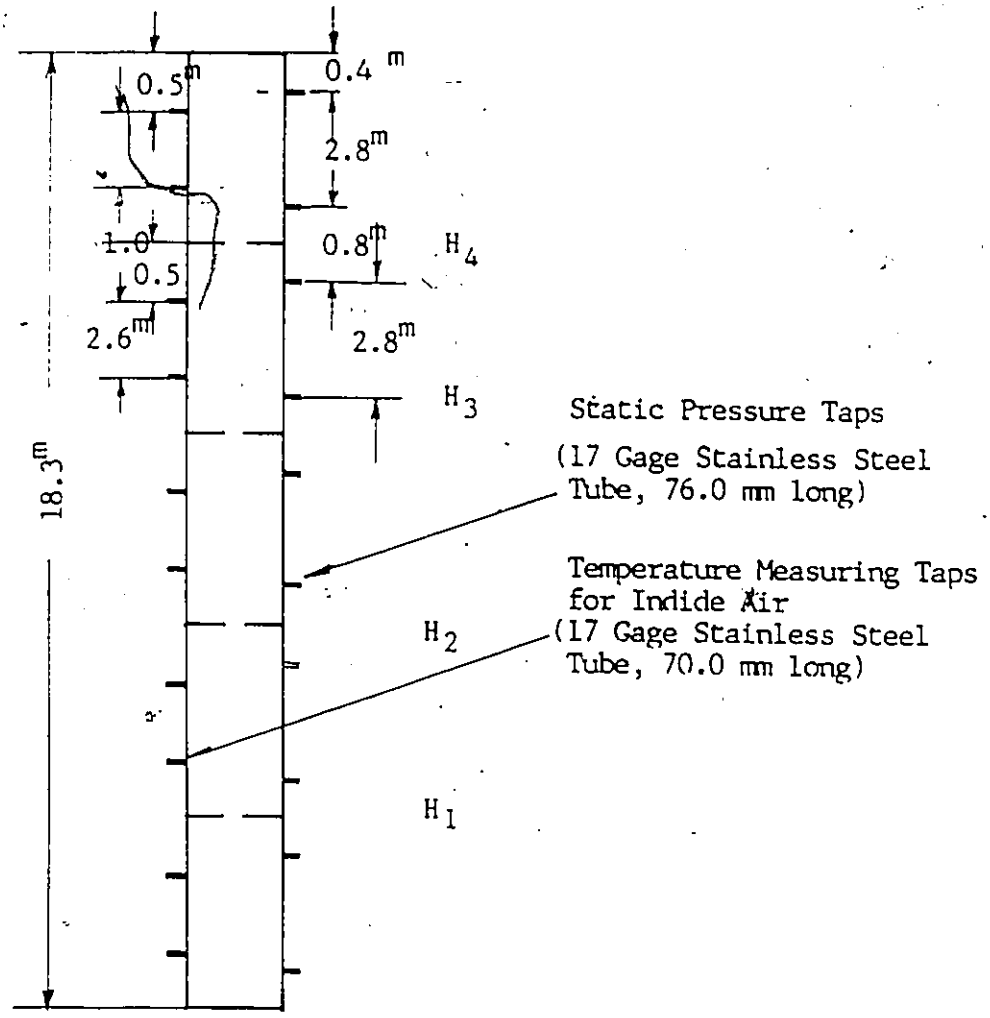

Fig.4.1.10 Installations of Static Pressure Taps and Temperature Taps in Test Section with Partitions

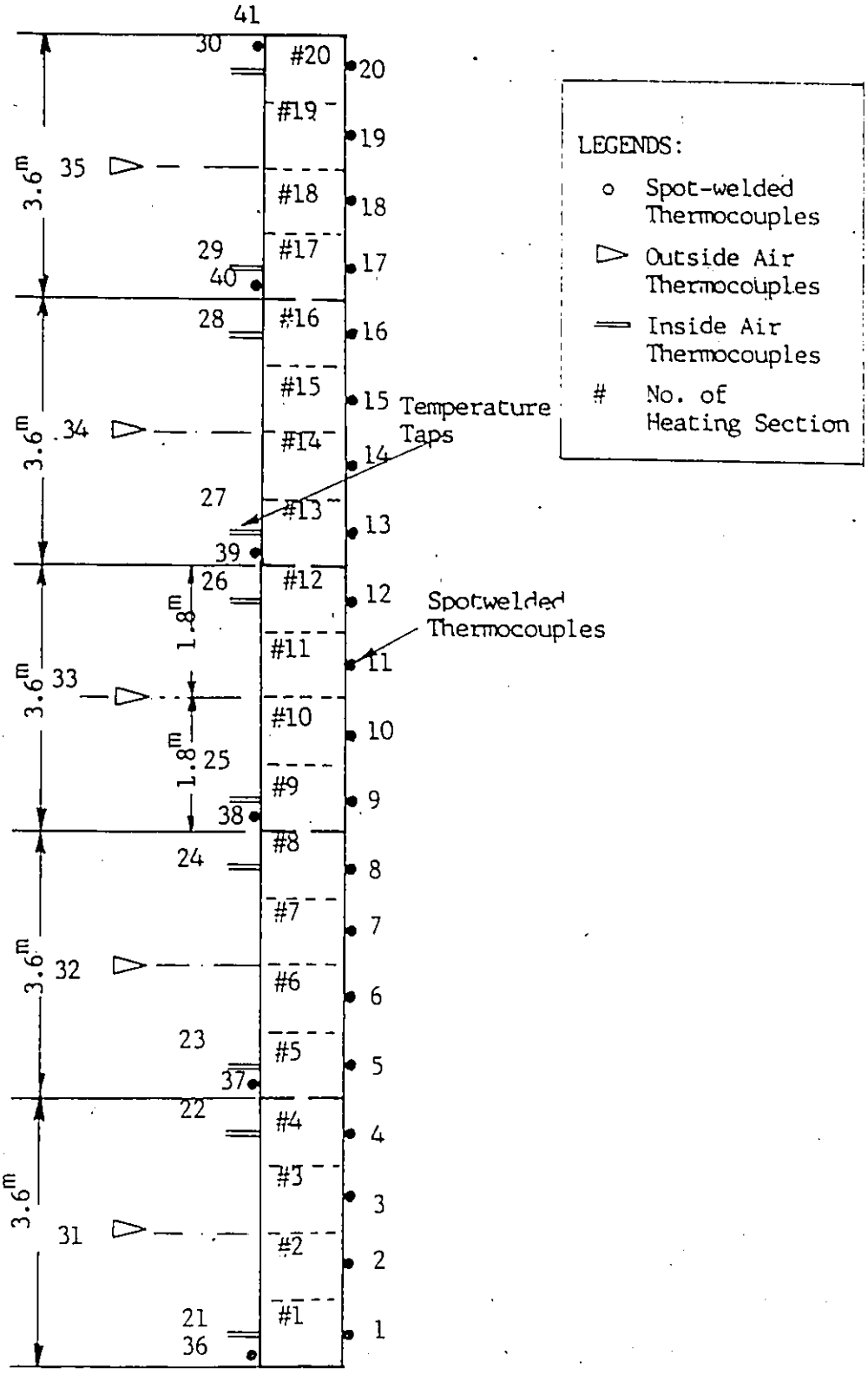

Fig.4.1.11 Schematic View of Installed Thermocouples in Test Section with Floor Partitions

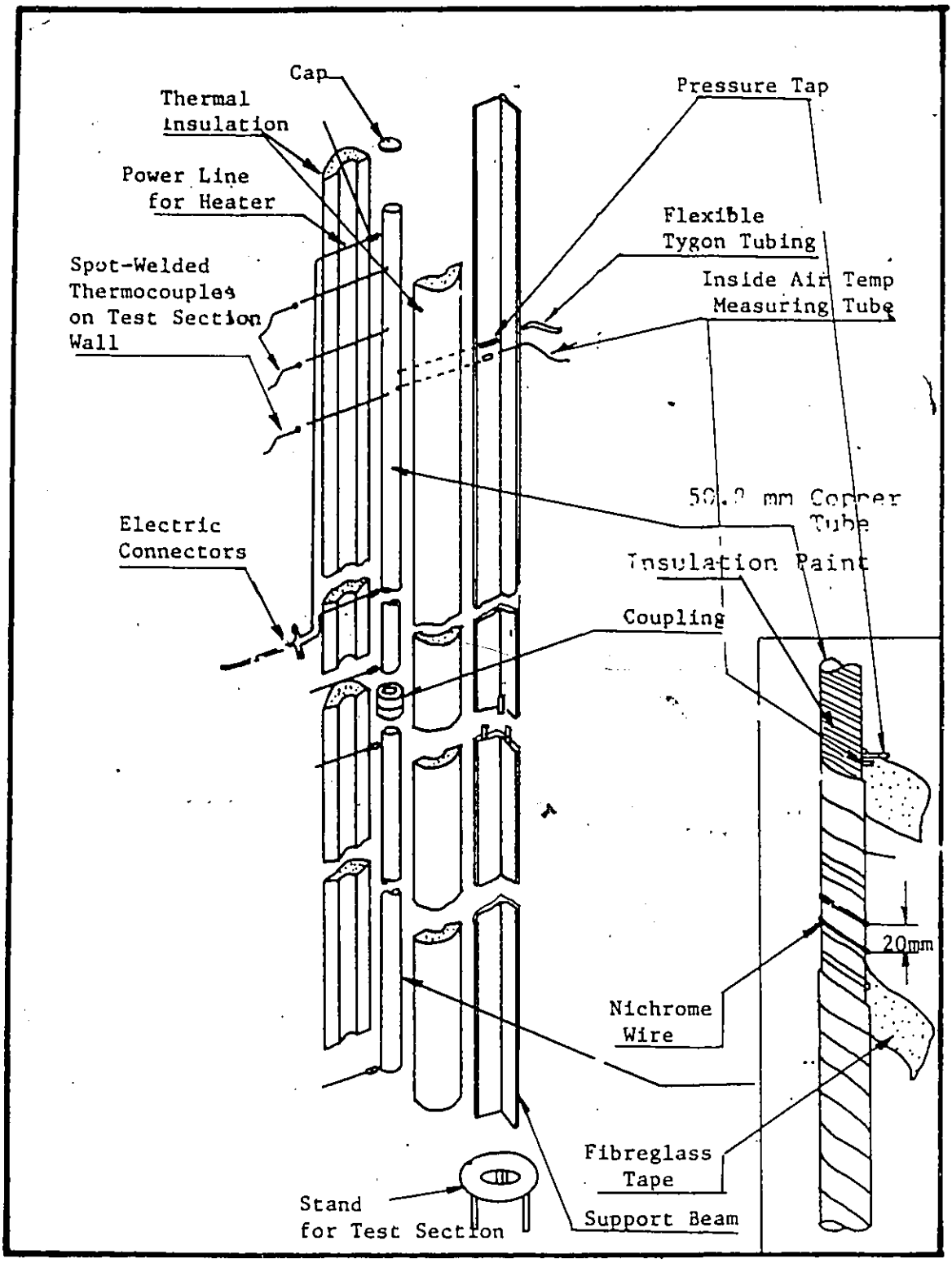

Fig.4.1.12. Sectional View of Test Section Assembly

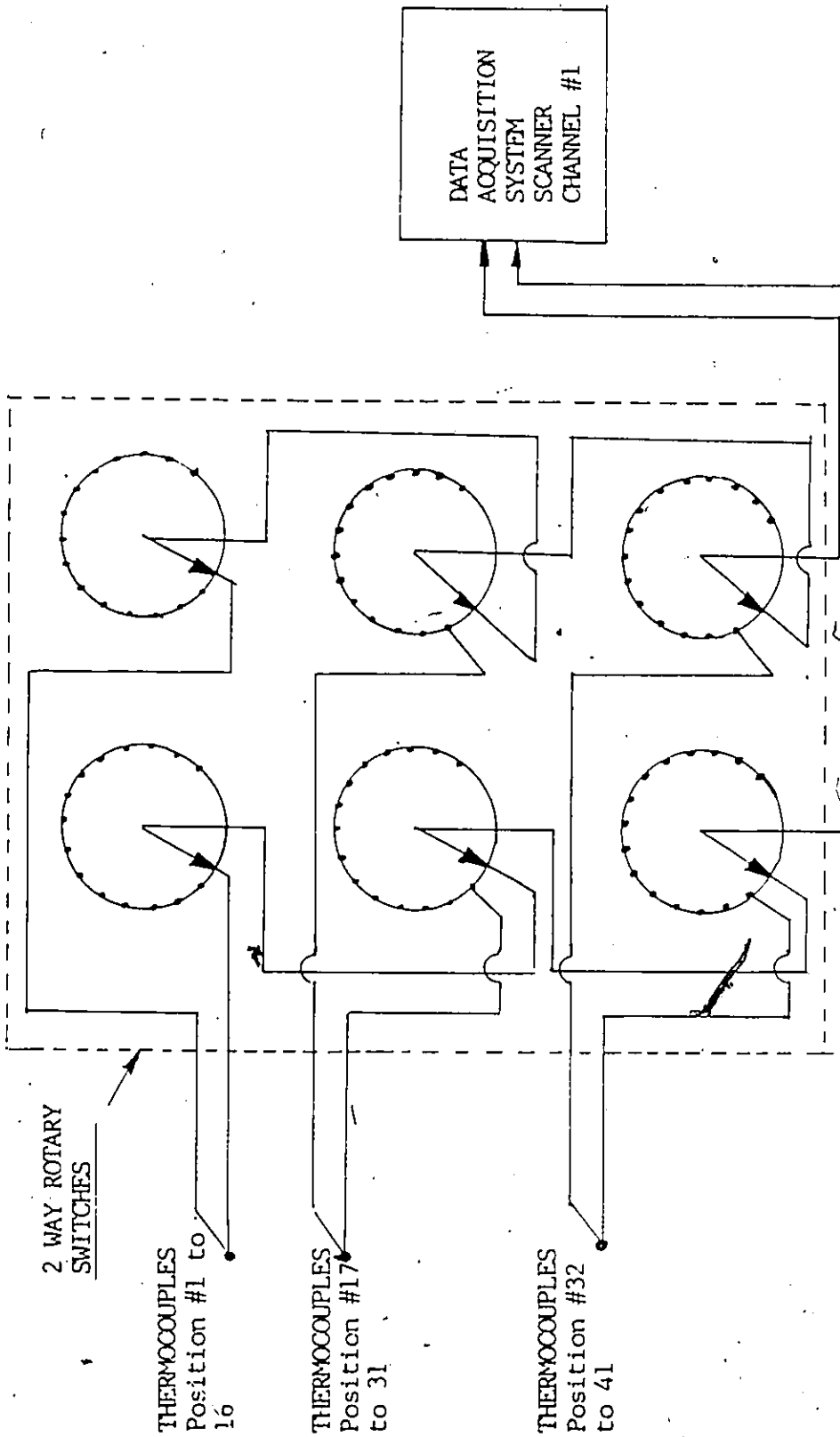

Fig.4.2.1 Temperature Measuring Circuit Loop

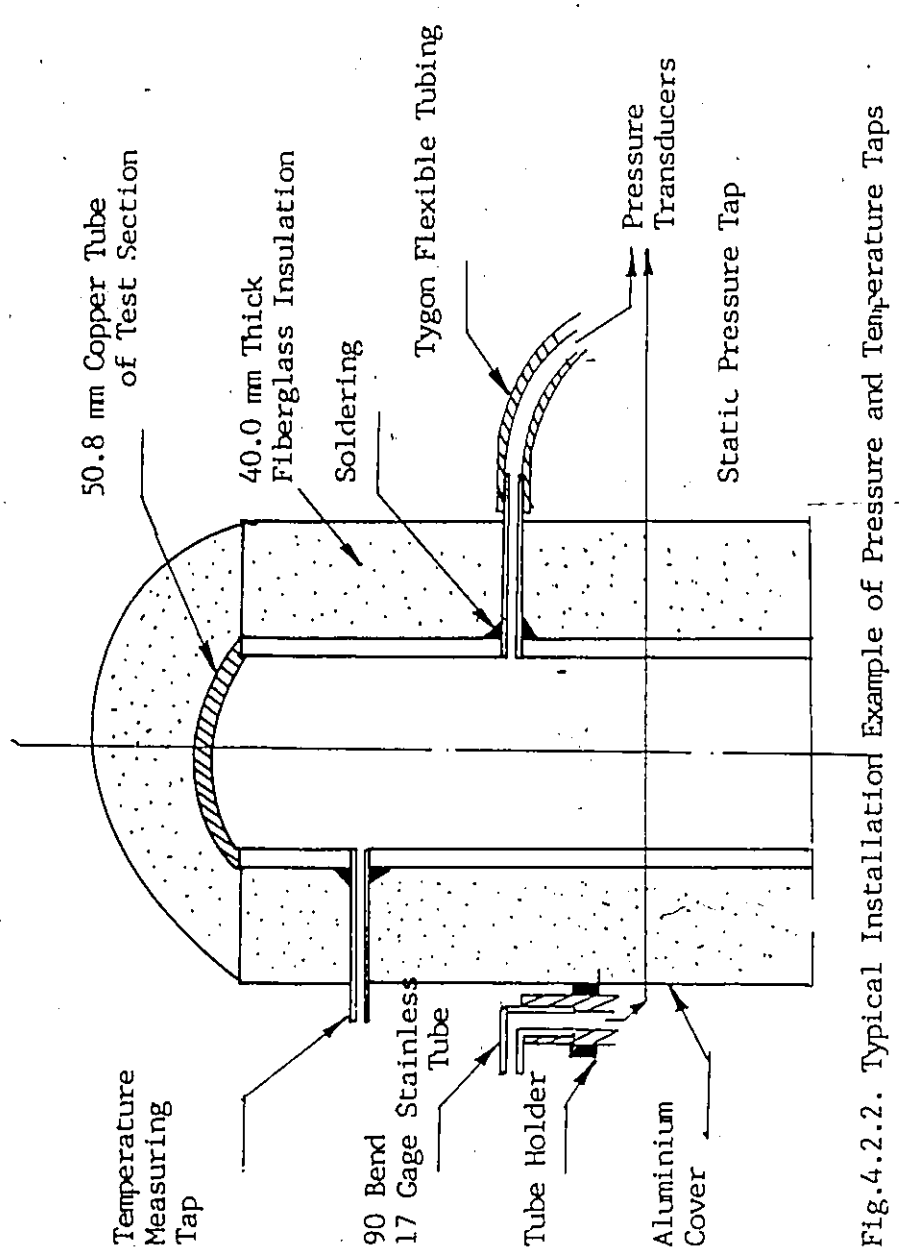

Fig.4.2.2. Typical Installation Example of Pressure and Temperature Taps

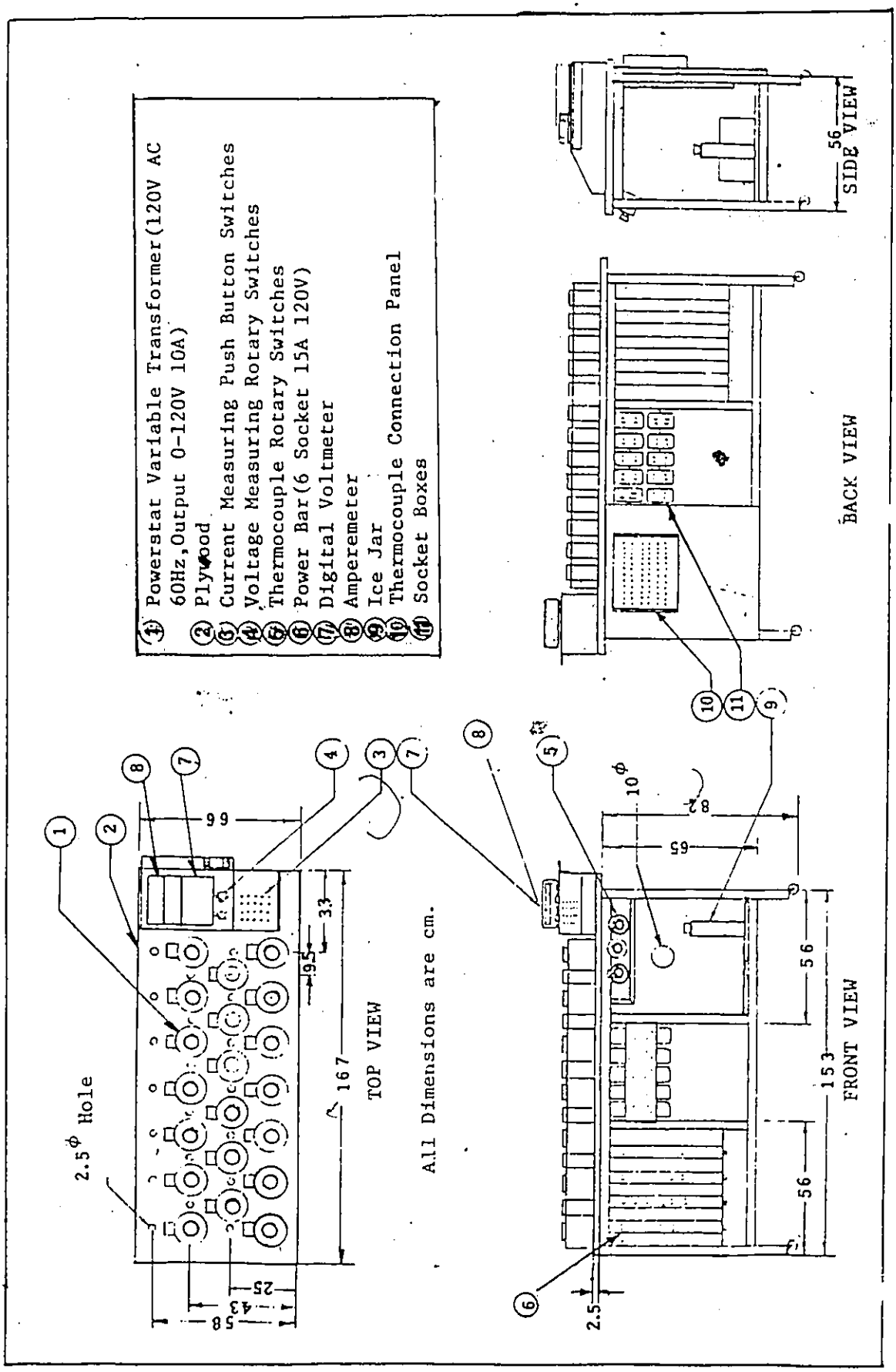

Fig.4.2.3. Set-Up of Power Supply and Control System for Heating Sections

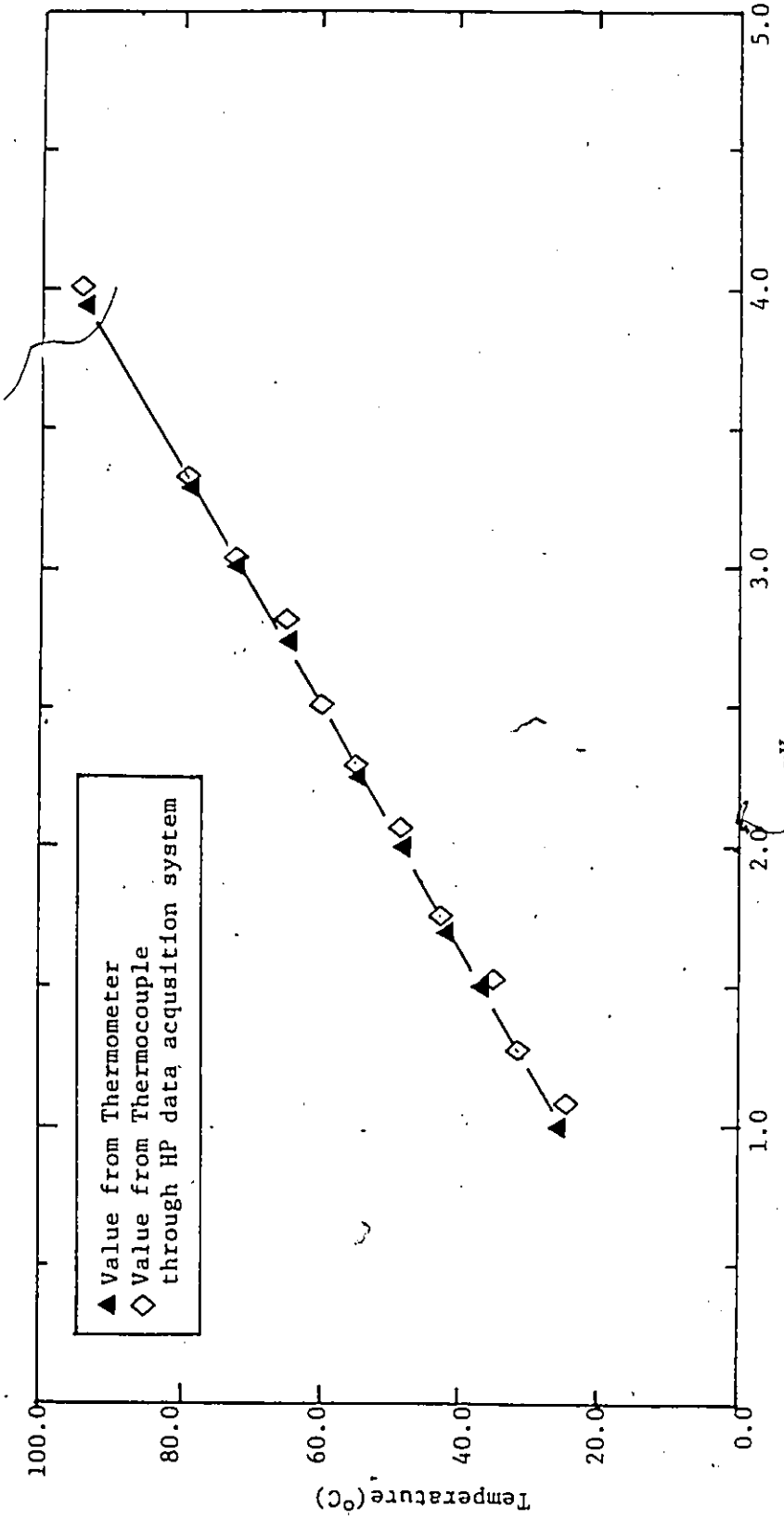

Fig.4.3.1. Typical Results of Thermocouple Calibration

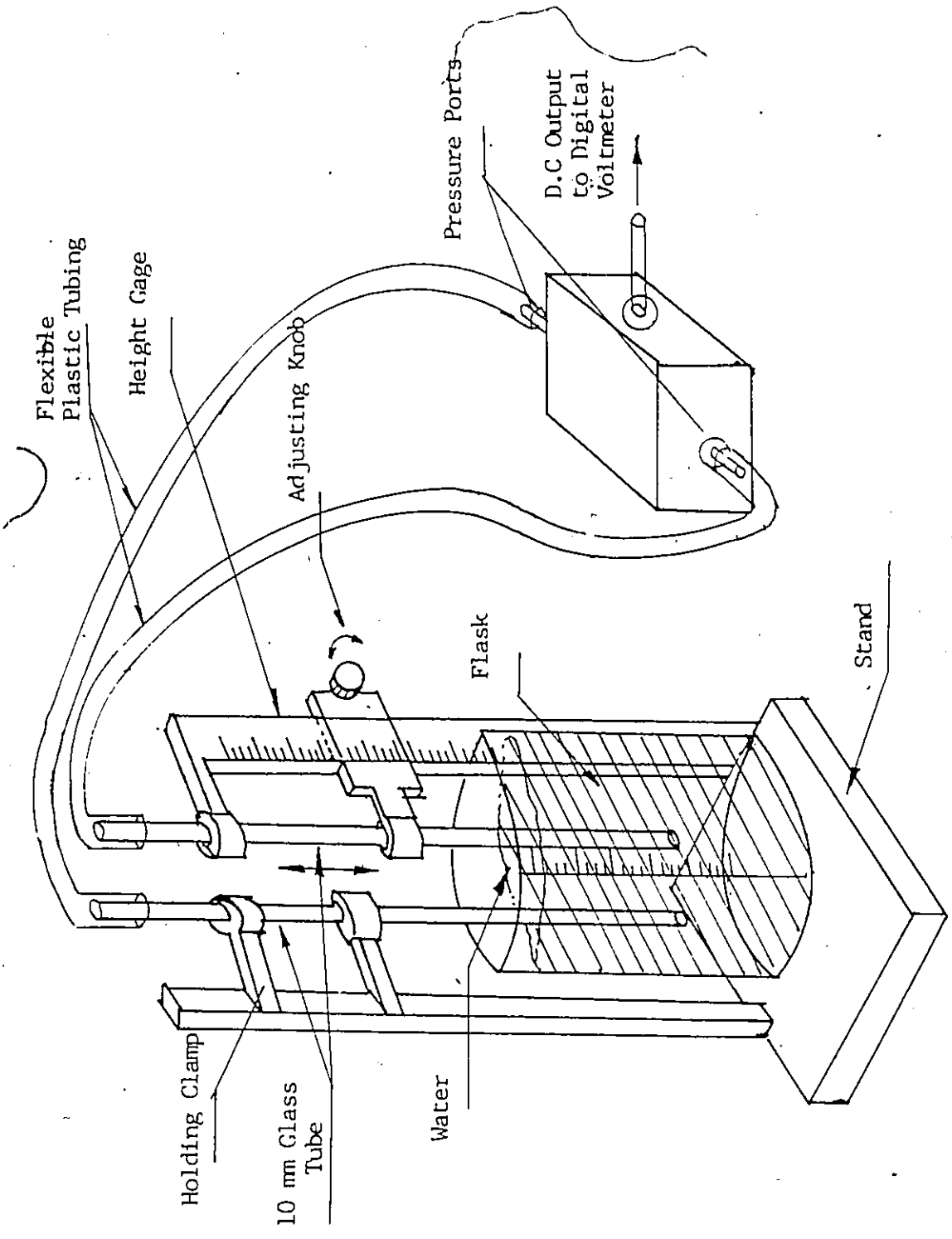

Fig.4.3.2. Set-Up of Simplified Pressure Calibration Apparatus

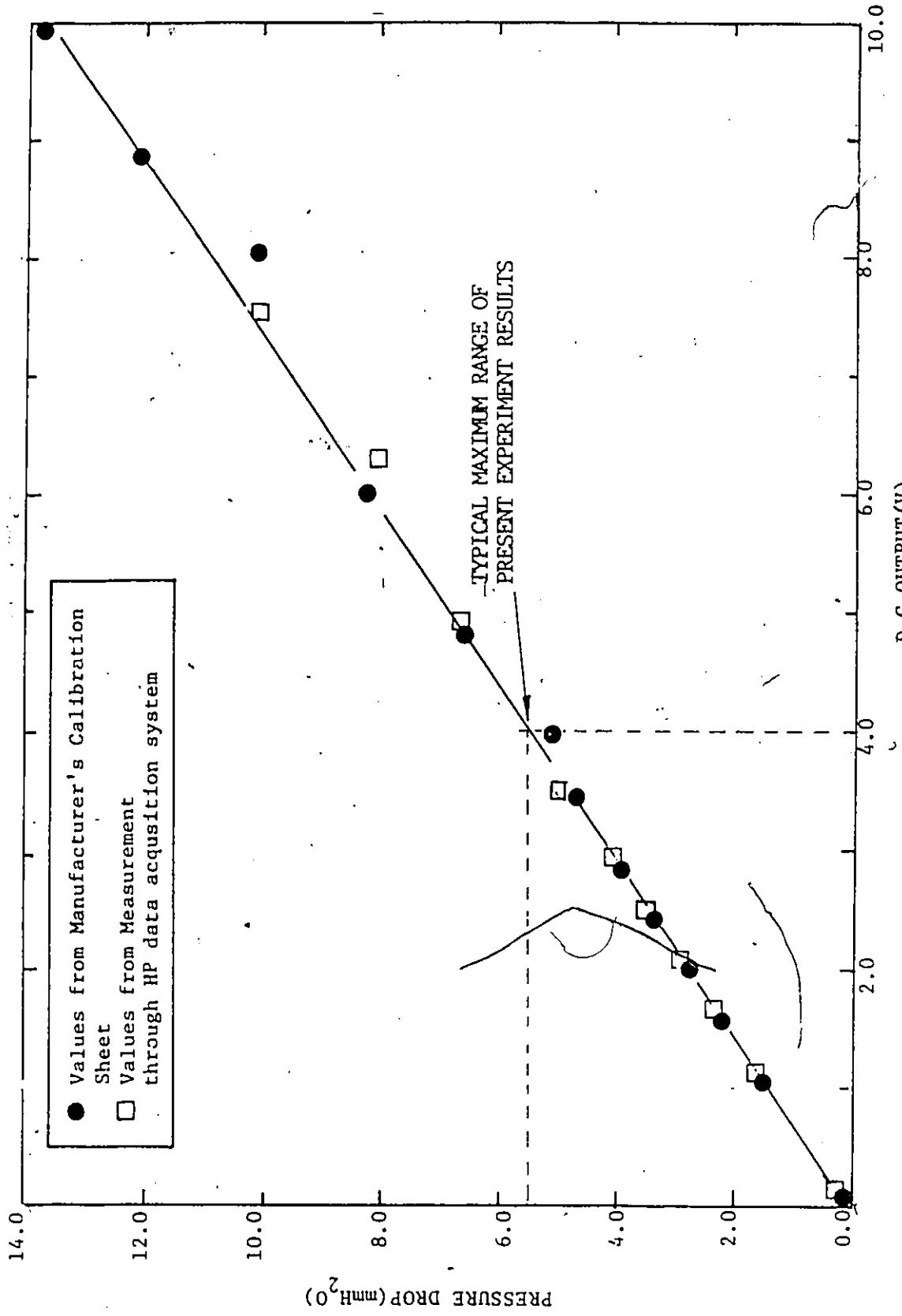

Fig.4.3.3. Typical Result of Pressure Transducer Calibration

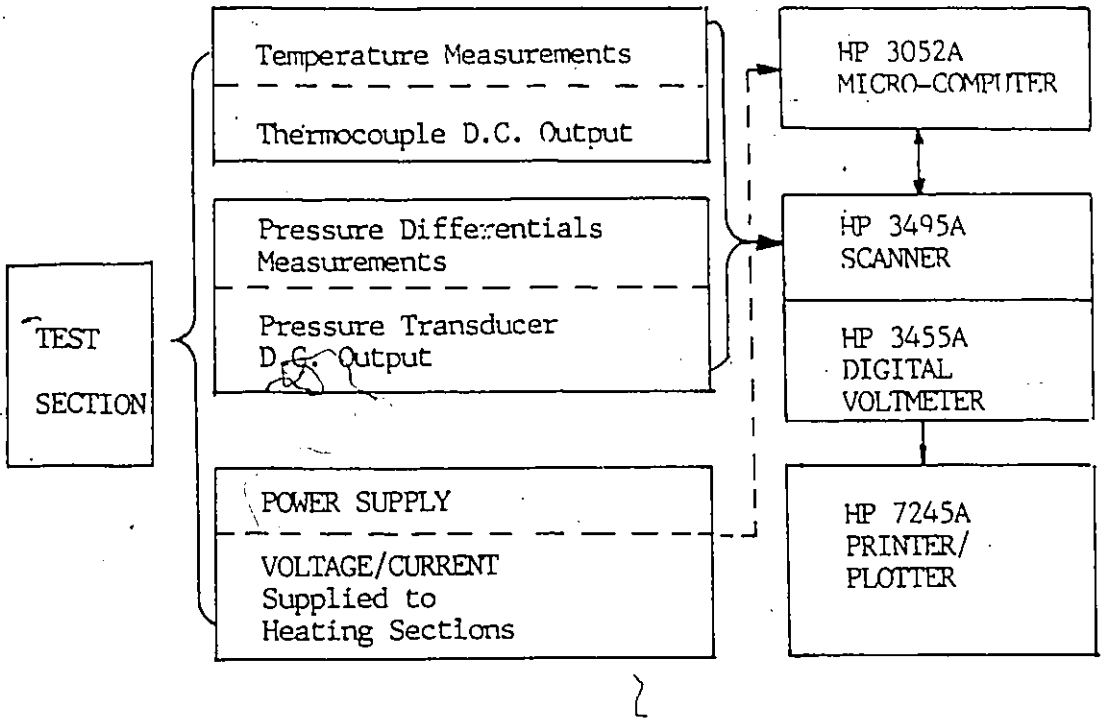

Fig.4.4.1. Schematic Diagram of Data Acquisition System used in Experimental Study

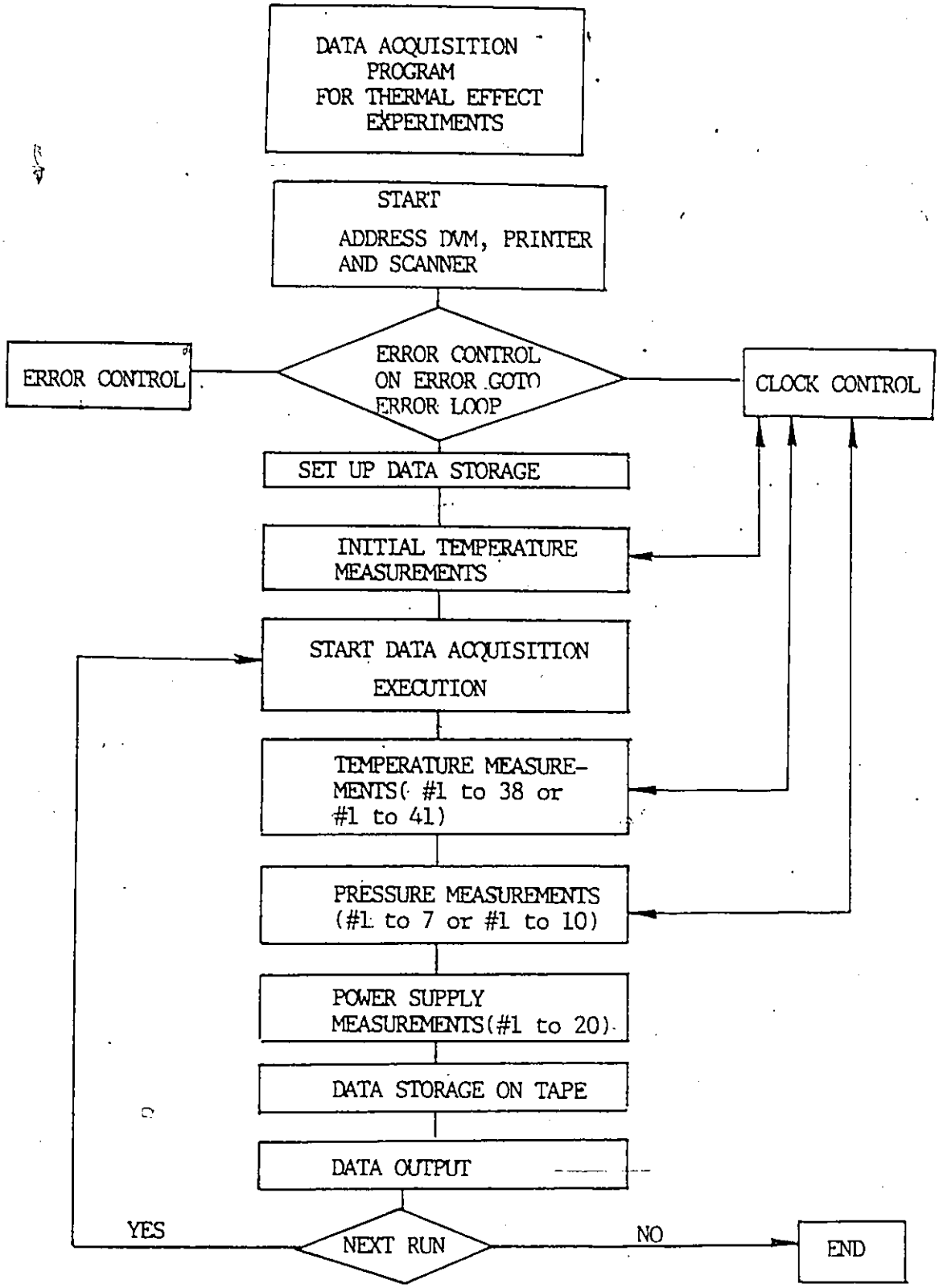

Fig.4.4.2. Flow Chart of Data Acquisition Procedures

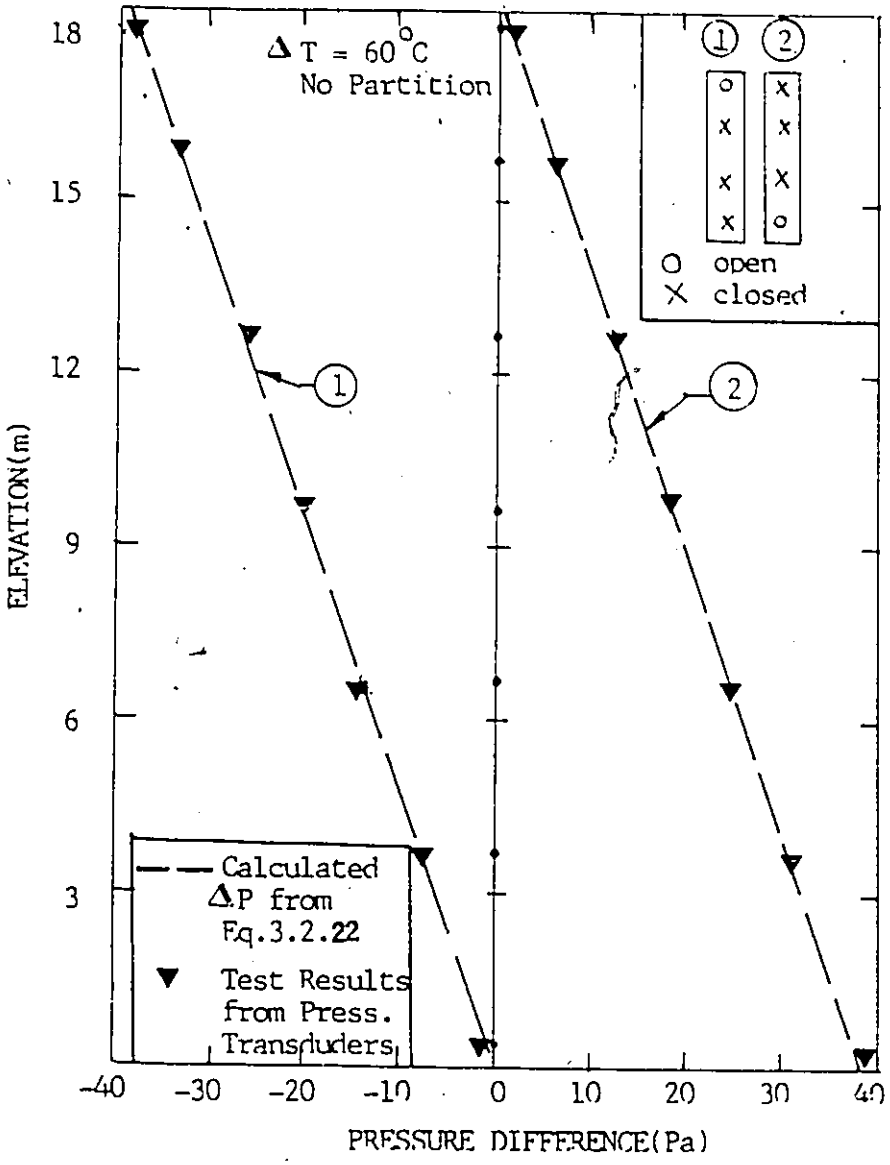

Fig.4.5.1 Test Results of Test Section with No Partitions and Pressure Transducers

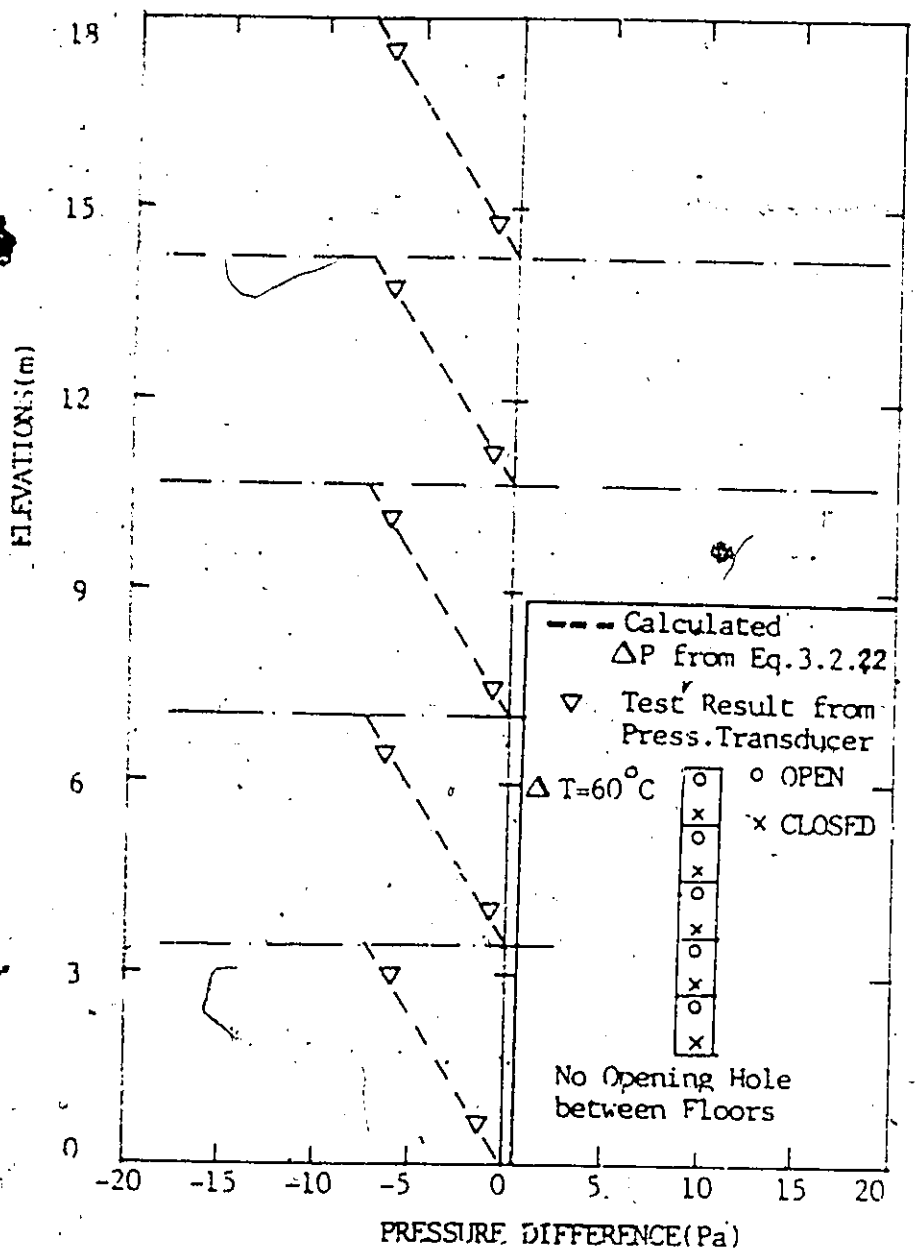

Fig.4.5.2. Test Results of Test Section with Partitions and Pressure Transducers

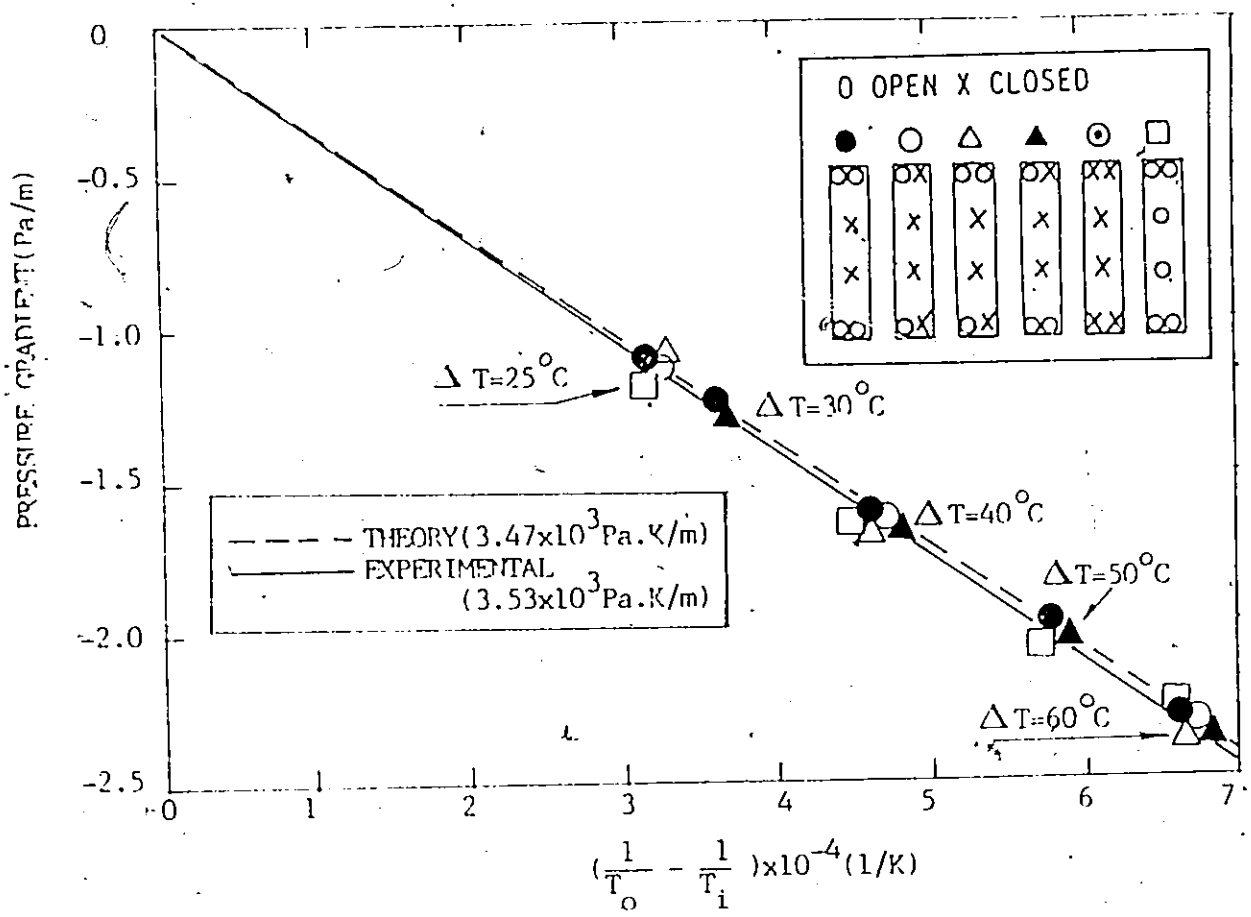

Fig.5.1.1. Pressure Gradient due to Thermal Effect in Case with No Partitions

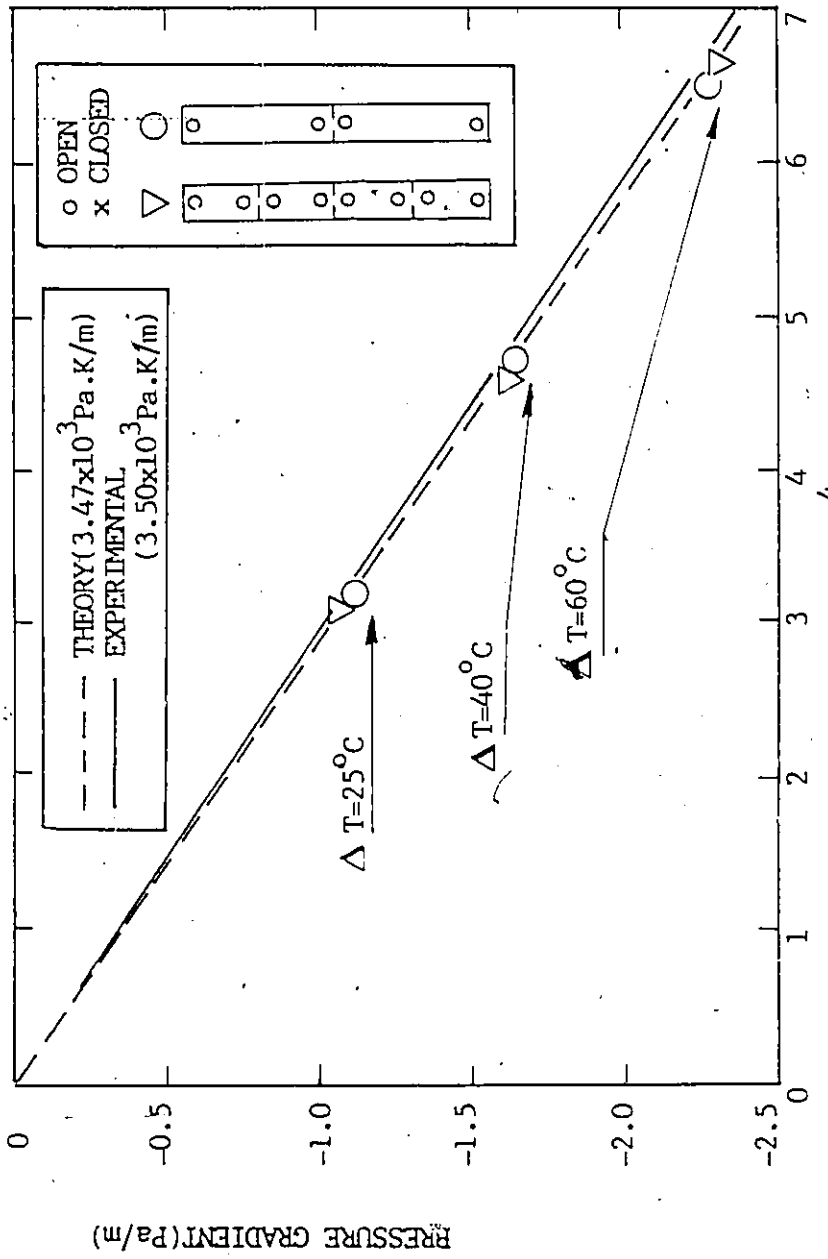

Fig.5.1.2. Pressure Gradient due to Thermal Effect in Partitioned Case

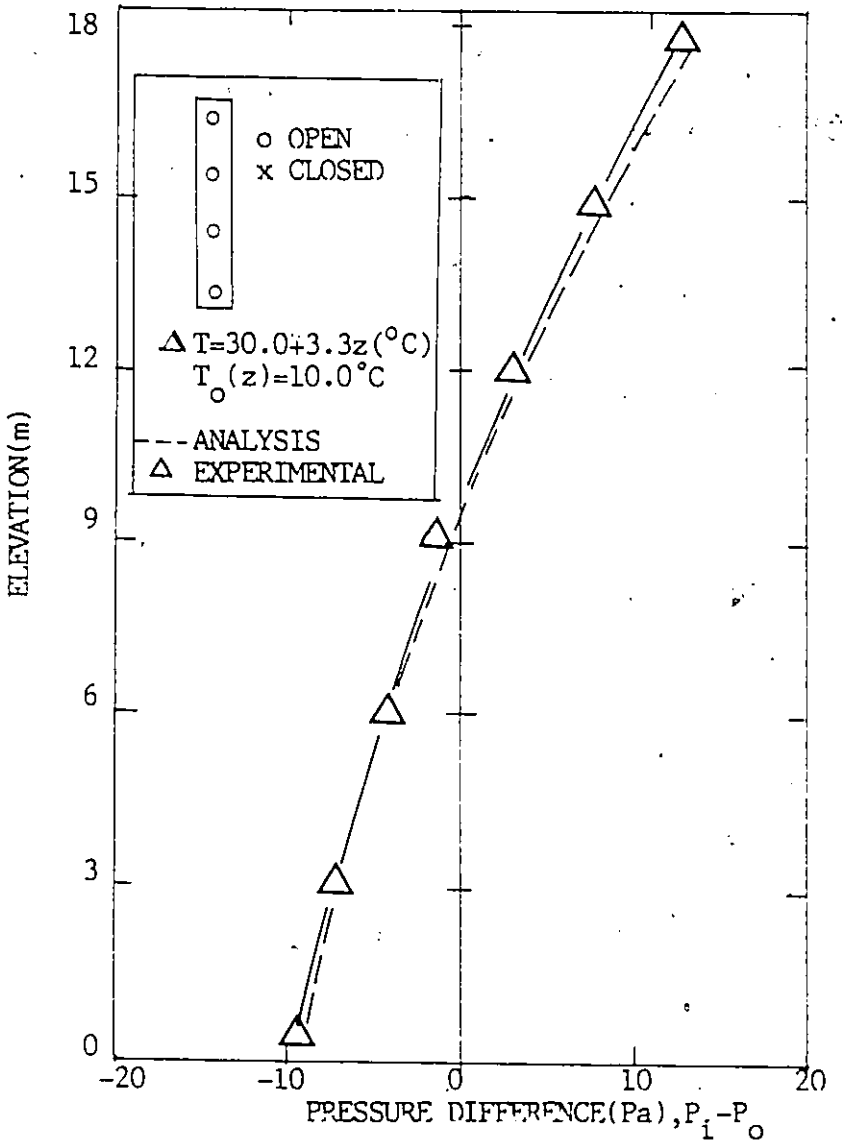

Fig.5.1.3. Validity Test of Thermal Effect Equation for Non-Uniform Temperature

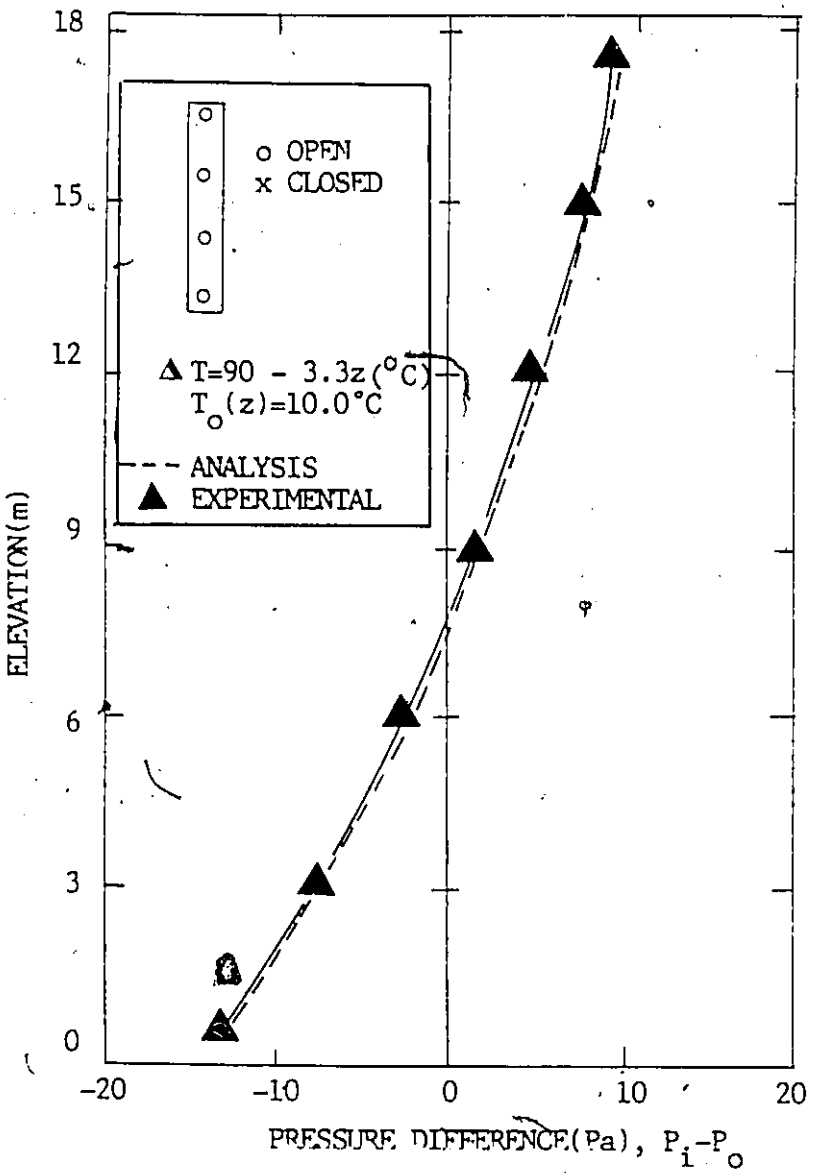

Fig.5.1.4. Validity Test of Thermal Effect Equation for Non-Uniform Temperature

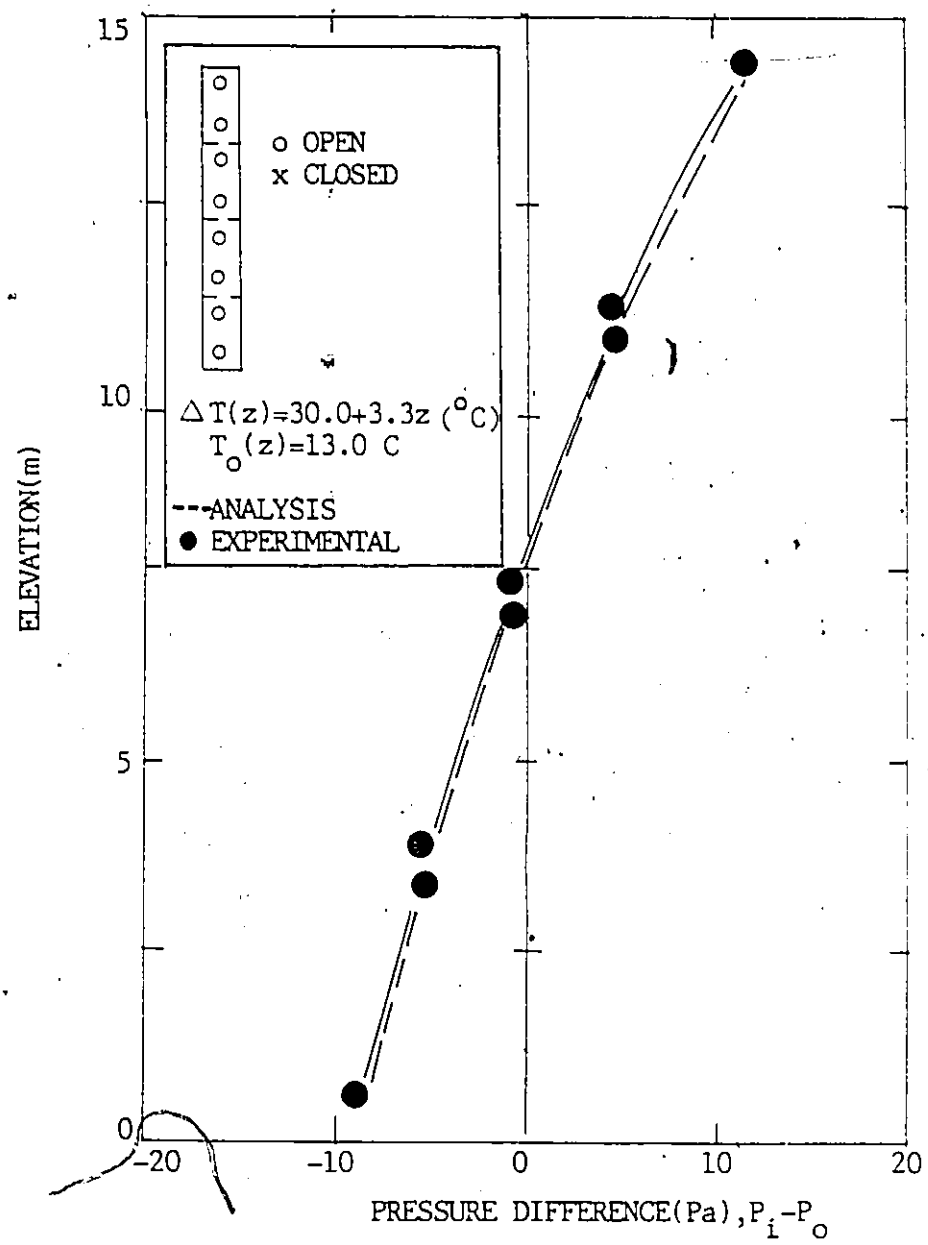

Fig.5.1.5. Validity Test of Non-Uniform Temperature Thermal Effect Equation for Partitioned Case

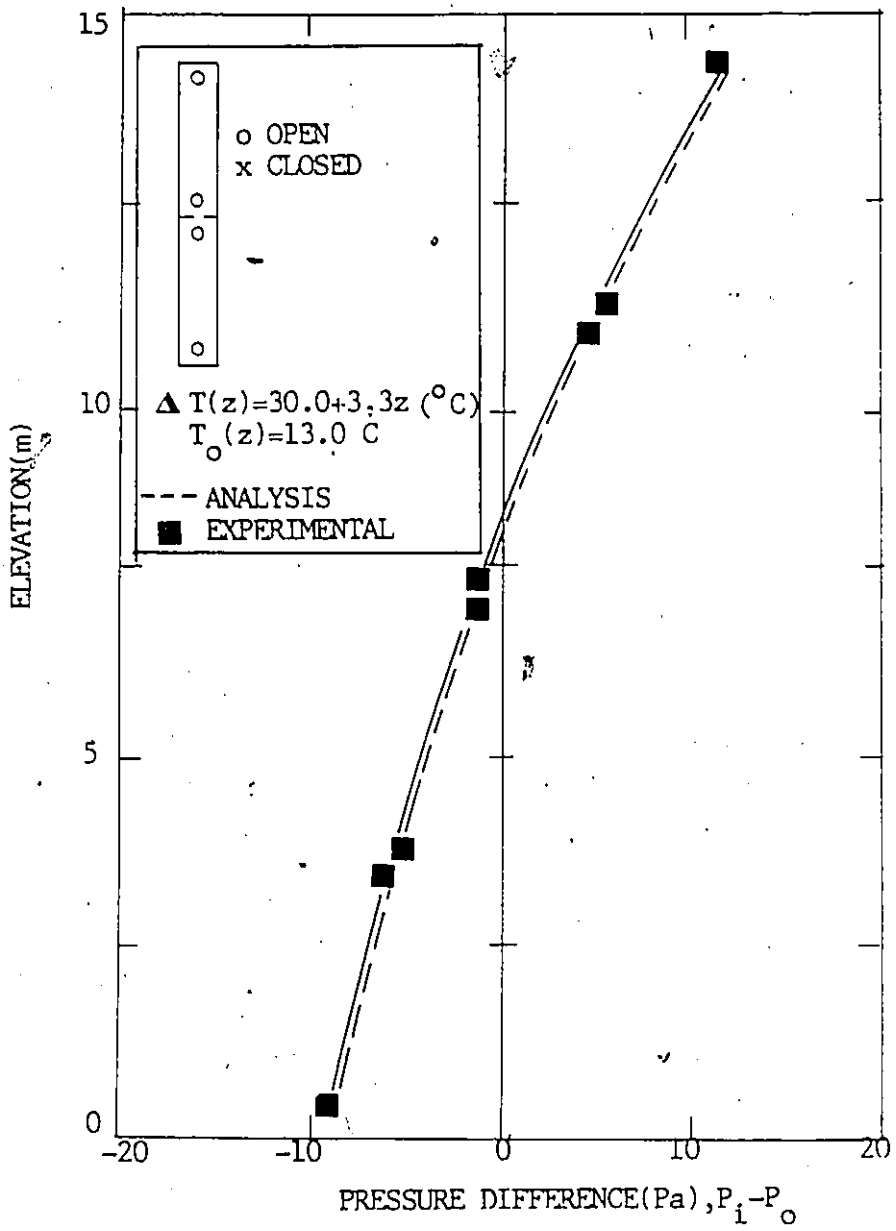

Fig.5.1.6. Validity Test of Non-Uniform Temperature Thermal Effect Equation for Partitioned Case

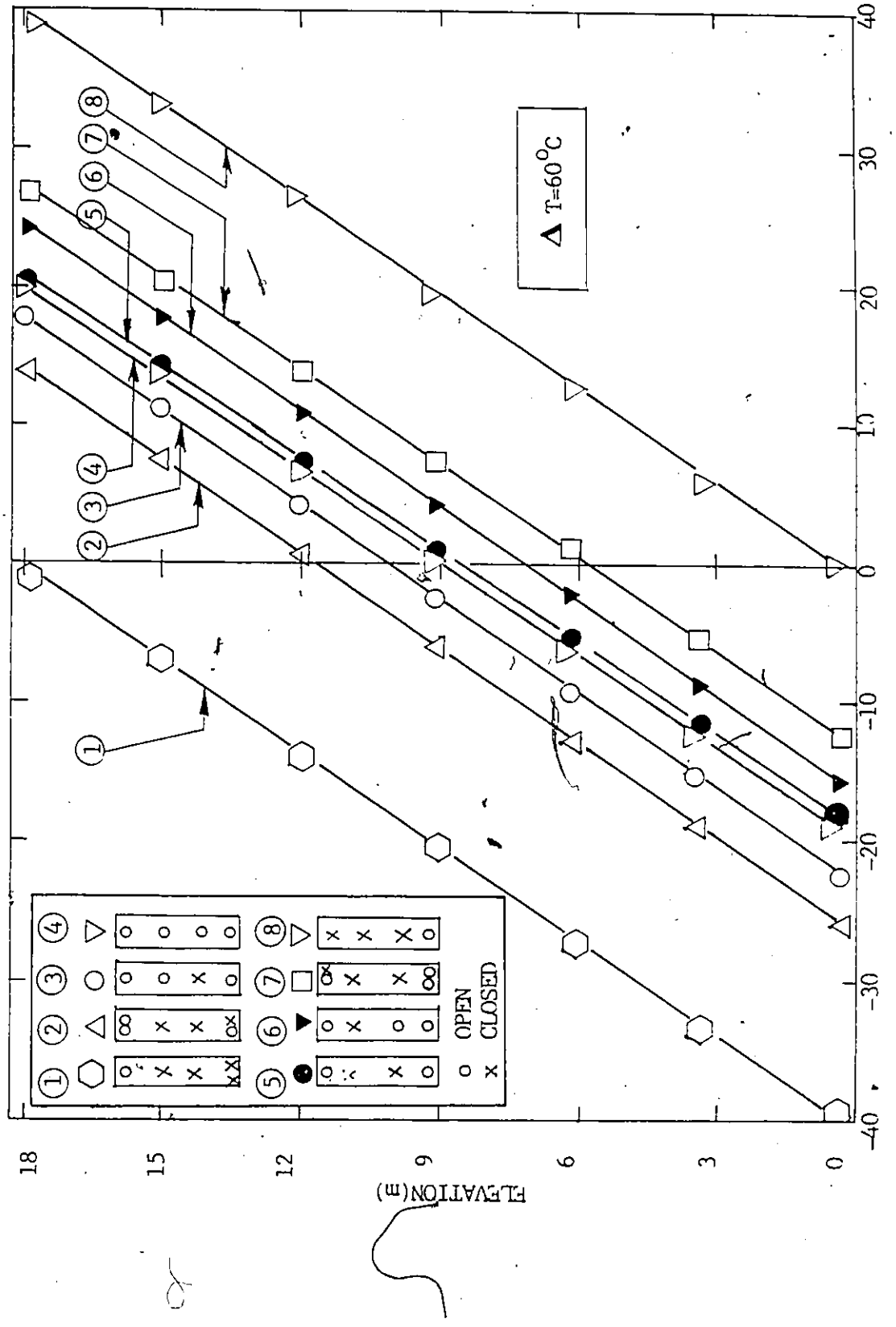

Fig.5.2.1. Experimental Pressure Differential Profiles under Temperature Difference of 60°C

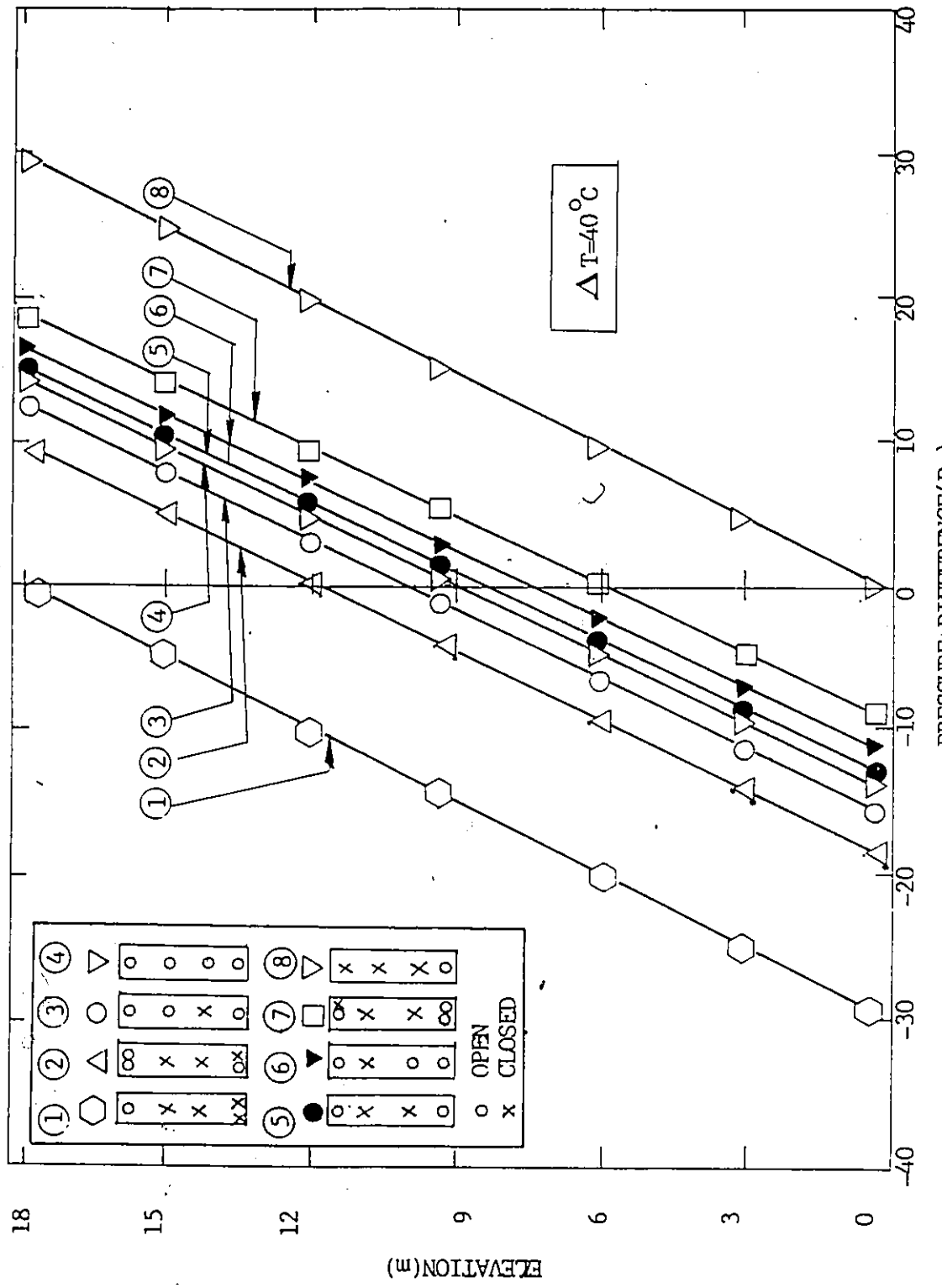

Fig.5.2.2. Experimental Pressure Differential Profiles under Temperature Difference of 40°C

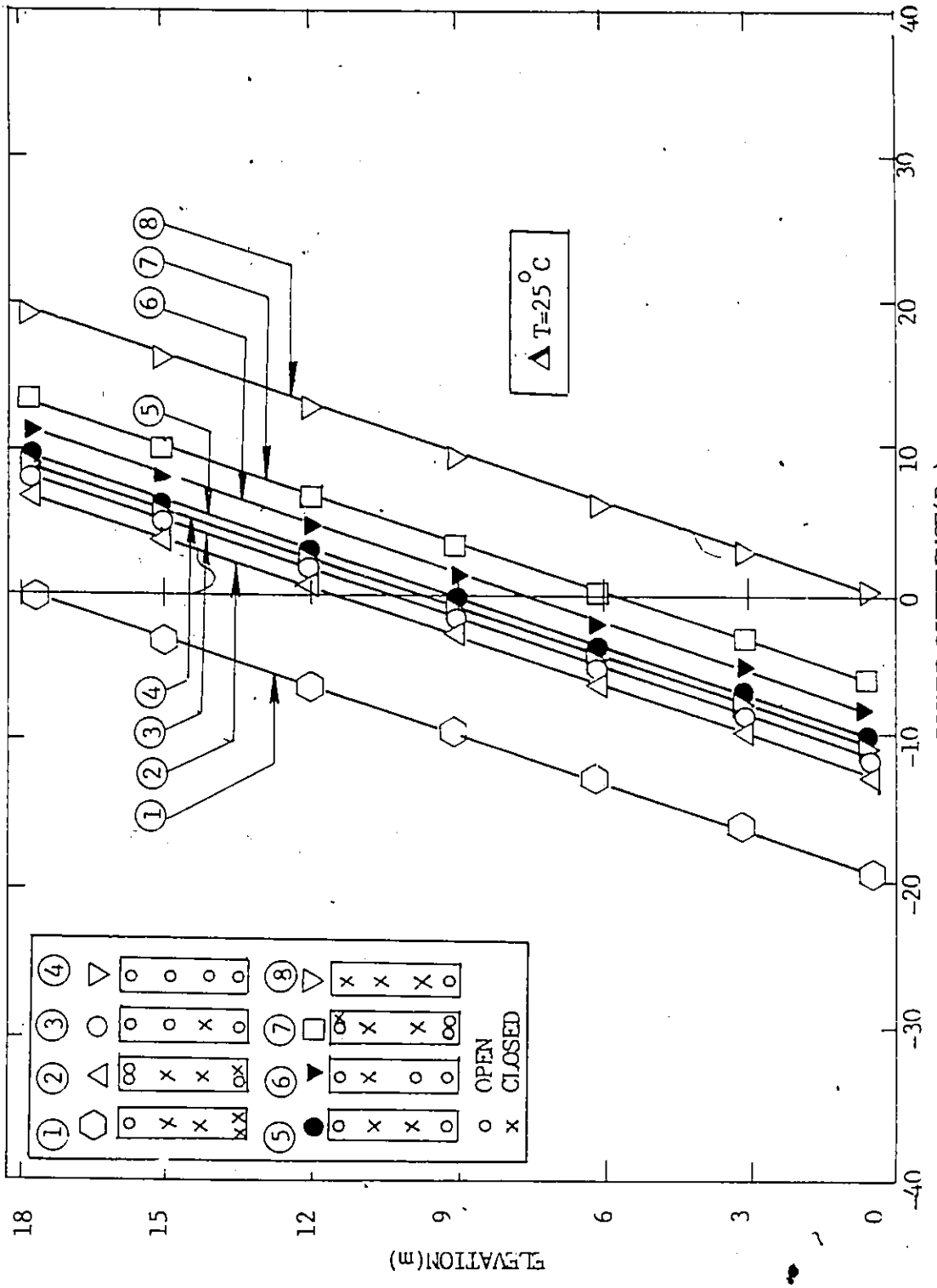

Fig.5.2.3. Experimental Pressure Differential Profiles under Temperature Difference of 25°C

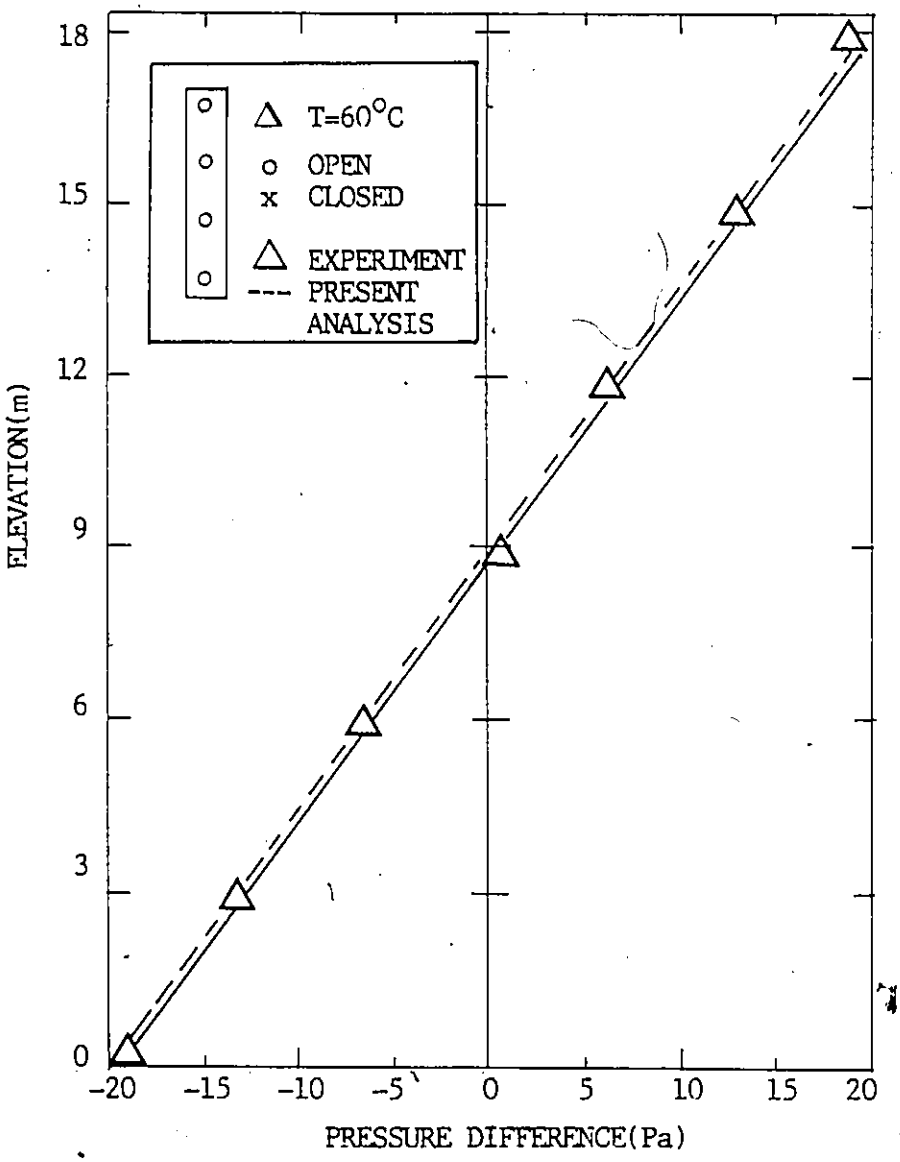

Fig.5.2.4. Comparison of Pressure Differential Profile

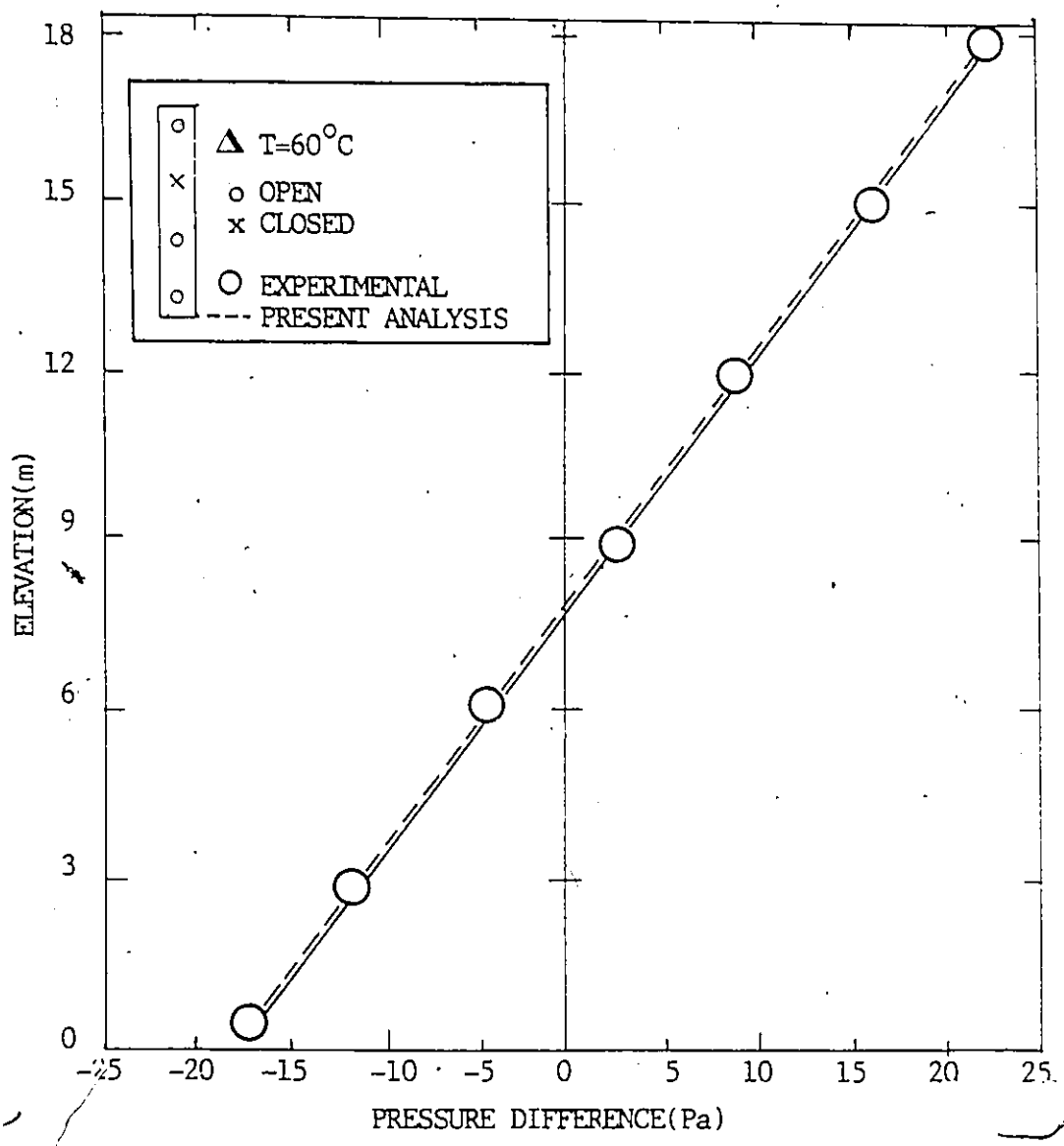

Fig.5.2.5. Comparison of Pressure Differential Profile

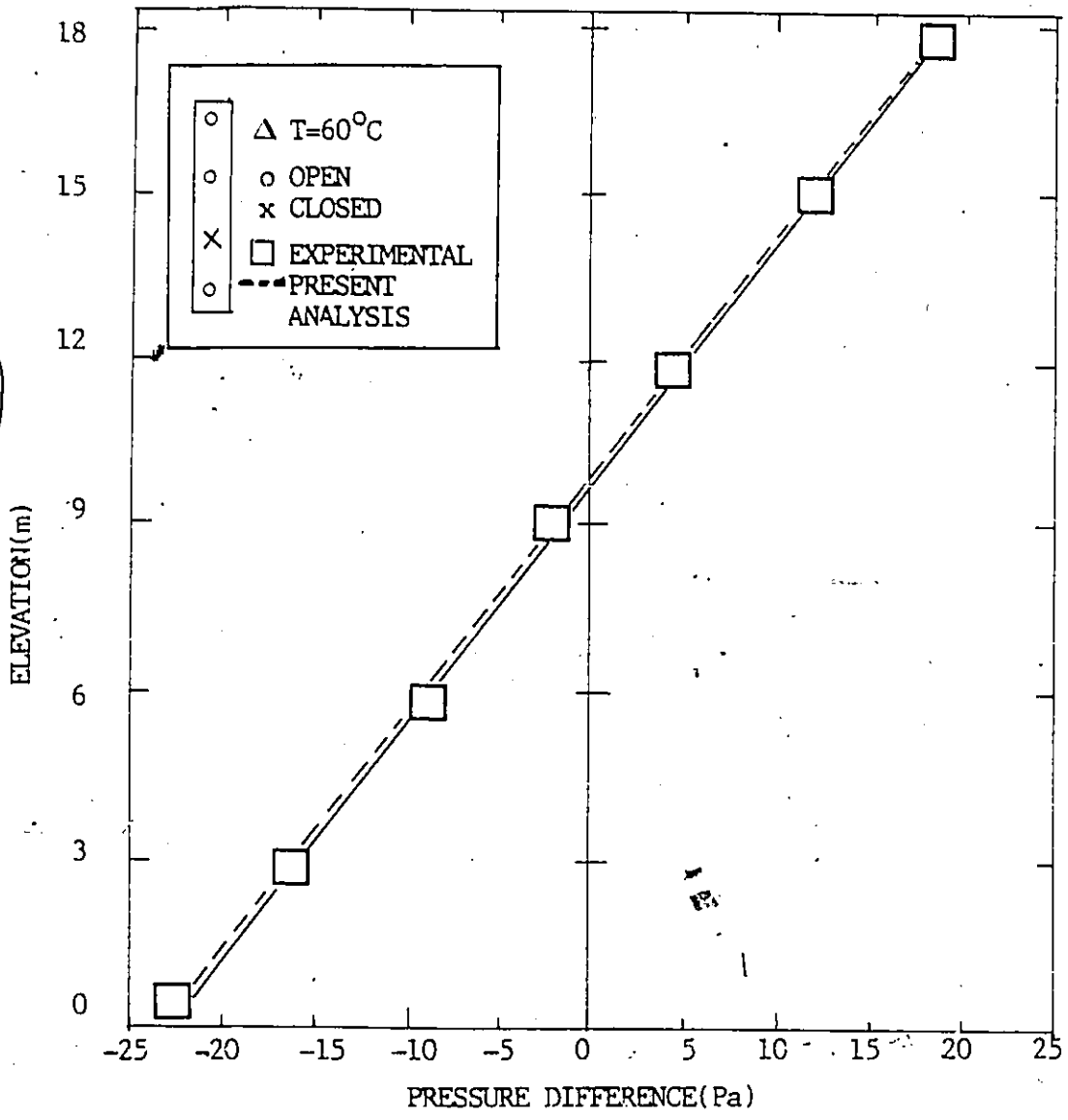

Fig.5.2.6. Comparison of Pressure Differential Profile

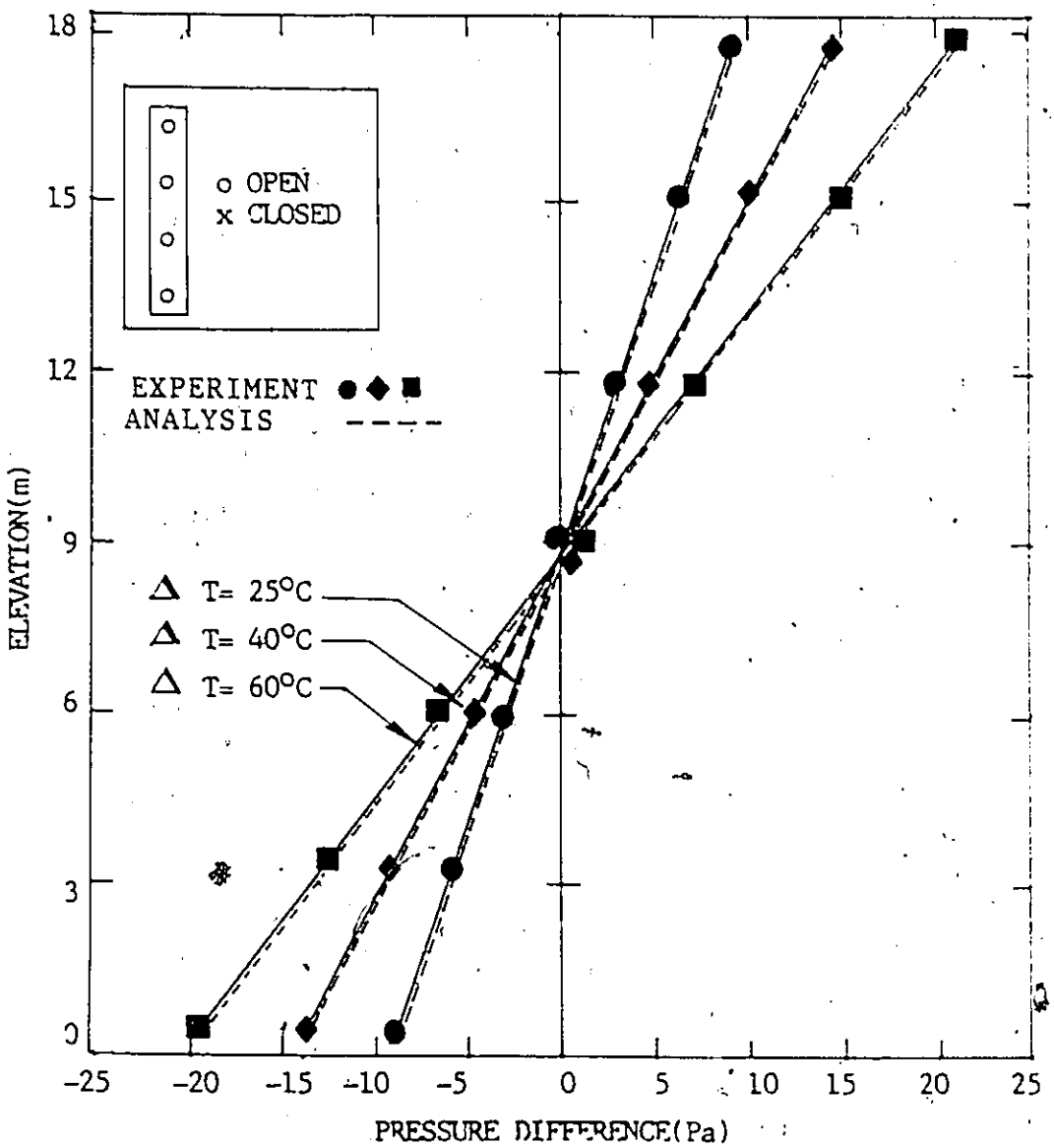

Fig.5.2.7 Effect of Temperature on Thermal Effect

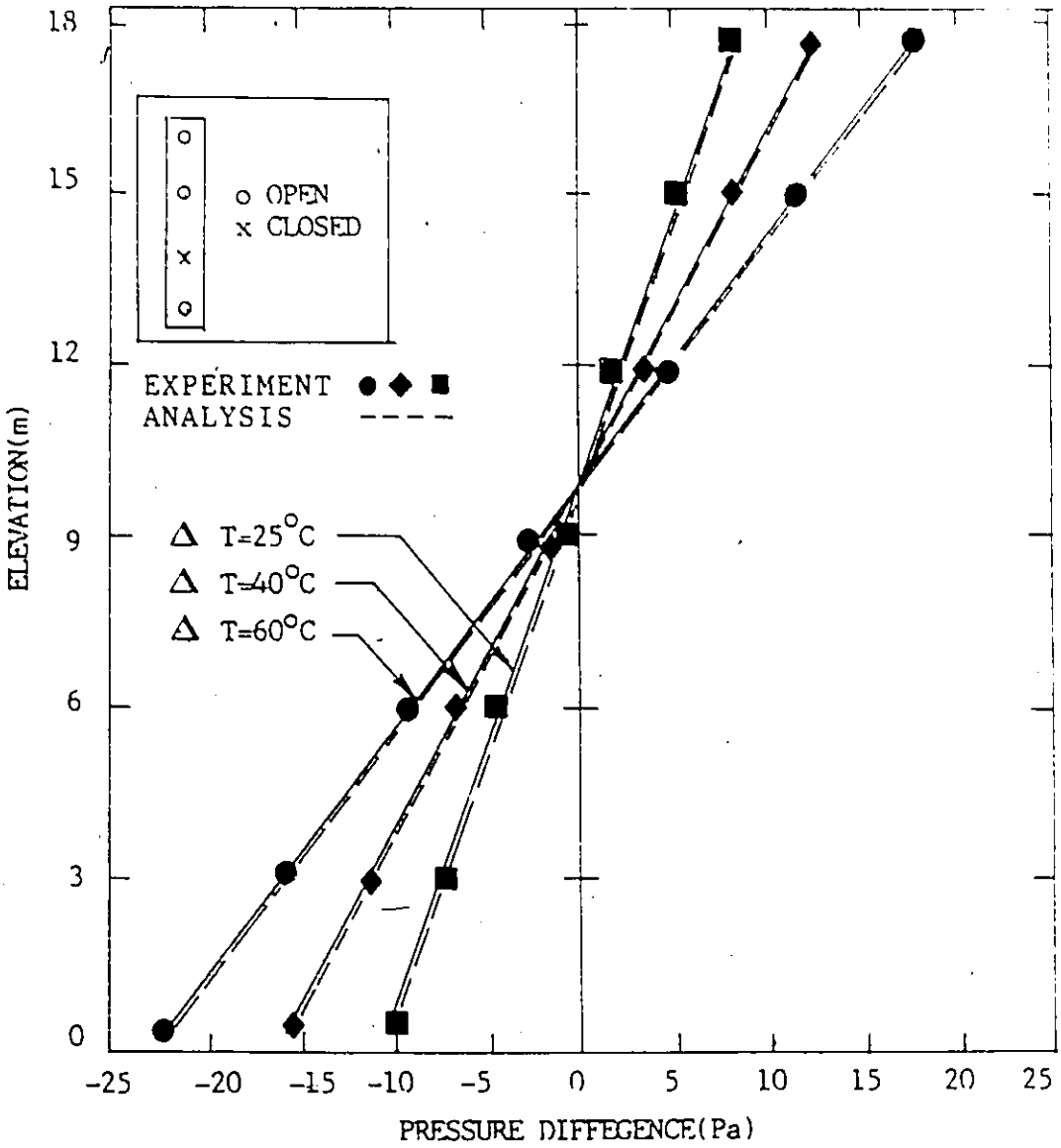

Fig.5.2.8 Effect of Temperature on Thermal Effect

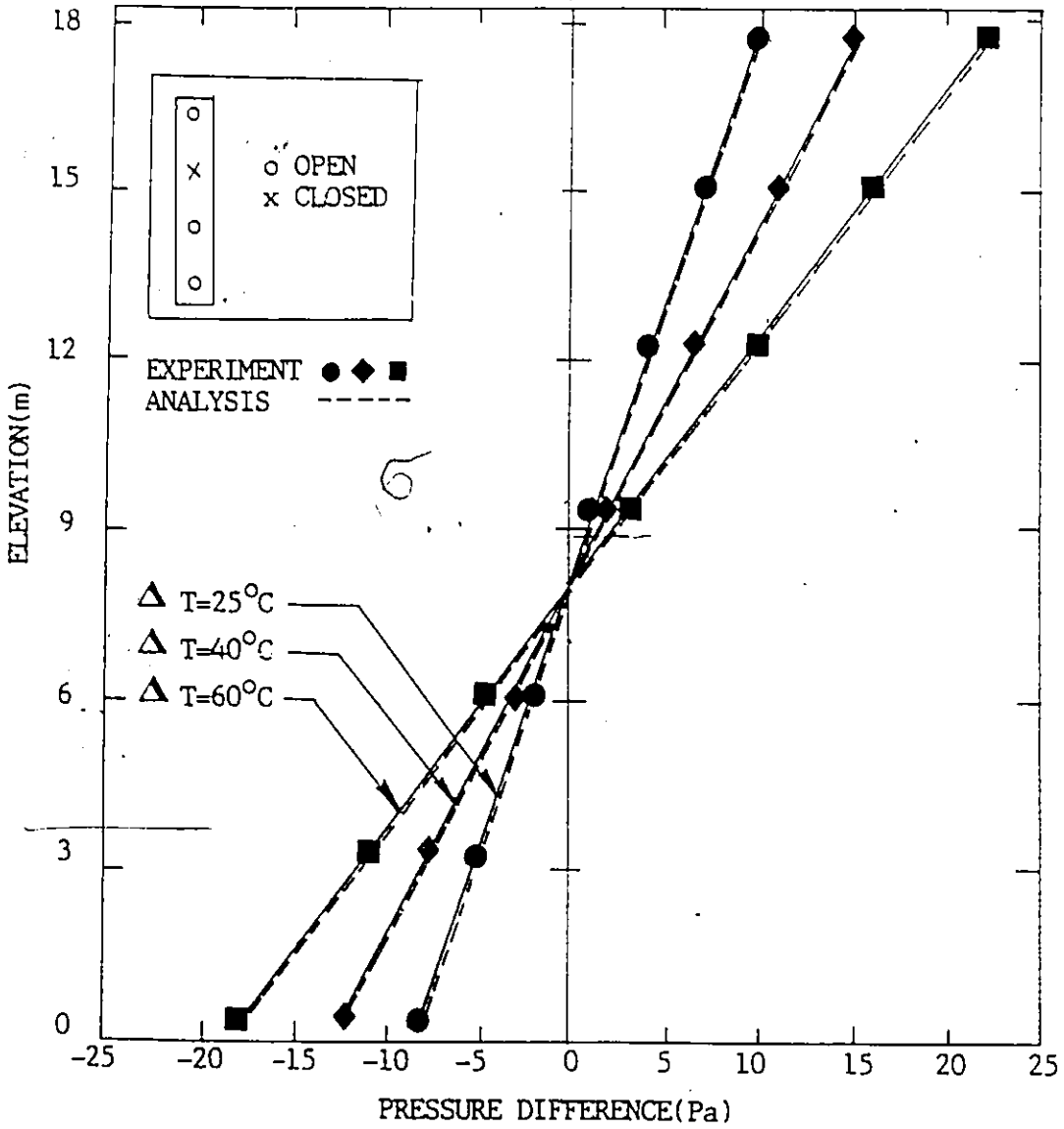

Fig.5.2.9 Effect of Temperature on Thermal Effect

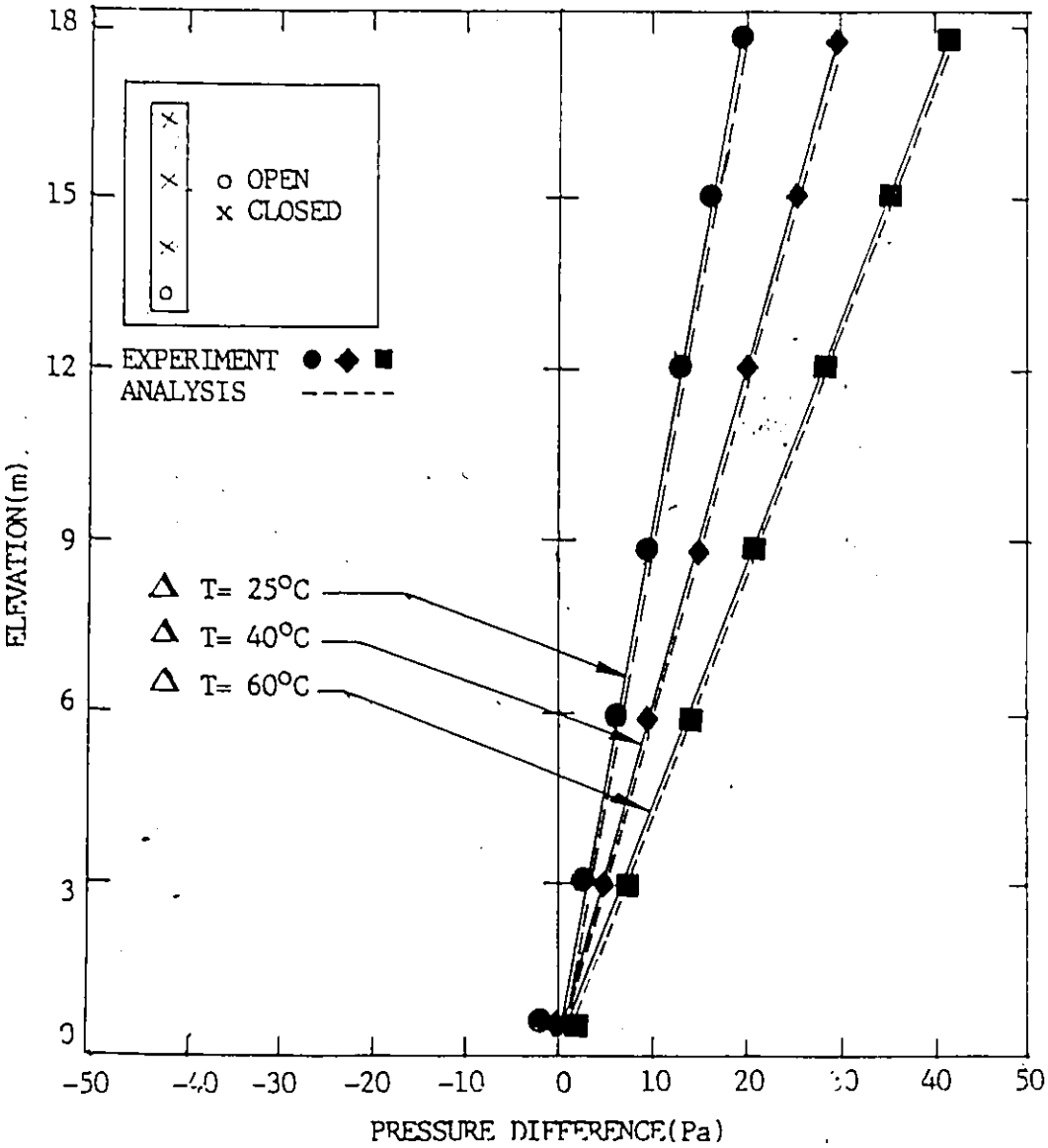

Fig.5.2.10 Effect of Temperature on Thermal Effect

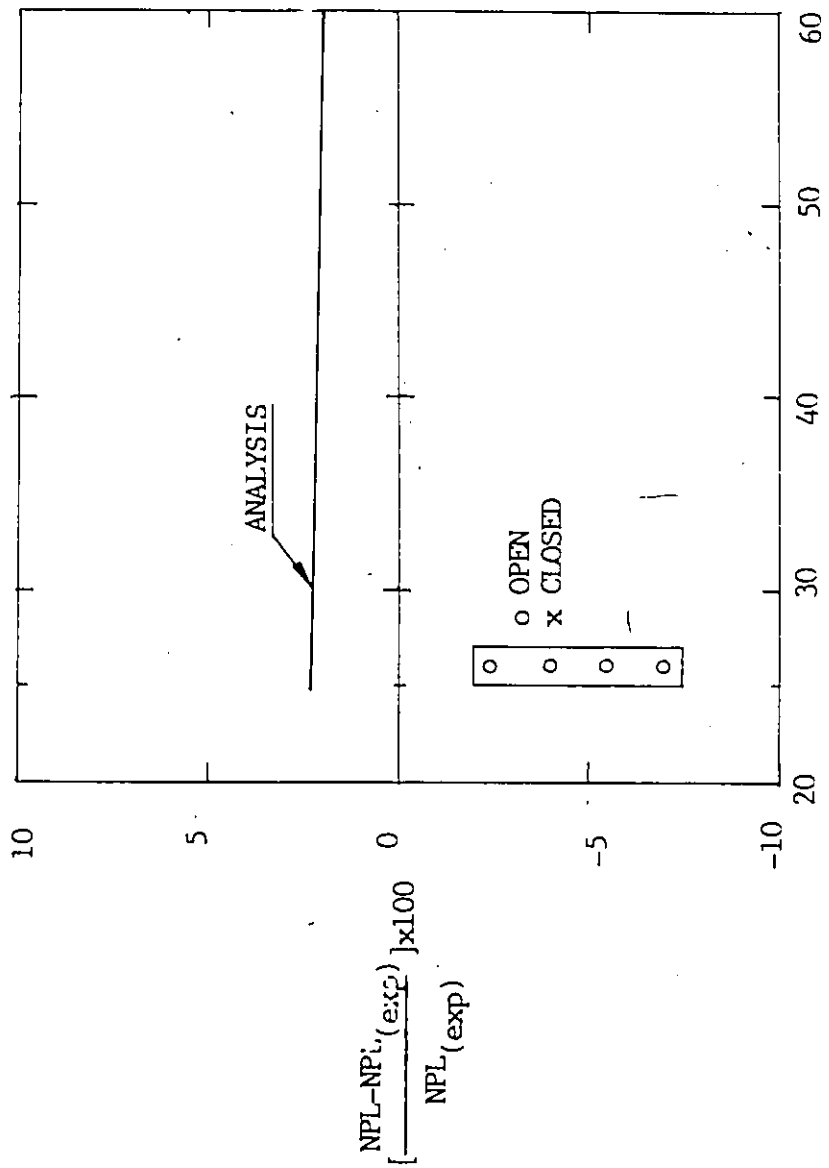

Fig.5.2.11 Test Result of Present Model for NPL

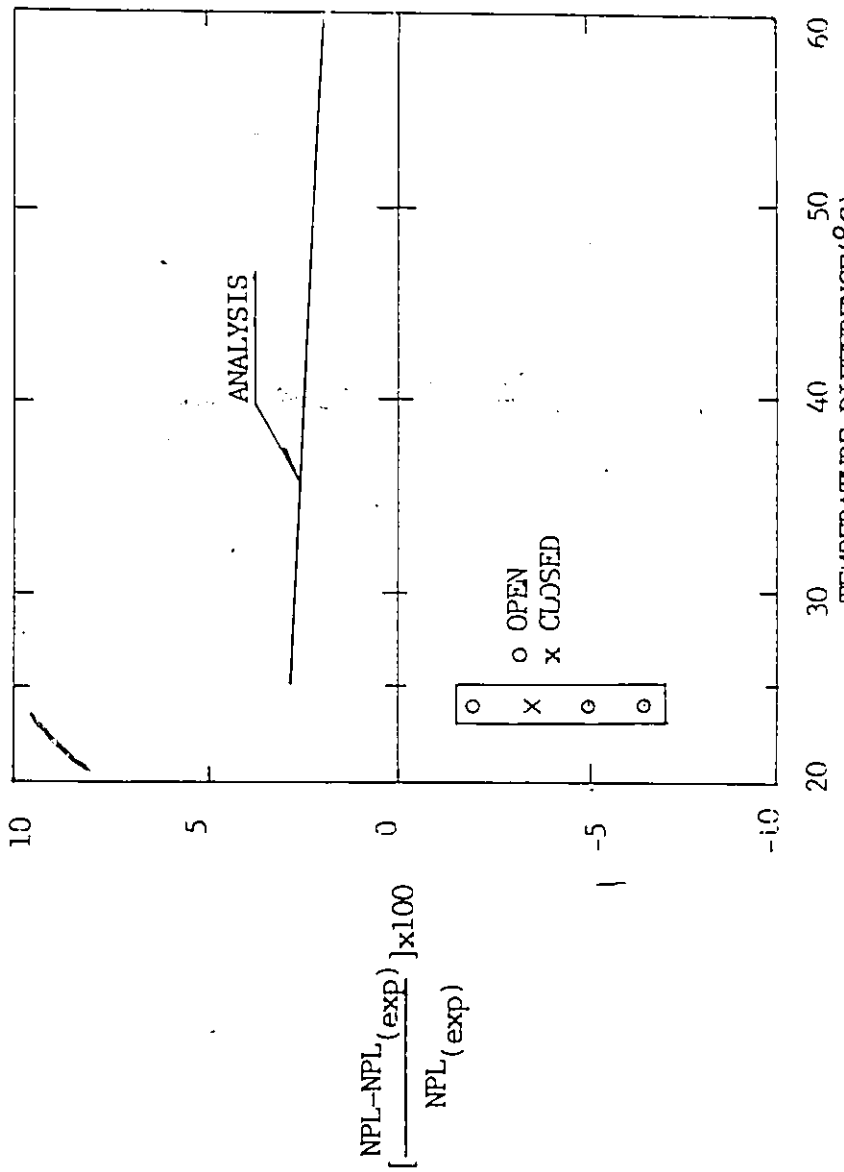

Fig.5.2.12 Test Result of Present Model for NPL

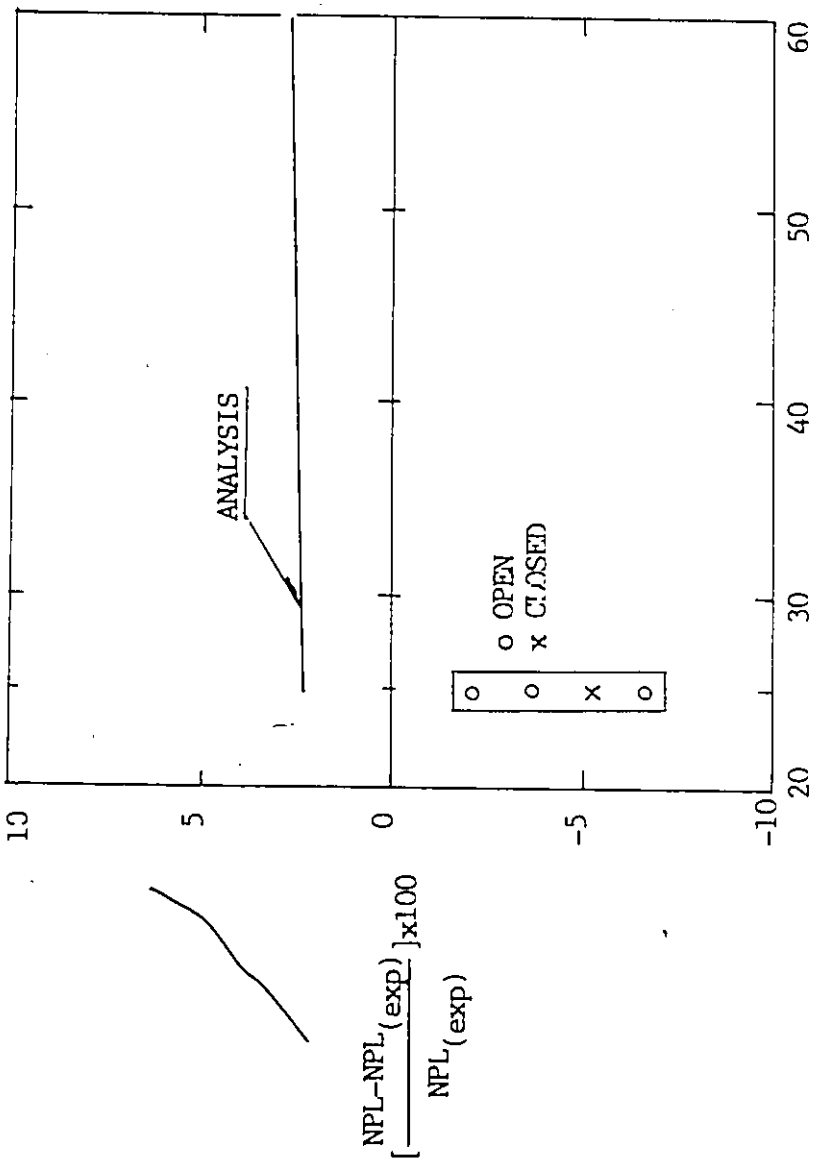

Fig.5.2.13 Test Result of Present Model for NPL

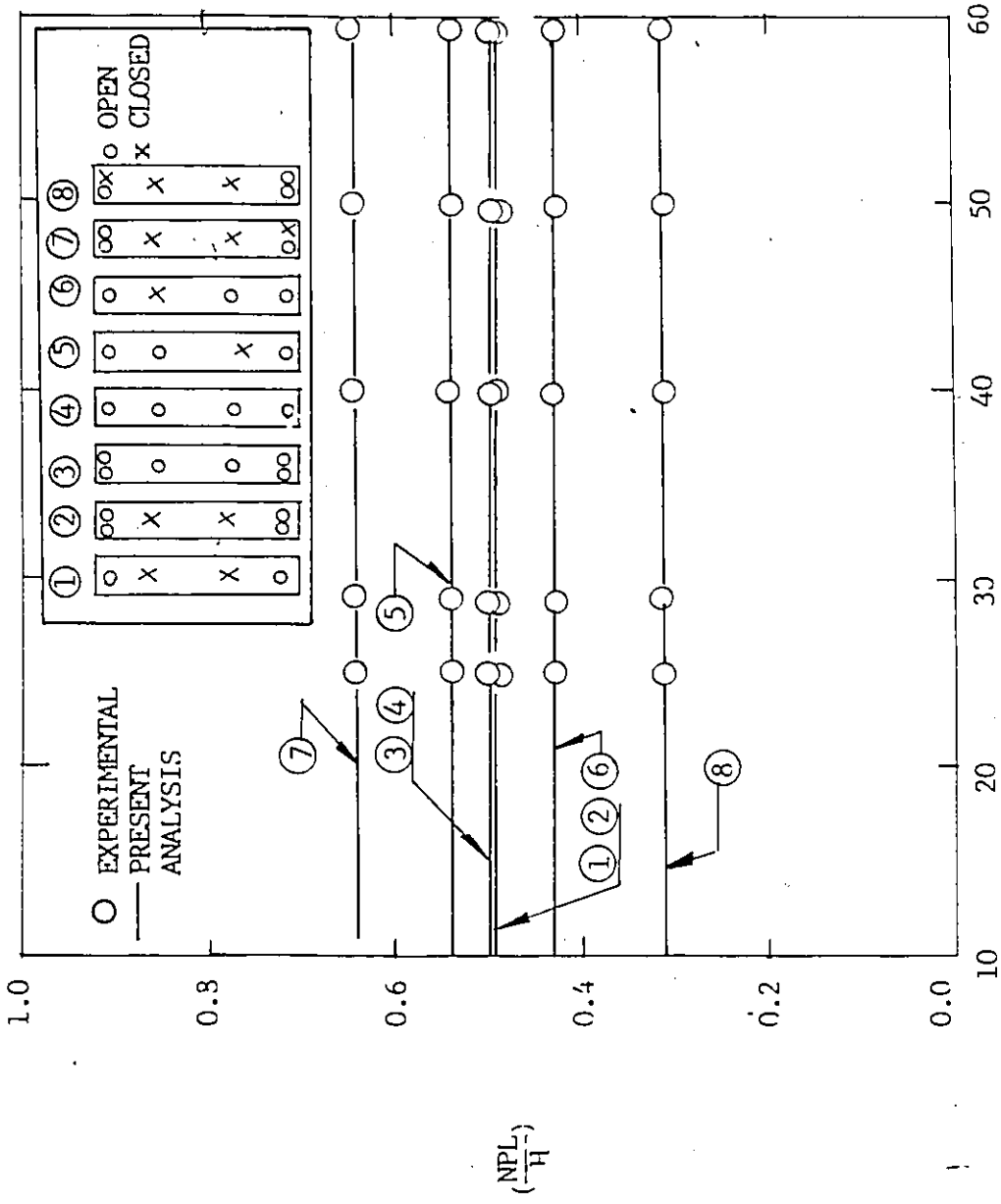

Fig.5.2.14 Effect of Temperature Difference on NPL

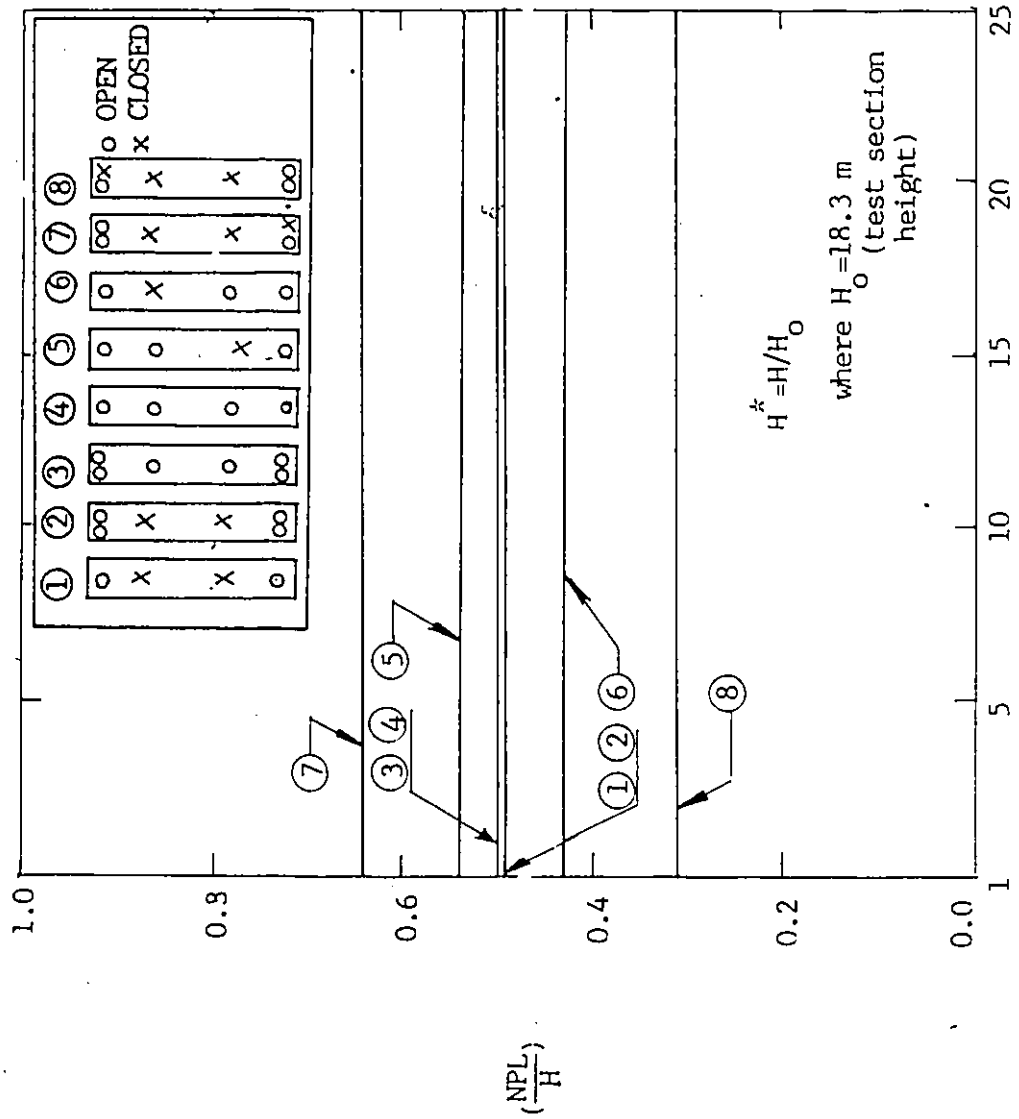

Fig.5.2.15 Effect of Building Height on NPL

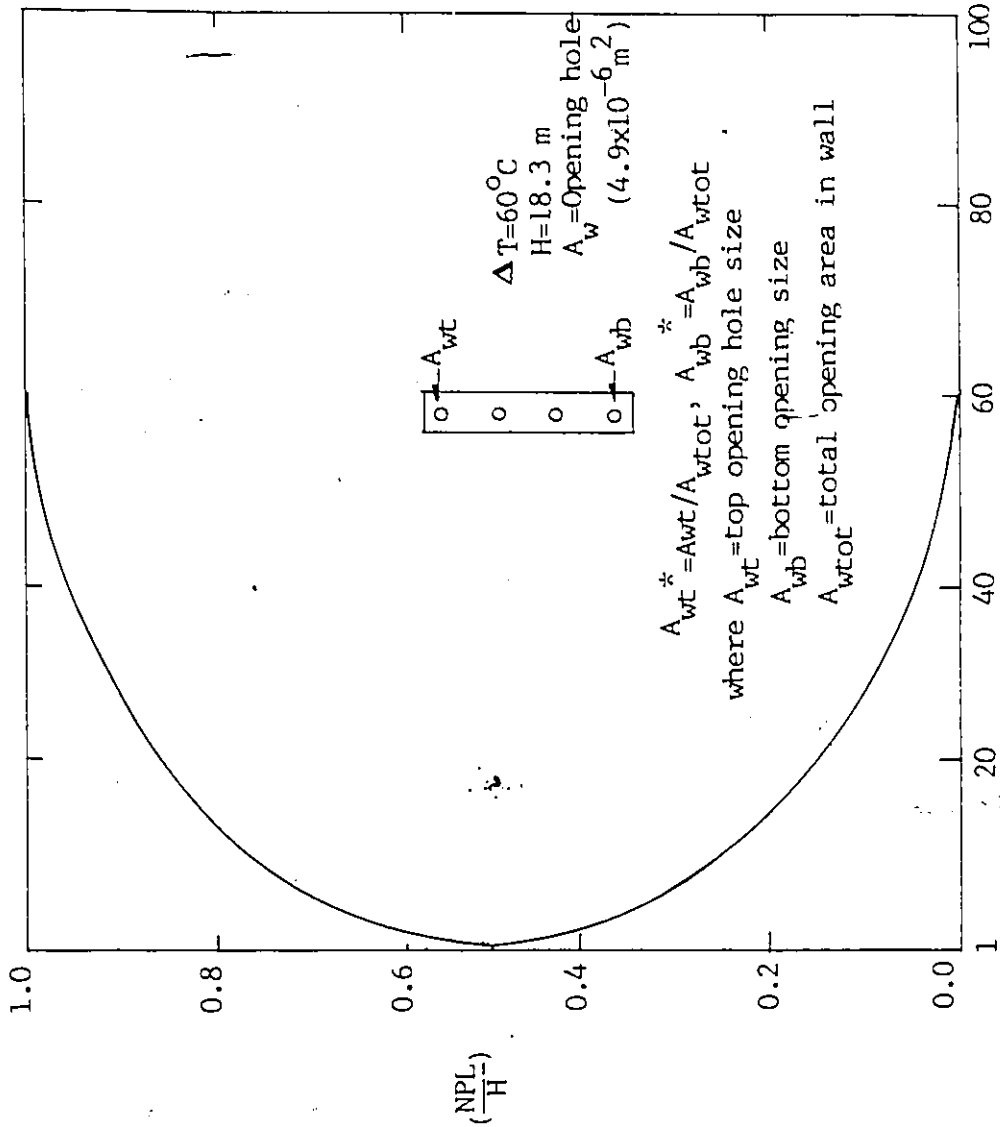

Fig.5.2.16 Effect of Enlargement of Top or Bottom Opening only on NPL

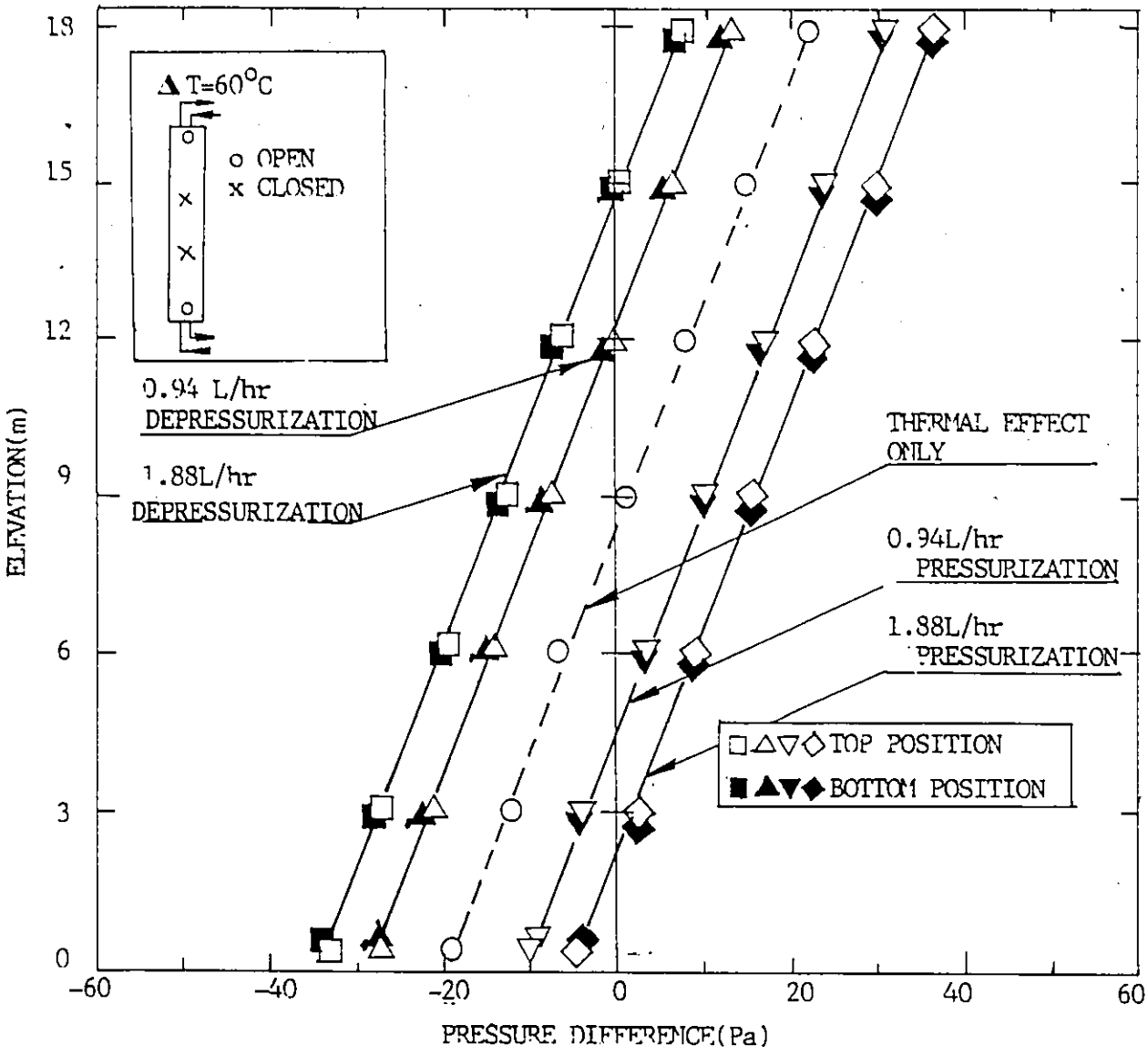

Fig.5.2.18 Effect of Ventilation on Thermal Effect(Top and Bottom Opening)

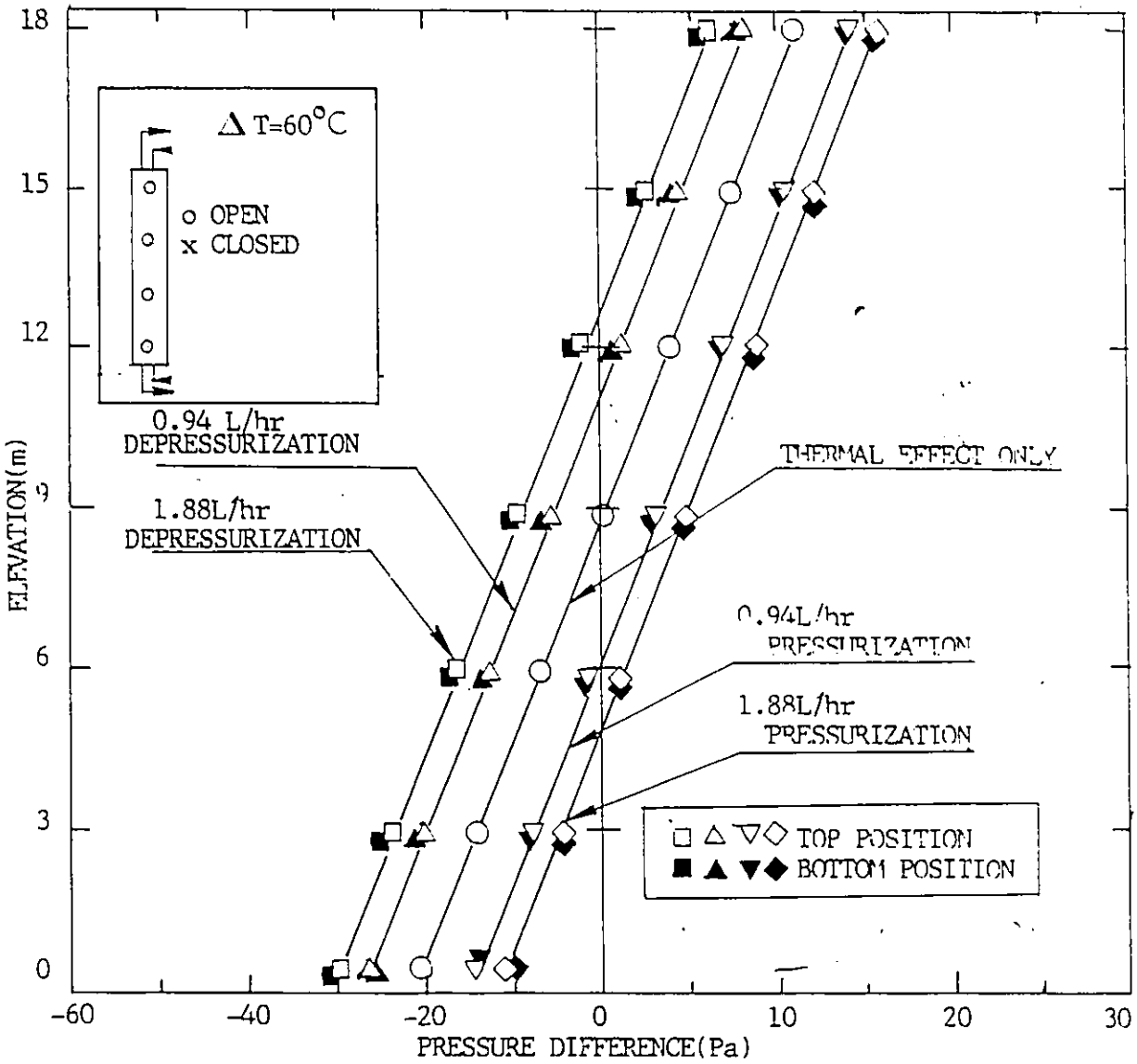

Fig.5.2.18 Effect of Ventilation on Thermal Effect(Four Openings)

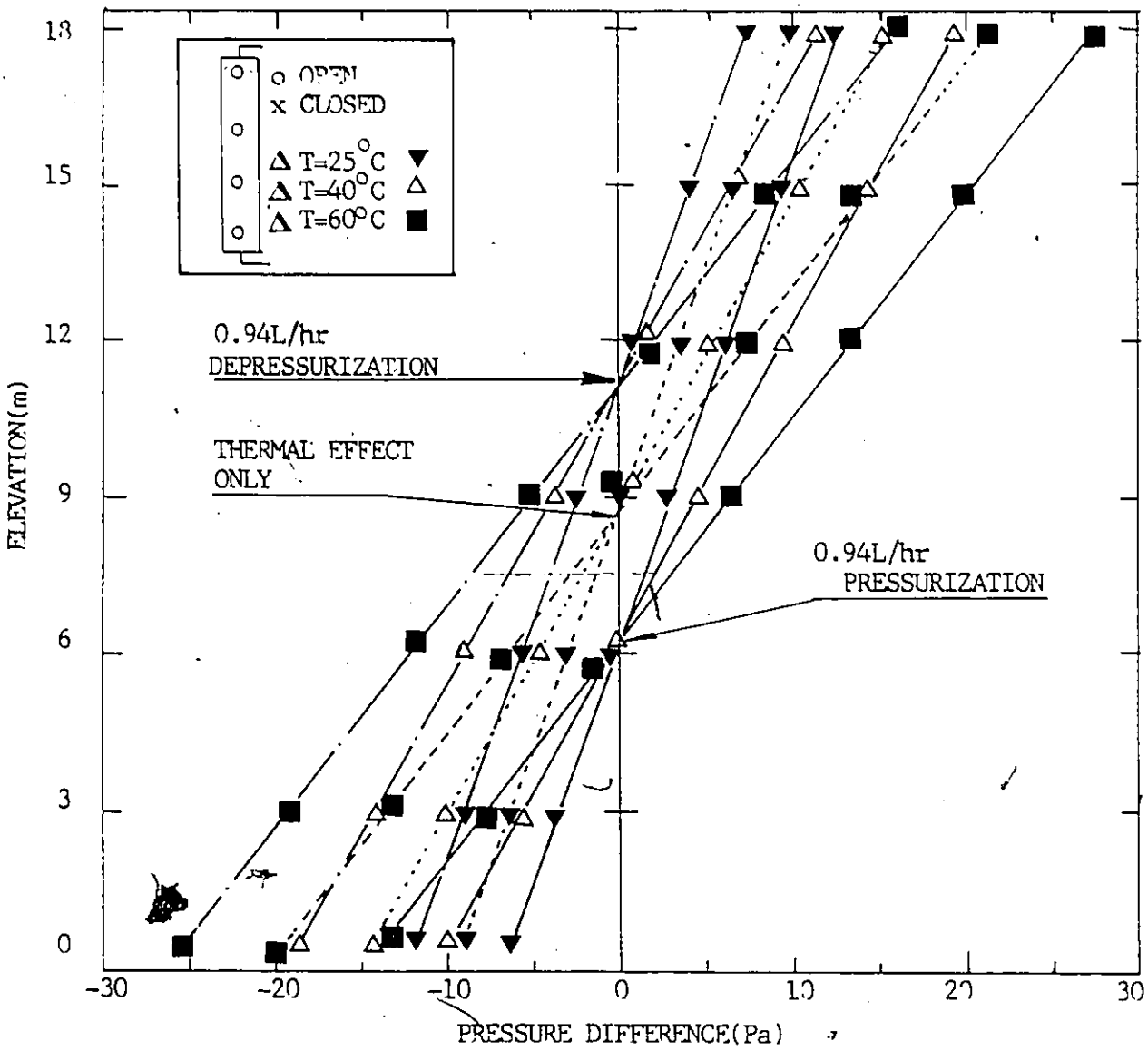

Fig.5.2.19 Combined Effect of Ventilation and Temperature on Thermal Effect

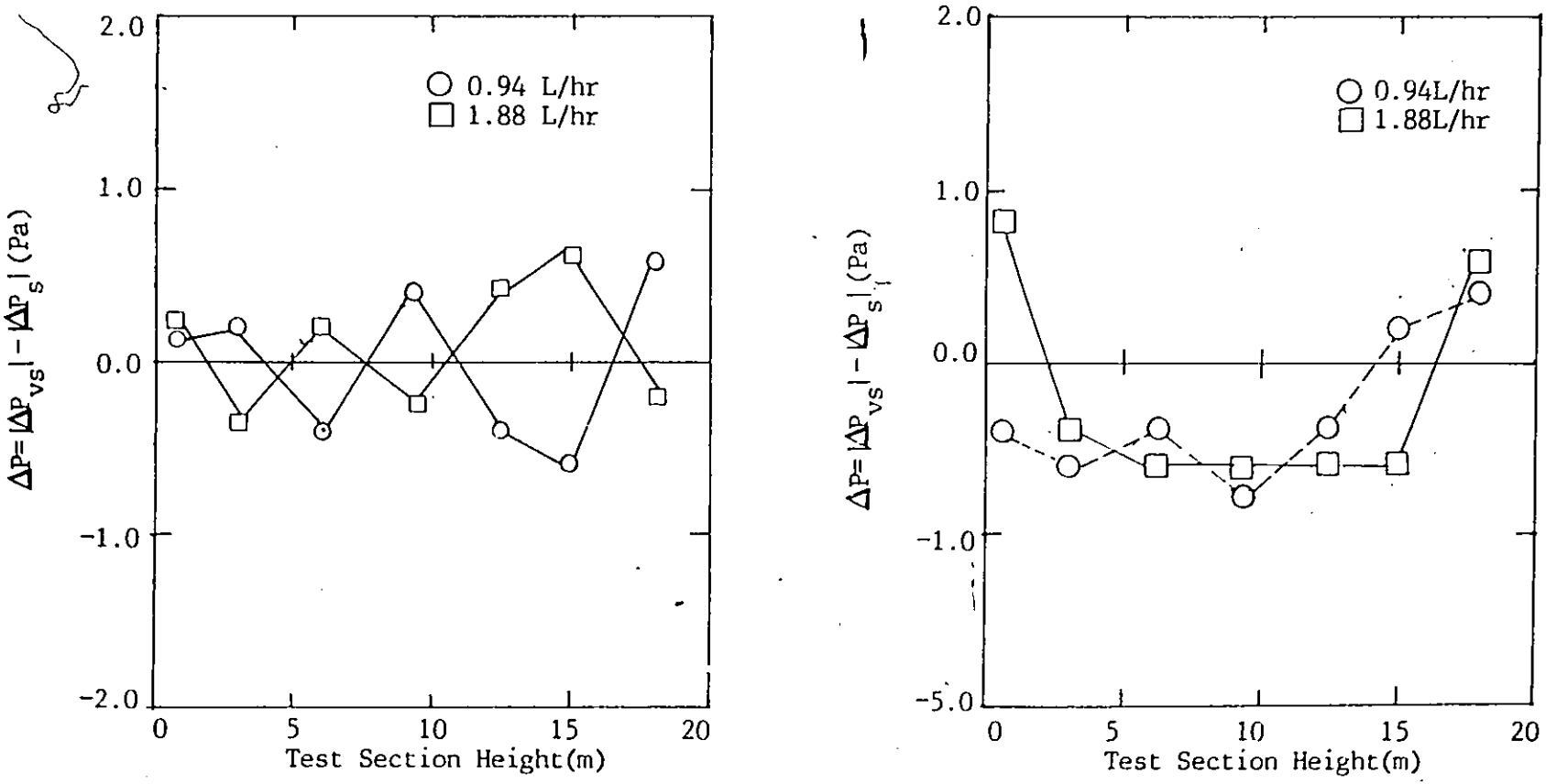

Fig.5.2.20 Effect of Applying Position of Mechanical Ventilation on Pressure Differential due to Thermal Effect

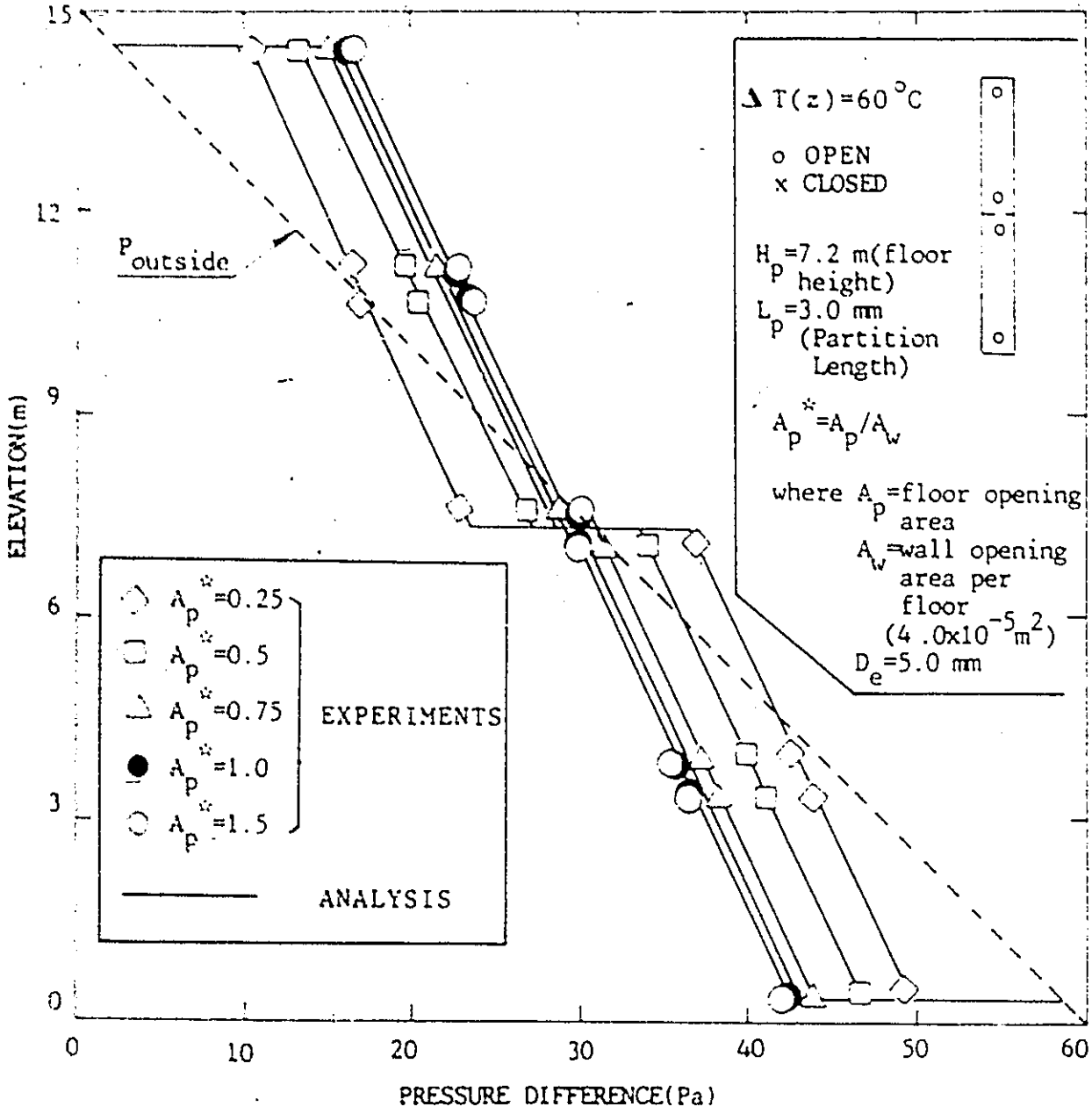

Fig.5. .1 Pressure Differential Profile for Two Floor Partitioned Case

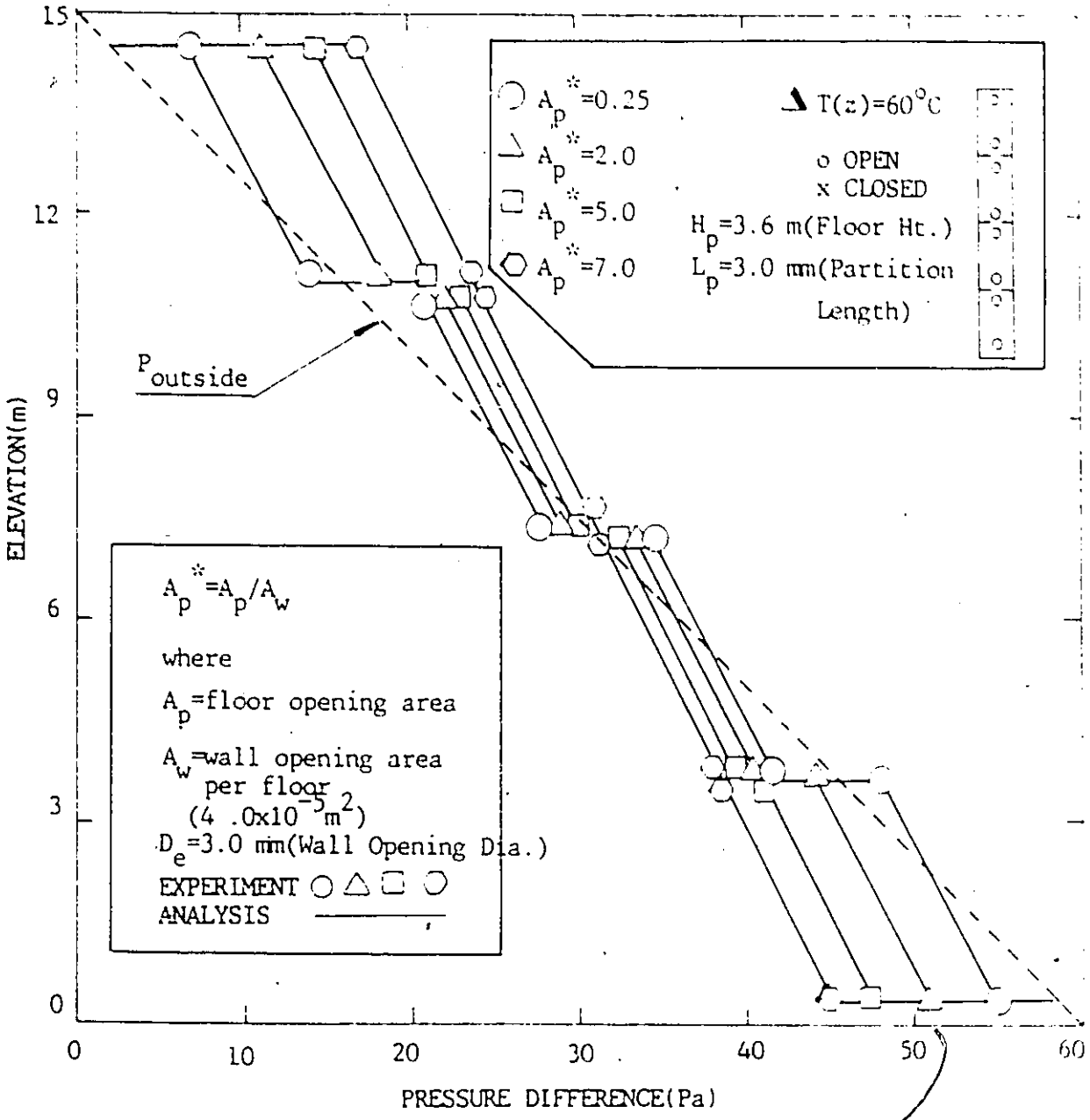

Fig.5.3.2 Pressure Differential Profile for Four Floor Partitioned Case

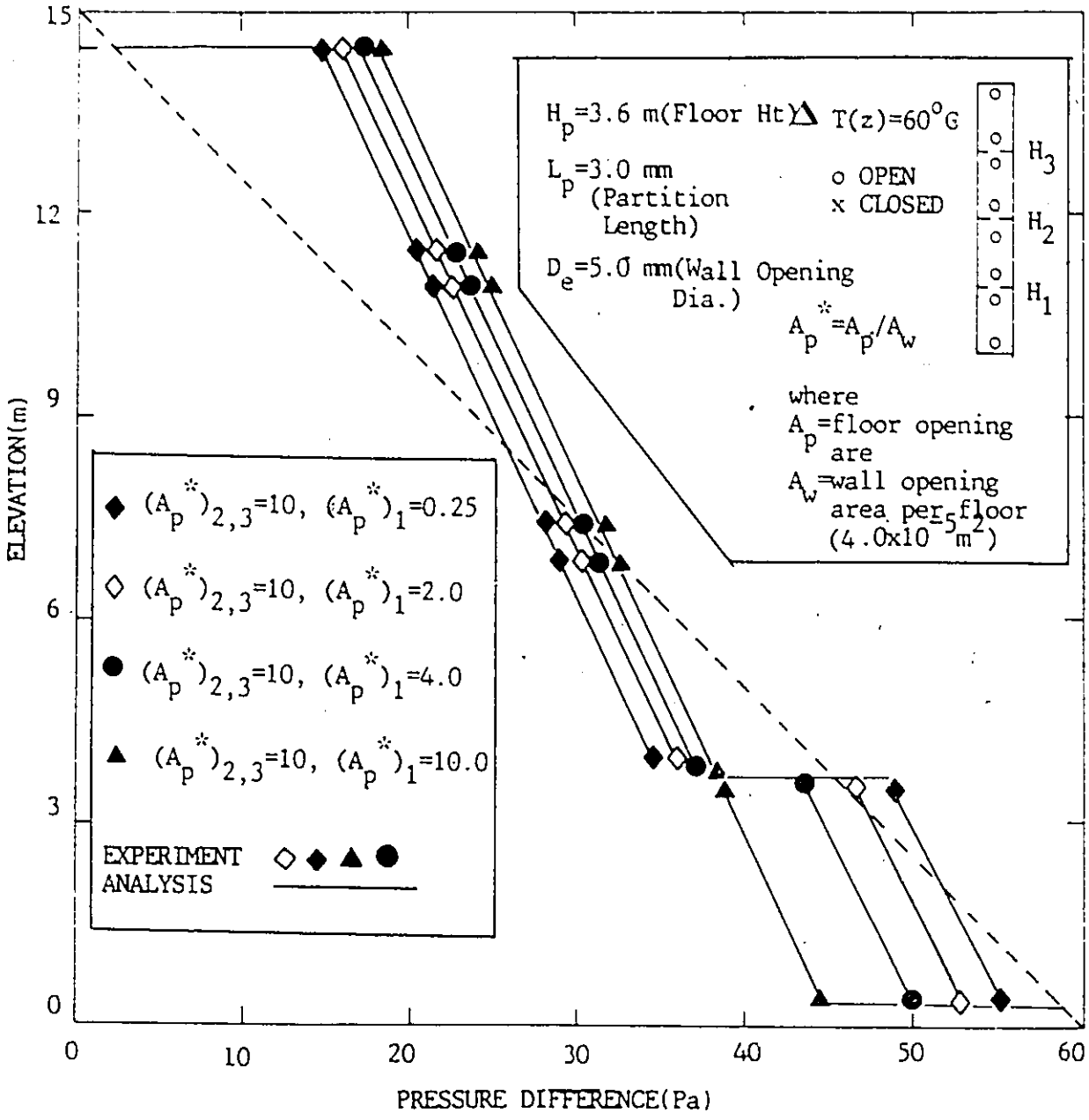

Fig.5.3.3 Pressure Differential Profile with Different Floor Opening Arrangements

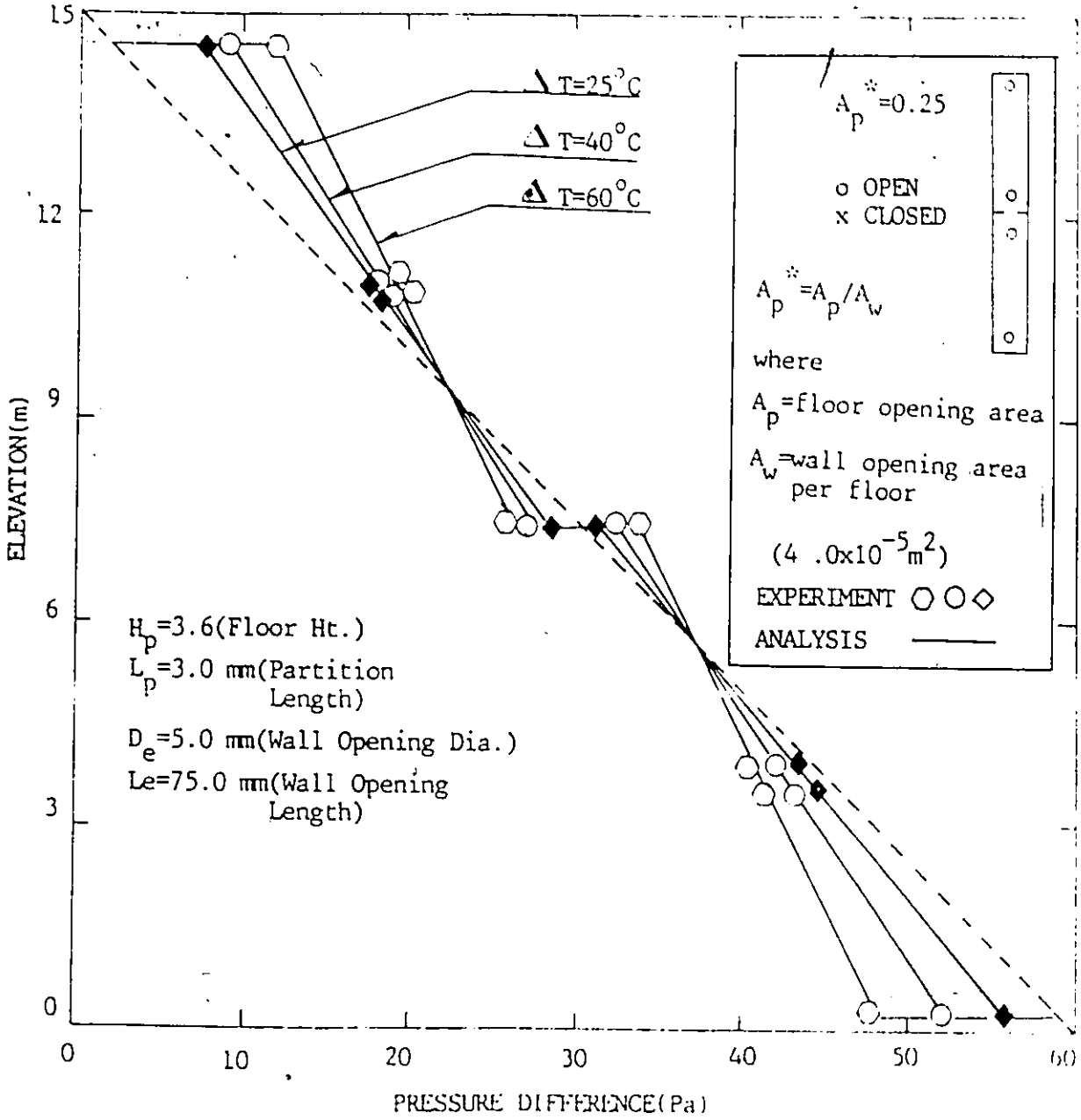

Fig.5.3.4 Effect of Temperature Difference on Pressure_Profile for Two Floor Case

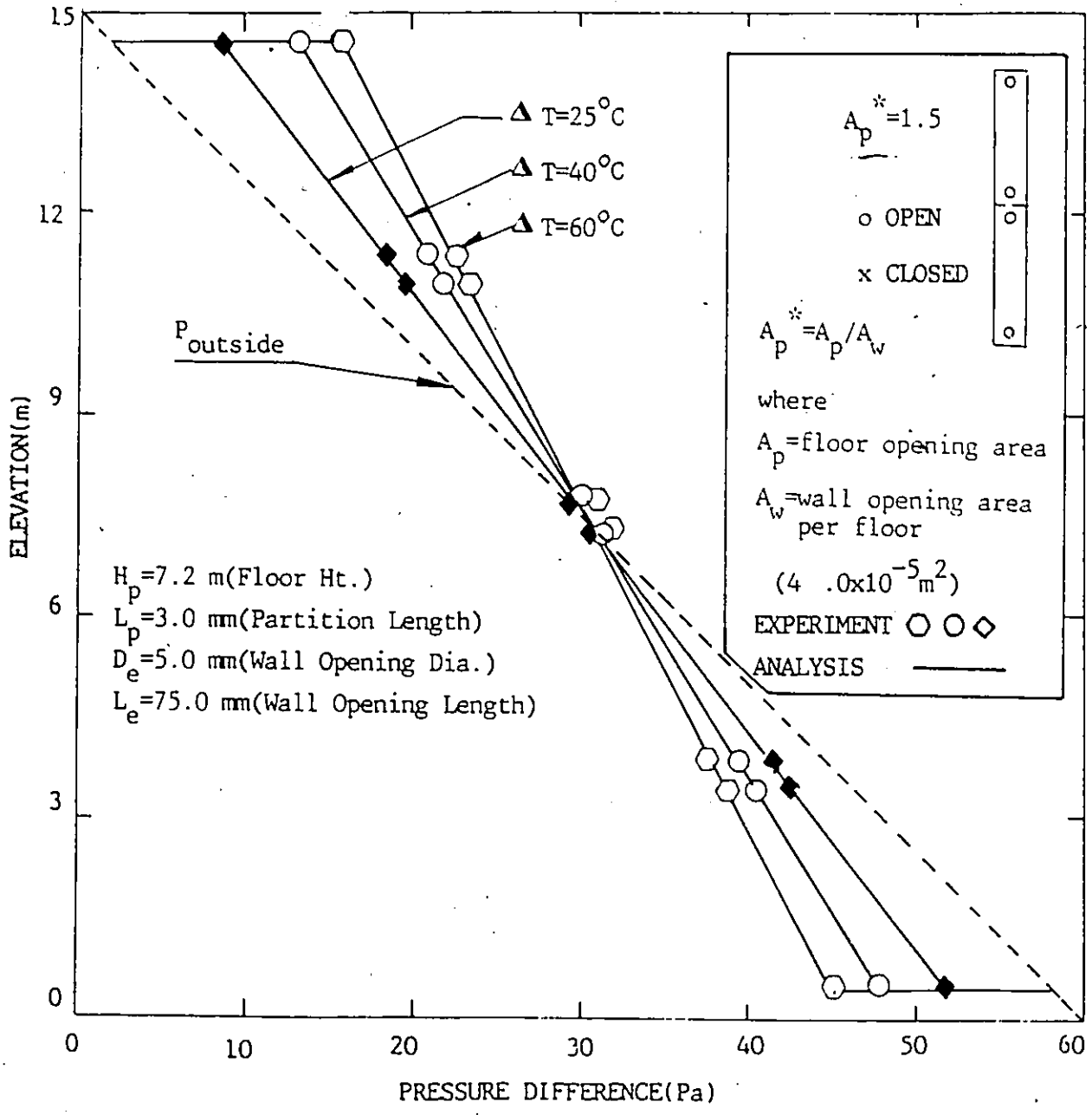

Fig.5.3.5 Effect of Temperature Difference on Pressure Profile for Two Floor Case

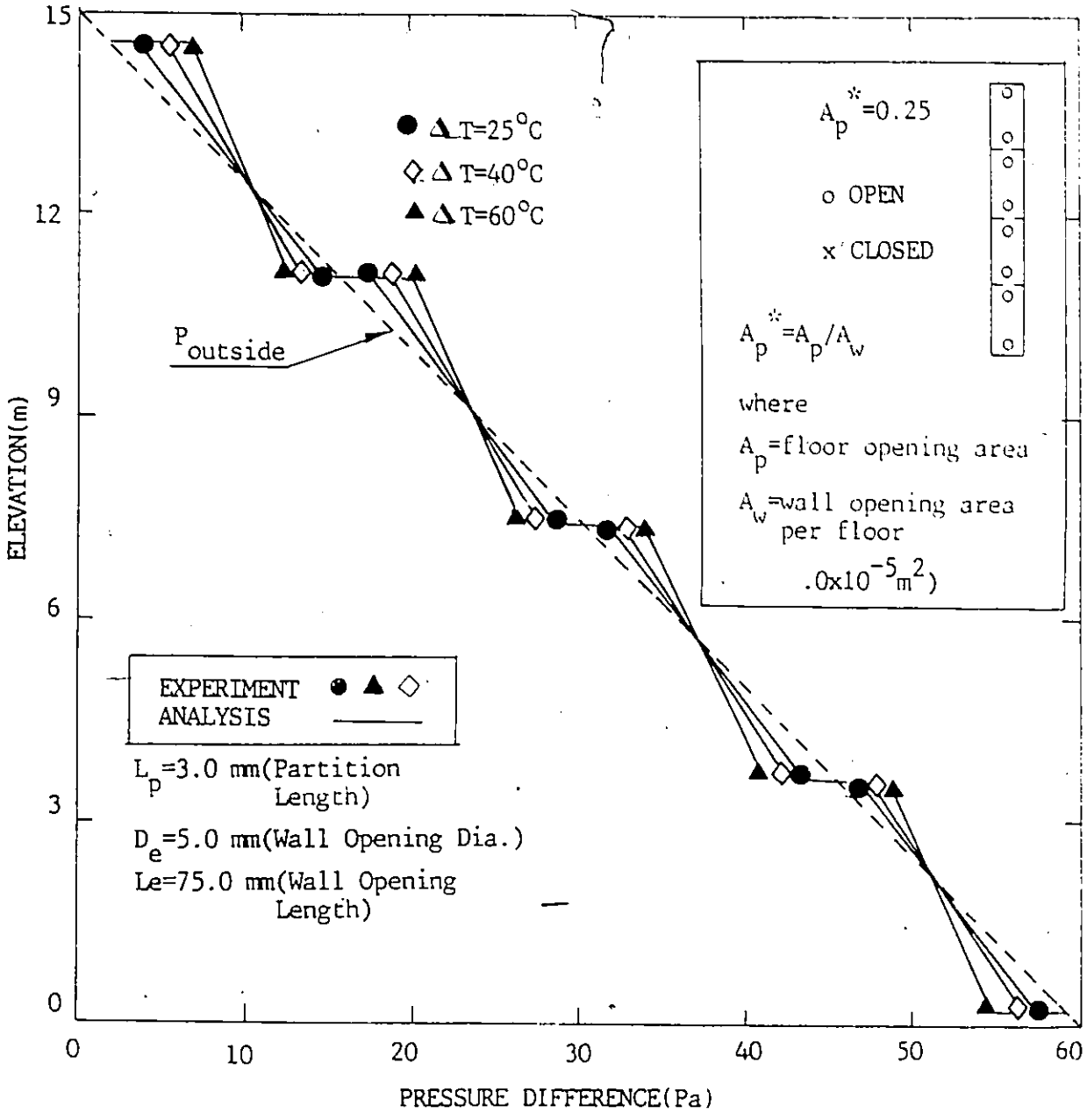

Fig.5.3.6 Effect of Temperature Difference on Pressure Profile for Four Floors Case

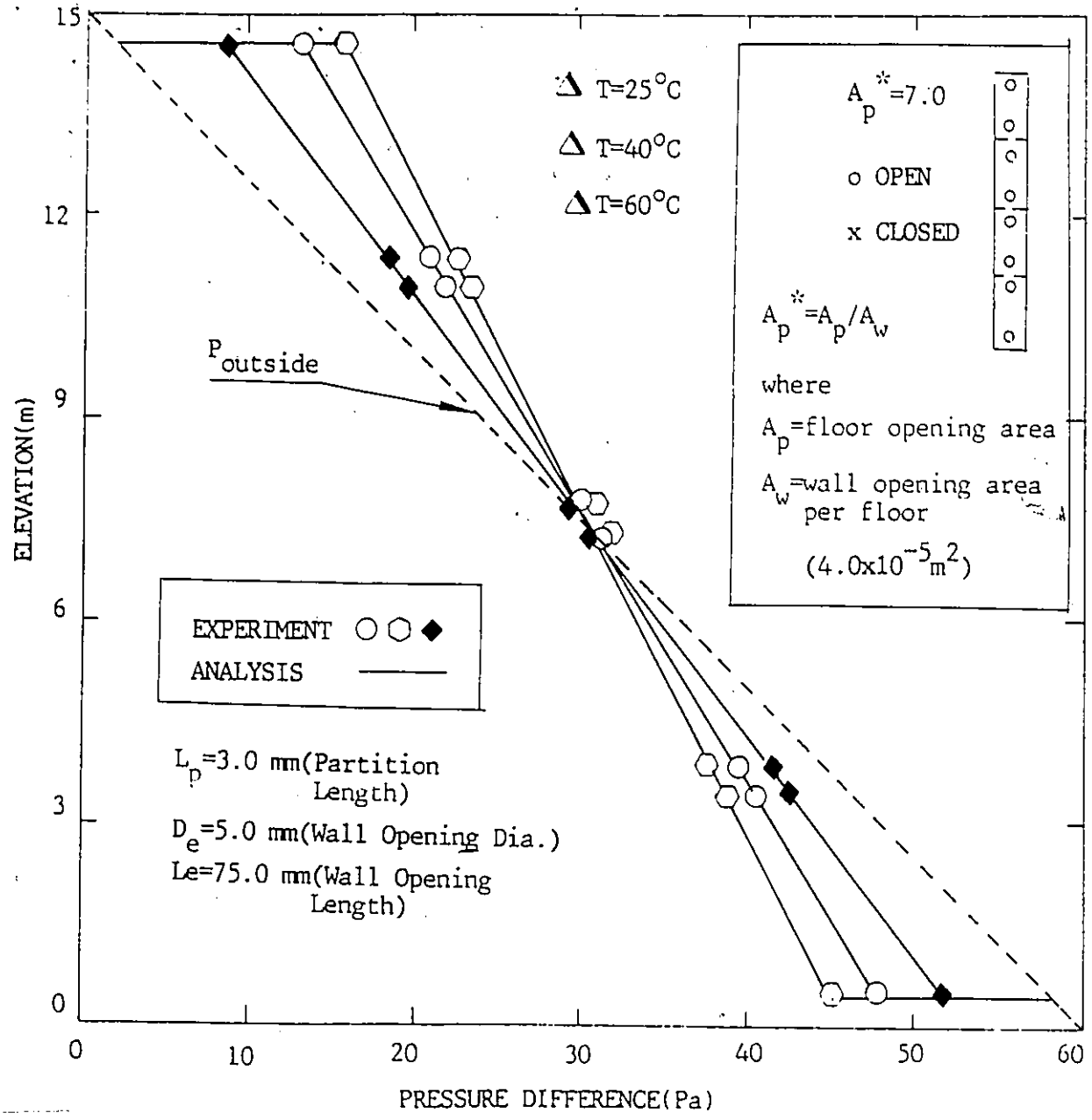

Fig.5.3.7 Effect of Temperature Difference on Pressure Profile for Four Floors Case

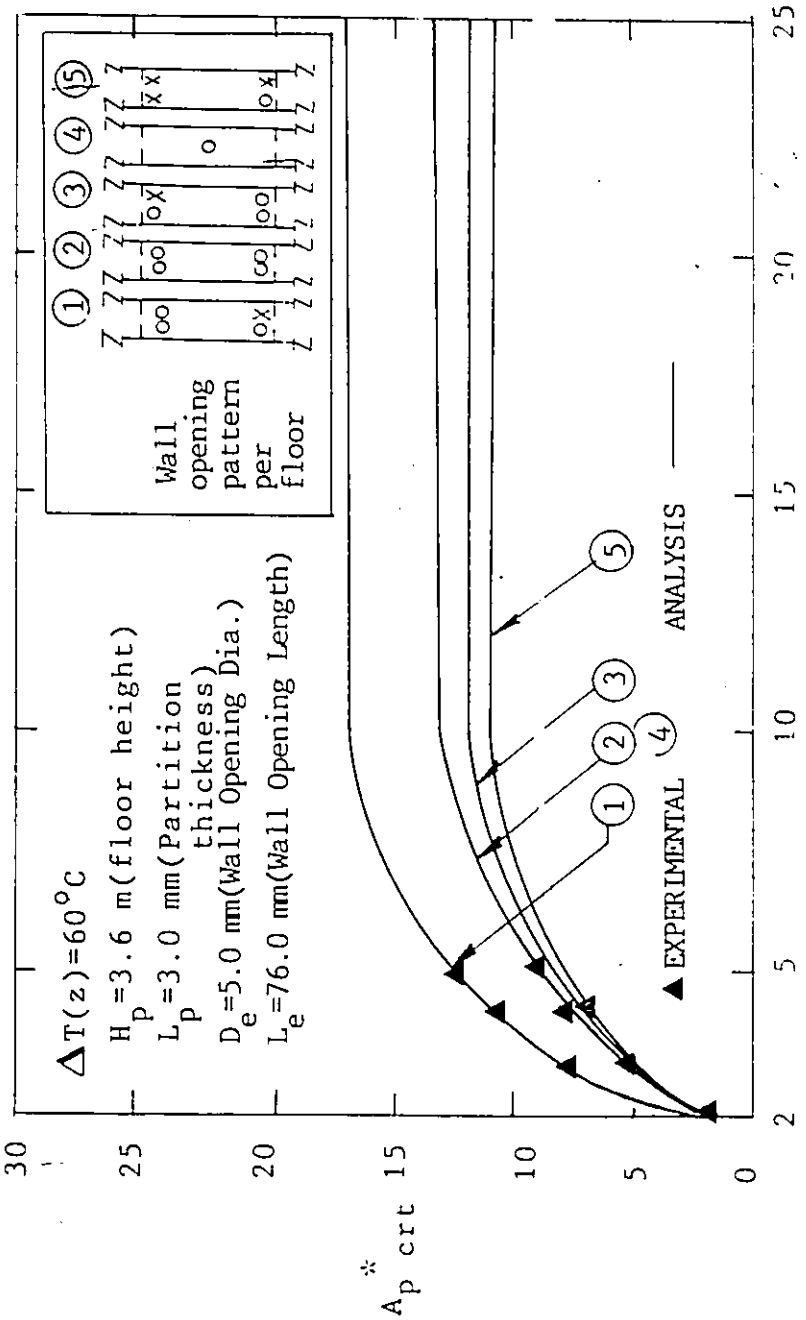

Fig.5.3.8 Effect of Number of Floor Numbers on Value of $A^*_{p\ crt}$

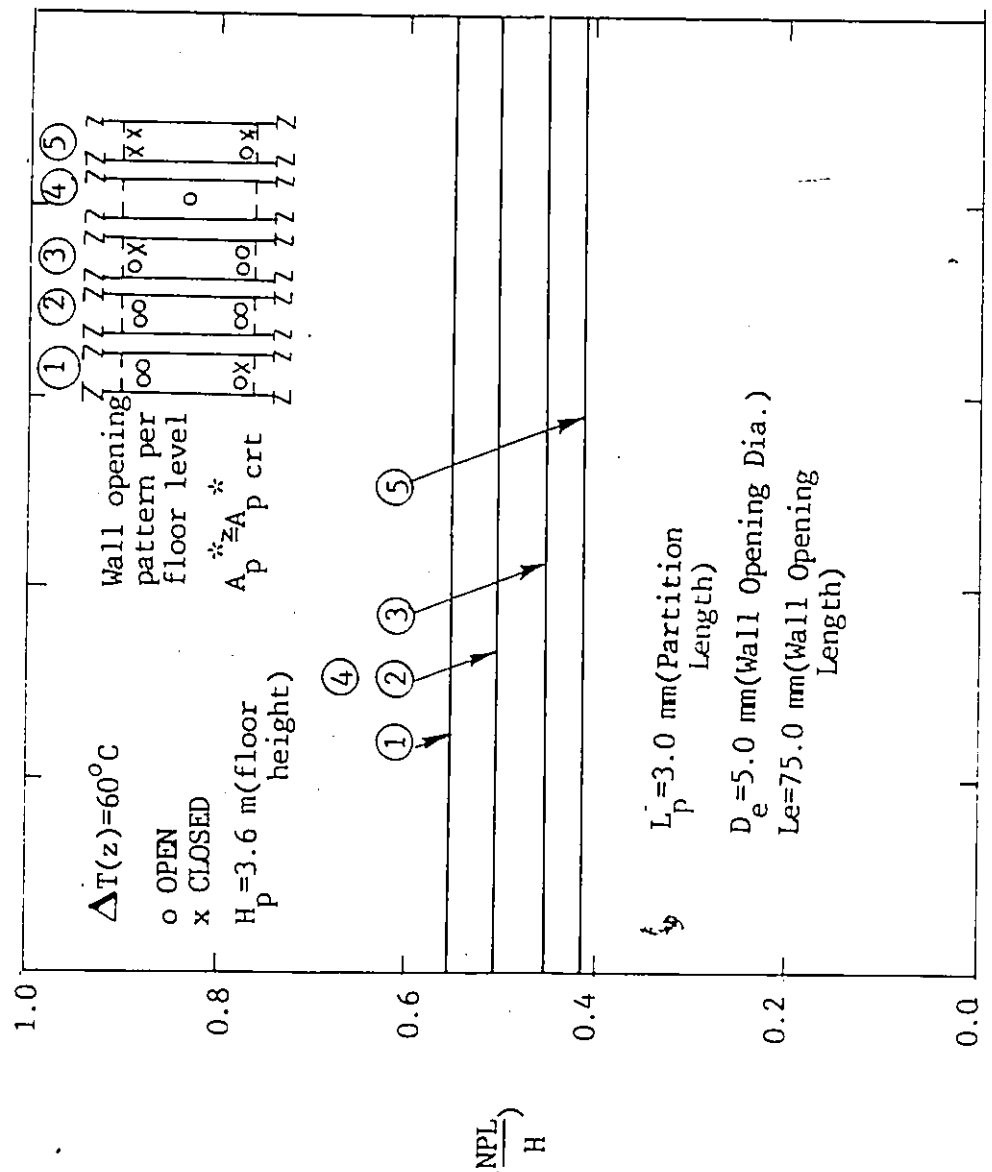

Fig.5.3. 9 Effect of Vertical Dimensions of Building on NPL for Partitioned Building

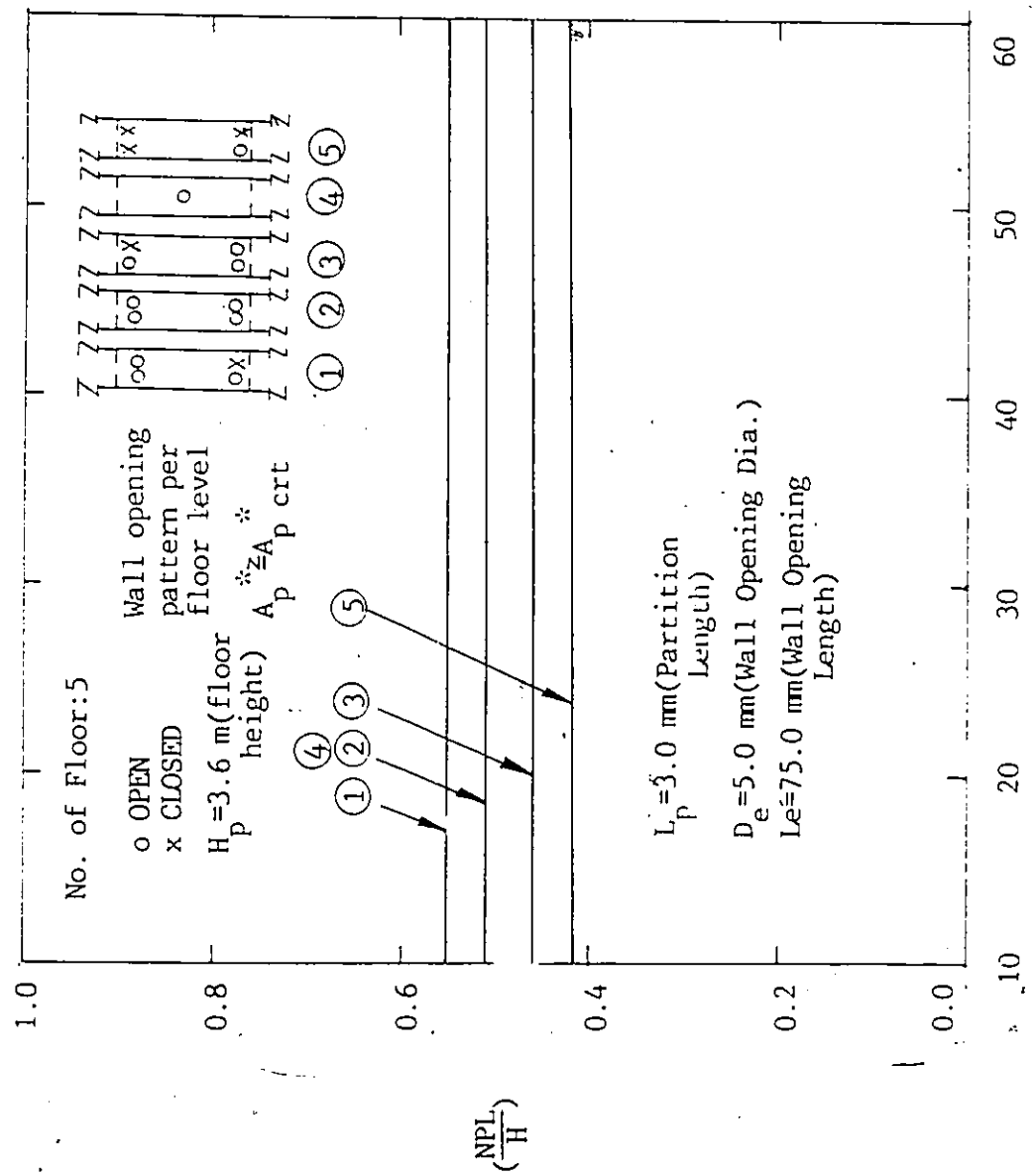

Fig.5.3.10 Effect of Temperature Difference on NPL for Partitioned Building

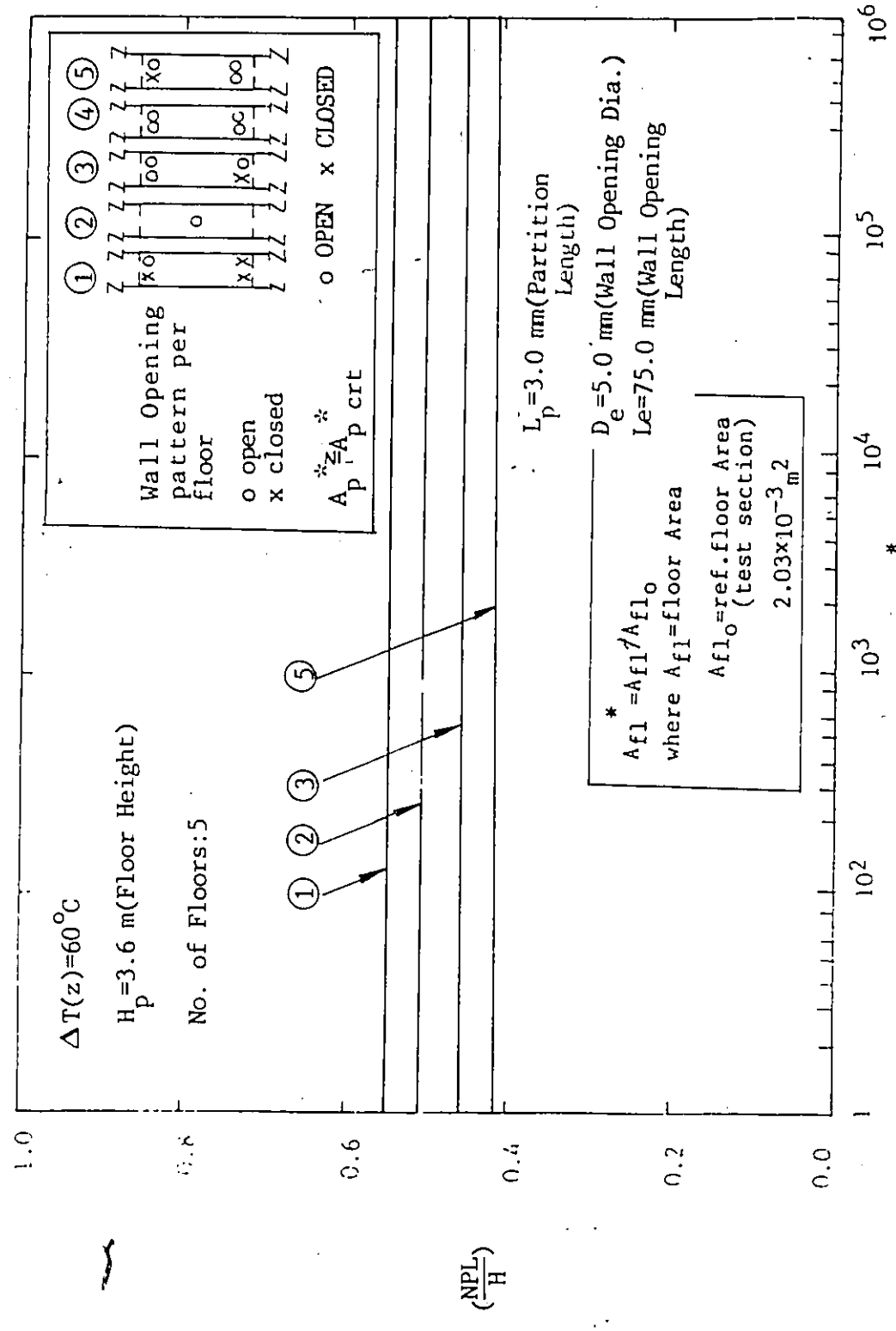

Fig.5.3.11 Effect of Floor Dimensions on NPL for Partitioned Case

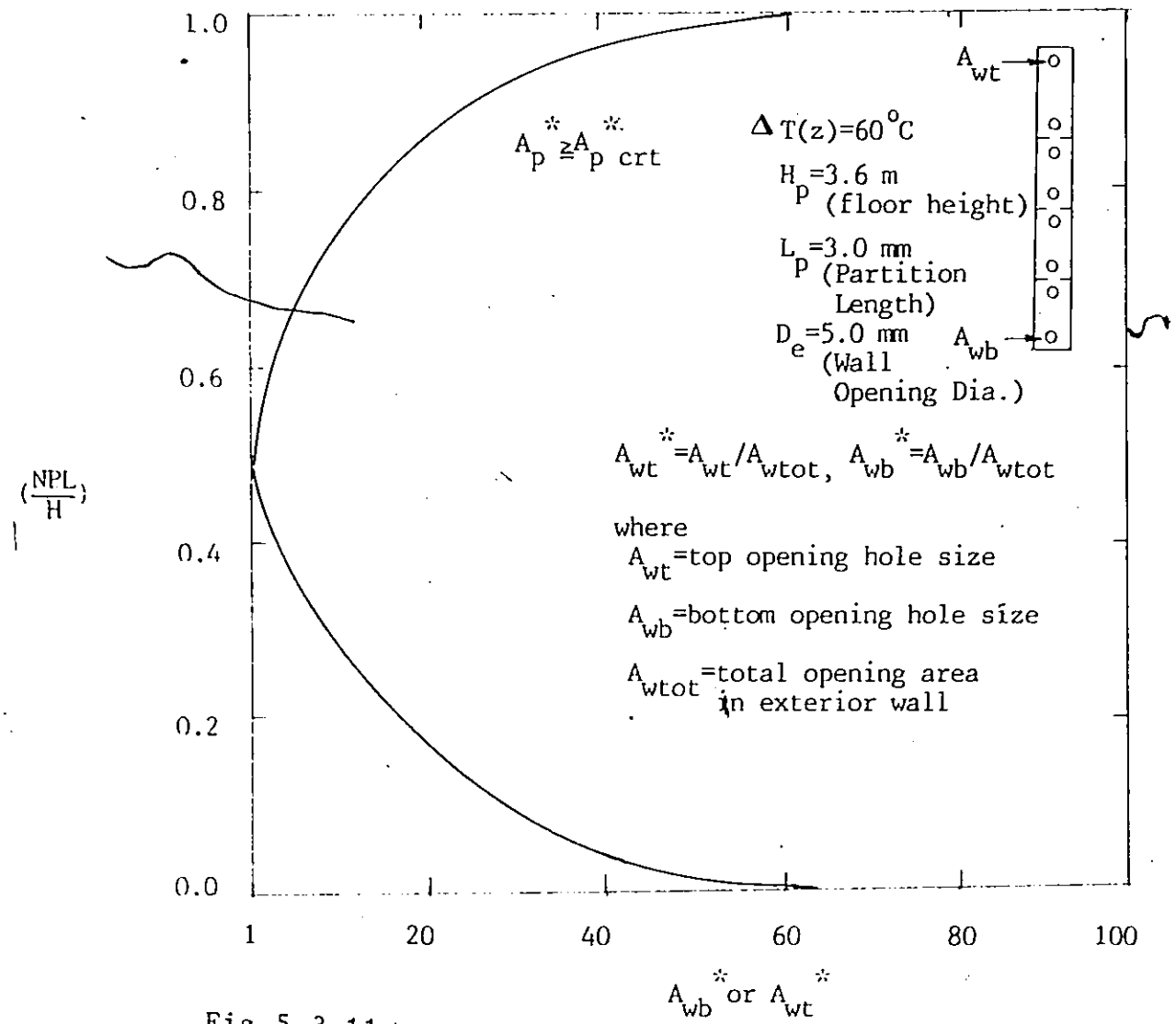

Fig.5.3.11 Effect of Enlargement of Top or Bottom Opening Area on NPL.

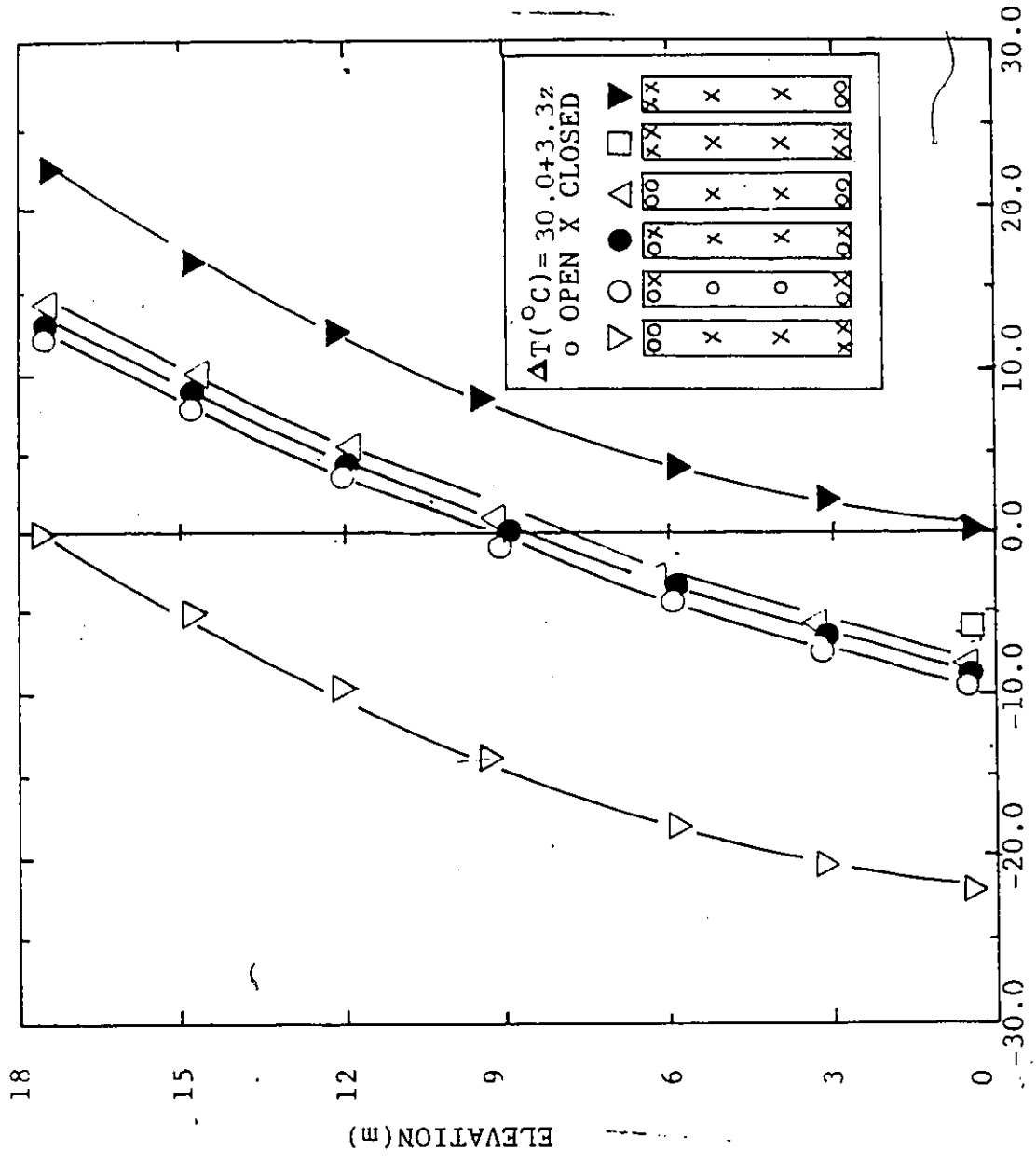

Fig.5.4.1 Experimental Pressure Differential Profiles under Non-Uniform Distribution of Inside Wall.

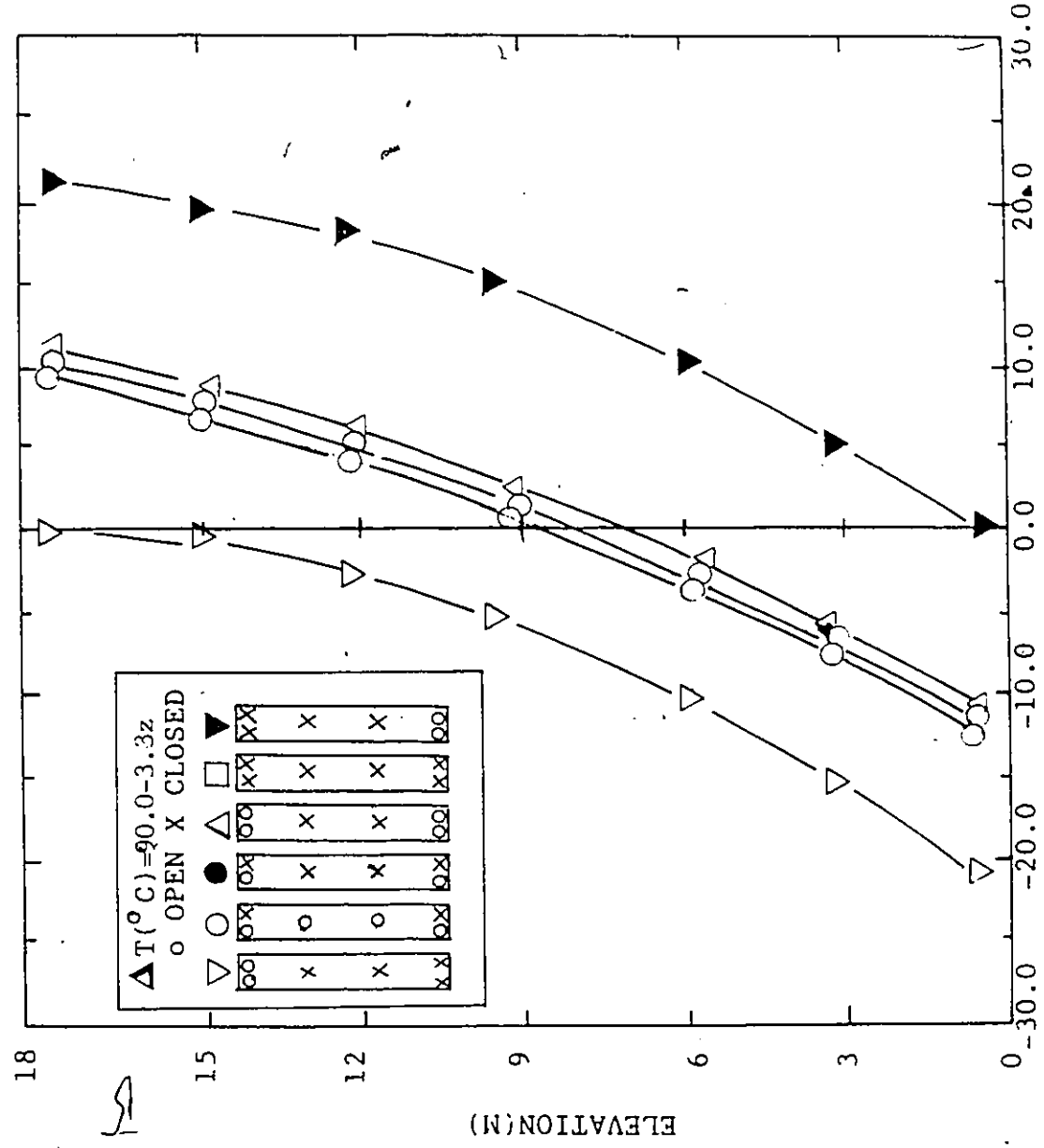

Fig.5.4.2 Experimental Pressure Differential Profile under Non-Uniform Temperature Profile of Inside Wall

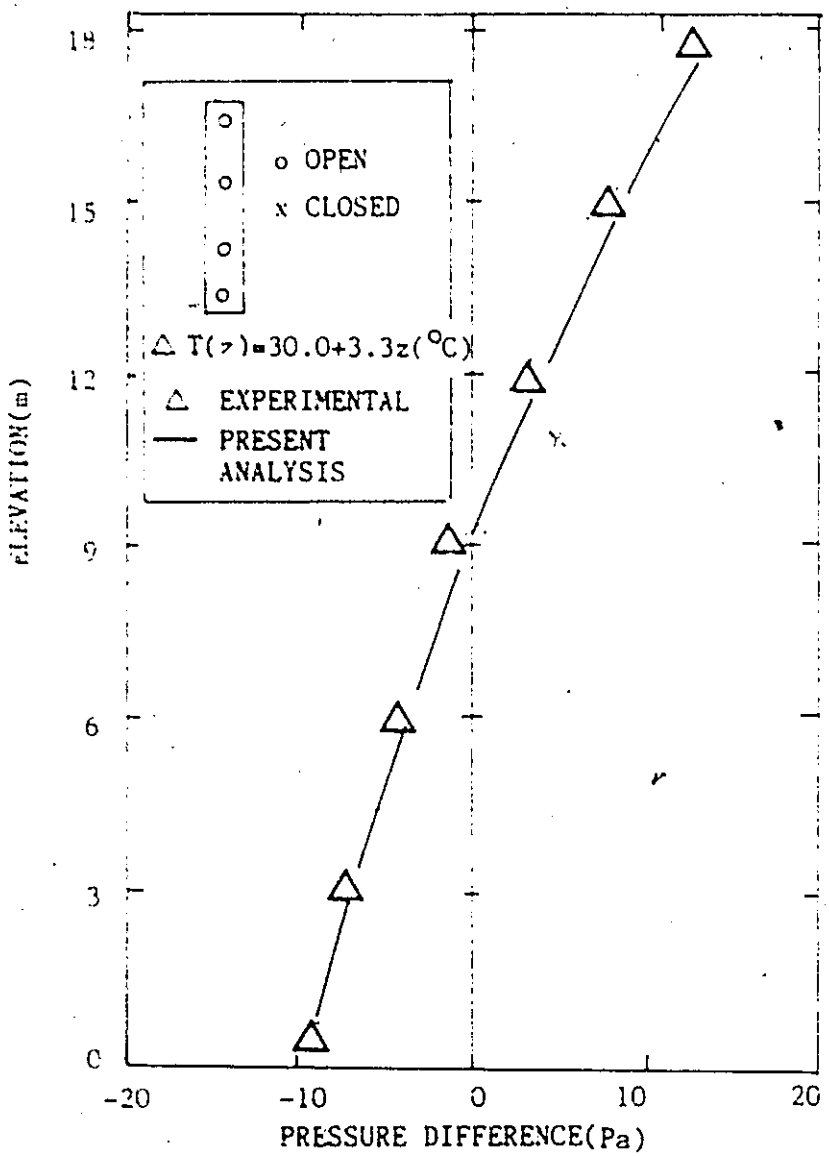

Fig.5.4.3 Comparison of Computed Pressure Differential with Experimental

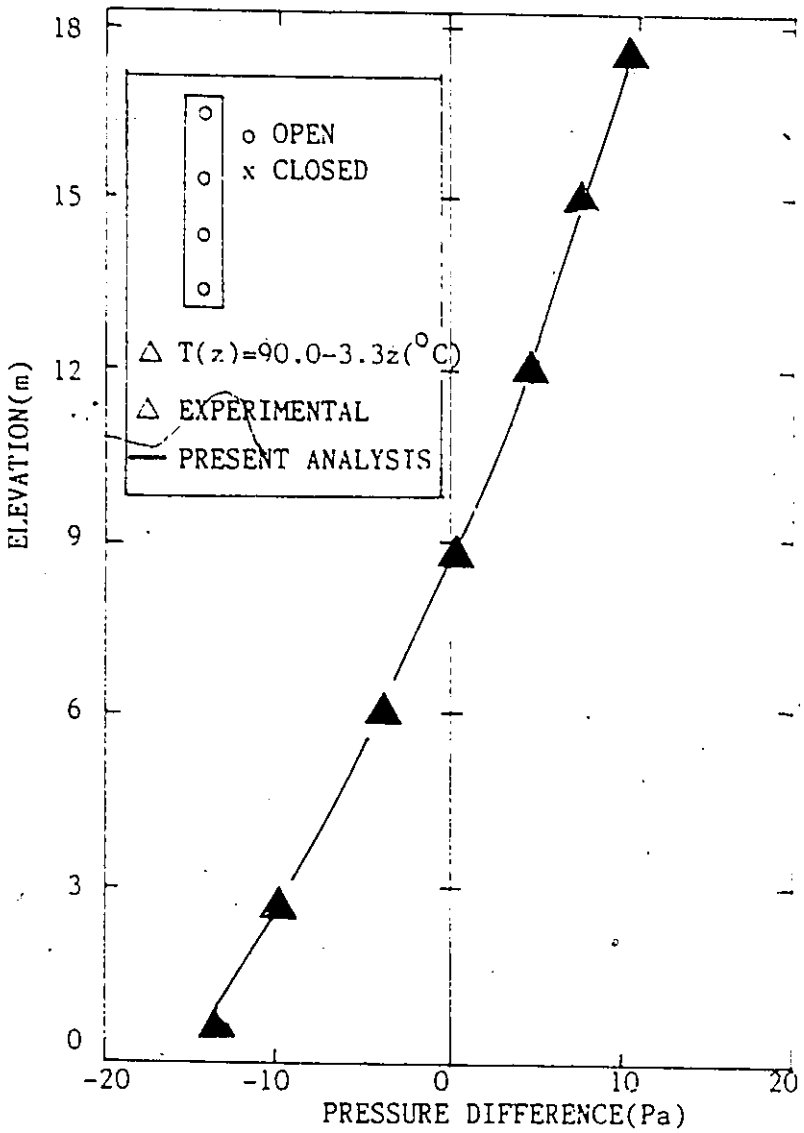

Fig.5.4.4 Comparison of Computed Pressure Profile with Experimental

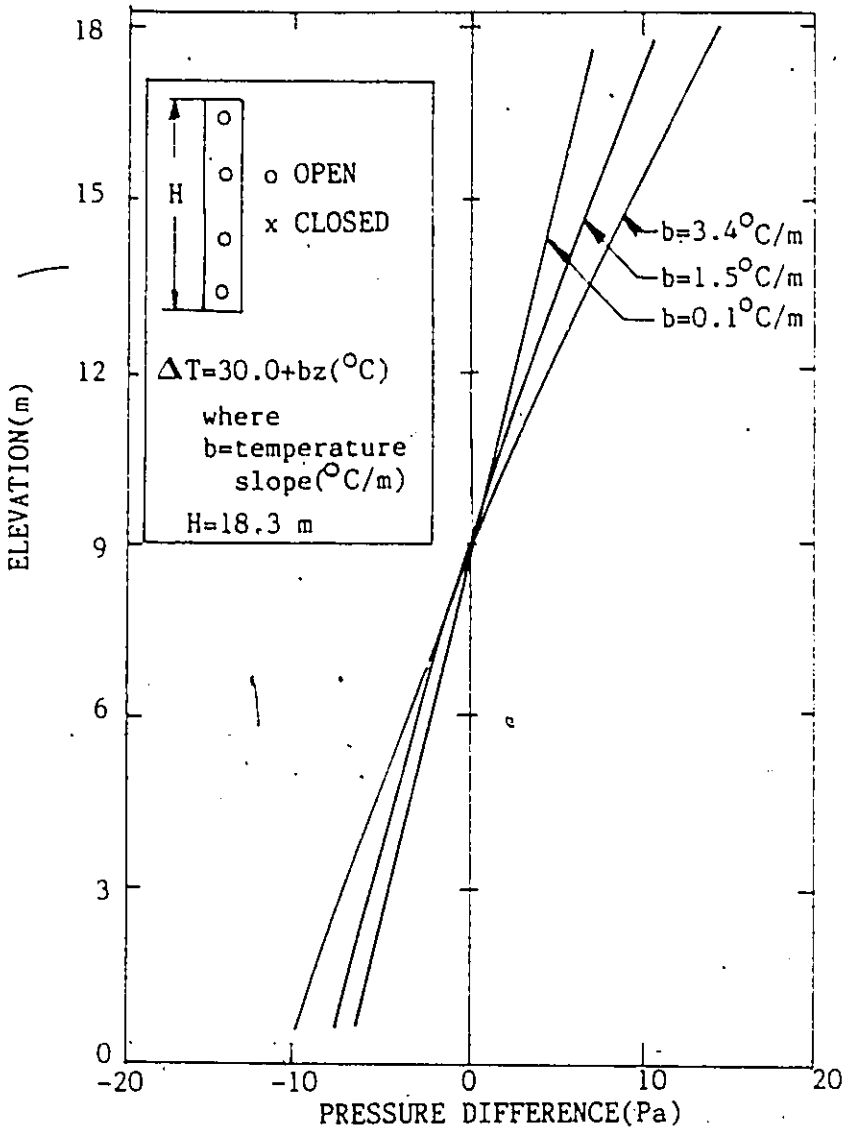

Fig.5.4.5 Effect of Temperature Slope of Inside Wall on Pressure Profile

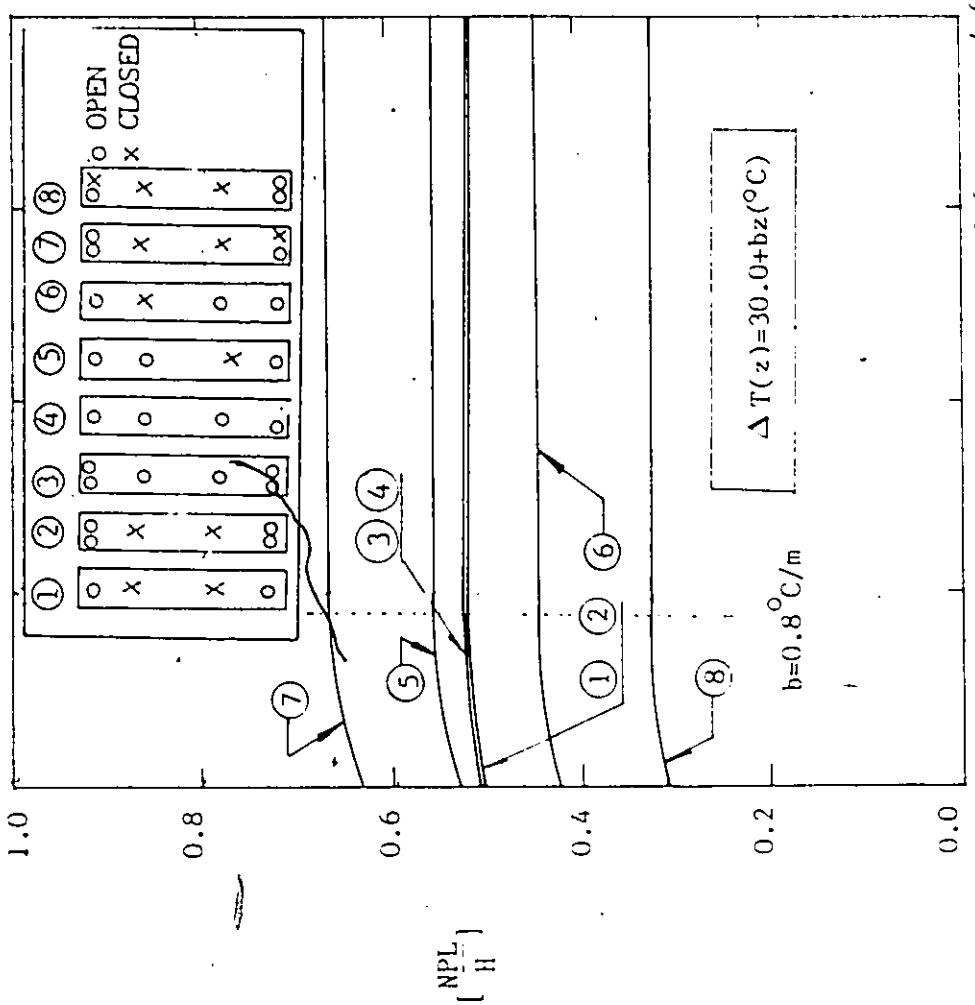

Fig.5.4.6 Effect of Temperature Slope of Inside Wall on NPL

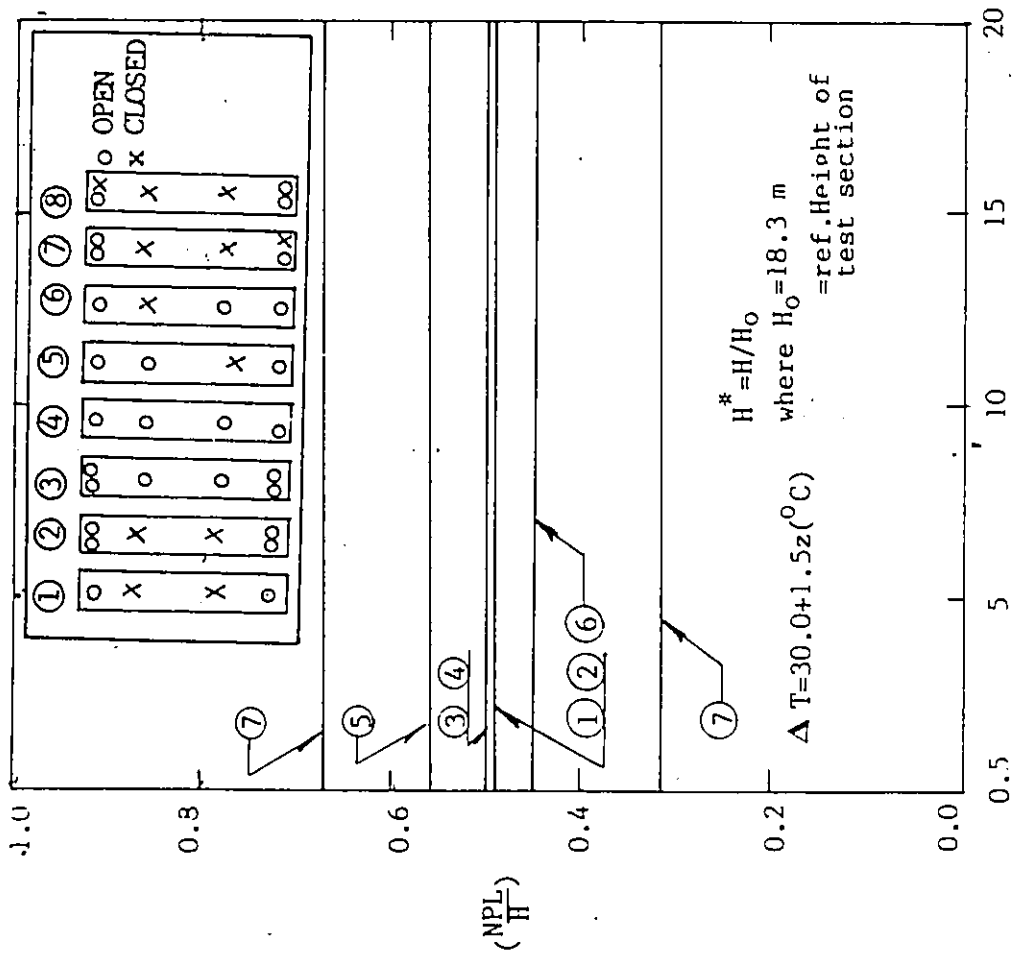

Fig.5.4.7 Effect of Vertical Dimensions of Building on NPL under Non-Uniform Temperature .

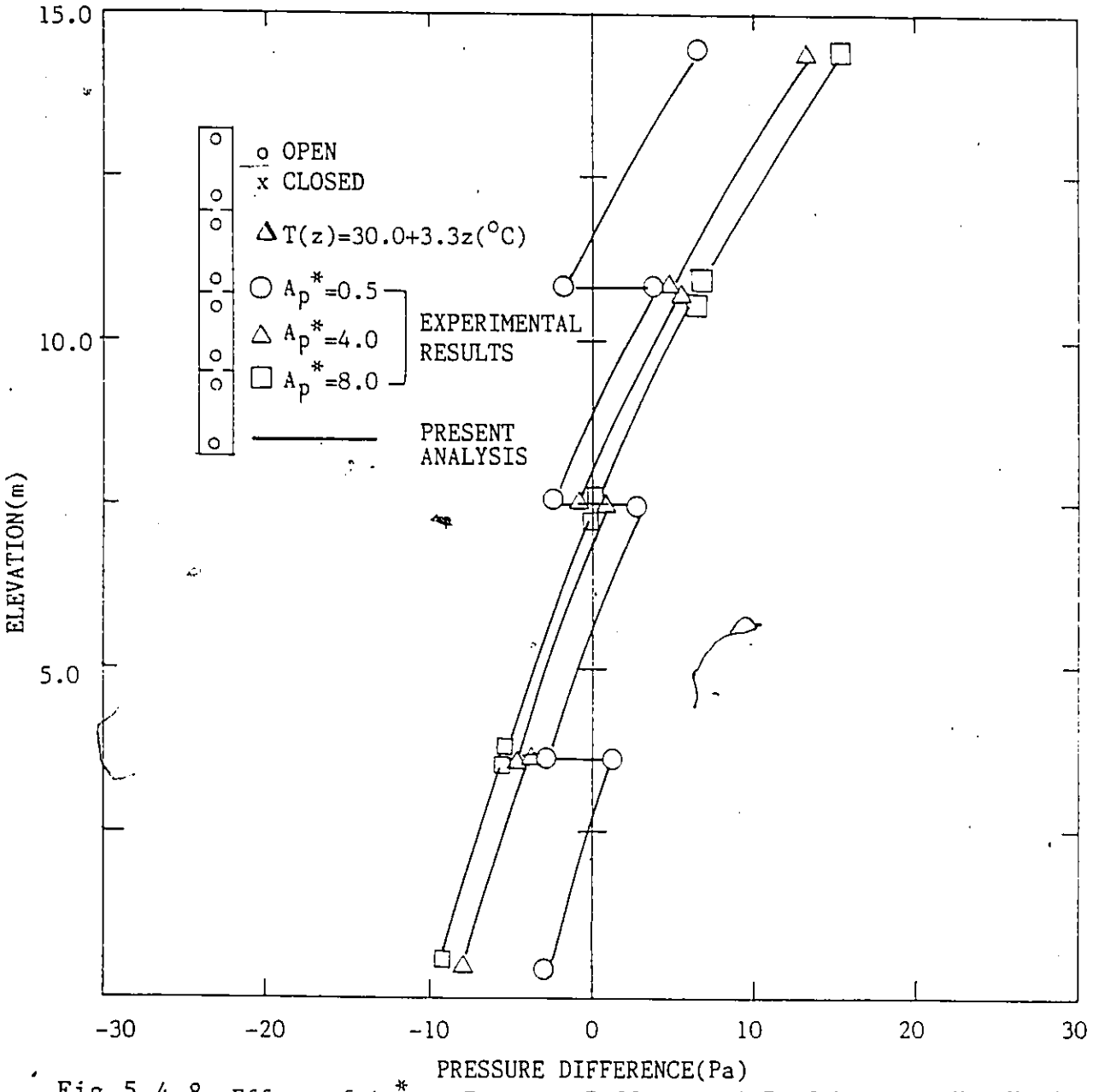

Fig.5.4.8 Effect of A_p^* on Pressure Differential Profile under Non-Uniform Temperature Distribution of Inside Wall.

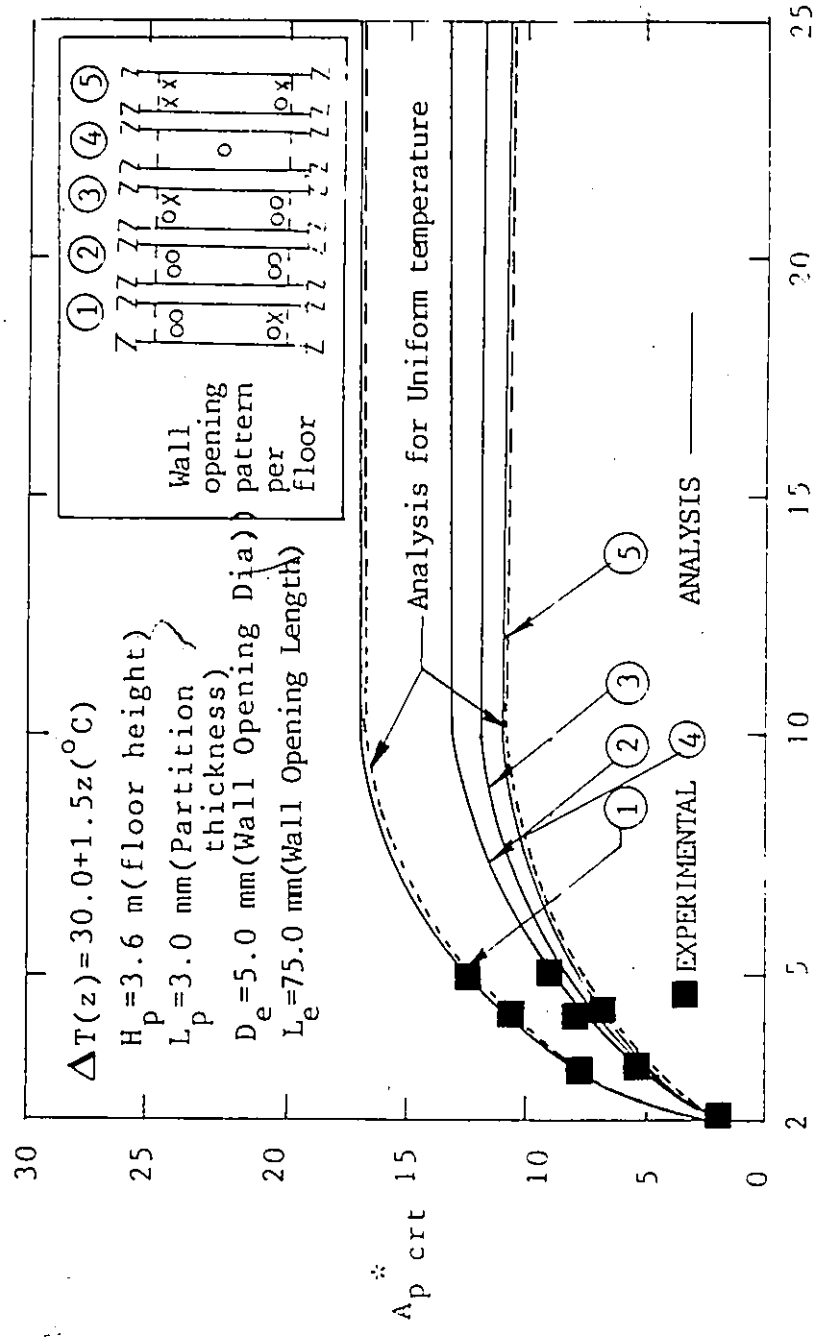

Fig.5.4.9 Effect of Number of Floors on $A^*_{p\ crt}$ for Non-Uniform Temperature Case

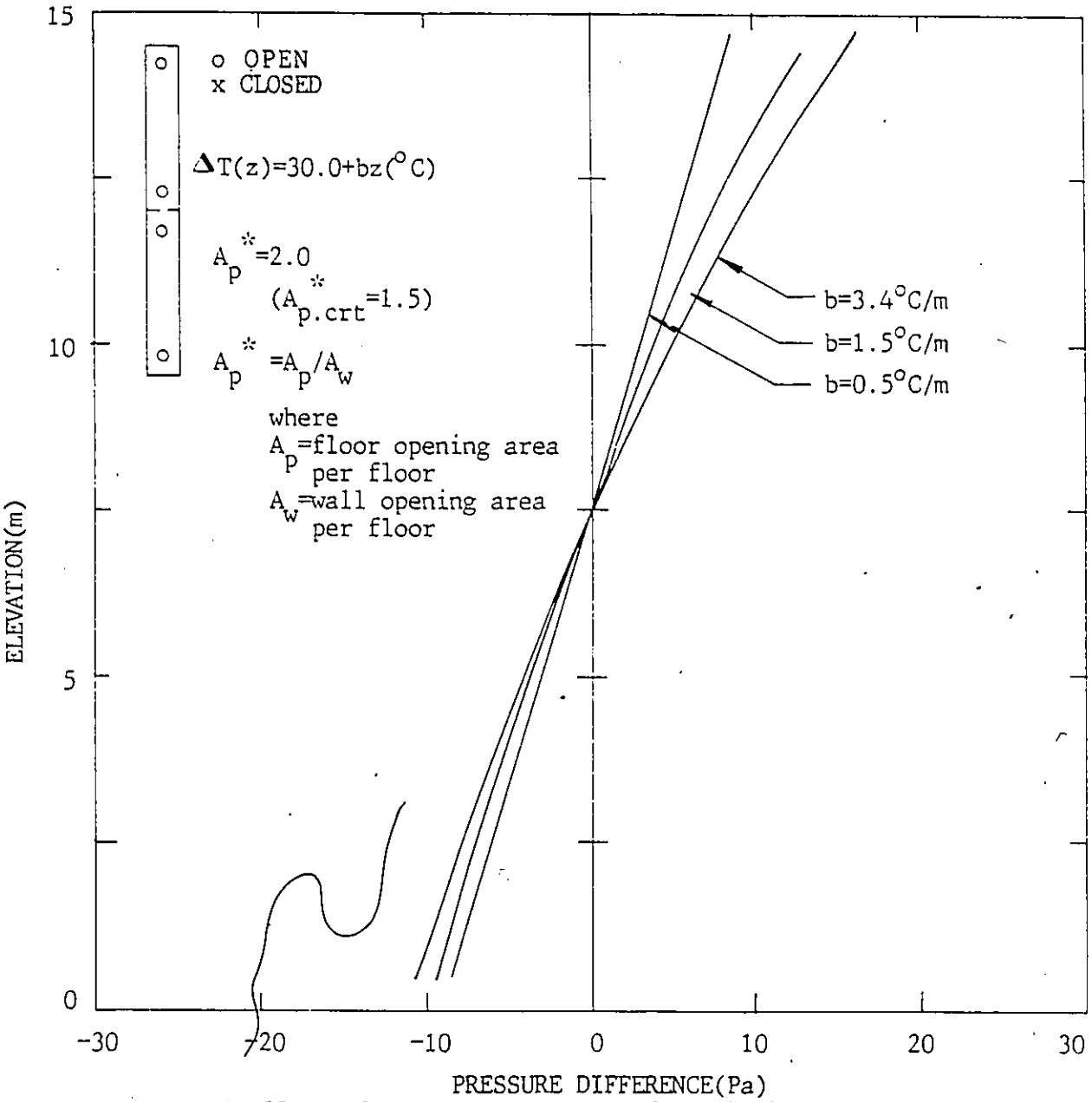

Fig.5.4.10 Effect of Temperature Slope of Building Inside on Pressure Differentials for Two Floor Partitioned Case

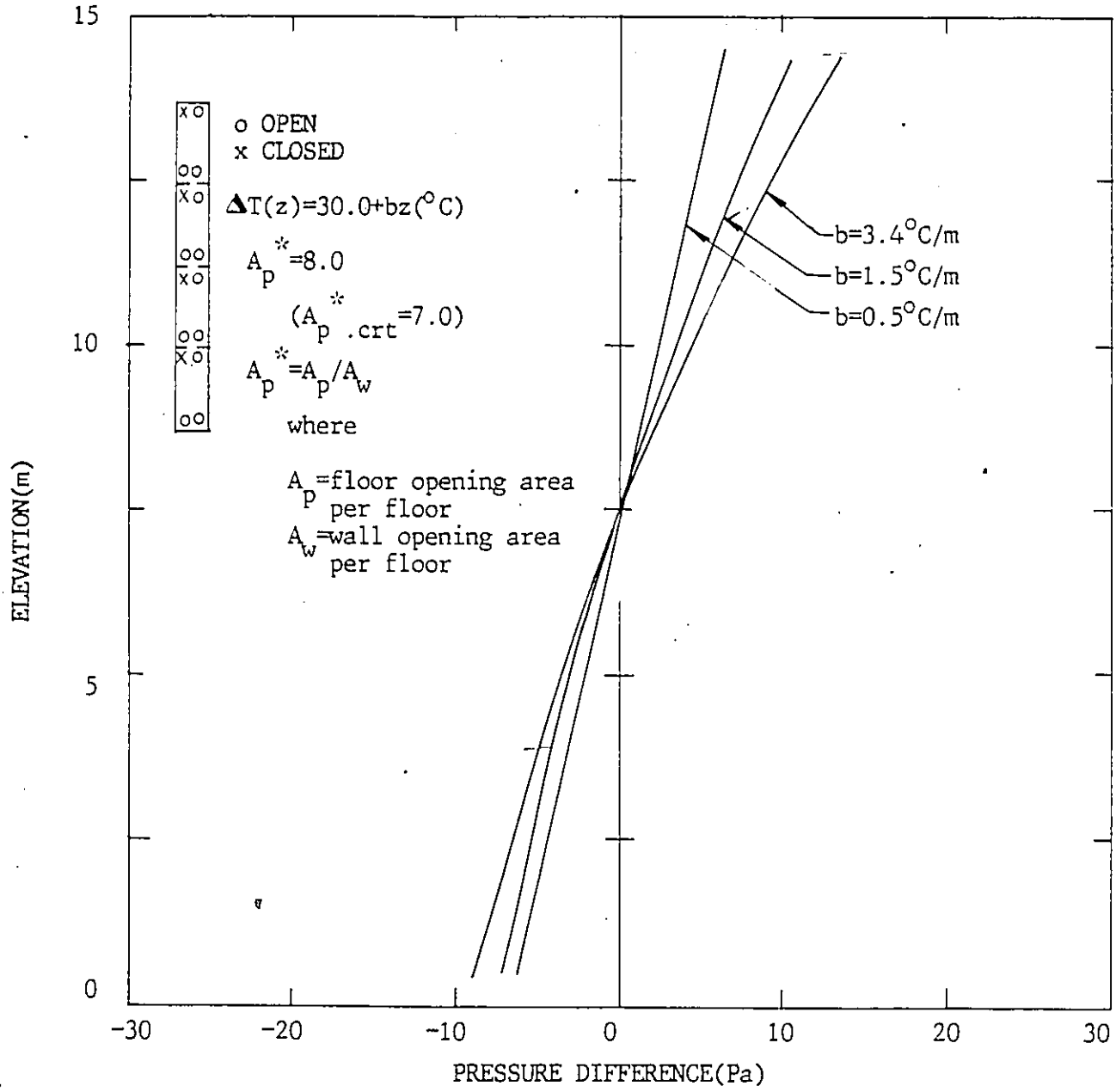

Fig.5.4.11 Effect of Temperature Slope of Building Inside on Pressure Differentials for Four Floor Partitioned Case

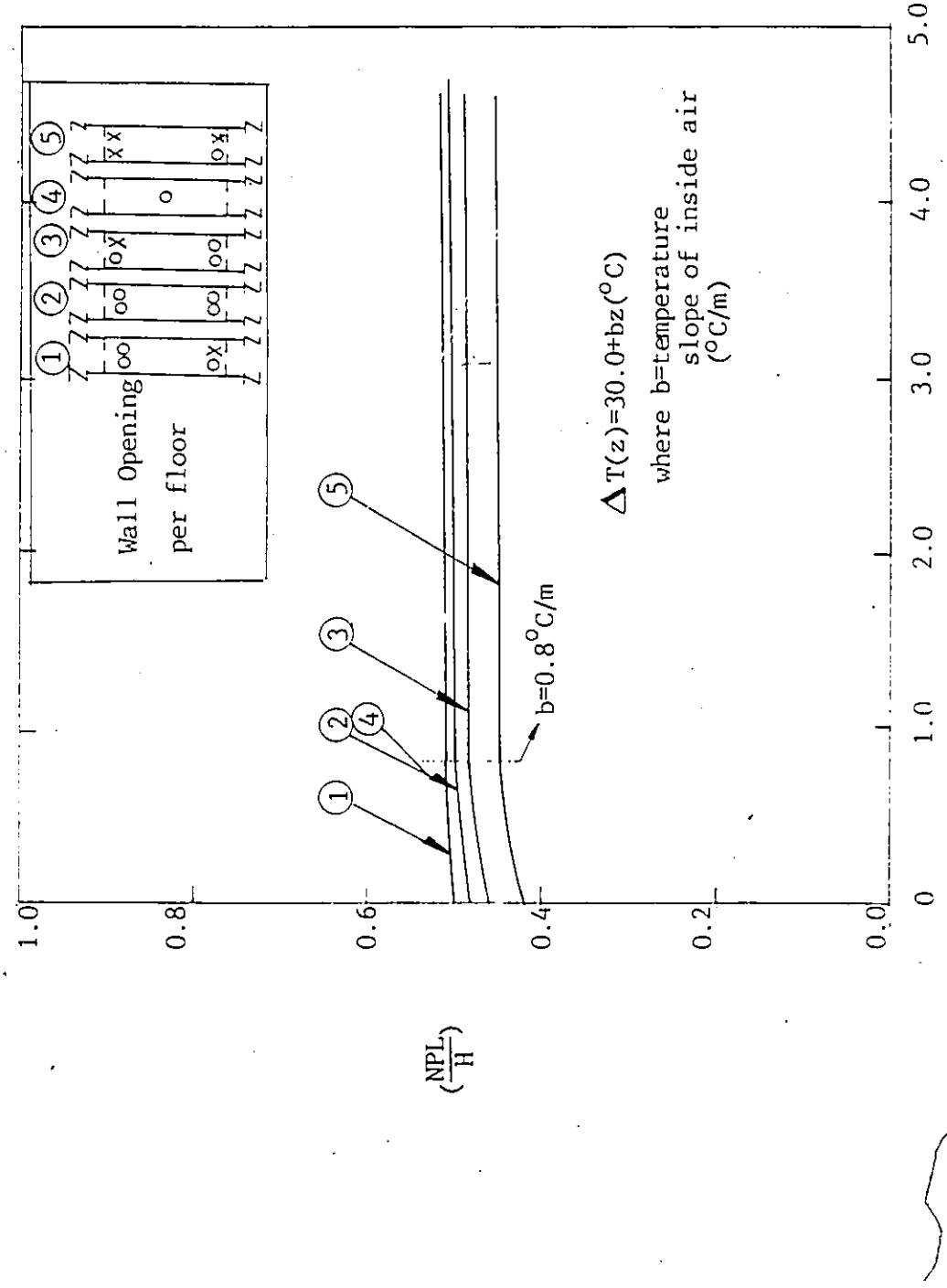

Fig.5.4.12 Effect of Temperature Slope on NPL for Partitioned Building

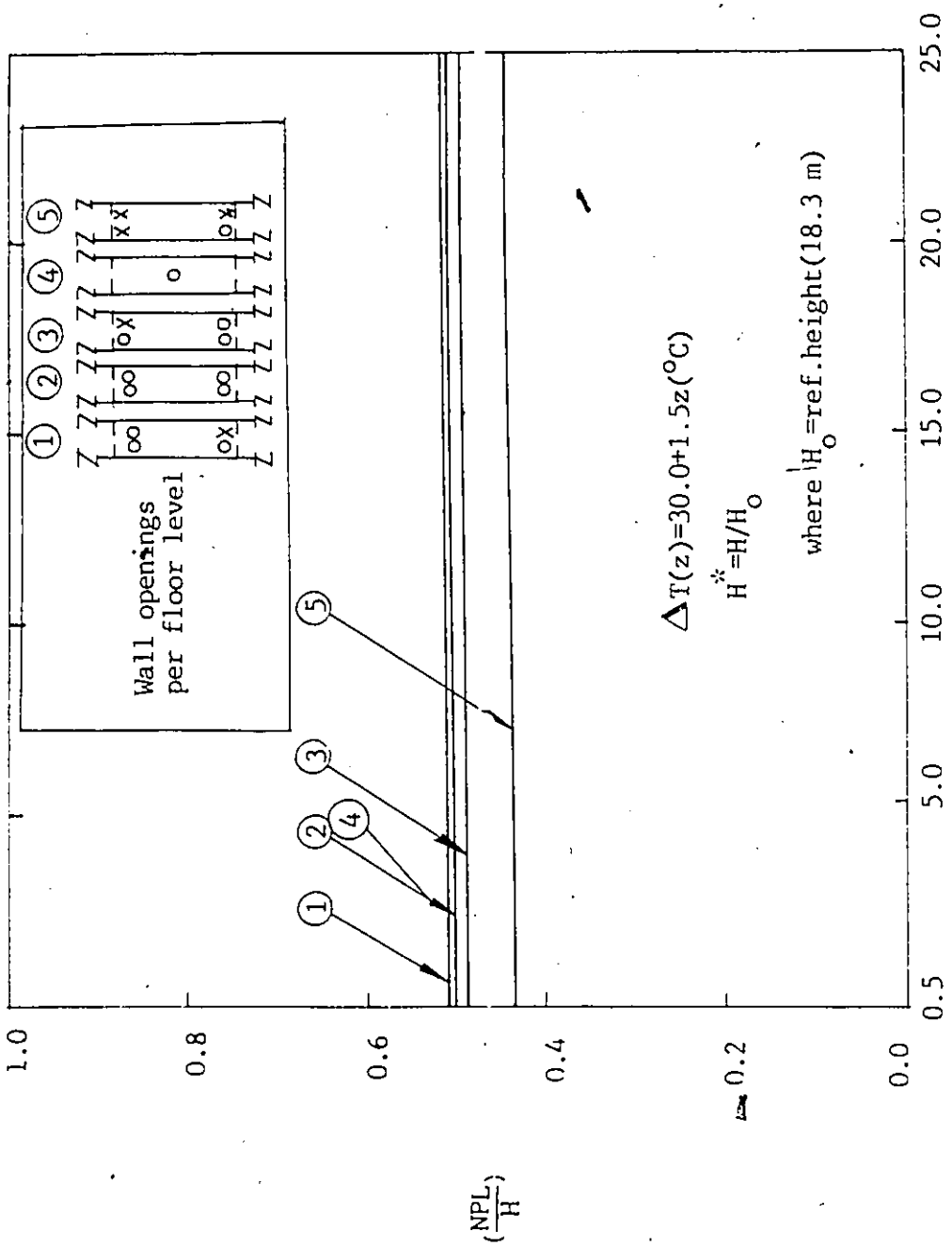

Fig.5.4.13 Effect of Vertical Dimensions of Building on NPL for Partitioned Case with Non-Uniform Temperature

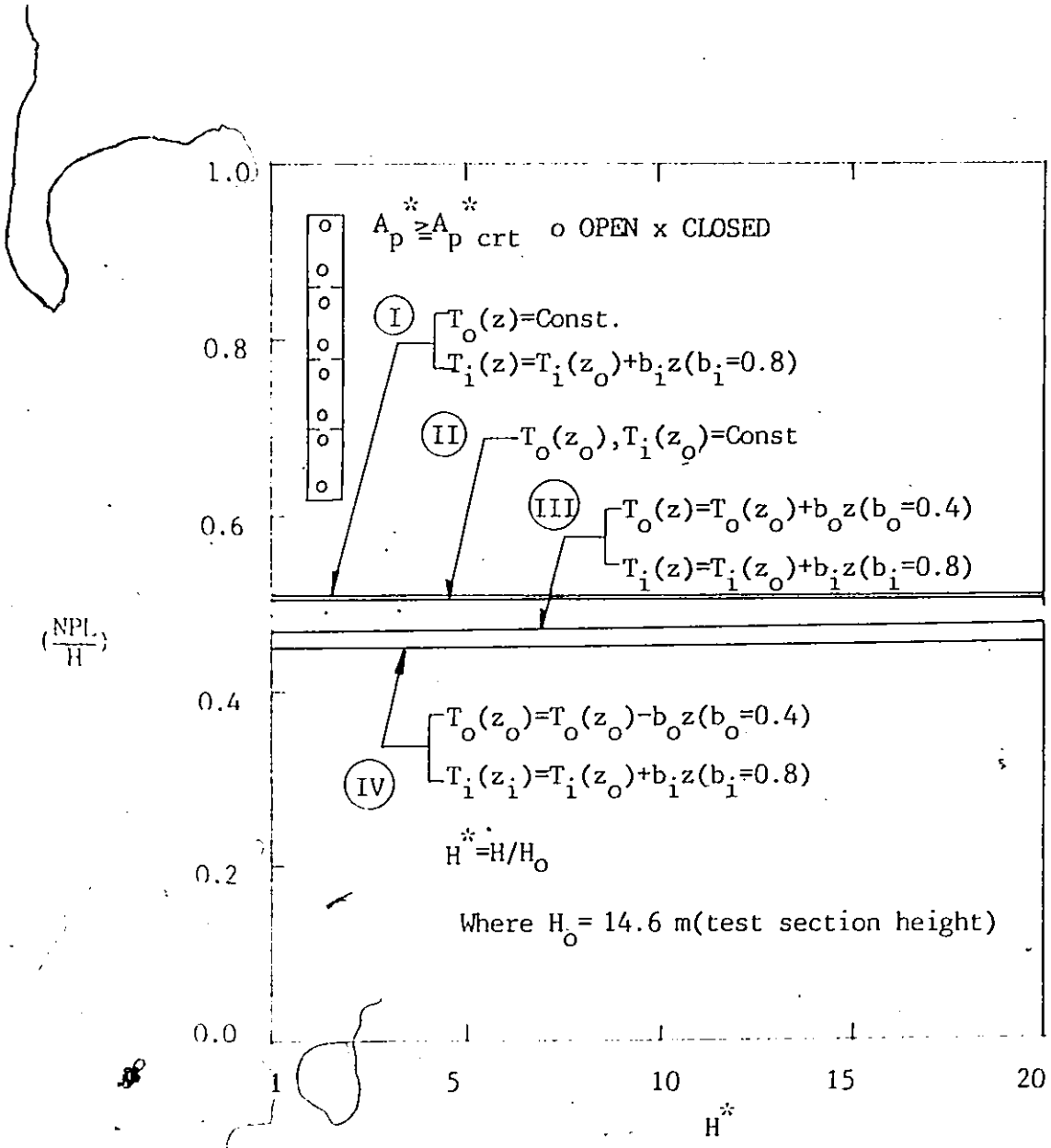

Fig.5.4.14 Effect of Temperature Slopes on NPL

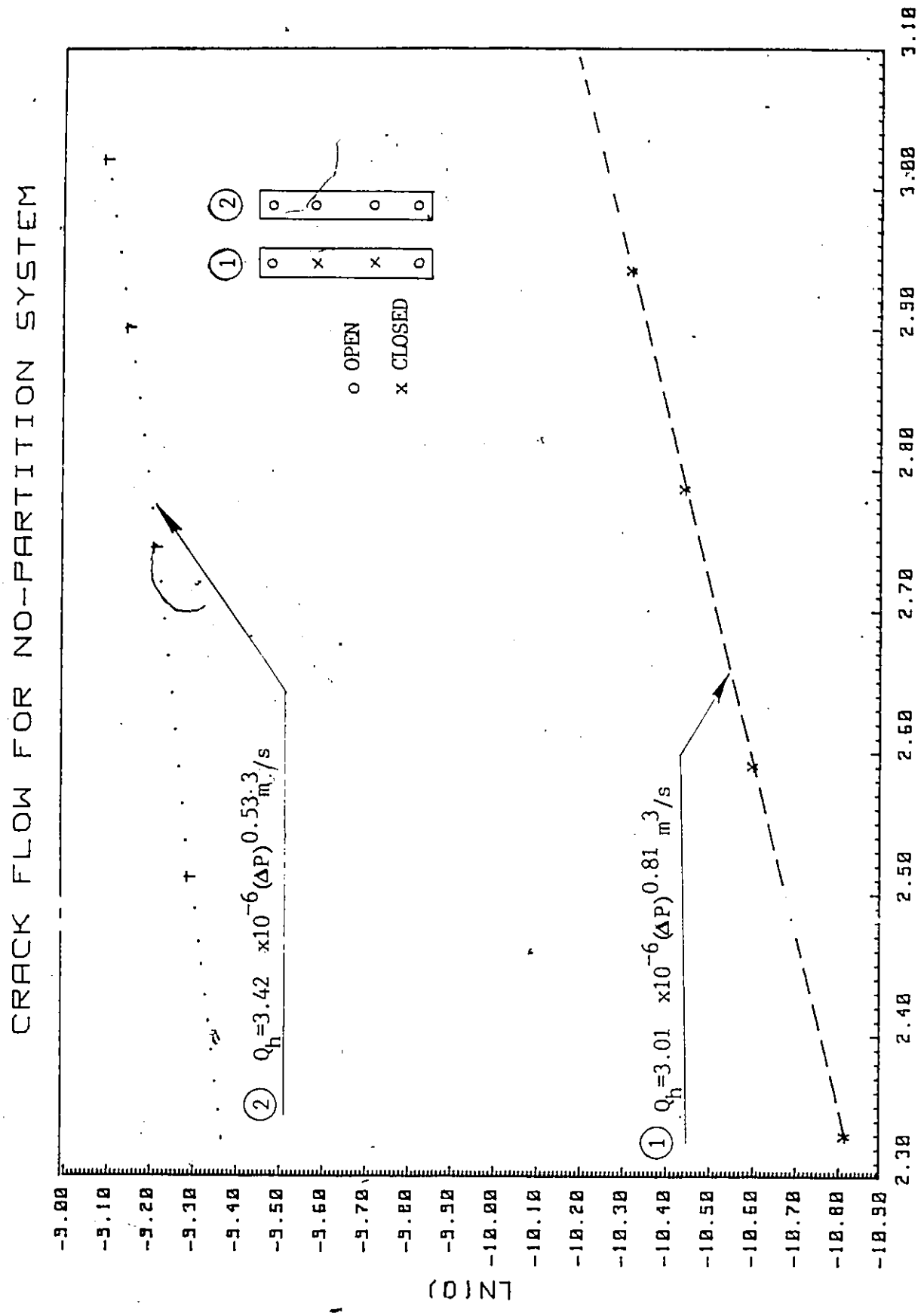

Fig.5.5.1 Correlated Result of Pressure Difference with Flow Rate for No-Partitioned Case

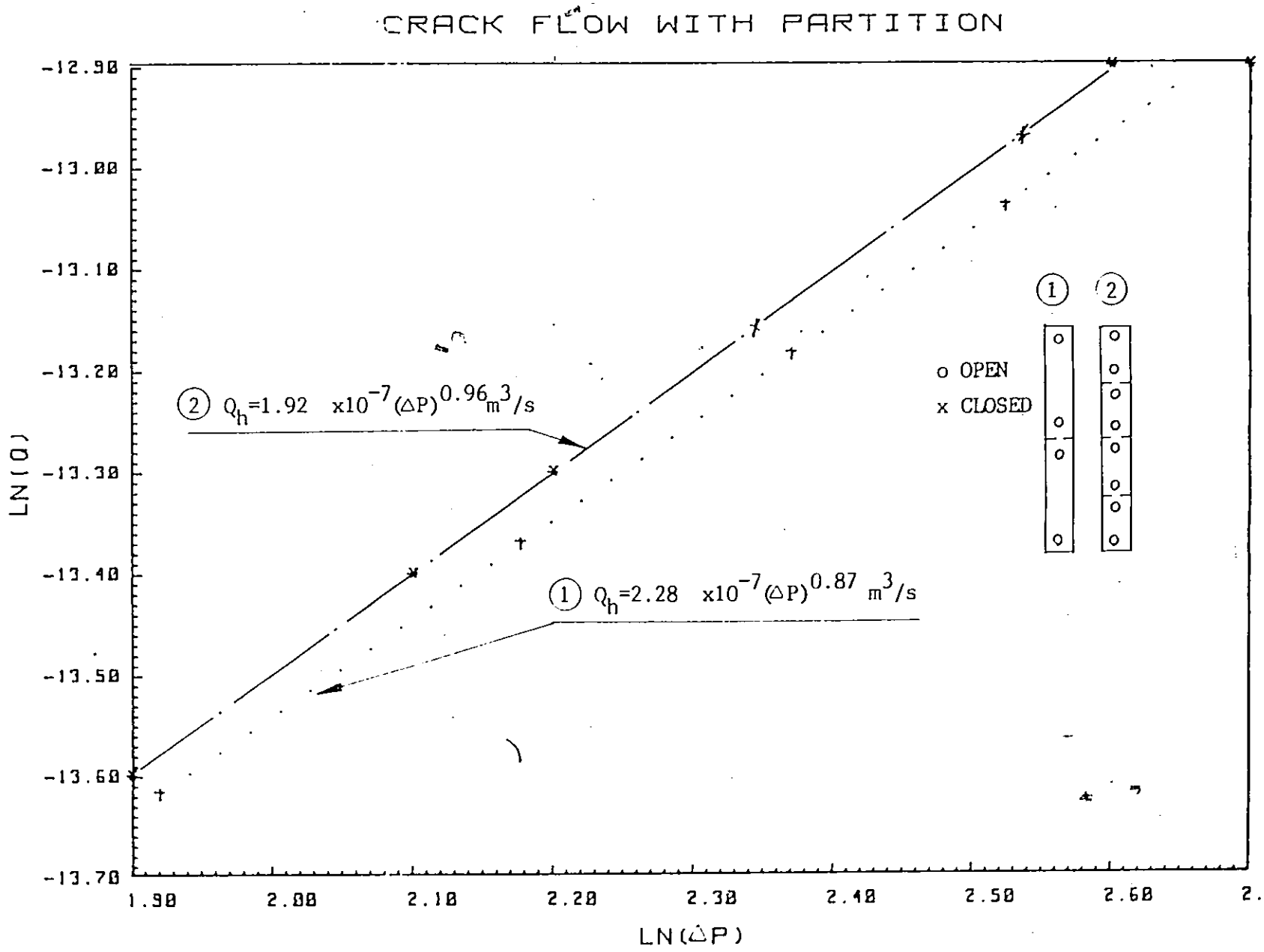

Fig.5.5.2 Correlated Result of Pressure Difference with Flow rate for Partitioned Case

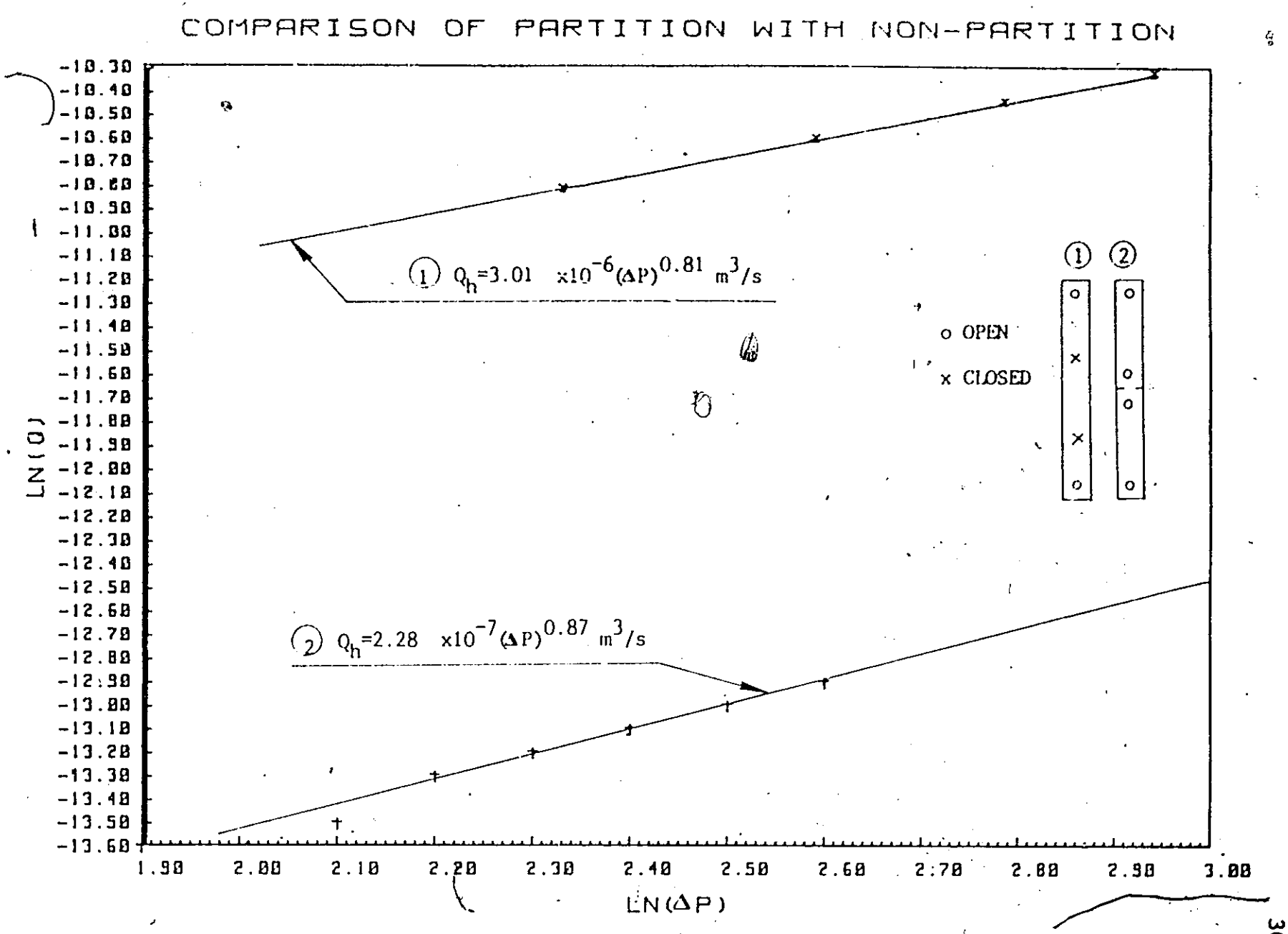

Fig.5.5.3 Comparison of Correlated Result of Partitioned Case with Non-Partitioned Case

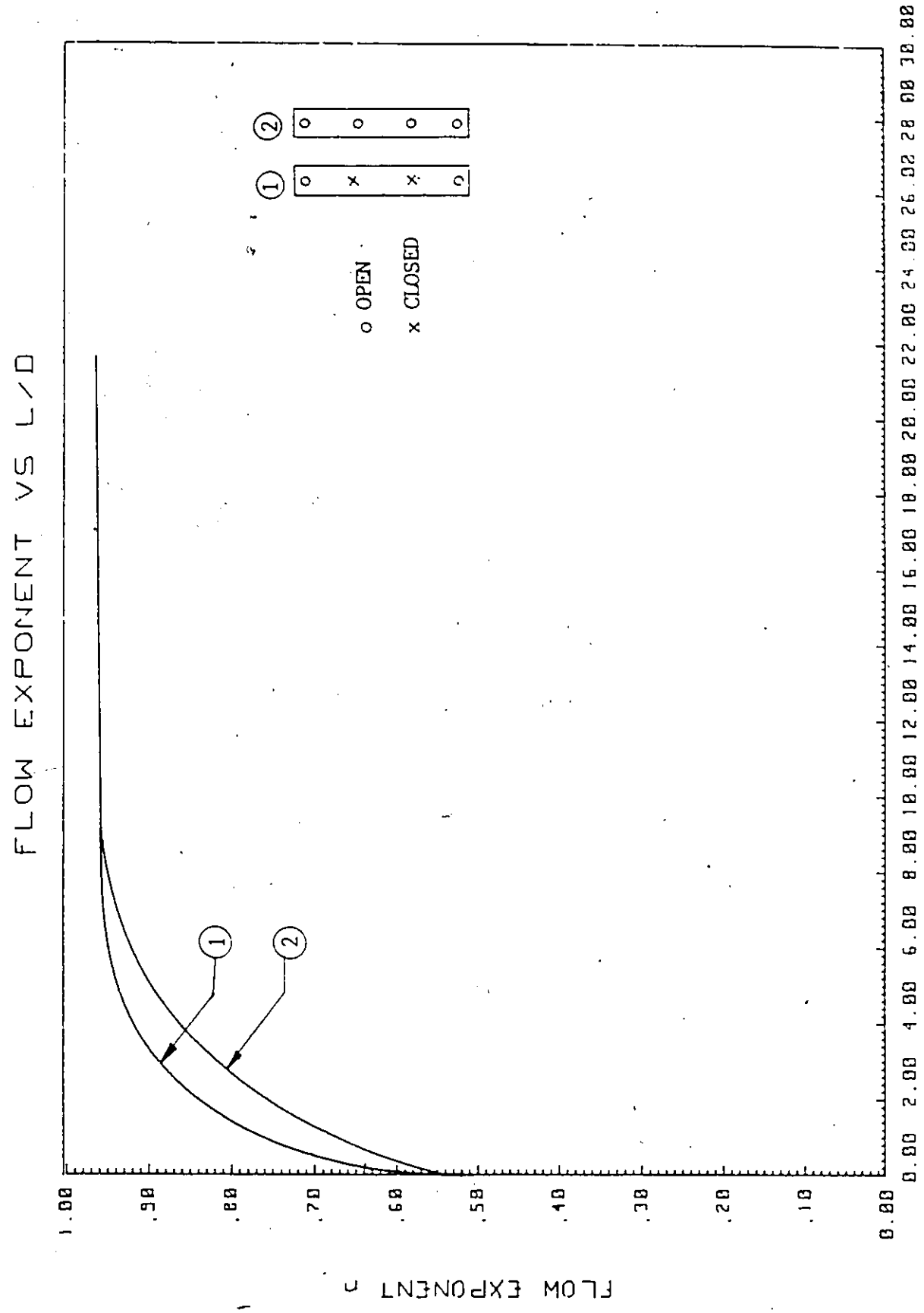

Fig.5.5.4 Effect of Opening Characteristics on Flow Exponent for Non-Partitioned Case

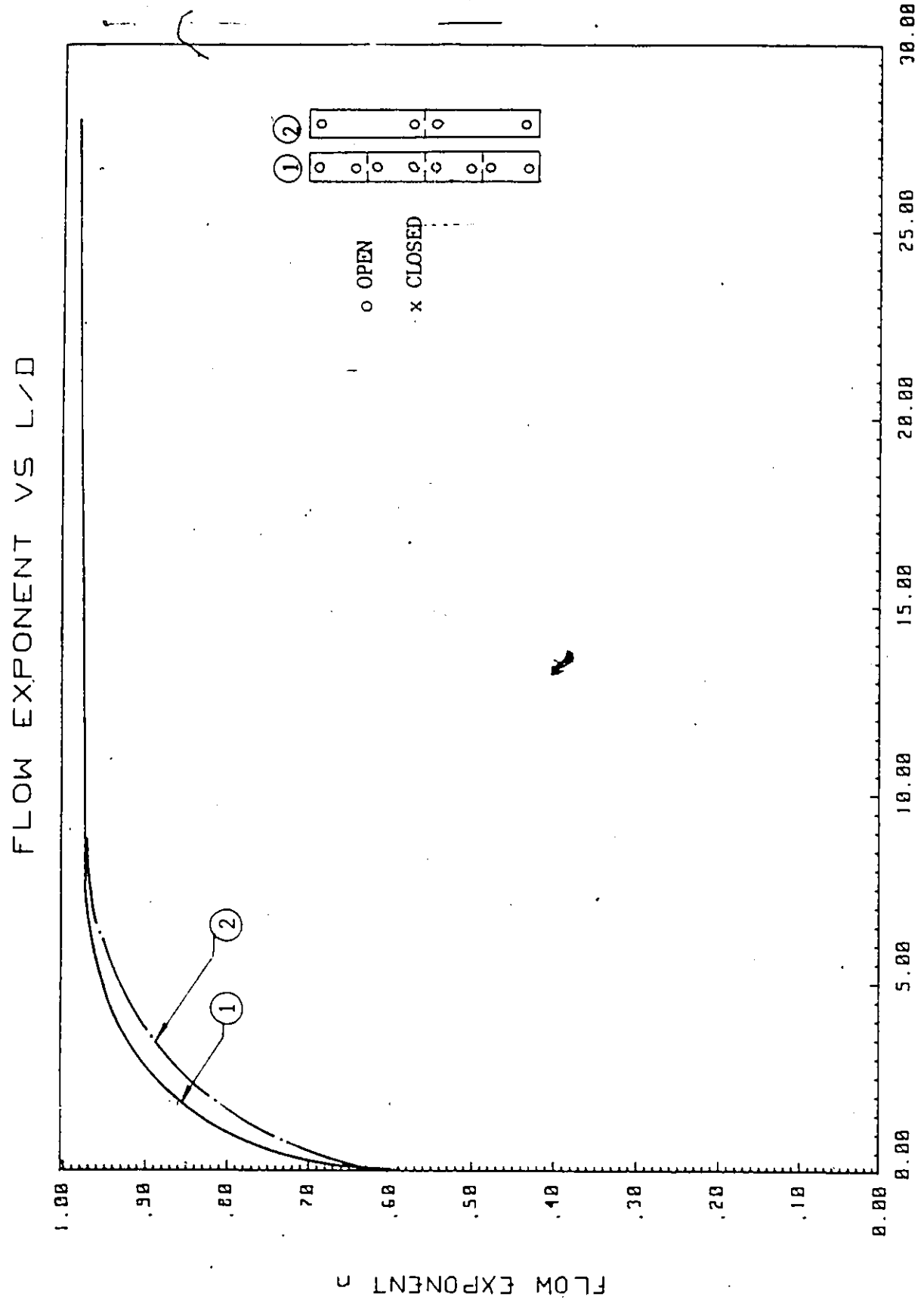

Fig.5.5.5 Effect of Opening Characyeristics on Flow Exponent for Partitioned Case

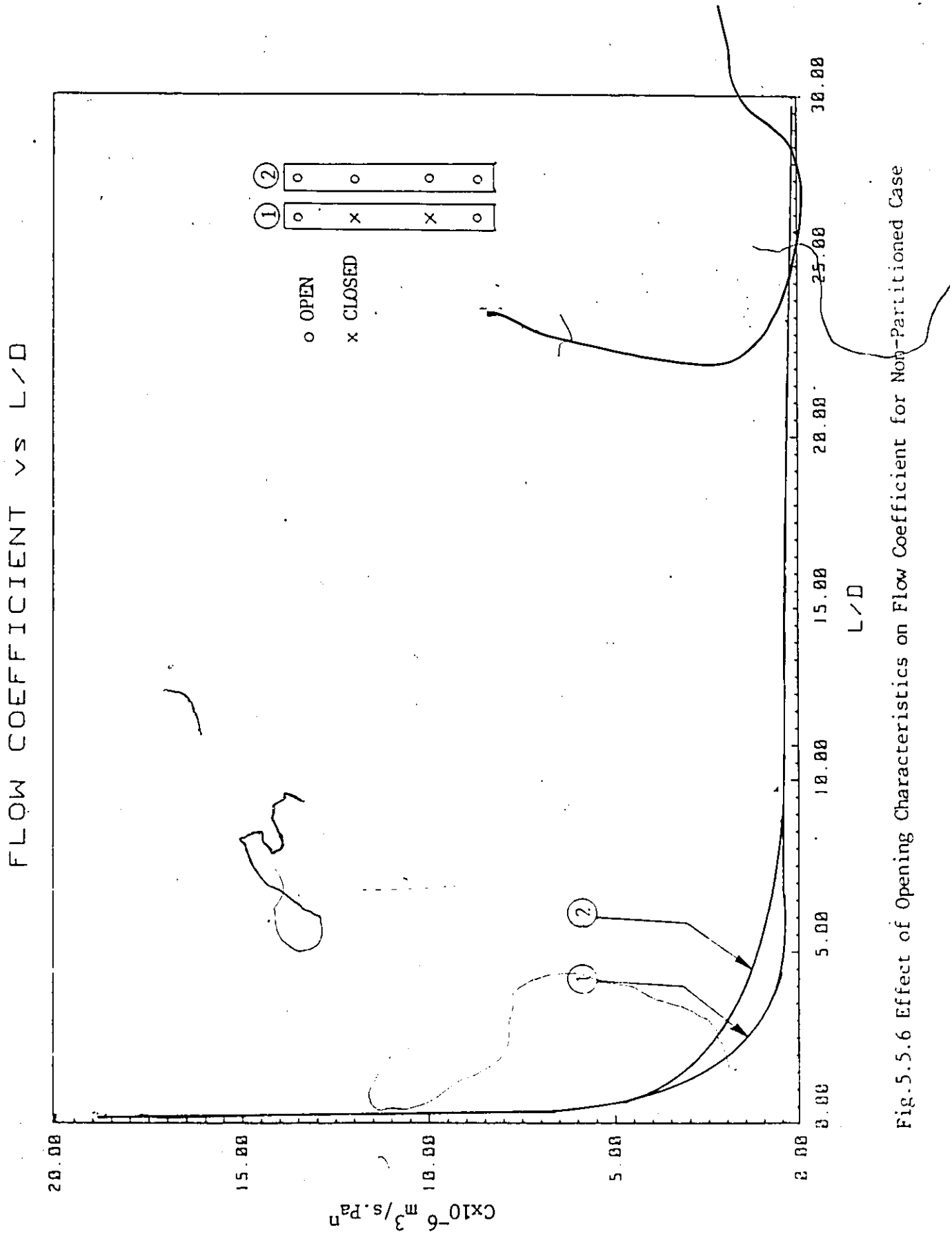

Fig.5.5.6 Effect of Opening Characteristics on Flow Coefficient for Non-Partitioned Case

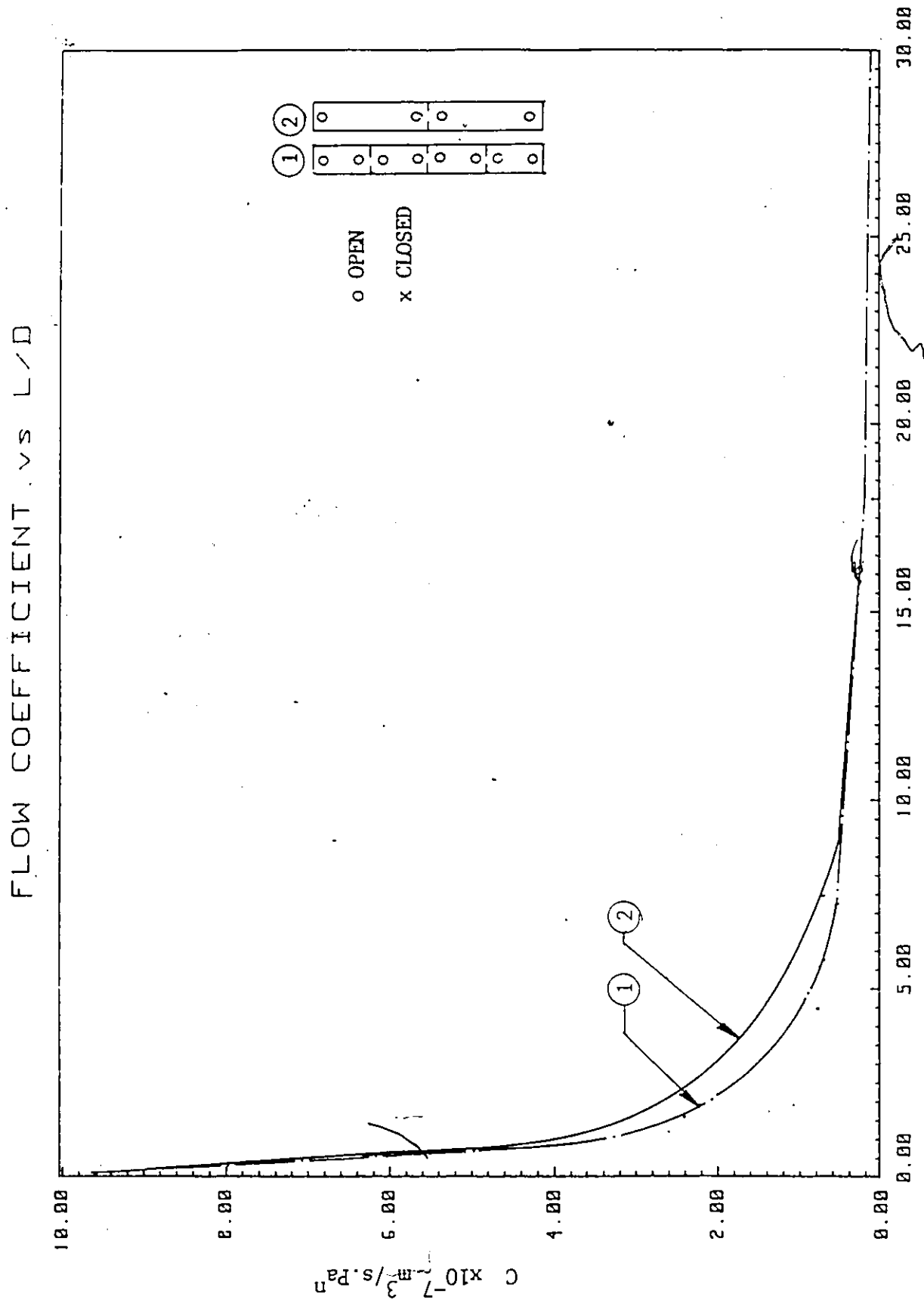

Fig.5.5.7 Effect of Opening Characteristics on Flow Coefficient for Partitioned Case

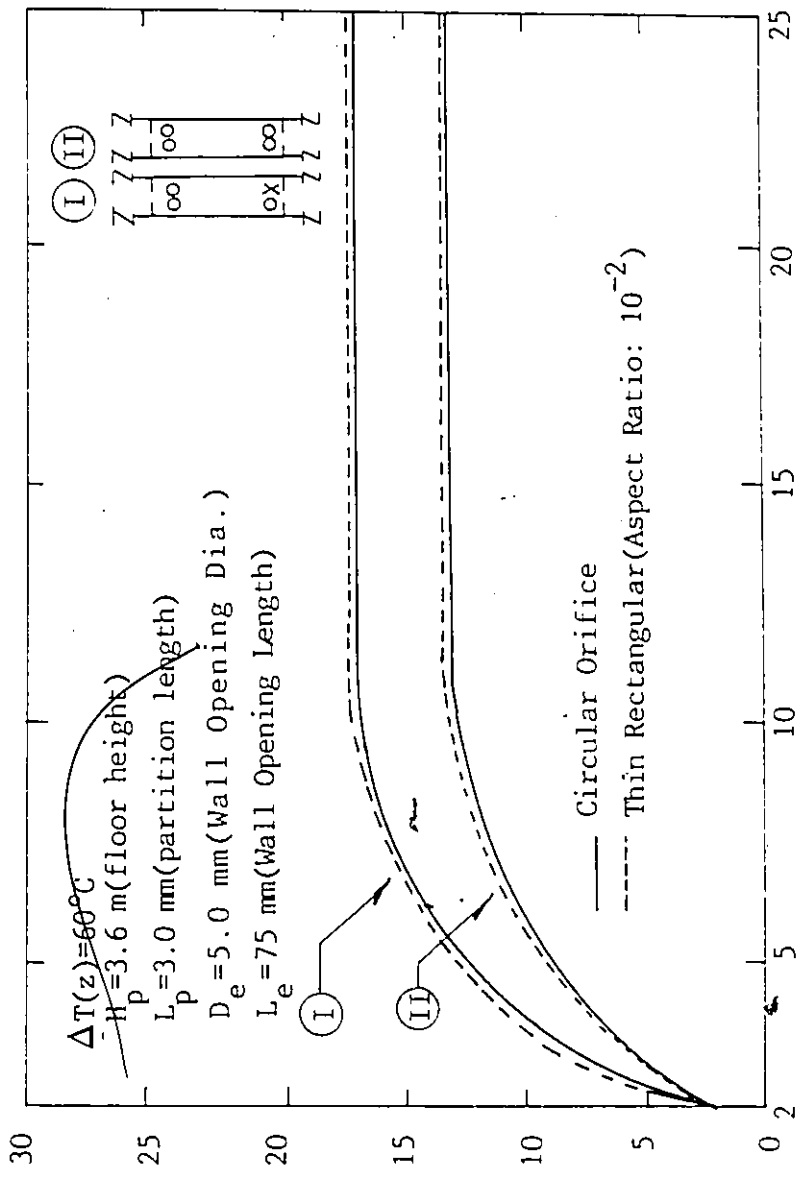

Fig.5.6.1 Effect of Crack Opening Shape on $A^*_{p\ crt}$

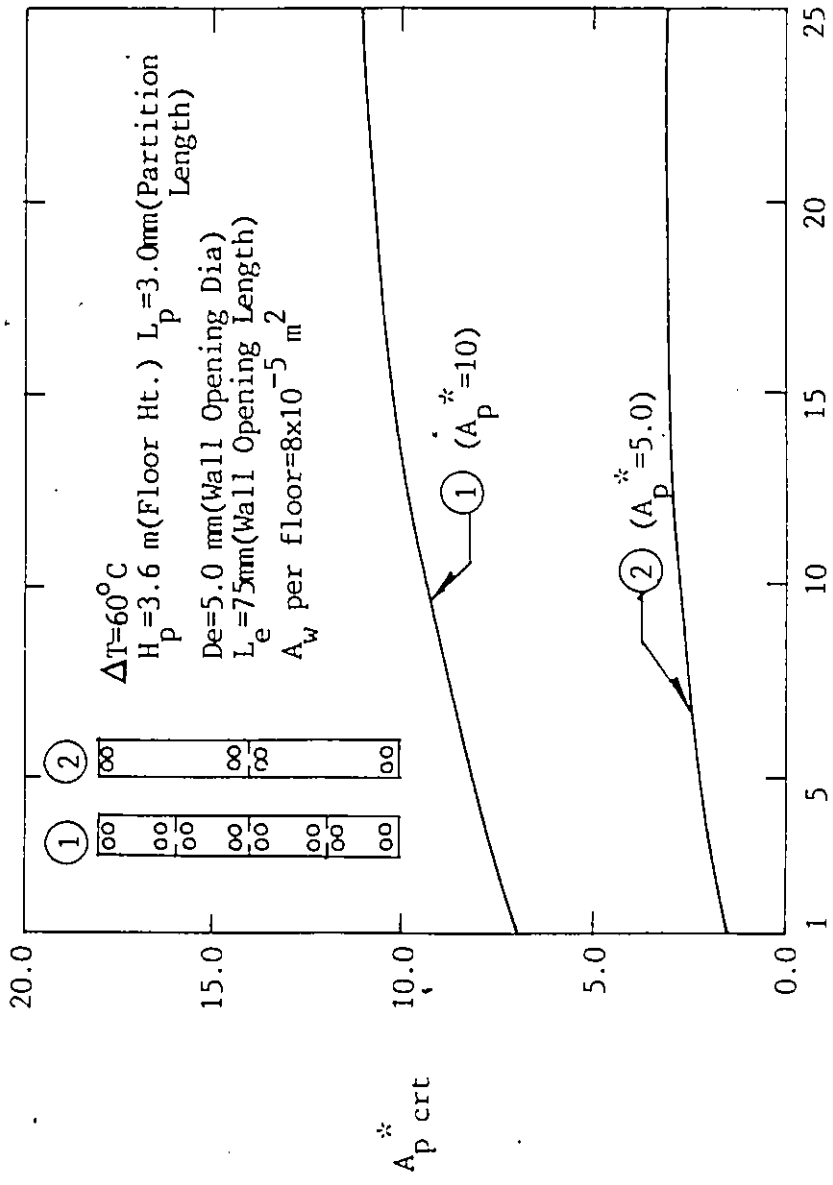

Fig.5.6.2 Effect of Dividing Floor Opening on $A_{p\ crt}^{*}$

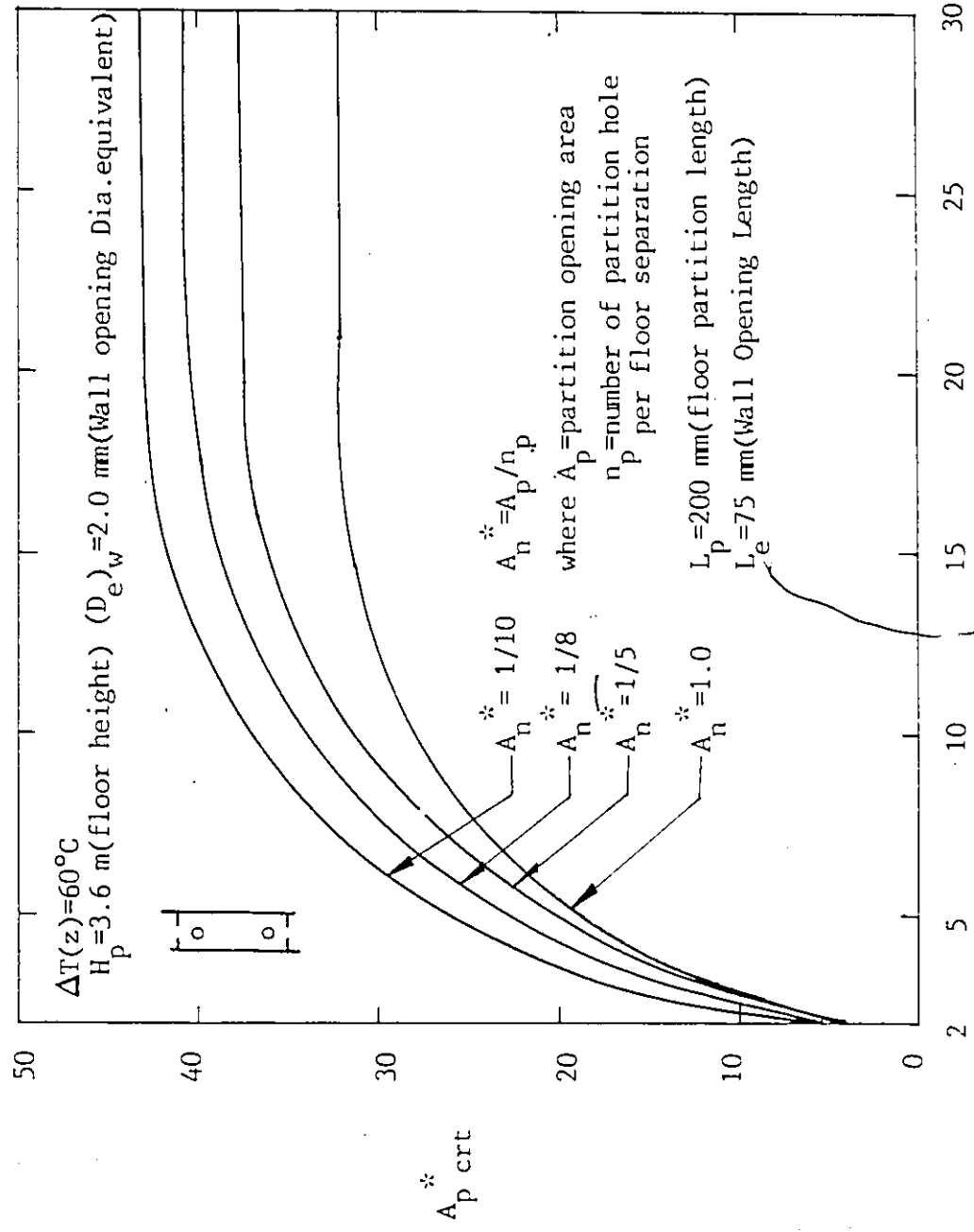

Fig.5.6.3 Effect of Number of Floor Openings for a large model bilding

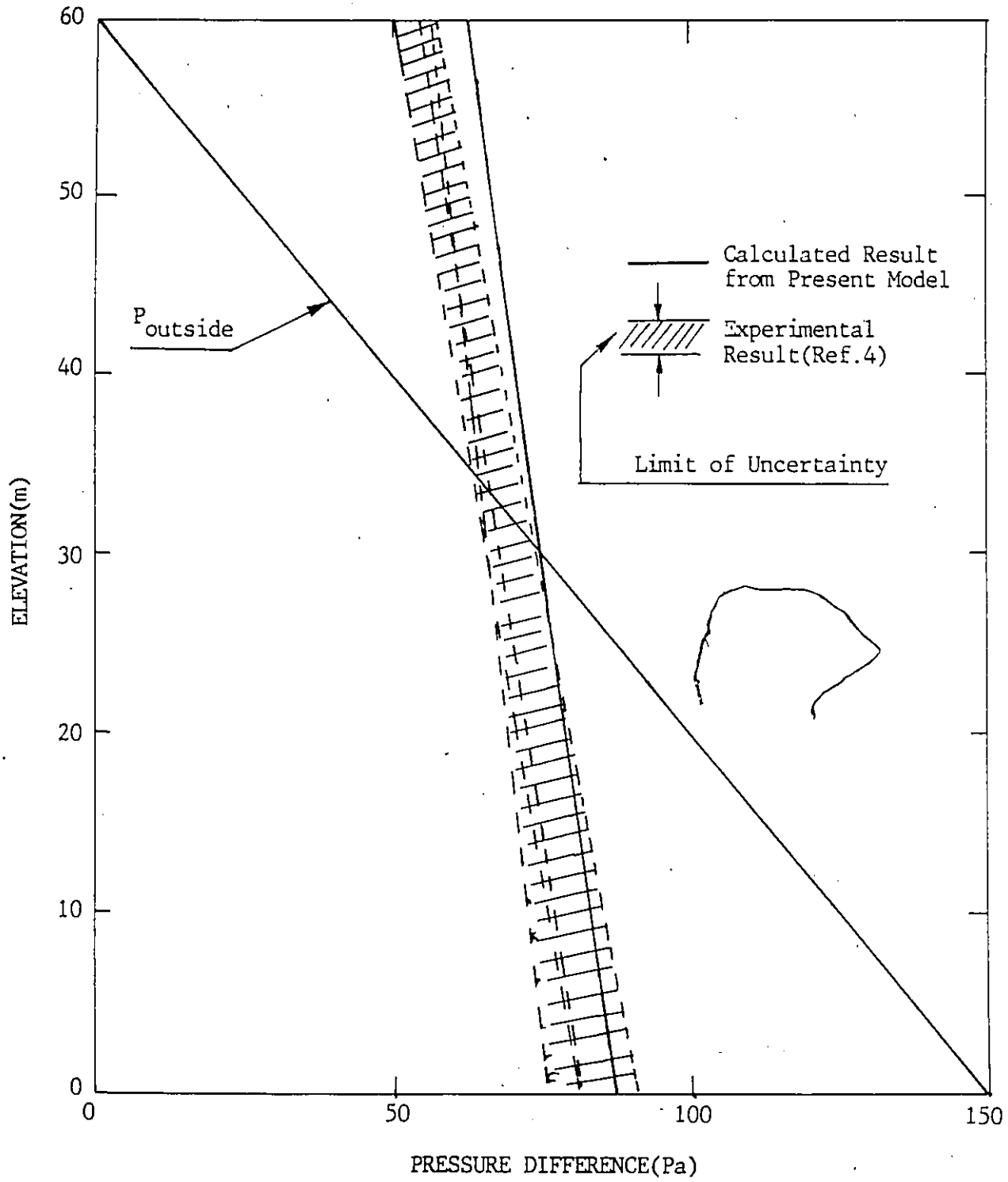

Fig.5.6.4 Comparison of Pressure Profile from Analysis with Experiment for Building A (Thompson Hall, University of Ottawa)

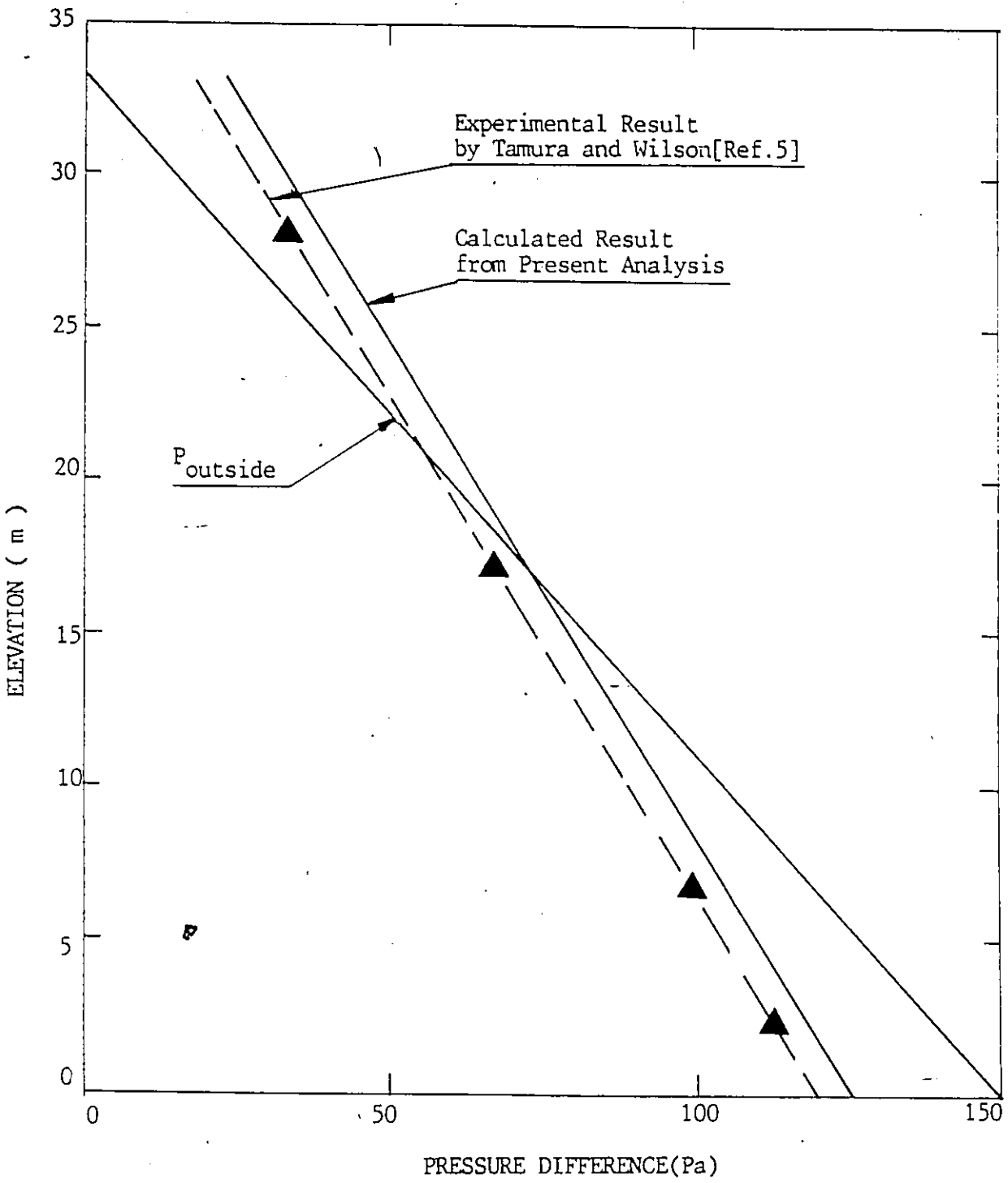

Fig.5.6.5 Comparison of Pressure Profile from Analysis with Experiment for Building E (an Office Building, Ottawa)

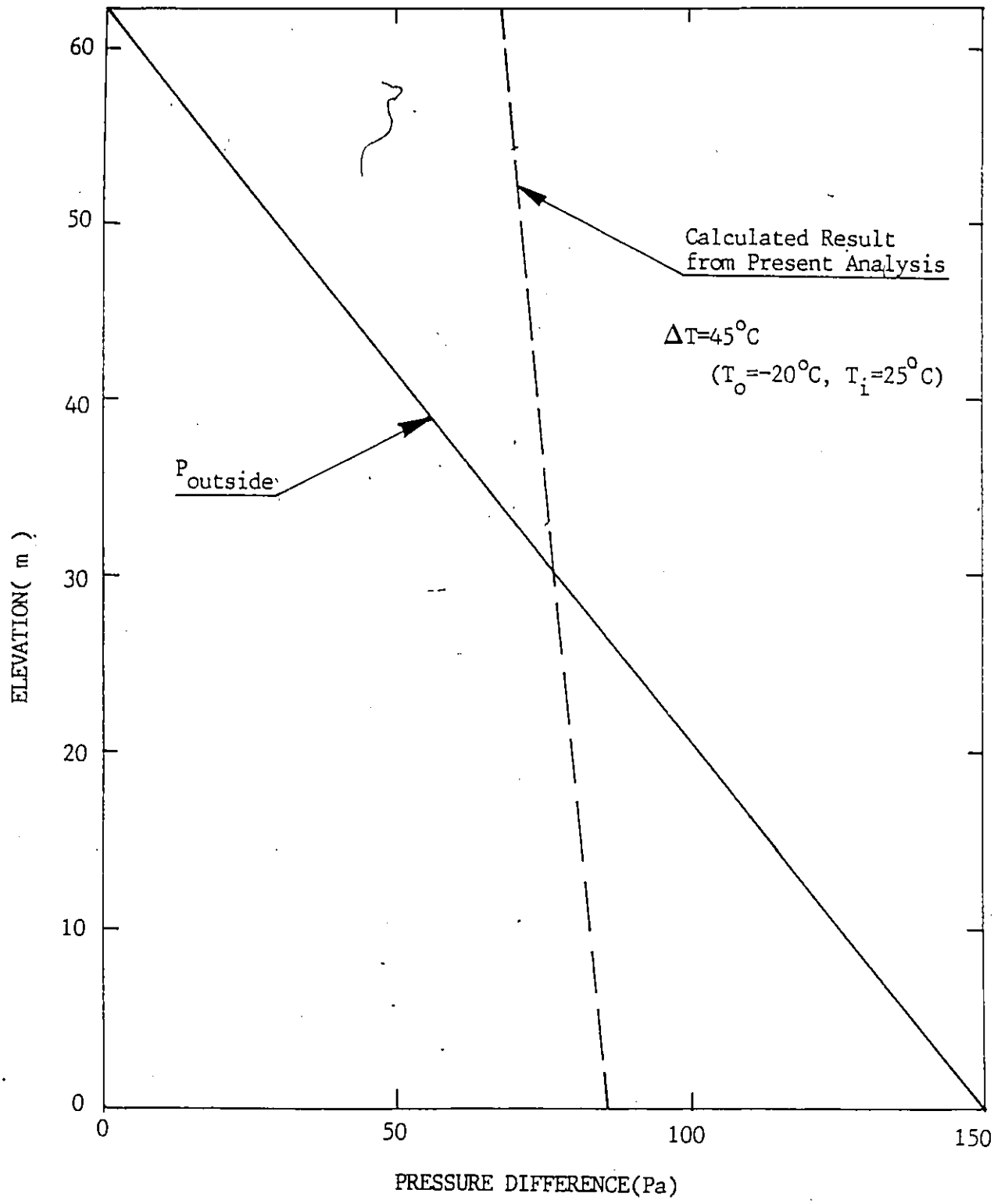

Fig.5.6.6 Pressure Profile obtained from Present Analysis for Building C (an Office Building, Ottawa)

Table 3.5.1 Calculated Values of $\overline{C}_x$ from Eq.3.3.6

(from Ref.29)

L/D	$\overline{C}_x$	L/D	$\overline{C}_x$
1	1143.3	15	120
2	759.7	17	110
3	580.0	20	93.1
4	280.0	25	70.0
5	230.0	30	68.0
6	210.0	35	67.0
8	170.0	38	65.0
10	145.5	38 $-\infty$	64.0

TABLE 5.6.1 Descriptions of Building

	Building A	Building B	Building C	Building D	Building E
No. of Floors	22	23	17	17	9
Typical Floor Dimensions (m x m)	25.6 x 20.7	31 x 37	26 x 38	26 x 38	26.8 x 42.6
Windows					
Type	Sealed double glazed, fixed	same as left	same as left	same as left	same as left
Typical frame size(m x m)	4.0 x 1.2	1.2 x 1.2	1.2 x 1.3	1.2 x 1.3	1.3 x 1.5
No. of windows per floor	36	64	110	110	32
Equivalent Wall Opening diameter(assumed crack width: 2 mm)	2.0	2.0	2.0	2.0	2.0
Elevators					
No. of Cars	3	4	6	6	5
Door Size(m x m)	1.1 x 2.2	1.22 x 2.2	1.17 x 2.13	1.17 x 2.13	1.2 x 2.2
Avg.Door Crack Width(mm)	12	10	10	12	13
Avg.Door Crack Depth(mm)	150	160	150	150	160
Equivalent Opening Dia. of Elevator Door Crack(mm)	24	20	20	24	26
Stairwells					
No. of stairs	2	2	2	2	2
Door Size(m x m)	0.92 x 2.13	0.93 x 2.13	0.93 x 2.13	0.93 x 2.13	0.93 x 2.13
Avg. Door Crack Width(mm)	4.0	3.0	5.0	5.0	5.0
Avg. Door Crack length(mm)	25	30	35	35	25
Equivalent Opening Dia. of Stair Door Crack(mm)	8	6	10	10	10

1) Building A: Thompson Hall, University of Ottawa
2) Building B: Tower Building, Carlton University, Ottawa
3) Building C: Tower A Building, Government Building, 303 River Road, Ottawa
4) Building D: Tower B Building, Government Building, 303 River Road, Ottawa
5) Building E: Office Building, Government Building, 2785 Riversise Dr., Ottawa

APPENDIX A-1

DATA ACQUISITION SYSTEM

The details of the data acquisition system used in all aspect of the present experimental studies is described as follow. This is a system which is consisted of a Hewlett Packard (HP) desk top computer and four other HP peripheral instruments.

(1) HP 9835A Desk Top Computer

The desk top computer constituting the data acquisition system has memory capacity of 115 K bytes, complete I/O capacity, a built-in tape cartridge drive for data storage on cassette tape (217 K byte per tape), and an interactive key board with a 12" green monitor.

The computer is used throughout the present study for the data acquisition of experimental data, data processing, data storage, and data reductions.

(2) HP 3455A Digital Voltmeter

The digital voltmeter included in the data acquisition system has a capacity of up to 24 readings per second with 1 micron-volt sensitivity, true RMS, auto system testing and auto-calibration capability. This digital voltmeter is used for all temperature and pressure measurements. All the measurement data are in the form of D.C. signals from either the pressure transducers or the thermocouples.

(3) HP 3495A Scanner

The scanner used throughout the experiments has capacity of 20 channels. The 20 channels of reference assembly are used for the purpose of scanning either the pressure differentials or temperatures in the testing apparatus. This scanner has taken the role of linking all the external instruments to the data acquisition system.

(4) HP 7245A Printer/Plotter.

This instrument has the capability of being a printer as well as a plotter. All the experimental data obtained and processed by the computer are printed out by this printer/plotter. In addition to this purpose of process, the printer/plotter is extensively used during the data reduction.

(5) HP 98035 Real Time Clock.

The real time clock connected to the computer is used as a real time reference as well as a trigger mechanism. Besides being used to trigger the digital voltmeter at certain time intervals for the acquisition of experimental data, this is also employed to set the system on idle for stabilization of the pressure transducers before taking regular measurements.

APPENDIX A-2 ERROR ANALYSIS

(1) Calibration of Thermocouples

Every thermocouple beads to be installed for each test model building in the present study were made from the same spool of the thermocouple wire supplied by manufacturer. Also every thermocouple beads were made by thermocouple welder with careful attentions.

Two of the thermocouple beads which were made for each test section were randomly selected and calibrated against a Fisher NR 15-155 standard precision thermometer having a temperature controlled oil bath in the range from 20 to 100 C.

In the calibration procedures above, readings from thermocouple were taken for each predetermined measuring point with a digital voltmeter, HP 3455A, with 1 micron-volt sensitivity and auto calibration capabilty, via channel # 1 of a scanner, HP 3495A, and then were compared to the reading from the thermometer. The results obtained from thermocouples were processed by a desk top computer, HP 9835A, which produced a hard copy of the processed data such as the listing of measurements, the standard diviation, and etc,.

As shown in Fig.4.3.1, each bead which was selected was tested for eleven testing temperature points with the above procedures. A typical example of the above calibration result is shown in Table A.2.1, in which the relative error between temperature readings from the standard thermometer and the values from thermocoulpe is presented.

As shown in the table, the relative error appears to be small and is not greater than ± 1.0 % or ± 0.5°C for all the ranges tested. For all other cases, the same trend shown above was observed.

(2) Temperature Distributions along Test Section Elevations

Fig.A.2.1 illustrates a typical example of the temperature distributions of the test section wall, the air inside, and the air outside along the elevations in the test section used in the present experimental studies.

The one shown in the figure is a case with no floor partitions, in which the test section was designed to have temperature difference of 60°C between inside and outside along height, and four exterior wall openings. In the results, the standard deviation of the mean of the

temperature measurements is taken as the experimental uncertainty of the corresponding measurement according to the standard error analysis method [68]. Typical results for this case are:

Temperature outside air : $20.1\pm0.6\,^{\circ}C$

Temperature inside wall : $79.3\pm0.2\,^{\circ}C$

Temperature inside air : $79.4\pm0.5\,^{\circ}C$

Hence, the temperature difference between inside and outside can be given as;

For inside wall of test section to air outside

$$\Delta T=(79.3\pm0.2)-(20.1\pm0.6)$$
$$=59.2\pm0.8\,^{\circ}C$$

For air inside to air outside

$$\Delta T=(79.4\pm0.5)-(20.1\pm0.6)$$
$$=59.3\pm1.1\,^{\circ}C$$

As can be seen in the result above, the largest uncertainty of temperature difference is not greater than $1.5\,^{\circ}C$ for the case. In the present study, the standard deviation of the temperature distribution along elevation

shown in Fig.A.2.1 was used as the experimental criteria in the creation of temperature conditions along the elevations of the test sections for all the experimental tests.

(3) Estimation of Uncertainty in Experimental Result

The experimental uncertainty can be estimated by using the standard method of error analysis [68]. The genearalized method finds the total uncertainty by taking the square root of the sum of the squares of the individual uncertainties which affect the result.

Suppose that x,....,z are measured with uncertainties dx,....,dz, and the measured values used to compute the function q(x,....,z). If the uncertainties in x,...,z are independent and random, then the fractional uncertainty in q is

$$\frac{dq}{q} = \sqrt{\left(\frac{dx}{x}\right)^2 + \ldots + \left(\frac{dz}{z}\right)^2} \qquad \text{(A.2.1)}$$

The pressure differential due to thermal effect is believed to be dependent only on the temperature of the building inside and outside. Assuming the thermal effect equation, Eq.1.1, is correct to determine the pressure difference, the uncertainty of the pressure difference due to thermal effect can be estimated from Eq.A.2.1.

The estimated uncertainties for the case shown in Fig.A.2.1 are;

$dT_i/T_i(air)=0.63$ %, $dT_w/T_w=0.25$ %, $dT_o/T_o=3.0$ %

Then

For air inside to air outside

$d\Delta P/\Delta P=[0.63^2 + 3.0^2]^{1/2} =3.1$ %

For inside wall to air outside

$d\Delta P/\Delta P=[0.25^2 + 3.0^2]^{1/2} =3.0$ %

As shown in the above result, the uncertainty of the pressure differentials due to the uncertainties involved in the temperature measurements is shown to be not significant.

Table A.2.1 Calibration Result of Thermocouple

(for Test Section with no Floor Partitions)

Readings from Standard Thermometer(A) °C	Values from T.C(B) °C	Difference A-B	Relative Error(%) (A-B)/A*100
25.2	25.4	-0.2	0.7
30.0	29.8	0.2	0.6
38.2	37.8	0.4	1.0
42.0	42.3	0.3	-0.7
50.0	50.1	-0.1	-0.2
58.1	58.2	-0.1	-0.2
60.0	59.5	0.5	0.8
65.3	64.9	0.4	0.6
70.0	70.2	0.2	0.3
80.2	80.1	0.1	0.1
97.0	97.2	-0.2	-0.2